AUS DEM INSTITUT FÜR KLINISCHE ZYTOBIOLOGIE UND ZYTOPATHOLOGIE
GESCHÄFTSFÜHRENDER DIREKTOR: PROF. DR. ROLAND LILL
DES FACHBEREICHS MEDIZIN DER PHILIPPS-UNIVERSITÄT MARBURG

TOWARDS AN UNDERSTANDING OF PEROXISOME DYNAMICS IN MAMMALIAN CELLS

INAUGURAL-DISSERTATION ZUR ERLANGUNG DES DOKTORGRADES DER HUMANBIOLOGIE
(DR. RER. PHYSIOL.)

DEM FACHBEREICH MEDIZIN DER PHILIPPS-UNIVERSITÄT MARBURG
VORGELEGT VON

NINA ANNA MARIA BONEKAMP
AUS WÜRSELEN

MARBURG, 2012

Angenommen vom Fachbereich Medizin der Philipps-Universität Marburg
am: 06.06.2012

Gedruckt mit Genehmigung des Fachbereichs.

Dekan: Prof. Dr. Matthias Rothmund
Referent: Prof. Dr. Roland Lill
Koreferent: Prof. Dr. Gerhard Schratt

1 INTRODUCTION

1.1 PEROXISOMES – AN OVERVIEW

1.1.1 Introducing a highly versatile organelle

Unlike mitochondria or the Golgi apparatus, both of which were discovered in the very end of the 19th century, peroxisomes were only identified using electron microscopy in 1954 by Rhodin as a part of his PhD thesis and then termed microbodies (Rhodin, 1954) (Fig. 1.1). Originally regarded as a "fossil organelle" or the cell's "garbage pail", they have gained considerable interest upon their subsequent biochemical characterization by de Duve and Baudhuin who discovered that the peroxisomal matrix contains a high number of hydrogen peroxide (H_2O_2)-producing oxidases as well as catalase, an H_2O_2-degrading enzyme (De Duve & Baudhuin, 1966) (Fig. 1.1 B). This observation coined the more functional name "peroxisome" for the organelle.

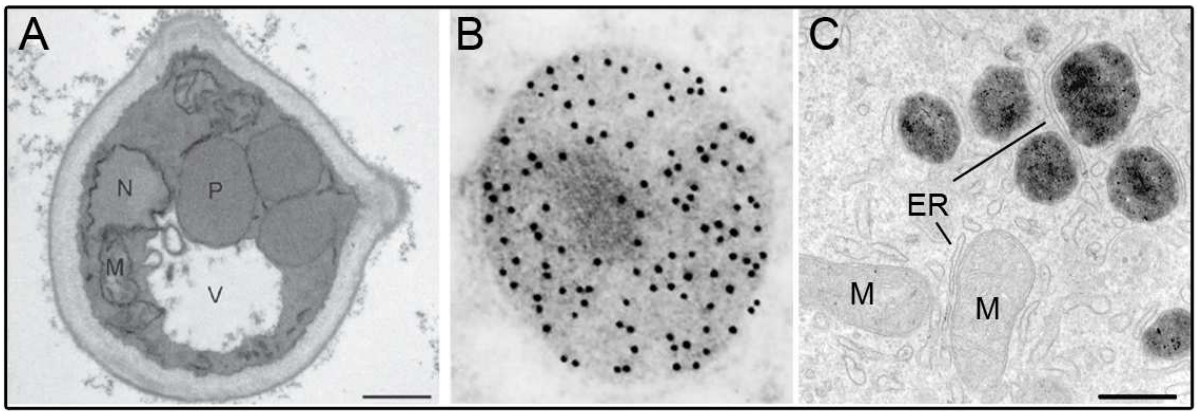

Fig. 1.1: Ultrastructure of peroxisomes.
(A) Ultrathin sections of peroxisomes in the methylotrophic yeast *Hansenula polymorpha* after growth on methanol (Krikken et al., 2009). (B) Rat liver peroxisomes labelled with specific antibodies against catalase followed by protein A-gold staining (Fahimi, 1992). Note that gold particles representing catalase distribute over the entire matrix sparing the crystalline cores. (C) Peroxisomes in rat hepatoma cells stained by alkaline DAB cytochemistry (Schrader & Yoon, 2007). Note the close association of peroxisomes (black structures) and mitochondria (M) with the endoplasmic reticulum (ER). M, mitochondria; N, nucleus; P, peroxisome; V, vacuole. Bars, 0.5µm (A, C). Magnification (B) × 58,000.

The identification of catalase as a key peroxisomal enzyme led to the introduction of the alkaline 3, 3'-diaminobenzidine (DAB) reaction for catalase that enabled the morphological characterization of peroxisomes by electron microscopy (Fahimi, 1968; Fahimi, 1969; Novikoff & Goldfischer, 1969) (Fig. 1.1 C). Subsequently, peroxisomes were shown to be ubiquitous organelles like mitochondria (Hruban et al., 1972), however, they disappear during

the development of red blood cells and sperm (Luers et al., 2006) and are absent in *Apicomplexa phylum* and amitochondriate parasites (Schluter et al., 2006).

In general, peroxisomes can be described as ubiquitous, single-membrane bound organelles that are devoid of DNA and contain a fine granular matrix (Fig. 1.1). About 85 genes in *Homo sapiens* and 61 genes in *Saccharomyces cerevisiae* have been identified that encode peroxisomal proteins, many of which are linked to peroxisome metabolism. Peroxisomes play a central role in lipid metabolism and detoxification, but also in the synthesis of ether phospholipids, bile acids and cholesterol (1.1.2), rendering them essential for cellular homeostasis and development. Their essential contribution to human health is exemplified by the severe consequences of peroxisomal dysfunctions (1.1.4). Despite this common ground, one of the most striking features of peroxisomes is their enormous plasticity, both on a metabolic and a morphological level. Peroxisomal enzyme composition varies immensely across species, even leading to the generation of specialized peroxisomal structures such as e.g. the glycosomes of trypanosomatids, the glyoxysomes of plants and the Woronin body of filamentous fungi, a very specialized peroxisome that serves the sole purpose of sealing septal pores upon injury (Jedd & Chua, 2000; Michels et al., 2005; Michels et al., 2006; Reumann & Weber, 2006). Interestingly, peroxisomal protein composition also varies within tissues and/or developmental stages of the same organism (Islinger et al., 2010), thus the term "multipurpose organelle" has proven to be a more than accurate designation for peroxisomes (Opperdoes, 1988; Islinger et al., 2010). Although peroxisomes display this striking heterogeneity in regard to their enzyme content, proteins involved in organelle biogenesis and maintenance – the so-called peroxins (Pex) - are evolutionary conserved throughout species. Pex genes have been identified based on genetic complementation in peroxisome-deficient yeast and mammalian cells (34 in yeast with approximately 20 mammalian and 23 plant homologues) (Kiel et al., 2006; Platta & Erdmann, 2007). Most of them are peroxisomal membrane proteins or associated with the membrane (1.1.5) (Table 1.2). Peroxisomes additionally show a remarkable plasticity in regard to their number and morphology. For instance, mammalian liver and kidney contain a high density of peroxisomes (accounting for around 2 % of the total hepatic protein content (Leighton et al., 1968)), whereas yeast cells in general only contain a few. Moreover, mammalian peroxisomes display a very heterogeneous morphology, since they may appear as spherical organelles with a diameter of around 0.1 – 0.2 µm, representing the common textbook image, but also enlarge to form rod-shaped (0.3 – 0.5 µm), long tubular structures (up to 5 µm) or even tubular-reticular networks (Yamamoto & Fahimi, 1987; Schrader et al., 1994; Schrader et al., 2000; Purdue & Lazarow, 2001). A

variety of peroxisomal shapes can also be observed on the ultrastructural level. Rat liver peroxisomes e.g. contain dense cores of urate oxidase, while bovine kidney peroxisomes display crystalline inclusions of α-hydroxyacid oxidase B, resulting in a rather polyhedric shape of the organelle (Hruban & Swift, 1964; Zaar et al., 1991). The Woronin bodies of *Neurospora crassa* on the other hand appear as hexagonal crystals (Jedd & Chua, 2000).

Despite their enormous plasticity and dynamic behaviour, peroxisomes do not exist as isolated entities, but are intimately linked to other organelles such as lipid droplets, the ER and especially mitochondria (Schrader & Yoon, 2007; Camoes et al., 2009) (1.3) (Fig. 1.1 C). Peroxisome homeostasis in general needs to remain adaptable to the metabolic state of the cell which is ensured by a combination of peroxisome multiplication or proliferation, the removal of excess organelles by autophagy (pexophagy) as well as by processes of peroxisome inheritance and motility (1.2).

1.1.2 Peroxisomal metabolism

Peroxisomes are essential for human health and development, since they fulfil a variety of metabolic functions, both in the breakdown and synthesis of key substrates. Over 50 enzymes have been identified in the peroxisomal matrix that catalyze the β-oxidation of very long chain fatty acids (VLCFAs), prostaglandins and eicosanoids, the oxidation of D-amino acids, alcohols, polyamines and uric acid (in non-primates) as well as the α-oxidation of branched chain fatty acids. Furthermore, peroxisomes play a key role in the detoxification of xenobiotics, reactive oxygen species (ROS), glyoxylate and the biosynthesis of ether lipids, cholesterol and bile acids (van den Bosch et al., 1992; Ferdinandusse et al., 2002; Hogenboom et al., 2004; Kunze et al., 2006; van der Klei et al., 2006; Wanders & Waterham, 2006b) (Fig. 1.2). Several specialized functions have evolved with plants, yeast and protozoa generally displaying a broader spectrum of activities. These include an involvement in photorespiration, jasmonic acid and auxin synthesis in plants as well as penicillin synthesis in fungi (Tolbert, 1981; van den Bosch et al., 1992; Heupel & Heldt, 1994; Kiel et al., 2005b; Nyathi & Baker, 2006). The fact that e.g. the biosynthesis of penicillin in fungal peroxisomes can be environmentally induced renders peroxisome research an attractive field of interest for biotechnology (Kiel et al., 2005b). Besides the classical functions listed above, peroxisomes have recently been shown to participate in the synthesis of biotin in fungi and to contribute to anti-viral innate immunity (Dixit et al., 2010; Tanabe et al., 2011).

As the various peroxisomal substrates are consumed by FAD-(or FMN)-coupled O_2-containing oxidases that produce H_2O_2 as a by-product, peroxisomes harbour an oxidative

metabolism. Detoxification of ROS is performed by catalase and a large set of resident peroxisomal antioxidant enzymes (1.1.3) (Fig. 1.2).

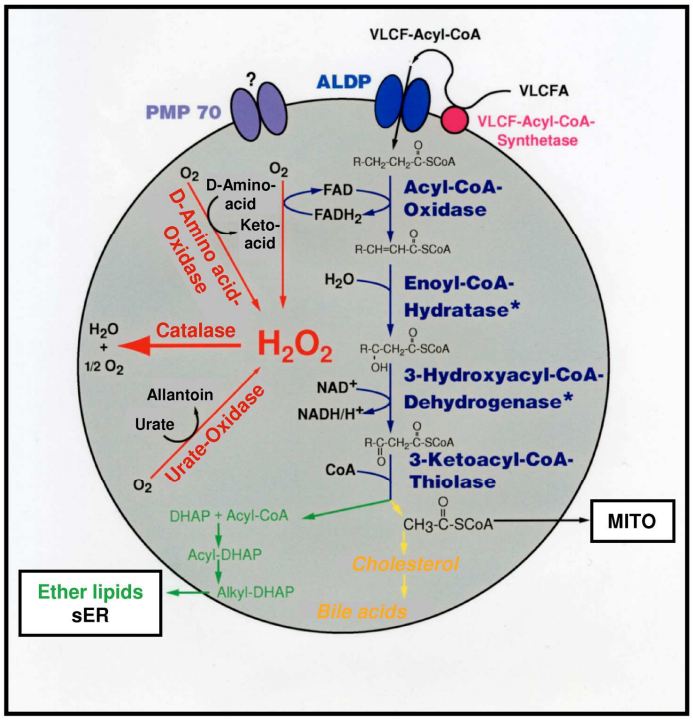

Fig. 1.2: Overview of the major peroxisomal metabolic pathways. Peroxisomal metabolism in the mammalian liver (adapted from Baumgart et al., 1997; Schrader & Fahimi, 2008).

Peroxisomal lipid metabolism

While fatty acid β-oxidation occurs exclusively peroxisomal in yeasts and plants, it coexists with the mitochondrial fatty acid β-oxidation in animal cells (Cooper & Beevers, 1969; Kunau et al., 1988; Poirier et al., 2006; Shen & Burger, 2009). However, only the peroxisomal acyl-CoA oxidases (AOX) show substrate specificity for very long chain fatty acids (VLCFA, ≥ C_{24}) and branched chain fatty acids (Mannaerts & Van Veldhoven, 1993; Mannaerts et al., 2000; Reddy & Hashimoto, 2001). Nonetheless, the basic set of fatty acid β-oxidation reactions carried out by both organelles remains the same and at the end of each cycle, fatty acids are shortened by two carbon atoms which are released as acetyl-CoA (Lazarow & De Duve, 1976; Wanders, 2004; Wanders & Waterham, 2006b) (Fig. 1.2). Upon reduction of fatty acid chain length to octanoyl-CoA, propionyl-CoA and acetyl-CoA, fatty acids are conjugated to carnitine and shuttled to mitochondria for full oxidation and energy production via the mitochondrial electron transfer chain (Ferdinandusse et al., 1999; Reddy & Hashimoto, 2001). Alternatively, they may serve as substrates for the generation of complex lipids within peroxisomes. Besides the prominent VLCFA docosahexaenoic acid (C26:0), peroxisomal substrates include pristanic acid, the bile acid intermediates di- and trihydroxycholestanoic acid (DHCA, THCA) and long-chain dicarboxylic acids. 3-methyl fatty acids such as phytanic acid or xenobiotics cannot directly serve as a substrate for the β-

oxidation machinery, hence they are degraded by peroxisomal α-oxidation, i.e. that they are oxidatively decarboxylated to generate 2-methyl-fatty acids which can be β-oxidized (Casteels et al., 2003; Jansen & Wanders, 2006; Wanders & Waterham, 2006a). In higher eukaryotes, peroxisomes are the sole site of α-oxidation.

Ether phospholipid synthesis

The term ether phospholipid denominates a special class of phospholipids which contain an ether-linkage instead of an ester linkage at the *sn*-1 position of glycerol. Ether lipids may contain an 1-O-alkyl linkage or an 1-O-alk-enyl linkage, the latter class is referred to as plasmalogens. Plasmalogens are important constituents of the neuronal myelin sheath, thus loss of peroxisomal functions is often accompanied by neurodegenerative processes (Faust et al., 2005; Hulshagen et al., 2008) (1.1.4). The biosynthesis of ether phospholipids involves the cooperation of peroxisomal and ER resident enzymes. Initial synthesis of acyl dihydroxyacetone phosphate (DHAP) and the generation of the eponymous ether bond is carried out by peroxisomal enzymes, while the generated alkyl-DHAP is then conversed into alkyl-glyceraldehyde 3-phosphate either in peroxisomes or at the ER. The final steps of ether phospholipid synthesis are performed exclusively at the ER (Heymans et al., 1983; Brites et al., 2004; Gorgas et al., 2006; Wanders & Waterham, 2006a).

Glyoxylate detoxification

Peroxisomes detoxify glyoxylate by the action of the enzyme alanine glyoxylate:aminotransferase (AGT) which catalyzes the transamination of glyoxylate to glycine with alanine. Unless it is detoxified, glyoxylate will be reduced to glycolate or oxidized to oxalate; in contrast to the water soluble glycolate, oxalate precipitates as calcium oxalate (Danpure, 2006).

1.1.3 Peroxisomes and reactive oxygen species

Although mitochondria are usually considered to be the major producer of ROS within the cell, peroxisomes contribute considerably to cellular ROS homeostasis due to their oxidative metabolism. In fact, they consume 20 % of the total amount of oxygen in rat liver while they produce 35 % of the cell's H_2O_2 (Boveris et al., 1972). Superoxide radicals are also generated within peroxisomes by the action of xanthine oxidase acting in purine catabolism in rat liver peroxisomes (Angermuller et al., 1987; Engerson et al., 1987). Additionally, reactive nitrogen species (RNS) are produced within peroxisomes by the inducible form of nitric oxide

synthase (iNOS) that catalyzes the oxidation of L-arginine to nitric oxide (Stolz et al., 2002) (Table 1.1). In order to handle the massive generation of ROS, peroxisomes harbour not only catalase, their key enzyme, but a large set of other antioxidant enzymes, such as copper/zinc and manganese superoxide dismutase (SOD), glutathione peroxidase, peroxiredoxins and epoxide hydrolase (Dhaunsi et al., 1992; Singh et al., 1994; Singh, 1996; Immenschuh & Baumgart-Vogt, 2005; Bonekamp et al., 2009; Antonenkov et al., 2010; Bonekamp et al., 2011a; Fransen et al., 2011) (Table 1.1)

Type of ROS/RNS	Generating reaction	Produced in PO by	Scavenged in PO by
Hydrogen peroxide (H_2O_2)	$O_2^{\bullet-} + H^+ \rightarrow HO_2^{\bullet}$, $2\ HO_2^{\bullet-} \rightarrow H_2O_2 + O_2$	Acyl-CoA oxidase (several) Urate Oxidase Xanthine Oxidase D-Amino Acid Oxidase D-aspartate Oxidase Pipecolic acid oxidase Sarcosine Oxidase L-alpha-hydroxy acid oxidase Polyamine oxidase	Catalase Glutathione Peroxidase Peroxiredoxin 1 PMP20
Superoxide anion ($O_2^{\bullet-}$)	$O_2 + e^- \rightarrow O_2^{\bullet-}$	Xanthine Oxidase	MnSOD CuZnSOD
Nitric oxide ($^{\bullet}NO$)	L-Arg + NADPH + H^+ + O_2 → NOHLA + $NADP^+$ + H_2O, NOHLA + ½ NADPH + ½ H^+ + O_2 → L-citrulline + ½ $NADP^+$ + $^{\bullet}NO$ + H_2O	Nitric oxide synthase	

Table 1.1: Overview of ROS/RNS generated in mammalian peroxisomes (PO).
NOHLA, N^{ω}-hydroxy-L-arginine, SOD, superoxide dismutase (adapted from Bonekamp et al., 2009)

Interesting findings regarding a dynamic, morphological response of peroxisomes to oxidative stress have been made in the plant system. Using live-cell imaging, plant peroxisomes were shown to respond to increasing oxidative stress in a two-fold manner: upon exposure to hydrogen peroxide or hydroxyl radicals, they were shown to develop small membrane protrusions – so-called peroxules - out of the previously spherical peroxisome in a time span of 10-120 seconds. Longer exposure or higher dosage of stressors resulted in a decline in peroxisome movement and their increased elongation and division (Sinclair et al., 2009). Similarly, mammalian peroxisomes respond to UV irradiation and H_2O_2 exposure with an elongation of the compartment (Schrader et al., 1999), hence peroxisomal elongation and/or proliferation might serve as a first line of defence counteracting oxidative stress. Changes in peroxisomal motility and a slight increase in number were also observed in plant cells after cadmium exposure (Rodriguez-Serrano et al., 2009). Notably, only the generation of intra-peroxisomal oxidative stress triggered a peroxisomal response and the resulting motility change was assumed to improve inter-organellar cross-talk, uptake of metabolites or to scavenge ROS in places of need. Due to the highly oxidative environment, peroxisomes require several safeguarding mechanisms ensuring proper organelle function: catalase itself was shown to be closely associated with more oxidation-prone proteins, but also increased its

activity in response to acute stress up to a certain threshold (Anand et al., 2009). Moreover, a peroxisomal Lon protease was identified in rat and *H. polymorpha* whose deletion led to an increase in protein oxidation, possibly removing damaged proteins to ensure functionality and thus contributing to intra-peroxisomal quality control (Kikuchi et al., 2004; Aksam et al., 2007). Apart from that, severely damaged organelles are removed by autophagy. Peroxisomes have further been linked to oxidative stress-related conditions such as neurodegeneration, carcinogenesis and aging (Cimini et al., 2009; Kou et al., 2011; Titorenko & Terlecky, 2011). In the case of aging, the fidelity of the peroxisomal matrix import system diminishes with age due to initial ROS-dependent modifications, resulting in a senescent cellular phenotype (Legakis et al., 2002; Terlecky et al., 2006). Moreover, the age-dependent "loss" of catalase leads to an accumulation of H_2O_2 and other ROS in peroxisomes which may facilitate H_2O_2 diffusion to the cytoplasm, where it may modulate signalling pathways and/or promote oxidative damage (Legakis et al., 2002). Aging also impairs the activities of other peroxisomal proteins, as was uncovered by mass-spectrometric analyses of kidney and liver peroxisomes (Mi et al., 2007).

1.1.4 Peroxisomal disorders

The pivotal role of peroxisomes in human health and development can be deduced from the severe phenotype of peroxisomal disorders, a group of inherited diseases in which either peroxisome biogenesis or single enzyme functions are disturbed. Based on this distinction, they are commonly subdivided into the peroxisome biogenesis disorders (PBDs) or peroxisomal (single) enzyme deficiencies (PEDs) (Steinberg et al., 2006; Wanders & Waterham, 2006a).

The PBDs are nowadays grouped into the Zellweger spectrum disorders (ZSD) and the rhizomelic chondrodysplasia punctata 1 (RCPD 1). ZSD is a collective term incorporating the Zellweger spectrum (ZS), neonatal adrenoleukodystrophy (NALD) and infantile Refsum disease (IRD), as patients suffer from the same clinical presentation of liver disease, neurodevelopmental delay, retinopathy and perceptive deafness within the first month of life, albeit to different degrees (Brosius & Gartner, 2002; Faust et al., 2005; Wanders & Waterham, 2005; Steinberg et al., 2006; Fidaleo, 2010). The ZS, initially referred to as cerebro-hepato-renal syndrome, shows the severest phenotype with an incidence of 1:50.000 births. Its initial characterization demonstrated the essential role of peroxisomes in human health (Goldfischer et al., 1973). ZSDs arise due to mutations in different peroxins, the peroxisomal membrane proteins required for peroxisome maintenance (1.1.5) (Table 1.2).

Mutations in at least 12 different peroxins were linked to the pathology of ZSD (Sacksteder & Gould, 2000; Steinberg et al., 2006). As Zellweger patients suffer from a complete absence of peroxisomes, toxic peroxisomal substrates (such as VLCFA, THCA and DHCA) accumulate while there is a shortage of essential peroxisomal products (such as plasmalogens) in every tissue. The consequences are especially detrimental in the brain, spinal cord and peripheral nerves in line with the central role of peroxisomes in the generation of plasmalogens which are essential for the formation of the myelin sheath (Faust et al., 2005; Hulshagen et al., 2008; Baes & Aubourg, 2009). As the accompanying developmental defects already start *in utero*, only supportive postnatal treatments are available based on dietary supplements and restrictions that merely counteract milder forms. The fact that ZSD presents with a low number of cases and a high variability restrains the development of new treatments. The other form of PBDs, RCPD1, presents differently from ZSD and is linked to mutations in PEX7, the gene encoding the import receptor for a subset of peroxisomal matrix proteins (Gould & Valle, 2000) (1.1.5.1).

The PEDs are grouped according to the biochemical pathway affected, e.g. ether lipid biosynthesis, peroxisomal β-oxidation, peroxisomal α-oxidation, glyoxylate detoxification and ROS metabolism (Wanders & Waterham, 2006a). The most common PED is the X-linked adrenoleukodystrophy (X-ALD) with an incidence of 1:15.000 males in France. Patients present with an accumulation of VLCFAs in the plasma, fibroblasts and other cell-types, resulting from mutations in the ABCD1 gene which encodes the adrenoleukodystrophy protein (ALDP). ALDP is an ABC transporter in the peroxisomal membrane, closely related to other metabolite transporters such as PMP70, and mediates the import of acyl-CoA esters of VLCFA into peroxisomes. Interestingly, its role was confirmed only recently (van Roermund et al., 2008; Wanders et al., 2010). In X-ALD, the accumulated VLCFAs were suggested to increase oxidative stress and thus lead to oxidative modification in nervous tissues (Schonfeld & Wojtczak, 2008). Furthermore, the VLCFA C26:0 may promote oxidative stress via mild inhibition of the mitochondrial electron transfer chain (ETC), which in combination with compromised cellular GSH levels, results in oxidative lesions (Fourcade et al., 2008). Other PEDs affecting peroxisomal β-oxidation were identified such as e.g. the AOX deficiency or D-bifunctional protein (DBP) deficiency. Interestingly, patient fibroblasts of AOX or DBP-deficient patients revealed peroxisomes that were enlarged in size and reduced in number (Chang et al., 1999). Except for X-ALD, all peroxisomal disorders are inherited in an autosomal-recessive manner. Similar to PBDs, PED treatment remains limited to supportive therapy based on the restriction of peroxisomal substrates or supplementation of

products. However, treatment options are available for patients suffering from primary oxaluria type I, a disease that results from AGT impairment. Interestingly, AGT mutations have been identified that introduce a mitochondrial targeting signal into the enzyme, leading to its mistargeting and subsequent loss of action (Danpure, 2006). As a result, oxalate deposits are formed in the kidneys (impairing renal function), but ultimately the failure in oxalate clearance results in its deposition in all tissues. As a treatment option, high oxalate concentrations can be diminished by inhibiting oxalate synthesis and increasing oxalate solubility (Danpure, 2005).

In addition to the classical peroxisomal disorders, other pathologies are now closer linked to peroxisomal function than previously assumed, including Alzheimer's disease (AD), diabetes and cancer. Interestingly, peroxisome proliferation has neuroprotective effect counteracting β-amyloid (Abeta) toxicity (Santos et al., 2005). Thus, the modulation of peroxisomal and peroxisome-related proteins after acute and chronic insults with the toxic Abeta peptide was investigated to determine the neuroprotective role of peroxisomes upon Abeta-related oxidative injury (Cimini et al., 2009). Additionally, peroxisomal generation of H_2O_2 is involved in fatty acid-induced toxicity in insulin-producing pancreatic β-cells, thus contributing to the complex pathology of type 2 diabetes (Gehrmann et al., 2010; Elsner et al., 2011). Human carcinoma cells often display a significant reduction or even complete absence of peroxisomes (Lauer et al., 1999; Frederiks et al., 2010). These conditions might compromise cellular antioxidant capacity and facilitate further oxidative DNA damage, thus contributing to a more malignant behaviour. Furthermore, disorders affecting proteins of the peroxisomal growth and division machinery (the dynamin-like protein 1), and thus peroxisome dynamics, have been identified and are addressed in detail later on (Waterham et al., 2007) (1.2.2.2).

1.1.5 Peroxisomal protein import

As peroxisomes are devoid of DNA, and thus all peroxisomal proteins are encoded in the nucleus, matrix and membrane proteins are synthesized on free ribosomes in the cytosol and imported post-translationally into pre-existing organelles (Lazarow & Fujiki, 1985). The processes of peroxisomal matrix and membrane protein import are mediated by independent sets of evolutionary conserved peroxins (Distel et al., 1996). Up until now, around 34 peroxins have been identified in lower eukaryotes (based on studies using *S. cerevisiae*, *P. pastoris*, *Y. lipolytica* and *N. crassa*), while around 18 mammalian and 23 plant peroxins have

been characterized (Kiel et al., 2006; Platta & Erdmann, 2007). An overview is given in Table 1.2.

Peroxin	Organism				Localization	Domains	Proposed function
Pex1p	m	p	f	y	membrane (cytosol)	AAA ATPase	Matrix protein import, export of Pex5p
Pex2p	m	p	f	y	integral PMP	RING finger	Matrix protein import, translocation
Pex3p	m	p	f	y	integral PMP		Membrane biogenesis, PMP import
Pex4p		p	f	y	peripheral PMP	E2 enzyme	Matrix protein import, Pex5p ubiquitination
Pex5p	m	p	f	y	Cytosol/ membrane	TPRs	Matrix protein import, PTS1 (and PTS2) receptor
Pex6p	m	p	f	y	membrane (cytosol)	AAA ATPase	Matrix protein import, export of Pex5p
Pex7p	m	p	f	y	Cytosol/ membrane	WD40 repeats	Matrix protein import, PTS2 receptor
Pex8p			f	y	peripheral PMP (matrix)		Matrix protein import
Pex9p				*Yl*	(ORF wrongly identified, antisense sequence of Pex26p)		
Pex10p	m	p	f	y	integral PMP	RING finger	Matrix protein import, translocation
Pex11p	m	p	f	y	(integral) PMP		Proliferation and division
Pex12p	m	p	f	y	integral PMP	RING finger	Matrix protein import translocation
Pex13p	m	p	f	y	integral PMP	SH3	Matrix protein import, docking
Pex14p	m	p	f	y	(integral) PMP	Coiled-coil	Matrix protein import, docking
Pex15p				*Sc*	integral PMP		Matrix protein import, Pex1p/Pex6p anchor
Pex16p	m	p	f	*Yl*	(integral) PMP		Membrane biogenesis
Pex17p				y	peripheral PMP	Coiled-coil	Matrix protein import, docking
Pex18p				*Sc*	Cytosol/ membrane		Matrix protein import, PTS2 import
Pex19p	m	p	f	y	Cytosol/ membrane	Farnesylation motif	Membrane biogenesis, PMP import
Pex20p			f	y	Cytosol/ membrane		Matrix protein import, PTS2 import
Pex21p				*Sc*	Cytosol/ membrane		Matrix protein import, PTS2 import
Pex22p		p	f	y	integral PMP		Matrix protein import, Pex4p anchor
Pex23p			f	y	integral PMP	Dysferlin	Proliferation
Pex24p			f	y	integral PMP		Proliferation

Pex25p			y	peripheral PMP		Proliferation
Pex26p	m	f		integral PMP		Matrix protein import, Pex1p/Pex6p anchor
Pex27p			*Sc*	peripheral PMP		Proliferation
Pex28p			*Sc*	integral PMP		Proliferation (Pex24p ortholog)
Pex29p			y	integral PMP		Proliferation
Pex30p			*Sc*	integral PMP	Dysferlin	Proliferation (Pex23p ortholog)
Pex31p			*Sc*	integral PMP	Dysferlin	Proliferation
Pex32p			y	integral PMP	Dysferlin	Proliferation
Pex33p		*Nc*		membrane	Coiled-coil	Matrix protein import, Biogenesis
Pex34p			y	integral PMP		Proliferation

Table 1.2: Overview of the peroxins (Pex).
Organisms: m, mammals; p, plants; f, filamentous fungi; y, yeasts; *Nc*, *N. crassa*; *Sc*, *S. cerevisiae*; *Yl*, *Y. lipolytica*. RING, really interesting new gene; SH3, Src-Homology 3.

1.1.5.1 Import of peroxisomal matrix proteins

Peroxisomal matrix protein import is accomplished using four consecutive steps: the binding of the cargo protein to its import receptor, the docking of the receptor-cargo complex to the peroxisomal membrane, membrane translocation of the cargo and receptor recycling (for review, see Ma & Subramani, 2009; Lanyon-Hogg et al., 2010; Rucktaschel et al., 2011) (Fig. 1.3).

Depending on their inherent peroxisomal targeting signal (PTS), peroxisomal matrix proteins utilize either the PTS1-Pex5p or the PTS2-Pex7p-mediated import pathway. The majority of peroxisomal proteins contain a PTS1 at their extreme C-terminus. It was initially identified as the tri-peptide sequence SKL in firefly luciferase (Gould et al., 1987), but has been expanded to the general consensus sequence [S/A/C]-[K/R/H]-[L/M] (Gould et al., 1989; Aitchison et al., 1991; Elgersma et al., 1996; Purdue & Lazarow, 1996; Kragler et al., 1998; Lametschwandtner et al., 1998). Some proteins (e.g. mammalian catalase) require additional interactions or upstream sequences to enhance Pex5p-binding specificity (Maynard & Berg, 2007; Ma & Subramani, 2009). Upon completion of protein synthesis, the PTS1 is recognized by its specific import receptor, the cytosolic Pex5p (Brocard et al., 1994; Terlecky et al., 1995). In mammals, a short (Pex5S) and a long mRNA isoform (Pex5L) are expressed; interestingly, the long isoform functions as a Pex7p co-receptor (Otera et al., 2000). The C-terminal part of Pex5p mediates cargo binding via specific interactions between its TPR

repeats and the PTS1 peptide. There is an ongoing discussion about the stochiometry of Pex5p. It was shown to act as a monomer in solution (Costa-Rodrigues et al., 2004; Shiozawa et al., 2009), but also dimeric or tetrameric structures have been reported (Madrid et al., 2004). The second peroxisomal targeting signal, the N-terminal PTS2, was first identified in rat liver thiolase and is a conserved nonapeptide with the consensus sequence [R/K]-[L/V/I]-X5-[H/Q]-[L/A] (Swinkels et al., 1991; Rachubinski & Subramani, 1995). Notably, its presence varies greatly across species. While the PTS2-Pex7p-mediated import pathway is completely absent in the nematode *C. elegans* (Motley et al., 2000), it is only maintained in the yeast *S. cerevisiae* for the import of 3-ketoacyl thiolase and Gpd1 (Grunau et al., 2009; Jung et al., 2010), whereas about 60 proteins (a third of all matrix proteins) contain a PTS2 in *A. thaliana* (Reumann et al., 2009). Unlike the PTS1, the PTS2 is cleaved from the nascent protein upon import (Helm et al., 2007; Kurochkin et al., 2007). PTS2 proteins are recognized by their import receptor Pex7p, a member of the WD40 class of proteins. Although Pex7p itself appears to act as a monomer, it requires the assistance of auxiliary co-receptors (Rehling et al., 1996; Mukai & Fujiki, 2006; Grunau et al., 2009; Lanyon-Hogg et al., 2010). Pex5pL functions as a co-receptor for Pex7p in mammals and plants (Otera et al., 2000), while Pex18p/Pex21p (*S. cerevisiae*) or Pex20p (*H. polymorpha*, *N. crassa*, *P. pastoris* and *Y. lipolytica*) are utilized in different yeast species (Einwachter et al., 2001; Otzen et al., 2005; Leon et al., 2006b). These co-factors share structural similarities (Dodt et al., 2001; Schliebs & Kunau, 2006). Other proteins lacking a PTS such as *S. cerevisiae* acyl-CoA oxidase or mammalian Cu/ZnSOD enter peroxisomes using other pathways, for example by employing a piggy back mechanism via association with PTS1 proteins (McNew & Goodman, 1994; Yang et al., 2001; van der Klei & Veenhuis, 2006; Islinger et al., 2009).

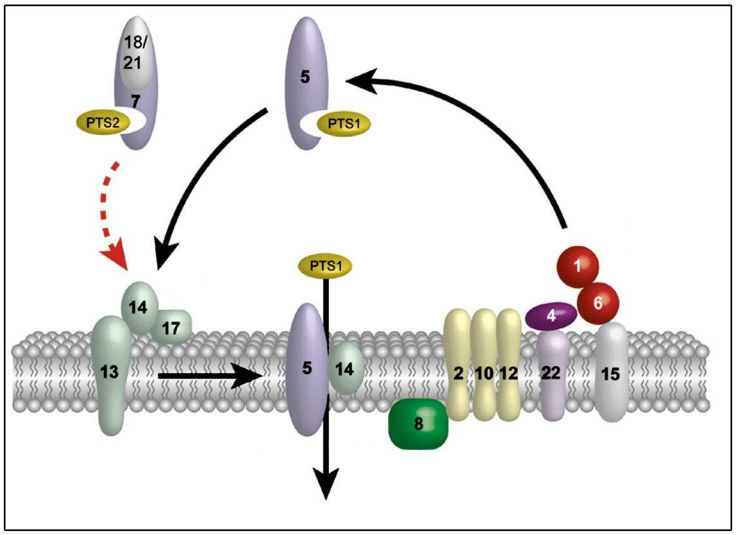

Fig. 1.3: Peroxisomal matrix protein import.
The receptor cycle in the yeast *S. cerevisiae* (see text for details) (adapted from Rucktaschel et al., 2011). Note that Pex17p and Pex8p do not exist in mammals. Moreover, Pex18p/Pex21p action is replaced by Pex5pL and the function of Pex22p/Pex4p is fulfilled by UbcH5a/b/c. In mammals, Pex26p anchors Pex6p at the membrane instead of Pex15p.

After cargo binding, the cargo-receptor complex docks at the peroxisomal membrane upon interaction with the resident docking complex, composed of the proteins Pex13p, Pex14p and additionally Pex17p in yeast. Importantly, neither Pex13p nor Pex14p have the capability to bind cargo directly, thus Pex5p needs to stay complexed with its cargo during the import procedure. Membrane translocation of peroxisomal matrix proteins is thought to occuran extended shuttle mechanism that allows the receptor-cargo complex to pass completely the membrane (Kunau, 2001). In line with this, Pex5p, Pex7p and Pex20p are cycling receptors that always remain protease-protected to a certain degree (Gouveia et al., 2003; Leon et al., 2006a; Leon et al., 2006b). Notably, peroxisomes possess the striking ability to import fully folded and even oligomeric proteins (Glover et al., 1994; McNew & Goodman, 1994). Furthermore, even gold particles coated with a PTS1 of 9 nm size are imported (Walton et al., 1995), which is achieved without disruption of membrane compartmentalisation or any indication of the existence of static membrane pores (analogous to nuclear pores). To accommodate these features, a transient membrane pore composed of Pex5p oligomers has been proposed to form at the peroxisomal membrane (Erdmann & Schliebs, 2005) for whose existence evidence has been provided recently (Meinecke et al., 2010). Nevertheless, another elegant model was proposed which suggests that peroxisomal cargo can reach the peroxisomal membrane enfolded by Pex5p due to its natively unfolded state and might thus be translocated due to membrane embedding by Pex5p monomers (Grou et al., 2009a). The membrane translocation step itself is independent of ATP (Gouveia et al., 2003; Miyata & Fujiki, 2005). Cargo release into the peroxisomal lumen was suggested to be mediated by Pex8p, a protein which contains both PTS and therefore competes with Pex5p and Pex7p; however it has only been identified in yeast and fungi so far (Rehling et al., 2000). Cargo receptor recycling is an ATP-dependent process that requires the action of two protein subcomplexes and includes mono-ubiquitination of Pex5p. The so-called receptor-release complex consists of Pex1p and Pex6p, two proteins of the AAA family of ATPases, and additionally Pex4p and Pex22p in yeast (Ma & Subramani, 2009; Rucktaschel et al., 2011). Pex1p interacts with Pex6p which is anchored at the peroxisomal membrane by Pex15p (*S. cerevisiae*) or Pex26p (mammals) (Matsumoto et al., 2003). The RING-finger proteins (Pex2p, Pex10p and Pex12p) are E3 protein-ubiquitin ligases, while Pex22p serves as a docking site for the E2 ubiquitin-conjugating enzyme Pex4p (Wiebel & Kunau, 1992; Platta et al., 2009). Mammals lack the Pex4p/Pex22p complex and instead utilize the cytosolic UbcH5a/b/c family (Grou et al., 2008). To initiate receptor release, a conserved cysteine residue in the N-terminus of Pex5p is mono-ubiquitinated by Pex12p (Williams et al., 2007;

Grou et al., 2009b) upon which it is extracted from the peroxisomal membrane by the action of Pex1p and Pex6p (Miyata & Fujiki, 2005; Platta et al., 2005). Subsequent de-ubiquitination of Pex5p can either occur by de-ubiquitinating enzymes or non-enzymatic processes (Grou et al., 2009b). If there is a delay in receptor release, Pex5p is poly-ubiquitinated, resulting in its degradation by the 26S proteasome (Kiel et al., 2005a; Platta et al., 2007) which provides a quality control mechanism for peroxisomal protein import. Poly-ubiquitination of Pex5p is thought to occur by the action of Pex2p and Pex10p (Williams et al., 2008; Platta et al., 2009). Ubiquitination of the PTS2 co-receptors Pex18p and Pex20p was also observed (Brown & Baker, 2008).

1.1.5.2 Insertion of peroxisomal membrane proteins

If peroxisomal matrix protein import is impaired, cells still contain peroxisomal remnant structures, the so-called ghosts, which retain a full set of peroxisomal membrane proteins (PMPs) (Santos et al., 1988; Brown & Baker, 2003; Schrader & Fahimi, 2008). Thus, peroxisomal membrane protein insertion is mediated in a manner completely distinct from matrix protein import (Fig. 1.4). The complete absence of peroxisomal membranes is only observed upon deletion or impairment of the peroxins Pex3p, Pex16p and Pex19p (Hohfeld et al., 1991; Baerends et al., 1996; Eitzen et al., 1997; Honsho et al., 1998; Matsuzono et al., 1999), identifying those as key factors of peroxisome membrane biogenesis. In contrast to the well-defined peroxisomal matrix targeting signals, no clear consensus sequence was identified for PMPs. However, specific membrane targeting sequences (mPTS) were determined in a variety of proteins displaying a different topology (Van Ael & Fransen, 2006). Depending on the protein, the mPTS varies greatly in length, but is usually comprised of a transmembrane segment and a cluster of basic amino acids (Baerends et al., 2000; Honsho & Fujiki, 2001; Jones et al., 2001; Rottensteiner et al., 2004). Peripheral peroxisomal membrane proteins harbour an mPTS and a protein interaction domain (Girzalsky et al., 2006). Most PMPs are targeted to the peroxisomal membrane in a manner dependent on Pex19p interaction (Class I PMPs) (Sacksteder et al., 2000; Snyder et al., 2000; Fransen et al., 2001; Halbach et al., 2005; Hadden et al., 2006; Halbach et al., 2006). Pex19p is farnesylated and shuttles between the cytosol and the peroxisomal membrane (Kammerer et al., 1997; Gotte et al., 1998; Rucktaschel et al., 2009). The multifunctional Pex19p simultaneously serves as an import receptor as well as a chaperone for newly-synthesized PMPs and has further been characterized as both an insertion factor and assembly/disassembly factor at the peroxisomal membrane (Fransen et al., 2001; Fransen et al., 2004; Jones et al., 2004; Shibata et al., 2004). While the C-terminal part of Pex19p facilitates PMP binding (Mayerhofer et al., 2002;

Shibata et al., 2004; Fransen et al., 2005; Matsuzono et al., 2006), the N-terminal part mediates peroxisomal membrane targeting through interaction with Pex3p.

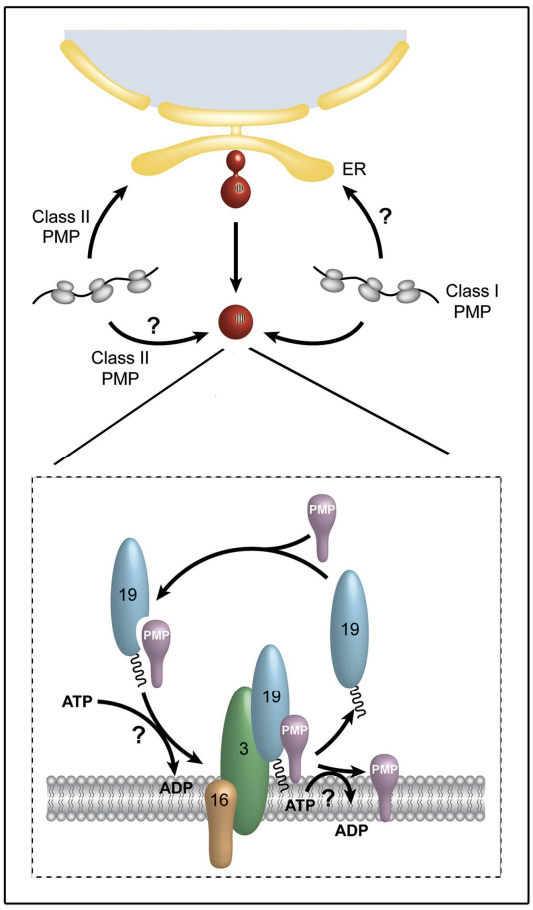

Fig. 1.4: Peroxisomal membrane protein insertion.
(upper panel) Topogenesis of peroxisomal membrane proteins. Two routes are proposed for the targeting of peroxisomal membrane proteins (PMPs). Class I proteins are directly imported into existing peroxisomes. Class II proteins are first targeted to ER where they concentrate in pre-peroxisomal vesicles which then are targeted to existing peroxisomes or function as an origin for *de novo* formation of peroxisomes.
(lower panel) Pex19p-dependent import of PMPs. Class I peroxisomal membrane proteins (PMPs) harbour a peroxisomal membrane protein targeting signal (mPTS) which is recognized in the cytosol by the import receptor and/or PMP-specific chaperone Pex19p. Cargo-loaded Pex19p docks to the peroxisomal membrane via association with its docking factor Pex3p. Then the PMP is inserted into the membrane in an unknown manner but presumably with assistance of Pex19p, Pex3p and, in some organisms, Pex16p (adapted from Rucktaschel et al., 2011).

Upon binding of Pex19p to newly-synthesized PMPs, the cargo-receptor complex is recruited to the peroxisomal membrane via the docking factor Pex3p, an integral membrane protein (Fang et al., 2004; Fransen et al., 2005; Matsuzono et al., 2006). It binds the cargo-receptor complex with a higher affinity than Pex19p alone which thus facilitates docking of the complex to the peroxisomal membrane (Soukupova et al., 1999; Ghaedi et al., 2000a; Ghaedi et al., 2000b; Hunt & Trelease, 2004; Haan et al., 2006; Pinto et al., 2006). In addition to that, Pex3p was implied to be involved in peroxisome inheritance in *S. cerevisiae* (Chang et al., 2009; Munck et al., 2009). Subsequently, the PMP is inserted into the peroxisomal membrane by an unknown mechanism and Pex19p is recycled back to the cytosol (Matsuzono & Fujiki, 2006).

The exact function of the membrane biogenesis factor Pex16p remains elusive. It is only present in higher eukaryotes and the yeast *Y. lipolytica*, however, protein topology of Pex16p between species differs substantially: it is defined as an integral membrane protein in mammals, but supposedly resides within the peroxisomal lumen in *Y. lipolytica* (Eitzen et al.,

1997; Honsho et al., 1998; Honsho et al., 2002) where it was suggested to act as an intra-peroxisomal regulator of organelle fission (Eitzen et al., 1997). Interestingly, mammalian Pex16p was shown to be co-translationally inserted into the ER prior to its trafficking to peroxisomes (Kim et al., 2006). In line with this, a small number of PMPs, such as Pex3p and Pex16p, was suggested to be inserted into peroxisomes in a Pex19p-independent manner (Class II PMPs) due to their lack of a Pex19p-binding domain (Fujiki et al., 2006). They are initially targeted to the ER, but, in order to release e.g. Pex3p from the ER, Pex19p is required (Hoepfner et al., 2005; Kragt et al., 2005; Tam et al., 2005). However, full-length Pex3p was also shown to directly interact with Pex19p and then be inserted into the peroxisomal membrane in a Pex16p-dependent fashion (Matsuzaki & Fujiki, 2008). Therefore, peroxisome membrane biogenesis can be initiated by the formation of a pre-peroxisomal membrane that carries either Pex3p or Pex16p, both of which are capable to develop into mature peroxisomes. Depending on the peroxin present (Pex3p or Pex16p), the respective missing PMP is targeted and inserted in a Pex19p-dependent manner to generate import competent peroxisomes.

1.2 PEROXISOME DYNAMICS

1.2.1 Models of peroxisome biogenesis: "growth and division" vs. "*de novo* synthesis"

Peroxisomes were once implied to originate from virtually any organelle, including the Golgi complex, lysosomes and the ER (Novikoff & Essner, 1960; Rouiller & Jezequel, 1963; Novikoff & Shin, 1964). Subsequently, peroxisomal proteins were shown to be synthesized on free ribosomes in the cytosol (Goldman & Blobel, 1978) and then imported post-translationally into peroxisomes, therefore, the classical "growth and division" model was proposed (Lazarow & Fujiki, 1985). According to the latter, peroxisomes grow by import of protein and lipid components into pre-existing peroxisomes and their subsequent division into smaller organelles, rendering them autonomous like mitochondria. The protein machinery orchestrating peroxisomal growth and division will be discussed in detail in the next section (1.2.2).

In the last decade, strong evidence was provided for an alternative mechanism of peroxisomal *de novo* formation from the ER (Mullen et al., 2001; Titorenko & Rachubinski, 2001b; van der Klei & Veenhuis, 2002; Geuze et al., 2003; Mullen & Trelease, 2006; Tabak et al., 2006;

Titorenko & Mullen, 2006; Hettema & Motley, 2009; Saraya et al., 2010; Nuttall et al., 2011). A close relationship between the ER and peroxisomes has long been indicated; e.g. ultrastructural studies demonstrated close contacts between peroxisomes and the ER (Novikoff & Novikoff, 1972), including direct, luminal connections between the organelles in mouse dendritic cells (Geuze et al., 2003). Furthermore, some peroxisomal proteins such as Pex16p are known to travel to the ER prior to peroxisomes in *Y. lipolytica,* mammals and plants (Titorenko & Rachubinski, 1998; Karnik & Trelease, 2005; Kim et al., 2006). The exciting observation that yeast or mammalian cells devoid of peroxisomes due to deletions of Pex3p, Pex16p or Pex19p (1.1.5.2) are able to form peroxisomes *de novo* from the ER upon re-introduction of the respective missing gene finally challenged the prevailing model of an autonomous peroxisomal growth and division {Faber, 2002, Haan, 2006`, Hoepfner`, 2005`, Kim`, 2006`, Kragt`, 2005`, Matzuzuno`, 1999`, Muntau`, 2000`, South`, 1999`, Titorenko`, 2001}. In different yeast species, *de novo* formation of peroxisomes was initiated by re-introduction of Pex3p which localized to specific spots at the ER membrane where it budded off in a Pex19p-dependent manner to generate a pre-peroxisomal structure (Hoepfner et al., 2005; Tam et al., 2005; Haan et al., 2006; Titorenko & Mullen, 2006). After subsequent assembly of the membrane and matrix protein import machinery, pre-peroxisomes acquire import-competence. In regard to the composition of pre-peroxisomal vesicles, at least *de novo* formation itself is independent of COPI- or COPII-dependent transport (Matsuzono et al., 1999; South et al., 2000; Voorn-Brouwer et al., 2001; Kim et al., 2006), although the COPII vesicle component Sec16B was recently shown to be involved in the ER export of Pex16p and Pex3p (Yonekawa et al., 2011). Peroxisome biogenesis from the ER is further suggested to be facilitated by the ER components Sec20, Sec39 and Dsl1 as well as Pex19p (and yet unidentified components) in *S. cerevisiae* (Perry & Rachubinski, 2007; Perry et al., 2009; Agrawal et al., 2011; Lam et al., 2011) and Emp24, Pex25p as well as Rho1 in *H. polymorpha* (Saraya et al., 2011). The contribution of the ER to PMP trafficking or peroxisomal *de novo* formation under wild-type conditions remains controversial. Elegant pulse-chase experiments in *S. cerevisiae* indicated that peroxisomes divide by growth and division under wild-type conditions, but that loss of peroxisomes can then be compensated by a slower, *de novo* pathway (Motley & Hettema, 2007). However, others suggest a major contribution of the *de novo* pathway in yeast and mammalian wild-type cells (Kim et al., 2006; Nagotu et al., 2010; van der Zand et al., 2010). Despite the ongoing debate on the extent of *de novo* formation to peroxisome biogenesis, it is clear that the ER provides lipids (and proteins) to peroxisomes and is intimately linked to peroxisome homeostasis. Instead of vesicular trafficking, exchange

of components between the two organelles might be facilitated via contact sites or direct luminal connections, as peroxisomes were observed in close apposition with the ER (Geuze et al., 2003 2003, Tabak, 2008). In line with this, a non-vesicular transfer of phospholipids between the ER and peroxisomes was shown to be completely independent of Pex3p or any Sec components (Raychaudhuri & Prinz, 2008).

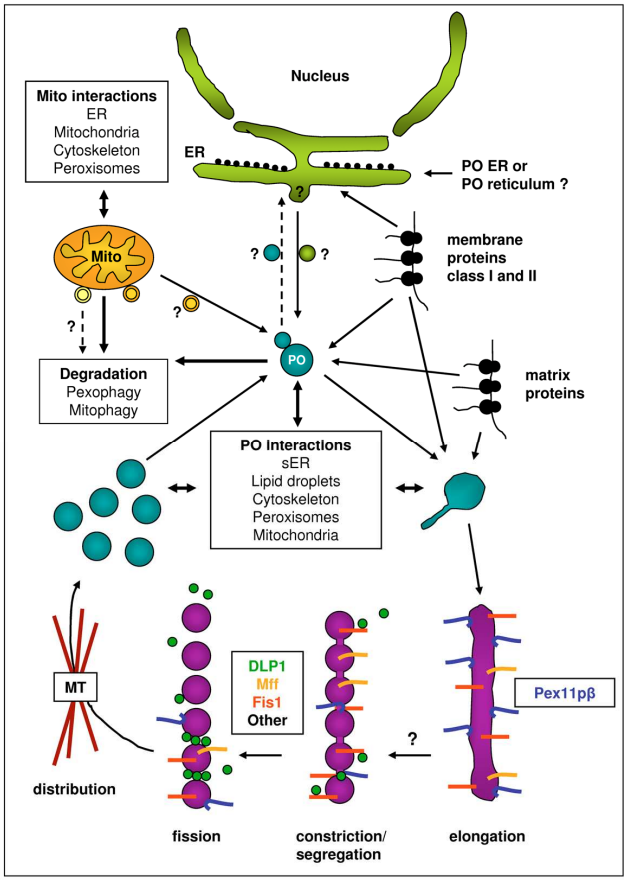

Fig. 1.5: Schematic view of peroxisome dynamics and interactions in mammalian cells.
Most peroxisomal matrix and membrane proteins (Class I PMPs) are synthesized on free polyribosomes in the cytosol and are post-translationally imported into pre-existing organelles. Other membrane proteins (Class II PMPs, early peroxins; e.g., Pex3p) are routed to peroxisomes via the ER. A retrograde peroxisome-to-ER transport might also exist. A novel vesicular mitochondria-to-peroxisome trafficking route has been described. A well defined sequence of morphological changes of peroxisomes, including elongation (growth), constriction, and final fission (division) contributes to peroxisome proliferation in mammalian cells. Pex11βp is involved in the elongation (tubulation) of peroxisomes, whereas DLP1, Mff and Fis1 mediate peroxisomal (and mitochondrial) fission. Proper intracellular distribution of peroxisomes formed by fission requires microtubules (MT) and motor proteins. Excess organelles are degraded by autophagy (pexophagy, mitophagy).
(adapted from Camoes et al., 2009).

1.2.2 The division machinery

Mammalian peroxisomes display a remarkably dynamic morphology. While they may appear as spherical organelles within the cytoplasm, they form tubular structures that acquire a “bead-on-a-string”-like morphology prior to their fragmentation into smaller organelles (Schrader et al., 1996a; Schrader et al., 1998b; Koch et al., 2003; Koch et al., 2004). This sequence of events is indicative of peroxisomal growth and division and occurs in a multi-step fashion by the action of a set of evolutionary conserved proteins throughout the yeast, mammalian and plant systems. Initial elongation of the peroxisomal membrane is mediated by the Pex11 family of proteins, and after subsequent constriction by a yet unidentified mechanism, final fission is carried out by dynamin-like GTPases (such as mammalian DLP1) that are recruited to the peroxisomal membrane by distinct membrane adaptors (Fis1, Mff)

(Fig. 1.5). Additionally, peroxisomes may also interconnect to form tubulo-reticular networks and a variety of morphologically distinct types of peroxisomes have been observed in different organs of mammalian organisms and cell lines (Hicks & Fahimi, 1977; Gorgas, 1987; Yamamoto & Fahimi, 1987; Roels et al., 1991; Fahimi et al., 1993; Schrader et al., 1994; Litwin & Bilinska, 1995; Schrader et al., 1996a; Schrader et al., 2000). In addition to growth and division, more complex structures such as elongated tubules or a peroxisomal reticulum may be related to other peroxisomal processes (e.g in metabolism, membrane signalling or stress protection), but information on the exact correlation between peroxisome dynamics/morphology and function is scarce.

1.2.2.1 The Pex11 family of proteins

The members of the Pex11 family of proteins represent a number of peroxisomal membrane proteins in fungi, plants and mammals that control peroxisome proliferation and regulate peroxisome morphology, size and number (Erdmann & Blobel, 1995; Marshall et al., 1995; Abe & Fujiki, 1998; Abe et al., 1998; Schrader et al., 1998b; Lingard & Trelease, 2006). They are conserved in yeasts, plants and mammals and several proteins and/or isoforms have been identified in each kingdom (Schrader & Fahimi, 2006; Hettema & Motley, 2009; Hu, 2010; Schrader et al., 2011). While Pex11 proteins were identified based on their capacity to modulate peroxisomal membrane elongation and peroxisome abundance, it has to be noted that not all Pex11 isoforms in a given species promote peroxisome membrane elongation or proliferation. In line with this, membrane association and topology may vary across organisms, ranging from a peripheral association in *S. cerevisiae* to multi-membrane spanning proteins in plants and mammals for (overview, see Schrader et al., 2011). The following section will provide an overview of the different Pex11 proteins across species and will give an insight into their mechanism of action.

Initially identified in *C. boidinii* as a inducible membrane protein upon peroxisome proliferation (and termed PMP31/32), the functional significance of Pex11p was only recognized upon deletion of its homologue in the yeast *S. cerevisiae* (*Sc*Pex11p) which led to the formation of one or two giant peroxisomes (Goodman et al., 1986; McCammon et al., 1990; Moreno et al., 1994; Erdmann & Blobel, 1995; Marshall et al., 1995; Sakai et al., 1995; Ma et al., 2006)} Besides Pex11p, additional proteins with weak similarity to the latter that influence peroxisome maintenance have been identified and termed Pex11-related or Pex11-like proteins (Thoms & Erdmann, 2005; Schrader et al., 2011). These include the oleic acid-inducible Pex25p and the non-inducible Pex27p in *S. cerevisiae* as well as GIM5a and GIM5b

in *Trypanosoma brucei* (Maier et al., 2001; Smith et al., 2002; Rottensteiner et al., 2003a; Tam et al., 2003; Voncken et al., 2003; Huber et al., 2011; Saraya et al., 2011). Moreover, *Sc*Pex28p/Pex29p, *Sc*Pex30p, *Sc*Pex31p/Pex32p as well as *Yl*Pex23p/Pex24p were shown to modulate peroxisome number (Brown et al., 2000; Tam & Rachubinski, 2002; Vizeacoumar et al., 2003). Other yeast species such as *H. polymorpha* contain Pex11C that shares a higher similarity with *Sc*Pex11p (Kiel et al., 2006), resembling the situation in mammals. Similarly, filamentous fungi also express three Pex11 isoforms that are involved in peroxisome proliferation and Woronin body differentiation (Kabeya et al., 2005; Kiel et al., 2005b; Kiel et al., 2006; Escano et al., 2009). Plants possess five obvious homologues of Pex11p (Pex11a-e) which display differences in their expression pattern and some functional redundancy (Lingard & Trelease, 2006; Orth et al., 2007; Hu, 2010). In the mammalian system, three Pex11p isoforms were identified that control peroxisome proliferation under both basal and induced conditions: Pex11pα, Pex11pβ and Pex11pγ (Abe & Fujiki, 1998; Abe et al., 1998; Passreiter et al., 1998; Schrader et al., 1998b; Li et al., 2002a; Tanaka et al., 2003; Shimizu et al., 2004). While Pex11pβ is constitutively expressed in all tissues, both Pex11pα and Pex11pγ display tissue-specific expression patterns, but are most prominent in the liver (Passreiter et al., 1998; Schrader et al., 1998b; Li et al., 2002a; Li et al., 2002b; Tanaka et al., 2003). Among the three isoforms, only Pex11pα is induced by peroxisome proliferators activating the nuclear transcription factor PPARα (1.2.4) and is thus regarded as the regulatable mammalian Pex11p isoform (Shimizu et al., 2004). Nonetheless, Pex11pα was shown to be dispensable for PPARα-mediated peroxisome proliferation in Pex11α knock-out mice and only required to mediate peroxisome proliferation after treatment with non-classical PPARα independent proliferators (Li et al., 2002a). Furthermore, the Pex11α knock-out (KO) mouse is viable and shows no obvious effects on peroxisome number or metabolism (Li et al., 2002a), Pex11β KO, however, causes neonatal lethality and defects similar to the ZS phenotype (Li et al., 2002b), confirming its role as the central regulator of peroxisome proliferation in mammals. As expected, peroxisome abundance in Pex11β KO mice is reduced, but peroxisomal protein import and metabolism are only slightly affected. A recent comparative analysis of primary neuronal cultures and brain samples from wild-type mice, Pex11β homozygous and heterozygous knock-outs indicated a higher degree of cell death in heterozygous than in wild-type mice (Ahlemeyer et al., 2012). Moreover, heterozygotes also showed delayed neuronal differentiation, indicating that deletion of a single allele of Pex11β already causes neuronal defects in mice, a factor underappreciated so far. Thus, as dysfunctions in PEX11 do not result in any large scale alterations of peroxisomal metabolism,

patients with a PEX11 defect might have remained undetected so far. All mammalian Pex11 isoforms are tightly associated with the peroxisomal membrane and are capable of forming homo-dimers (Li & Gould, 2003; Kobayashi et al., 2007; Koch et al., 2010). Hetero-dimers were also observed, however, no interaction between Pex11pα and Pex11pβ was detected (Koch et al., 2010). Furthermore, an interaction of Pex11pβ with Fis1, a tail-anchored protein involved in the recruitment of DLP1 (1.2.2.3), has been demonstrated (Kobayashi et al., 2007; Koch et al., 2010) (Fig. 1.6). Interestingly, mammalian Pex11pβ was not only shown to be able to promote peroxisome elongation upon expression, but was also observed to concentrate at constriction sites, indicating a non-uniform distribution of the protein at the peroxisomal membrane (Schrader et al., 1998b). Recently, its role as a key component in an multistep-maturation process of asymmetric peroxisomal growth and division was further characterized (Delille et al., 2010). Employing a dominant-negative Pex11pβ-mYFP (which blocked peroxisome growth and division at an early stage) and subsequent ultrastructural and pulse-chase analysis, Pex11pβ was indicated to initially localize to spherical, pre-existing organelles where initiates the formation of a nose-like protrusion at only one side of the peroxisome. The protrusion extends to form a membrane tubule that acquires a specific set of PMPs, segments and becomes import-competent for peroxisomal matrix proteins prior to its final fission by the action of Fis1 and DLP1 (Fig. 1.6). Importantly, predominantly newly-synthesized matrix proteins are imported into the newly formed constrictions, pointing to an inherent mechanism of peroxisomal quality control linked to growth and division (Delille et al., 2010). Transient expression of various Pex11 family members of different origins led to the formation of similar membrane protrusions in mammalian cells which developed into large stacks of peroxisomal membranes (Koch et al., 2010). This pattern of Pex11p-dependent formation of specific membrane subdomains and its role in inducing a differential distribution of PMPs was also detected in the yeast *H. polymorpha* (Cepinska et al., 2011).

The membrane deforming capacities of the various Pex11 proteins were recently linked to the presence of several N-terminal motifs within Pex11p that are conserved in yeast, fungi and human proteins and display amphipathic properties (Opalinski et al., 2011). Negatively charged liposomes, resembling the phospholipid composition of peroxisomes, were shown to hyper-tubulate upon the addition of a Pex11 peptide containing the most conspicuous amphipathic helix of *P. chrysogenum.* The conservation of the amphipathic properties and its helical structure is essential to mediate tubulation, an intrinsic property apparently conserved throughout species (Opalinski et al., 2011). Thus, Pex11p-induced membrane remodelling is

induced by the insertion of an amphipathic helix into one leaflet of the lipid bilayer which causes membrane asymmetry and bending (Drin & Antonny, 2010) (Fig. 1.6).

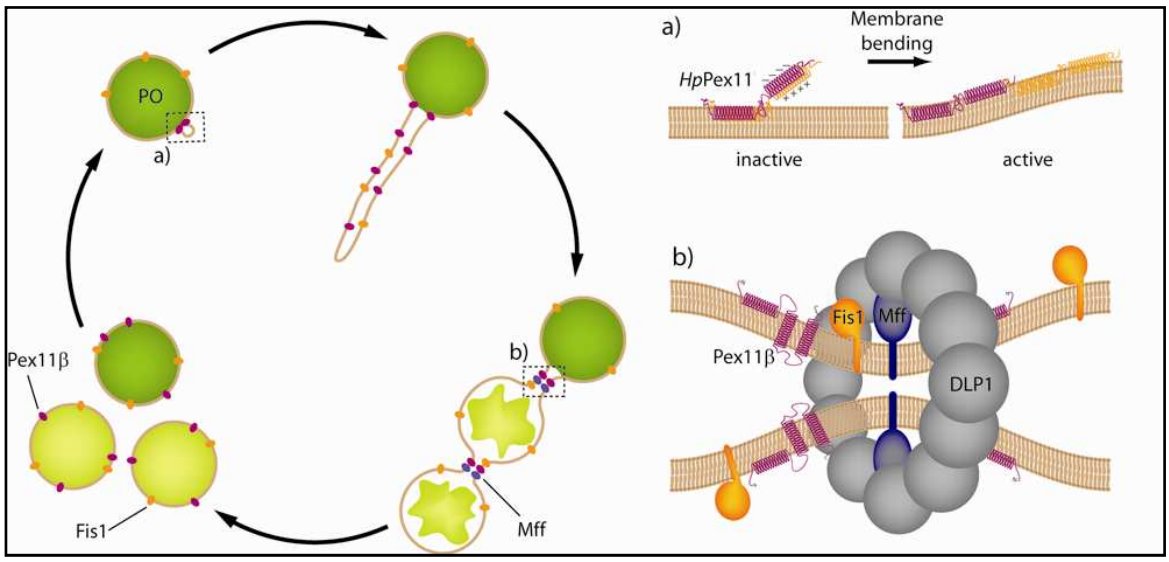

Fig. 1.6: Model of peroxisomal growth and division in mammalian cells.
A well defined sequence of morphological changes of peroxisomes, including elongation (growth), constriction, and final fission (division) contributes to peroxisome proliferation in mammalian cells. Targeting to and/or activation of Pex11pβ at pre-existing peroxisomes initiates membrane remodelling and the formation of a tubular membrane extension on one side of the peroxisome. (a) Peroxisomal membrane remodelling via Pex11p is induced by the insertion of an amphipathic helix into one leaflet of the lipid bilayer which causes membrane asymmetry and bending (based on data obtained with *Hp*Pex11p). Homodimerization may keep Pex11p in an inactive form. Subsequently, the extension grows and acquires a specific set of PMPs (e.g. Pex11pβ, Fis1), before it constricts and starts to import predominantly newly-synthesized matrix proteins. Pex11pβ and the Mff-DLP1 complex concentrate at the sites of con-striction, possibly driven by alterations in membrane curvature. (b) Cytosolic DLP1 is recruited by the membrane receptor Mff. After targeting, DLP1 self-assembles into large ring-like structures that hydrolyze GTP and sever the peroxisomal membrane. Fis1 may fulfil a regulatory function. (from Schrader et al., 2011).

In regard to the regulation of Pex11p itself by post-translational modifications and/or mechanisms, monomeric *Sc*Pex11p was suggested to be inactivated by homo-dimerization, hence dimerization was proposed to regulate membrane remodelling (Marshall et al., 1996). Furthermore, phosphorylation of *Sc*Pex11p at a S165/167 residue was recently shown to be required for Pex11p action (Knoblach & Rachubinski, 2010). However, studies on the post-translational regulation of Pex11 protein activity remain restricted to the yeast system up until now.

1.2.2.2 Peroxisome fission

The final fission step of peroxisomal growth and division is executed by the action of dynamin-like mechano-enzymes, i.e. the proteins dnm1 (and vps1) in yeast species, DLP1/Drp1 in mammals and DRP3A, DRP3B and DRP5B in plants (Hoepfner et al., 2001;

Koch et al., 2003; Li & Gould, 2003; Mano et al., 2004; Kuravi et al., 2006; Fujimoto et al., 2009; Kaur & Hu, 2009; Zhang & Hu, 2010). The dynamin superfamily of large GTPases includes the classical dynamins, dynamin-like proteins, Mx proteins and mitofusins in eukaryotic cells. They facilitate budding and scission events of transport vesicles, cytokinesis as well as the organelle division and fusion (for review, see Praefcke & McMahon, 2004; Heymann & Hinshaw, 2009). Classical dynamins contain five characteristic domains: the highly conserved GTPase domain as well as a middle domain and a GTP effector domain which are involved in the oligomerization and subsequent stimulation of GTPase activity. Additionally, they possess a PH domain facilitating lipid binding and a PRD mediating protein-protein interactions. Dynamin-like proteins lack one or more of the five classical domains and/or have acquired additional ones. Dynamins act as mechano-enzymes that constrict and deform membranes upon GTP hydrolysis (Sweitzer & Hinshaw, 1998; Takei et al., 1998; Takei et al., 1999). Mammalian dynamin-like protein 1 (abbreviated as DLP1 in the following) was localized to a variety of organelles, including the perinuclear region and the ER (Imoto et al., 1998; Yoon et al., 1998), but is primarily involved in the division of both mitochondria and peroxisomes (Bleazard et al., 1999; Labrousse et al., 1999; Sesaki & Jensen, 1999; Yoon et al., 2001; Koch et al., 2003; Li & Gould, 2003; Yoon, 2004). Furthermore, it contributes to the sorting of GPI-anchored, apical transport carriers at the Golgi complex (Bonekamp et al., 2010). Notably, DLP1 was the first protein identified to be a shared component of peroxisomal and mitochondrial fission (Schrader, 2006; Delille et al., 2009)(Fig. 1.7). The concept of sharing fission components between the two organelles extends to other kingdoms, as e.g. dnm1 in *S. cerevisiae* and DRP3B in *A. thaliana* are also implied in both peroxisomal and mitochondrial division (Kuravi et al., 2006; Fujimoto et al., 2009). Interestingly, the yeast *S. cerevisiae* uses two different types of DLPs, vps1 and dnm1, to mediate peroxisome fission. Both can complement each other, however, vps1 is utilized on glucose-grown conditions, while peroxisome proliferation induced upon growth on oleate depends on dnm1 (Motley & Hettema, 2007). At the peroxisomal membrane, mammalian DLP1 aligns in a spot-like pattern around the elongated, constricted tubules (Koch et al., 2003; Li & Gould, 2003; Koch et al., 2004); in this respect, membrane constriction might facilitate DLP1 association. DLP1 silencing by RNAi leads to the generation of elongated, constricted peroxisomes that display a prominent “beads-on-a–string”-like morphology, indicating that constriction of the peroxisomal membrane occurs by an independent, yet unidentified mechanism (Koch et al., 2003). This striking morphological appearance of division-arrested peroxisomes facilitated the discovery of a novel lethal disorder affecting the

fission of both mitochondria and peroxisomes, the DLP1 deficiency (Waterham et al., 2007). The patient died shortly after birth and suffered from microcephaly, abnormal brain development, optic atrophy and hypoplasia, while enzyme measurements indicated a persistent lactic acidemia and mildly elevated VLCFAs, pointing to mitochondrial and/or peroxisomal dysfunctions. Altered mitochondrial and peroxisomal morphology in patient skin fibroblasts suggested a defect in organelle fission and indeed, a point mutation in the middle domain of DLP1 was identified (A395D). A recent biochemical study linked this point mutation (and other mutations in the middle domain of DLP1) to a failure in the generation of higher order structures of DLP1 (Chang et al., 2010). Studies in DLP1 KO mice have demonstrated that the complete absence of DLP1 is embryonically lethal (Ishihara et al., 2009; Wakabayashi et al., 2009). Mice suffered from developmental abnormalities, particularly in the forebrain, heart and liver and impaired placenta development. Moreover, defects in neurite and synapse formation as well as a defect in neural tube formation were observed. Another mutation in the middle domain of DLP1 (C425F) has been linked to dilated cardiomyopathy in mice (Ashrafian et al., 2010). DLP1 action is furthermore extensively regulated by protein phosphorylation, sumoylation, ubiquitination and S-nitrosylation (Chang & Blackstone, 2010). Notably, starvation-induced phosphorylation of DLP1 by protein kinase A was demonstrated to decrease its recruitment to mitochondria and thus result in the formation of elongated mitochondrial networks that resist autophagic degradation (Gomes et al., 2011). However, studies on the effects of post-translational modifications of DLP1 are so far restricted to mitochondria.

The mechanistic basis of peroxisomal membrane constriction prior to fission remains to be elucidated. In *Y. lipolytica*, intra-peroxisomal lipid remodelling, and thus membrane constriction, was linked to the AOX-dependent modulation of *Yl*Pex16p activity (Guo et al., 2003). In mammalian cells, the concerted action of non-muscle myosin A, Rho kinase II and the actin cytoskeleton was recently suggested to mediate membrane constriction (Schollenberger et al., 2010).

1.2.2.3 Recruiting DLP1 to peroxisomal membranes – Fis1, Mff

As DLP1 lacks the PH domain necessary for direct lipid binding, it is recruited to mitochondrial and peroxisomal membranes by membrane adaptor proteins. Initially, the tail-anchored protein Fission 1 (Fis1) was implied to recruit DLP1 to mitochondria and peroxisomes, and thus mediate organelle division (Yoon et al., 2003; Koch et al., 2005; Kobayashi et al., 2007). The majority of Fis1 faces the cytosol (Mozdy et al., 2000) and TPR repeats in its N-terminus were suggested to facilitate protein-protein interactions (Suzuki et

al., 2003; Dohm et al., 2004; Suzuki et al., 2005). It is targeted to peroxisomes in a Pex19p-dependent manner where it acts in a complex with Pex11pβ (Kobayashi et al., 2007; Delille & Schrader, 2008).

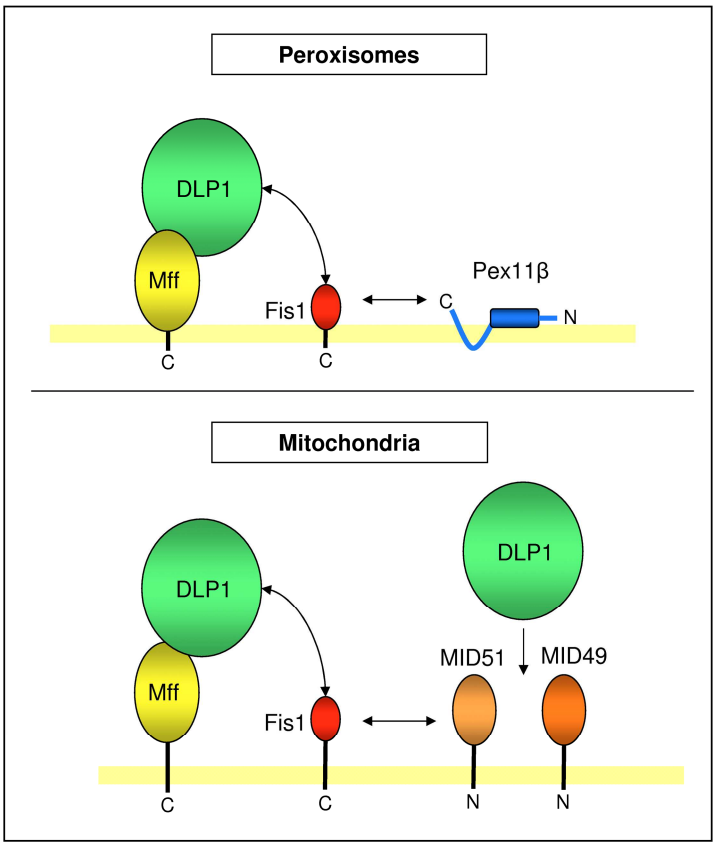

Fig. 1.7: Key fission proteins on peroxisomes and mitochondria in mammals.
Peroxisomes and mitochondria share key components of their fission machineries. DLP1 is a GTPase performing the final scission of constricted membranes and is recruited to the organelle from the cytosol by the tail-anchored membrane receptors Mff and Fis1. Whereas Mff appears to be the essential DLP1 receptor for organelle fission, Fis1 might fulfil regulatory functions. On peroxisomes, the peroxin Pex11pβ that is known to regulate peroxisome abundance and to elongate membranes prior to fission, is supposed to interact with Fis1, which might result in the assembly and/or recruitment of other components of the fission machinery. On mitochondria, the N-terminally anchored proteins MiD51 and MiD49 may sequester DLP1 thus inhibiting its function. Fis1 can potentially regulate the inhibitory effect of MiD51 on DLP1 function and mitochondrial fission (adapted from Schrader et al., 2011).

Another tail-anchored protein, the mitochondrial fission factor (Mff), was identified in a large scale siRNA screen in *D. melanogaster* and suggested to regulate fission of mitochondria and peroxisomes (Gandre-Babbe & van der Bliek, 2008). Detailed analysis of Mff recently revealed it to be the actual membrane receptor for DLP1, challenging the aforementioned role of Fis1 (Otera et al., 2010) (Fig. 1.7). Thus, the function of Fis1 at mitochondria and peroxisomes has to be reconsidered. Interestingly, Mff was only identified in metazoans (Gandre-Babbe & van der Bliek, 2008), thus the recruitment of the yeast DLP1 homologue dnm1 to mitochondria and peroxisomes still depends on the action of yeast Fis1. However, yeast Fis1 requires the additional action of the soluble molecular linkers Caf4 and Mdv1 (Motley & Hettema, 2007; Motley et al., 2008), two WD40 proteins that bind to yeast dnm1 as well as Fis1. Caf4 proteins have so far been only identified in *Saccharomyces* species and *C. glabrata*, but not in other yeast and fungi such as *H. polymorpha* (Delille et al., 2009). Additional factors involved in the recruitment and regulation of DLP1 action continue to emerge: MiD49 and MiD51/MieF, two novel N-terminally anchored mitochondrial membrane

proteins, have been found to recruit DLP1, at least to mitochondria (Palmer et al., 2011; Zhao et al., 2011). Similar to Mff, they are not found in yeast.

1.2.3 Peroxisome motility and inheritance

The intracellular distribution of peroxisomes in mammalian cells is achieved by a combination of microtubule-independent and dependent movement (Rapp et al., 1996; Schrader et al., 1996a; Schrader et al., 1996b; Wiemer et al., 1997; Huber et al., 1999; Thiemann et al., 2000; Schrader et al., 2003). Around 90 % of peroxisomes display short range, oscillating, microtubule-independent movements which enable contacts between neighbouring organelles (Rapp et al., 1996; Wiemer et al., 1997; Schrader et al., 2000). Those occur randomly, without any preferential direction. An involvement of the actin cytoskeleton was recently suggested to facilitate short-range movements and RhoA activity was implied to provide a switch between travelling on actin or microtubules, depending on its activation state (Schollenberger et al., 2010). For long range movements, peroxisomes utilize the microtubule cytoskeleton, covering mean distances of 10 µm with a velocity of 0.6 µm/second (Rapp et al., 1996; Wiemer et al., 1997; Schrader et al., 2000). This microtubule-dependent movement involves the action of dynein, kinesin, and dynactin (Schrader et al., 1996a; Schrader et al., 2003; Kural et al., 2005). Recently, anchoring of peroxisomal membranes to microtubules was demonstrated to be mediated by Pex14p, an essential component of the importomer (1.1.5.1). Tubulin was shown to associate with Pex14p and long-range microtubule-dependent movements were diminished in Pex14p-deficient fibroblasts, but were restored upon its re-introduction (Bharti et al., 2011). Whereas the formation of tubular peroxisomes is microtubule-independent (and is even induced upon microtubule depolymerisation) (Schrader et al., 1996a), intact microtubules are required for the proper distribution of the organelles (Schrader et al., 2003). Furthermore, microtubules are involved in Pex16p-dependent biogenesis of peroxisomes (Brocard et al., 2005).

In yeast and plant cells, the actin cytoskeleton and type V myosins are required for peroxisome movement and inheritance (Hoepfner et al., 2001; Jedd & Chua, 2002; Mano et al., 2002; Mathur et al., 2002; Muench & Mullen, 2003). It is important to note that regulated peroxisome transport is crucial for peroxisome inheritance in yeast species, as non-induced yeast cells contain just one or only a few peroxisomes. Thus, coordination of cell cycle-dependent division and transport to the daughter organelle is essential. The faithful partitioning of peroxisomes in yeasts is mediated by the proteins Inp1p and Inp2p in concert with Myo2p and Pex3p (Fagarasanu et al., 2005; Fagarasanu et al., 2006; Chang et al., 2009; Munck et al., 2009; Fagarasanu et al., 2010; Saraya et al., 2010). Within the mother cell,

peroxisomes are anchored at the cell cortex by the action of Inp1p and Pex3p, while some are actively transported into the bud due to the interaction of the motor Myo2p with the integral membrane protein Inp2. In contrast, mammalian cells contain hundreds of peroxisomes that are inherited in a rather random fashion.

1.2.4 Regulation of peroxisome abundance

Peroxisomes are known to be remarkably plastic organelles across species. In the following section, an overview will be given of the variety of stimuli influencing peroxisome abundance in mammals, yeast and plants. Moreover, the signal transduction mechanisms mediating peroxisome proliferation in the different kingdoms will be introduced.

The inherent capacity of mammalian peroxisomes to adjust their morphology and proliferate after application of external stimuli has been known for decades (Hess et al., 1965). Classical models of peroxisome proliferation in mammals include the peroxisomal response to peroxisome proliferators (Fahimi et al., 1982) and the regenerating rat liver after partial hepatectomy (Yamamoto & Fahimi, 1987). Ultrastructural studies revealed that peroxisomes in the regenerating rat liver display a very heterogeneous morphology, exhibiting tail-like membrane extensions and elongated forms, but also forming interconnections (Fahimi, 1969). In mammals, peroxisome proliferation is induced by the application of a high-fat diet, cold exposure, hypolipidemic drugs (such as fibrates), industrial compounds and environmental pollutants such as phtalates and plasticizers (Hess et al., 1965; Svoboda & Azarnoff, 1966; Lazarow & De Duve, 1976; Reddy et al., 1980; Fahimi et al., 1982; Bentley et al., 1993). However, it is important to note that different species respond with different intensities to peroxisome proliferators (PP), e.g. a massive peroxisome proliferation upon PP treatment is only observed in rodents, but not in humans (Islinger et al., 2010). Similarly, prolonged PP exposure gives rise to hepatocellular tumours in rodents, but not humans (Reddy et al., 1980; Kluwe et al., 1982; Reddy et al., 1982; Gariot et al., 1983; Moody et al., 1991). In addition to an increase of peroxisome number, PP treatment in rodents also leads to the induction of peroxisomal enzymes e.g. associated with fatty acid β-oxidation. Induction of proliferation and peroxisomal enzymes is dose-dependent and occurs at the protein and mRNA level (Beier et al., 1988; Schad et al., 1996). However, some chemicals may induce proliferation without simultaneous induction of β-oxidation enzymes (Baumgart et al., 1990) and vice versa (Lazarow et al., 1982). In mammalian cell culture models, a profound tubulation of peroxisomes was further observed upon addition of growth factors and unsaturated fatty acids, microtubule depolymerisation or after UV irradiation and H_2O_2 exposure (Schrader et

al., 1998a; Schrader et al., 1999). A similar increase in peroxisome number and size is induced in yeast species and fungi after shifting cells to growth media that contain e.g. alkanes, oleic acid, methanol, D-amino acids, and purines, and thus substrates that require peroxisomal metabolic functions (Veenhuis et al., 1987; Schrader & Fahimi, 2006; van der Klei et al., 2006). For instance, 80 % of the cytoplasmic volume of the methylotrophic yeast *H. polymorpha* may be occupied by peroxisomes when shifting to methanol-containing cultures (Veenhuis et al., 2003). As peroxisomes are the only site of β-oxidation in yeast, fungi and plant cells (Kunau et al., 1988), the regulation of their numbers is essential for utilization of fats. Plant peroxisomes respond to seed germination, herbicides, clofibrate as well as stress signals like ROS and ozone with peroxisome proliferation (Castillo et al., 2008). Interestingly, mussel peroxisomes proliferate extensively after exposure to crude petroleum, thus peroxisome proliferation may serve a valuable indicator of marine pollution (Fahimi & Cajaraville, 1995).

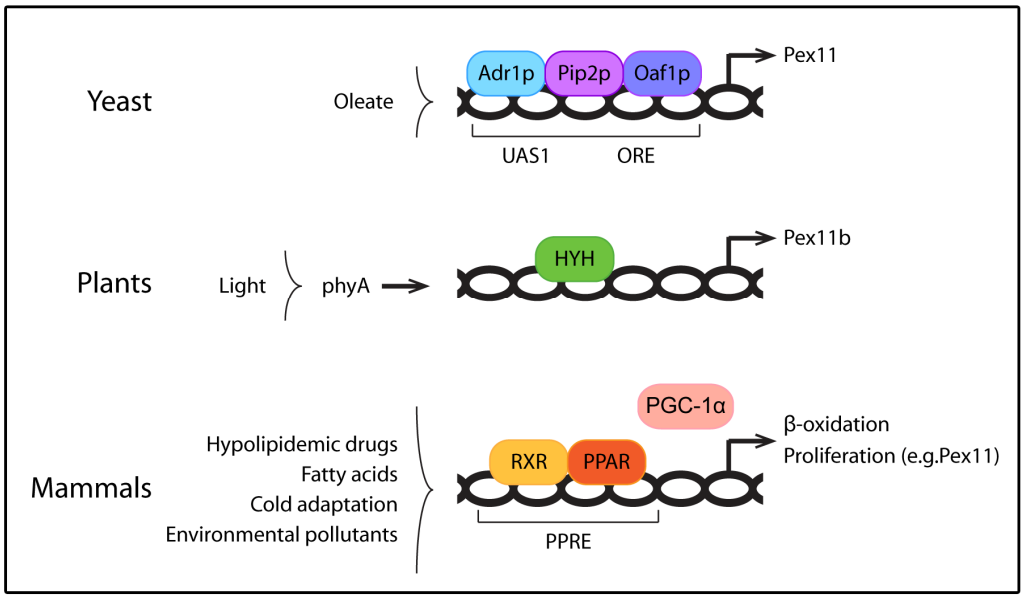

Fig. 1.8: Transcriptional regulation of peroxisome proliferation in different species.
In most organisms, peroxisome proliferation is preceded by the induction of genes associated with fatty acid β-oxidation and membrane elongation (e.g. Pex11). Activation of these pathways depends on several environmental and developmental conditions. In yeast, growth in the presence of oleic acid induces the dimerization of the transcription factors Oaf1p and Pip2p that, together with Adr1p, bind the oleate response element (ORE) and upstream activation sequence 1 (UAS1). In plants, light induces the expression of peroxisomal genes by the action of phyA and the binding of the transcription factor HYH to the PEX11b promoter. In mammals, peroxisome proliferator-activated receptor alpha (PPARα) and retinoid X receptor (RXR) co-ordinately bind to the PPAR response element (PPRE) to upregulate gene expression. Recently, other mechanisms independent of PPARα have also been described (e.g. PGC-1α dependent) (adapted from Ribeiro et al., 2011).

Peroxisome proliferation in mammals is regulated by the activation of the peroxisome proliferator activating receptor (PPAR)α. PPARs are nuclear encoded transcription factors which belong to the family of steroid/retinoid/thyroid receptors of which three subtypes were

identified: alpha, beta (delta) and gamma (Issemann & Green, 1990). PPARs form hetero-dimers with the retinoid X receptors (RXRs) and bind to specific DNA sequences known as peroxisome proliferator response elements (PPREs) (Fig. 1.8). PPREs not only regulate all peroxisomal lipid β-oxidation enzymes, but also other proteins (Schoonjans et al., 1996). Various peroxisome proliferators such as fibrates, hypolipidemic drugs and PUFAs activate PPARα which then regulates processes linked to lipid metabolism, lipoprotein synthesis and inflammatory response (Feige et al., 2006). PPARα is highly expressed in rodents, but only moderately in humans (Klaunig et al., 2003). Upon deletion of PPARα, KO animals are viable and maintain basic peroxisome functions (Lee et al., 1995), indicating that PPARα is not required for constitutive expression of peroxisomal genes. In rodents, PPARα-mediated peroxisome proliferation was linked to carcinogenesis in liver, pancreas and testis (Reddy et al., 1980; Reddy & Lalwani, 1983; Rabu & High, 2007), but the proliferators as such do not elicit a genotoxic response. Thus, tumour formation was linked to increased ROS damage (Qi et al., 2000), as the induction of various peroxisomal β-oxidation enzymes without concomitant induction of antioxidant enzymes (e.g. catalase) generates an intra-peroxisomal ROS imbalance, initiating ROS-related protein damage throughout the whole cell. PP induced peroxisome proliferation in mammals is linked to the induction of Pex11α as it is the only Pex11 isoform carrying a PPRE (Shimizu et al., 2004). However, Pex11α was shown to be only essential for peroxisome proliferation induced by non-classical proliferators, but was neglectable for proliferation stimulated by PPARα-dependent PPs (Li et al., 2002a). Thus, other PPARα-independent mechanisms of peroxisome proliferation might contribute profoundly to peroxisome homeostasis. In line with this, the transcriptional co-activator PGC1α was shown contribute to combined peroxisome and mitochondrial proliferation in brown adipose tissue after thermogenic stimuli in a PPAR-independent mechanism (Bagattin et al., 2010). Notably, these observations were made in rodent and human cells. As AOX or MFE2-deficient cell lines display a reduction in peroxisome number (Chang et al., 1999), a contribution of an intra-peroxisomal metabolic stimulus controlling peroxisomal abundance is discussed (Purdue & Lazarow, 2001), but was proposed to act independent of Pex11p (Li & Gould, 2002). Similar to the mammalian system, upon shift to oleate-containing growth media, the transcription factor Pip2-Oaf1 is activated in yeast that binds to oleate response elements (ORE) in the promoters of fatty acid response genes (Einerhand et al., 1993; Filipits et al., 1993; Rottensteiner et al., 1996; Karpichev & Small, 1998; Baumgartner et al., 1999; Rottensteiner et al., 2003b) (Fig. 1.8). Besides the OREs, several fatty acid response genes also contain an upstream activation sequence (UAS1) that is targeted by the transcription

factor Adr1 (Simon et al., 1992). These transcription factors induce the expression of Pex11p and the peroxisomal acyl-CoA oxidase Fox1p, while Pip2 additionally induces Pex25p (Gurvitz et al., 2001; Gurvitz & Rottensteiner, 2006). In methylotrophic yeasts, peroxisomal alcohol oxidase, the key enzyme for methanol oxidation (Ozimek et al., 2005), is regulated by the Adr1 homologue Mxrp1 in *P. pastoris* (Lin-Cereghino et al., 2006) and by Mpp1 in *H. polymorpha* (Leao-Helder et al., 2003). In plants, a light-induced signal transduction mechanism activating peroxisome proliferation has been identified (Hu & Desai, 2008). Far-red light is perceived by the receptor phyA which in turn facilitates binding of the transcription factor HyH to the promoter region of the Pex11B gene (Fig. 1.8). Although plant peroxisomes respond to fibrate addition with proliferation, no orthologues for PPARα or Pip2 have so far been identified in plants (Castillo et al., 2008; Kaur & Hu, 2009).

Upon withdrawal of stimuli, excess peroxisomes are degraded (Yokota, 1993; Tuttle & Dunn, 1995; Kiel et al., 2003). This is achieved by a combination of autophagy and membrane disruption by 15-lipoxygenase (Iwata et al., 2006). Around 70 % of peroxisomes are removed by autophagy in mammalian cells (Iwata et al., 2006). For autophagic removal, excess peroxisomes are first surrounded by ER membranes to create an autophagosome that fuses with lysosomal compartments. Upon fusion of double membranes, digestion of peroxisomes occurs. Peroxisome degradation is characterized in more detail in the yeast system and there termed pexophagy (Klionsky & Ohsumi, 1999; Kim & Klionsky, 2000; Dammai & Subramani, 2001; Farre & Subramani, 2004; Dunn et al., 2005; Monastyrska & Klionsky, 2006). Another mechanism of peroxisome degradation requires the action of 15-lipoxygenase which binds to organelles and disrupts their membrane, resulting in a release of contents into the cytoplasm (van Leyen et al., 1998). The mechanism of 15-lipoxygenase recruitment to peroxisomes remains to be elucidated, but leaking peroxisomal proteins are then degraded by the proteasome.

1.3 THE PEROXISOME-MITOCHONDRIA CONNECTION

Mitochondria and peroxisomes are both ubiquitous subcellular organelles that fulfil essential metabolic functions. While mitochondria have often been reduced to the powerhouse of the cell, they are essential for a variety of other processes such as controlling cellular redox-state, calcium homeostasis, apoptosis and the biosynthesis of iron-sulphur clusters (Rizzuto et al., 2000; Lill & Muhlenhoff, 2005; McBride et al., 2006). Although mitochondria and peroxisomes vary in some essential aspects, as e.g. mitochondria contain their own DNA, possess a double membrane and are of different evolutionary origin, several findings indicate

that they share an intricate relationship on a metabolic, dynamic and pathological level (Schrader & Yoon, 2007; Camoes et al., 2009).

On a metabolic level, peroxisomes and mitochondria obviously co-operate in the in the β-oxidation of fatty acids in animals (1.1.2): Shortened acyl-CoA esters generated by the peroxisomal β-oxidation machinery may be shuttled to mitochondria to be fully oxidized for energy generation (Wanders, 2004; Schrader & Yoon, 2007). Furthermore, both organelles co-operate in thermogenesis in brown adipose tissue (BAT) (Nedergaard et al., 1980; Binns et al., 2006). Mitochondria in BAT possess the ability to uncouple oxidation from ATP production, thus generating heat, whereas peroxisomal β-oxidation is an inherently uncoupled process (1.1.2) (Nicholls & Locke, 1984; Sell et al., 2004). Moreover, co-operation in the glyoxylate cycle in yeast, the glycolate cycle and photorespiration of plants as well as biotin synthesis of fungi was demonstrated (Veenhuis et al., 1989; Reumann & Weber, 2006; Fujimura et al., 2007; Tanabe et al., 2011). Additionally, both organelles are essential for ROS detoxification (Antonenkov et al., 2009; Bonekamp et al., 2009; Bonekamp et al., 2011a; Fransen et al., 2011). In line with a co-ordinated metabolic cooperation, the transcriptional co-activator PGC1α, a essential regulator of mitochondrial biogenesis (Puigserver et al., 1998; Puigserver et al., 1999), was recently shown to modulate peroxisome proliferation after thermogenic stimuli in BAT (Bagattin et al., 2010). Moreover, peroxisomes and mitochondria were shown to co-operate in antiviral defence (Dixit et al., 2010): the RIG-I-like receptor adaptor protein MAVS, curiously another tail-anchored protein like Fis1 and Mff, was localized to mitochondria and peroxisomes. Upon viral infection, peroxisomal MAVS mediates short-term defence by induction of interferon-independent response genes, while mitochondrial MAVS stimulates interferon-dependent genes in order to stabilize the antiviral response.

In addition to their metabolic co-operation, mitochondria and peroxisomes are both very dynamic organelles that can drastically change their morphology and number. Interestingly, both were shown to share key components of their fission machinery, the GTPase DLP1 as well as its membrane adaptors Fis1 and Mff (1.2.2) (Schrader & Fahimi, 2006; Camoes et al., 2009; Schrader et al., 2011). As a result, the first combined disorder of mitochondrial and peroxisomal fission was described (Waterham et al., 2007). Sharing of fission machinery components appears to an evolutionary conserved concept in plants, yeast and mammals (Mano et al., 2004; Lingard et al., 2008; Zhang & Hu, 2008; Delille et al., 2009; Nagotu et al., 2010). This mechanism might have been initiated when mitochondria lost their originally bacterial division components and thus adapted the peroxisomal ones (Osteryoung & Nunnari,

2003; Michels et al., 2005; Schrader & Fahimi, 2006). Unlike peroxisomes, however, mitochondria are further known to regulate their dynamics by complete fusion of mature organelles (Okamoto & Shaw, 2005). Peroxisomal fusion processes have only been implied in peroxisome biogenesis of *Y. lipolytica* (Titorenko & Rachubinski, 2000; Titorenko & Rachubinski, 2001a).

Aforementioned findings raise the question of how inter-organellar cross-talk is achieved. Indeed, a vesicular transport pathway from mitochondria to peroxisomes was identified (Neuspiel et al., 2008). Those mitochondria-derived-vesicles (MDVs) were shown to bud off the mitochondrial membrane in a DLP1 independent manner and a subpopulation of MDVs was observed to fuse with a small subpopulation of peroxisomes (Neuspiel et al., 2008). Vps35, a component of the retromer complex, was shown to regulate the formation of transport vesicles between mitochondria and peroxisomes (Braschi et al., 2010). Although the exact function of this vesicular pathway requires further analysis, it might contribute to the transport of metabolites, lipids, or proteins to peroxisomes. Alternatively, it might constitute a retrieval mechanism of peroxisomal proteins which have been mistargeted to mitochondria. Additionally, intra-organellar redox balance was indicated to facilitate inter-organellar communication (Ivashchenko et al., 2011). It was demonstrated that mitochondrial redox balance is very sensitive to perturbations of peroxisomal redox state and a mechanism of direct cross-talk between the organelles was proposed. In line with this, damage or disturbances of one organelle may have deleterious effects on the other. For instance, inhibition of catalase not only leads to a decline in catalase levels and a subsequent peroxisomal H_2O_2 elevation, but also contributes to age-related mitochondrial dysfunction (Koepke et al., 2008). As a consequence, the inner mitochondrial membrane potential and mitochondrial ROS production were increased. Additionally, certain peroxisomal disorders result in an accumulation of peroxisomal substrates such as VLCFA and bile acid intermediates that directly affect mitochondria and their redox balance by inhibiting the electron transfer chain (Fourcade et al., 2008; Ferdinandusse et al., 2009). In line with this, Pex5-/- mice show an extremely altered mitochondrial morphology with marked abnormalities in various tissues (Baumgart et al., 2001). Vice versa, in microvesicular hepatic steatosis, mitochondrial β-oxidation is impaired, leading to an accumulation of triglycerides and the formation of lipid droplets. Pre-treatment of steatotic rats with clofibrate, a peroxisome proliferator, which also enhanced catalase activity, partly reversed this phenotype (Natarajan et al., 2006). Thus, impairment of mitochondrial β-oxidation leads to a shift to

peroxisomal β-oxidation which results in an increase in ROS production due to higher activity of peroxisomal oxidases, inducing oxidative lesions in hepatic tissue.

1.4 OBJECTIVES

Peroxisomes are ubiquitous subcellular organelles that catalyze numerous metabolic processes, some of which are carried out in co-operation with other cell organelles such as the ER, lipid droplets and mitochondria in particular. The crucial role of peroxisomes for human health is exemplified by the severe phenotype of peroxisomal disorders. However, peroxisomes are not merely static organelles, but display a remarkable degree of plasticity in regard to their number and morphology. Peroxisome dynamics have been shown to be regulated by a combination of peroxisomal membrane elongation, subsequent fission and intracellular distribution via the microtubule cytoskeleton. Moreover, a multitude of external stimuli was identified to induce peroxisome elongation and/or proliferation; however, there is only limited knowledge on their intracellular signal transduction onto the peroxisomal level.

In mammals, peroxisomal growth and division is initialized by an elongation of the peroxisomal membrane which is mediated by the action of Pex11pβ, a constitutively expressed member of the Pex11 family of proteins. After subsequent constriction of the membrane tubule by a yet unidentified mechanism, final fission is carried out by the dynamin-like GTPases DLP1 that is recruited to the peroxisomal membrane by the membrane adaptor proteins Fis1 and Mff. Interestingly, the latter components are shared with mitochondria.

In the recent years, evidence has been provided that organelle dynamics and their proper regulation are intricately linked to organelle function and/or distribution. In line with this, a patient with a lethal defect of mitochondrial and peroxisomal fission was identified. Thus, the aim of this thesis was to gain further insight into the processes contributing to and regulating peroxisome dynamics in mammalian cells. This thesis is comprised of three parts: in the first section, the contribution of a potential fusion between mature peroxisomes to peroxisome dynamics, analogous to mitochondria, was investigated. Moreover, it was addressed if components of the mitochondrial fusion machinery are also shared by peroxisomes. In the second part, the regulation of peroxisome dynamics at the organelle itself was investigated by characterizing Pex11pβ, the key mediator of peroxisome elongation/proliferation in mammalian cells, biochemically. Furthermore, modulations of Pex11pβ activity by post-translational mechanisms were addressed. In the final part, different groups of external stimuli were characterized in regard to their capacity to alter peroxisome dynamics in order to study the regulation of peroxisome dynamics on a transcriptional level in mammalian cell culture. The results obtained in this study will help to clarify the following basic cell biological questions:

- Peroxisome dynamics: Do mammalian peroxisomes fuse? Does the fusion of mature peroxisomes contribute to the regulation or organelle dynamics in a manner analogous to mitochondria? If not, are there other yet uncharacterized processes involved in peroxisome dynamics? Are mitochondrial fusion proteins also shared between mitochondria and peroxisomes as are components of the fission machinery?
- Modulation of peroxisome dynamics by Pex11pβ action: What is the exact topology of human Pex11pβ? Is the protein targeted to the ER in peroxisome-deficient patient fibroblasts? Is human Pex11pβ regulated by phosphorylation and/or oligomerization?
- Alterations of peroxisome dynamics: Do peroxisomes respond to distinct classes of external stimuli (apoptotic insults, oxidative stress, metabolic stimuli) with a change in peroxisome dynamics? Can the observed phenotype be correlated to a specific metabolic state/function? Can pancreatic rodent AR42J cells usually utilized to study zymogen granule biogenesis serve as physiological model system for peroxisome dynamics? Does external stimulation affect the expression of the three mammalian Pex11 isoforms? Are they all regulated in a similar manner?

2 MATERIALS AND METHODS

2.1 EQUIPMENT

Centrifuges

- Centrifuge 5810R (Eppendorf, Hamburg, Germany)
- Heraeus Fresco 17 Centrifuge (Thermo Scientific, Waltham, MA, USA)
- Heraeus Pico 17 Centrifuge (Thermo Scientific, Waltham, MA, USA)
- Minispin plus (Eppendorf, Hamburg, Germany)
- Avanti Centrifuge J-251, Rotors JA-25.50 and JA-14 (Beckman Coulter, Fullerton, USA)
- Optima LE-80K Ultracentrifuge, Rotor Ti80 (Beckman Coulter, Fullerton, USA)

Incubators and shakers

- Incubator for bacterial cultures (Binder, Tuttlingen, Germany)
- Incubator shaker for bacterial cultures Innova 4400 (New Brunswick Scientific, Edison, USA)
- Magnetic stirrer Agimatic-N (JP Selecta, Barcelona, Spain)
- Mini Rocker MR-1 (Biosan, Riga, Latvia)
- Shaker REAX 2 (Heidolph Instruments, Heidelberg, Germany)
- Shaker, horizontal Unimac 1010 (Heidolph Instruments, Heidelberg, Germany)
- Thermomixer comfort (Eppendorf, Hamburg, Germany)
- Ultra Low -80°C freezer (Sanyo, Sakata, Japan)
- Vortex Genius 3 (IKA, Staufen, Germany)
- Water bath (Memmert, Schwabach, Germany)

Cell culture

- CO_2 incubator (Sanyo, Sakata, Japan)
- CO_2 incubator HeraCell (Heraeus/Kendro Laboratory Products, Hanau, Germany)
- Safety cabinet HeraSafe (Heraeus/Kendro Laboratory Products, Hanau, Germany)
- Peristaltic pump Masterflex 701572 (Cole-Parmer, Vernon Hills, USA)
- Pump Laboport (KNF Neuberger, Freiburg, Germany)
- Electro Cell Manipulator (ECM) 630 (BTX Harvard Apparatus, Holliston, MA, USA)

Optical equipment and microscopes

- Leica DMIL microscope (Leica, Heidelberg, Germany; cell culture)
- Olympus IX81 microscope; PlanApo 100x/1.40 oil objective (Olympus Optical, Hamburg, Germany)
- Camera F-View II CCD and Soft Imaging software (Soft Imaging Systems, Münster, Germany)
- Zeiss LSM 510 confocal microscope; Plan-Apochromat 63x and 100x/1.4 oil objectives (Carl Zeiss, Oberkochen, Germany)

- Zeiss LSM 510 live cell equipment: Heating insert P, CTI controller 3700 digital, Tempcontrol 37-2 (PeCon GmbH, Erbach, Germany)
- Leica TCS SP2 AOBS confocal microscope; PlanApo 100x/1.40 oil objective (Leica, Wetzlar, Germany)
- Andor Revolution XD spinning disk confocal microscope (Andor technology, Belfast, Northern Ireland)
- AlphaImager HP (Alpha Innotech, San Leandro, USA)
- BioRad Molecular Imager FX (BioRad, Munich, Germany)
- Phospho-Imager FLA-3000 (Fujifilm Europe GmbH, Düsseldorf, Germany)
- Calibrated Imaging Densitometer GS-710 (Bio-Rad, Munich, Germany)
- Photometer Ultrospec 100 pro (Amersham Biosciences, Uppsala, Sweden)
- Qubit fluorometer (Invitrogen, Carlsbad, CA, USA)
- NanoDrop nanospectrophotometer 2000 (Fisher Scientific – NanoDrop products, Wilmington, DE, USA)
- Tecan M200 infinite plate reader (Tecan Group Ltd., Männedorf, Switzerland)

Electrophoretic and blotting equipment

- Horizontal PerfectBlue Gel System Mini (Peqlab Biotechnology, Erlangen, Germany)
- Electrophoresis power supply EPS 2A200 (Amersham Biosciences, Uppsala, Sweden)
- Electrophoresis power supply EPS 601 (Amersham Biosciences, Uppsala, Sweden)
- Slap mini gel chamber (Keutz, Reiskirchen, Germany)
- Trans-Blot SD SemiDry transfer cell (BioRad, Munich, Germany)

Other equipment

- Autoclave Uniclave 88 (AJC, Lisbon, Portugal)
- Bag Sealer Folio (Severin, Sundern, Germany)
- Balance Vicon (Acculab/Sartorius, Göttingen, Germany)
- Balance, analytical BP 221S (Sartorius, Göttingen, Germany)
- Centrifuge beakers, 250 ml (Beckman, Munich, Germany)
- Centrifuge tubes, 50 ml (Nalgene, Rochester, USA)
- Cryomed N_2 storage (Forma Scientific, Waltham, USA)
- Drying Oven (Sanyo, Sakata, Japan)
- Easypet (Eppendorf, Hamburg, Germany)
- Microwave KOR-63A5 (Daewoo, Butzbach, Germany)
- pH meter PB-11 (Sartorius, Göttingen, Germany)
- Research pipettes, 2.5 µl, 10 µl, 100 µl, 1000 µl (Eppendorf, Hamburg, Germany)
- Thermal Cycler MyCycler (Bio-Rad, Munich, Germany)
- X-Ray cassette (Roth, Karlsruhe, Germany)
- Autoradiography cassette BAS Cassette 2040 (Fujifilm Europe GmbH, Düsseldorf, Germany)
- Fujifilm Imaging Plate BAS-MP 2040S (Fujifilm Europe GmbH, Düsseldorf, Germany)
- Ultracentrifuge adapters for reaction tubes (Rotor: 70Ti; Beckman Coulter) (Beranek Laborgeräte, Heidelberg, Germany)
- BioRad GelAir gel dying system (BioRad, Munich, Germany)
- Haemocytometer Neubauer counting chamber improved (Roth, Karlsruhe, Germany)
- Metal rings for clone selection (inner diameter: 10 mm), self-made

2.2 CONSUMABLES

Product	Source
Centrifuge tubes, 250 mL	Nalgene, Rochester, NY, USA
Centrifuge tubes, 50 mL	Nalgene, Rochester, NY, USA
Cover slips, round, 12 and 18 mm diameter	Menzel, Braunschweig, Germany
Cryovials, 2 mL	Greiner Bio-One, Frickenhausen, Germany
Cuvettes, semimicro	Plastibrand/Brand, Wertheim, Germany
Dishes for agar plates	Greiner Bio-One, Frickenhausen, Germany
Dishes for tissue culture, 35, 60, 100 mm	Greiner Bio-One, Frickenhausen, Germany
Dishes for tissue culture, 6, 12 and 24 well	Greiner Bio-One, Frickenhausen, Germany
Dishes for tissue culture, 96 well, black well, flat, microclear bottom	Greiner Bio-One, Frickenhausen, Germany
Electroporation cuvettes, 4 mm gap	Molecular BioProducts, San Diego, USA
Filter for medium, Sartolab P20, 0.2 µm	Sartorius, Goettingen, Germany
Folded filters	Macherey-Nagel, Düren, Germany
Glass bottom dishes, 35 mm	MatTek, Ashland, USA
Hyperfilm ECL	Amersham Biosciences, Uppsala, Sweden
Microcentrifuge tubes, 0.2 mL	Axygen, Union City, CA, USA
Microcentrifuge tubes, 0.5 mL for Qubit	Axygen, Union City, CA, USA
Microcentrifuge tubes, 0.5, 2 mL	Sarstedt, Nürnbrecht, Germany
Microcentrifuge tubes, 1.5 mL	Greiner Bio-One, Frickenhausen, Germany
Microcentrifuge tubes, 1.5mL, SafeLock	Eppendorf, Hamburg, Germany
Microscope slides, frosted end	Menzel, Braunschweig, Germany
Needle, Sterican 20 G x 1", 0.45 x 25 mm	B. Braun, Melsungen, Germany
Needle, Sterican 26 G x 1", 0.45 x 25 mm	B. Braun, Melsungen, Germany
Pipette tips, 20, 200, 1000 µL	Sarstedt, Nümbrecht, Germany
Protran Nitrocellulose Transfer Membrane	Whatman, Dassel, Germany
Reaction tubes, 15, 50 mL	Greiner Bio-One, Frickenhausen, Germany
Rubber policeman	Roth, Karlsruhe, Germany
Serological pipettes, 5, 10 mL	Greiner Bio-One, Frickenhausen, Germany
Silica Gel Orange	Roth, Karlsruhe, Germany
Syringe Inject, 10 mL	B. Braun, Melsungen, Germany
Syringe Omnifix-F, 1 mL	B. Braun, Melsungen, Germany
Tubes for bacterial cultures, 14 mL	Greiner Bio-One, Frickenhausen, Germany
Whatman filter paper, 3 mm	Whatman, Dassel, Germany

Table 2.1: Consumables

2.3 CHEMICALS AND REAGENTS

2.3.1 Chemicals

Chemical	Source
[P^{32}] orthophosphoric acid	PerkinElmer, Waltham, MA, USA
[S^{35}]-methionine	Hartmann Analytics, Braunschweig, Germany
2-7-dichlorodihydrofluorescein diacetate (H_2DCFDA)	Invitrogen, Carlsbad, CA, USA
2-Mercaptoethanol	Sigma, Steinheim, Germany
6-hydroxydopamine	Sigma, Steinheim, Germany
Acetic acid	Merck, Darmstadt, Germany

Chemical	Source
Acrylamide – RotiphoreseGel 30	Roth, Karlsruhe, Germany
Agar	Formedium, Hunstanton, England
Agarose NEEO	Roth, Karlsruhe, Germany
Albumin Fraction V (BSA)	Roth, Karlsruhe, Germany
Ammonium persulphate (APS)	Sigma, Steinheim, Germany
Ampicillin	Sigma, Steinheim, Germany
Arachidonic acid	MP Biochemicals, Illkirch, France
Bezafibrate	Boehringer-Mannheim, Mannheim, Germany
Bromophenol blue	Sigma, Steinheim, Germany
Calcium chloride	Sigma, Steinheim, Germany
CHAPS	Roth, Karlsruhe, Germany
Chloroform	Merck, Darmstadt, Germany
Copper	Sigma, Steinheim, Germany
Cycloheximide	Sigma, Steinheim, Germany
D(+)glucose monohydrate	Fluka/Sigma, Steinheim, Germany
Dexamethasone	Sigma, Steinheim, Germany
Digitonin	Sigma, Steinheim, Germany
Dimethyl sulphoxide (DMSO)	Sigma, Steinheim, Germany
Dithiothreitol (DTT)	Sigma, Steinheim, Germany
ECL advanced western blot detection kit	Amersham Biosciences, Uppsala, Sweden
Eicosatetraynoic acid (ETYA)	Alexis/Axxora, Grünberg, Germany
Ethanol	Merck, Darmstadt, Germany
Ethidium bromide solution	Fluka/Sigma, Steinheim, Germany
Ethylenediaminetetraacetic acid salt dehydrate (EDTA)	Sigma, Steinheim, Germany
FOY-305 protease inhibitor	Sanol-Schwarz, Monheim, Germany
G418 (Geneticin)	Sigma, Steinheim, Germany
Glycerol	Roth, Karlsruhe, Germany
Glycine	Sigma, Steinheim, Germany
HEPES sodium salt	Sigma, Steinheim, Germany
Hoechst 33528	Polysciences, Warrington, USA
Hydrochloric acid	Merck, Darmstadt, Germany
Hydrogen peroxide (30%)	Merck, Darmstadt, Germany
Isopropanol	Merck, Darmstadt, Germany
Kanamycin disulphate salt	Sigma, Steinheim, Germany
LB-Broth Miller	Formedium, Hunstanton, England
Malonate	Sigma, Steinheim, Germany
Menadione	Sigma, Steinheim, Germany
Methanol	Merck, Darmstadt, Germany
Milk, powder, low fat (Molico)	Nestlé, Linda-a-Velha, Portugal
MOPS sodium salt	Sigma, Steinheim, Germany
Mowiol 4-88 reagent	Calbiochem/Merck, Darmstadt, Germany
Nickel	Sigma, Steinheim, Germany
n-propylgallate	Fluka/Sigma, Steinheim, Germany
Oleic acid	Merck, Darmstadt, Germany
Palmitic acid	MP Biochemicals, Illkirch, France
Paraformaldehyde (powder)	Sigma, Steinheim, Germany
Paraquat (Methylviologen hydrate)	Sigma, Steinheim, Germany
PeqGold TriFast reagent	PeqLab, Erlangen, Germany
Phenylmethylsulphonyl fluoride (PMSF)	Sigma, Steinheim, Germany

Chemical	Source
Polyethyleneglycol (PEG) 6000	Fluka/Sigma, Steinheim, Germany
Ponceau S	Roth, Karlsruhe, Germany
Potassium chloride	Sigma, Steinheim, Germany
Potassium phosphate dibasic	Sigma, Steinheim, Germany
Protein A-Sepharose, 1 mg/ml	Sigma, Steinheim, Germany
Protein assay (Bradford)	Bio-Rad, Munich, Germany
Proteinase K	Sigma, Steinheim, Germany
Sodium azide	Sigma, Steinheim, Germany
Sodium bicarbonate	Sigma, Steinheim, Germany
Sodium carbonate	Sigma, Steinheim, Germany
Sodium chloride	Sigma, Steinheim, Germany
Sodium deoxycholate monohydrate	Sigma, Steinheim, Germany
Sodium dodecyl sulphate (SDS)	Sigma, Steinheim, Germany
Sodium fluoride	Sigma, Steinheim, Germany
Sodium hydroxide	Merck, Darmstadt, Germany
Sodium orthovanadate	Sigma, Steinheim, Germany
Sodium phosphate dibasic	Sigma, Steinheim, Germany
Sucrose	Sigma, Steinheim, Germany
Sudan Black	Merck, Darmstadt, Germany
Tetramethylethelenediamine (TEMED)	Fluka/Sigma, Steinheim, Germany
Trasylol (protease inhibitor)	Bayer, Leverkusen, Germany
Trichloroacetic acid (TCA)	Merck, Darmstadt, Germany
Tris	Roth, Karlsruhe, Germany
Triton X-100	Sigma, Steinheim, Germany
Water, treated with DEPC	Roth, Karlsruhe, Germany

Table 2.2: Frequently used chemicals

Further chemicals not listed in Table 2.2 were purchased from Sigma (Steinheim, Germany), Merck (Darmstadt, Germany), or Roth (Karlsruhe, Germany).

2.3.2 Loading dyes and markers

Product	Source
6x Orange Loading Dye	Fermentas, Burlington, Canada
Gene Ruler DNA Ladder Mix	Fermentas, Burlington, Canada
Kaleidoscope Precision Plus Protein Standard	BioRad, Munich, Germany
Precision Plus Proteins Standard	BioRad, Munich, Germany

Table 2.3: Loading dyes and markers

2.3.3 Kits

Product	Source
Nucleobond Xtra Midi Kit	Macherey-Nagel, Düren, Germany
Qiaprep Spin Miniprep Kit	Qiagen, Hilden, Germany
Qiaquick Gel Extraction Kit	Qiagen, Hilden, Germany
Quant-iT dsDNA BR Assay Kit	Invitrogen, Carlsbad, CA, USA
Quant-iT RNA Assay Kit	Invitrogen, Carlsbad, CA, USA
RNeasy Protect Mini Kit	Qiagen, Hilden, Germany

Table 2.4: Kits

2.3.4 Cell culture reagents

Product	Source
Chloroquine diphosphate	Fluka/Sigma, Steinheim, Germany
Collagen R solution (4mg/mL)	Serva, Heidelberg, Germany
DEAE-Dextran hydrochloride	Sigma, Steinheim, Germany
DMEM high glucose with L-glutamine	PAA Laboratories, Pasching, Austria
DMEM with L-glutamine, without sodium bicarbonate and phenol red, powder (supplemented with 3.7 g/l sodium bicarbonate and filtered upon use)	Sigma, Steinheim, Germany
Fetal Bovine Serum "Gold" (FBS)	PAA Laboratories, Pasching, Austria
Ham's F-12 with L-glutamine, powder (supplemented with 1.18 g/L sodium bicarbonate and filtered upon use)	Sigma, Steinheim, Germany
L-glutamine (100x)	Sigma, Steinheim, Germany
Lipofectamine reagent	Invitrogen, Karlsruhe, Germany
MEM essential medium (MEM) without L-glutamine, without L-methionine	Biowest S.A.S., Nuaille, France
N1 medium supplement for serum-free culture (100x)	Sigma, Steinheim, Germany
Penicillin/Streptomycin, 100x concentrate	PAA Laboratories, Pasching, Austria
Polyethylenimine (PEI) 25 kD	Sigma, Steinheim, Germany
Poly-L-Lysine	Sigma, Steinheim, Germany
Trypsin/EDTA	PAA Laboratories, Pasching, Austria
Turbofect transfection reagent	Fermentas, Burlington, Canada

Table 2.5: Frequently used cell culture reagents

2.4 IMMUNOLOGICAL REAGENTS

2.4.1 Primary antibodies

Antibody	Source	Dilution
Mouse mc anti-Actin 2G2	B. Jokusch, University of Braunschweig, Germany	WB 1:1000
Mouse mc anti-Myc epitope 9E10	Santa Cruz Biotechnology, Santa Cruz, USA	IF 1:200 WB 1:1000
Mouse mc anti-Pex19	BD Biosciences, San Jose, USA	WB 1:250
Mouse mc anti-Tom20	BD Transduction Laboratories, San Diego, USA	IF 1:200
Mouse mc anti-α-Tubulin	Synaptic Systems, Göttingen, Germany	IF 1:100; WB 1:1000
Rabbit pc anti-AOX	A. Völkl, University of Heidelberg, Germany	WB 1:2000 IF 1:200
Rabbit pc anti-ATP synthase α/β	H. Schägger, University of Frankfurt, Germany	WB 1:1000
Rabbit pc anti-carboxypeptidase A	Rockland Immunochemicals, Gilbertsville, USA	IF 1:800
Rabbit pc anti-GFP	Invitrogen, Carlsbad, CA, USA	IF 1:100; WB 1:1000; IP 1:333
Rabbit pc anti-OPA1	P. Belenguer, University of Toulouse, France	IF 1:100, WB 1:1000

Rabbit pc anti-Pex11β	Abcam, Inc, Cambridge, UK	IF 1:200, WB 1:500
Rabbit pc anti-Pex14	D. Crane, Griffith University, Brisbane, Australia	IF 1:1000
Rabbit pc anti-PMP70	A. Völkl, University of Heidelberg, Germany	IF 1:200, WB 1:1000
Sheep pc anti-Chymotrypsinogen	H. F. Kern, University of Marburg, Germany	IF 1:400

Table 2.6: Primary antibodies
Abbreviations: IF, immunofluorescence; IP, immunoprecipitation; mc, monoclonal; pc, polyclonal; WB, western blotting.

2.4.2 Secondary antibodies

Antibody	Source	Dilution
Donkey pc anti-mouse IgG conjugated to Alexa Fluor 488	Invitrogen, Karlsruhe, Germany	IF 1:400
Donkey pc anti-mouse IgG conjugated to tetramethylrhodamine 5 isothiocyanate (TRITC)	Jackson ImmunoResearch, West Grove, USA	IF 1:100
Donkey pc anti-rabbit IgG conjugated to Alexa Fluor 488	Invitrogen, Karlsruhe, Germany	IF 1:500
Donkey pc anti-rabbit IgG conjugated to TRITC	Jackson ImmunoResearch, West Grove, USA	IF 1:100
Donkey pc anti-sheep IgG conjugated to TRITC	Jackson ImmunoResearch, West Grove, USA	IF 1:100
Goat anti-mouse IgG conjugated to horseradish peroxidase (HRP)	BioRad, Munich, Germany	WB 1:2000
Goat anti-rabbit IgG conjugated to HRP	BioRad, Munich, Germany	WB 1:2000

Table 2.7: Secondary antibodies
IF, immunofluorescence; WB, western blotting.

2.5 MOLECULAR BIOLOGY REAGENTS

2.5.1 Enzymes and other reagents

Reagent	Source
Antarctic phosphatase	New England Biolabs, Ipswich, USA
dNTP's	New England Biolabs, Ipswich, USA
KOD Hot Start DNA polymerase	Novagen/Merck, Darmstadt, Germany
M-MuLV reverse transcriptase	New England Biolabs, Ipswich, USA
Oligo-dT(15) primer	Roche, Basel, Switzerland; Eurofins MWG Operon, Ebersberg, Germany
Restriction enzymes: *Bam*HI, *Bgl*II, *Eco*RI, *Hind*III, *Kpn*I, *Mlu*I, *Xho*I	New England Biolabs, Ipswich, USA; Fermentas, Burlington, Canada; Invitrogen, Karlsruhe, Germany
RNAse block	Stratagene, LaJolla, USA; New England Biolabs, Ipswich, USA
T4 DNA ligase	New England Biolabs, Ipswich, USA
Taq DNA polymerase	New England Biolabs, Ipswich, USA

Table 2.8: Molecular biology reagents

2.5.2 Plasmids

Name	Source/Reference
APP-GFP	O. da Cruz e Silva, University of Aveiro, Portugal
EGFP-*Hs*Pex26(275-305)-*Hs*ALDP(87-164) (pAH26)	R. Erdmann, University of Bochum, Germany
GFP-SKL	S. Gould, Johns Hopkins University School of Medicine, Baltimore, USA
Mfn 1-myc	A. Niemann, ETH, Zurich, Switzerland
Mfn 2-myc	A. Niemann, ETH, Zurich, Switzerland
Mfn1(K88T)-Myc	A. Niemann, ETH, Zurich, Switzerland
Mfn2(K109A)-Myc	A. Niemann, ETH, Zurich, Switzerland
Mfn2-IYFFT-Myc	M. Rojo, Paris, France
Mfn2-RRD-Myc	M. Rojo, Paris, France
Mito-DsRed	Clontech, Saint-Germain-en-Laye, France
Mito-GFP	R. Lill, University of Marburg, Germany
Myc-Pex11α	(Delille et al., 2010)
Myc-Pex11β	(Schrader et al., 1998b)
Myc-Pex11γ	(Delille et al., 2010)
pDsRed-C1-monomer	Clontech, Saint-Germain-en-Laye, France
pDsRed-Peroxi	Clontech, Saint-Germain-en-Laye, France
Pex11β-GFP	G. Dodt, University of Tübingen, Germany
Pex11β-Myc	(Schrader et al., 1998b)
Pex11β-mYFP	(Delille et al., 2010)
pKillerRed-C	Evrogen, Moscow, Russia
pKillerRed-Mito	Evrogen, Moscow, Russia
pmEYFP-C1	Clontech, Saint-Germain-en-Laye, France
PMP70-YFP	J. Gärtner, University of Göttingen, Germany
YFP-Pex11β	(Delille et al., 2010)

Table 2.9: Plasmids used for protein expression in this study
Mfn, mitofusin.

2.5.3 Constructs

Name	Template	Primer	Enzymes	Vector
KillerRed-ΔAOX1	AOX1 (*homo sapiens*)	KR-PO_fw/ KR-PO_rev	*Eco*RI/*Bam*HI	pKillerRed-C
DsRed-dPex26	EGFP-*Hs*Pex26(275-305)-*Hs*ALDP(87-164)	-	*Bgl*II/*Kpn*I	pDsRed-C1-monomer

Table 2.10: Constructs generated in this study

In frame insertion of all constructs was verified by sequencing (Eurofins MWG Operon, Ebersberg, Germany).

2.5.4 Primers

2.5.4.1 Mycoplasm PCR & Cloning

Name	Sequence (5' to 3')
GPO1	ACT CCT ACG GGA GGC AGC AGT A
MGSO	TGA ACC ATC TGT CAC TCT GTT AAC CTC
KR-PO_fw	TTGAATTCCATTCAAGCTGTCTTAAGGAGTTTATGTCTGCTG
KR-PO_rev	TTGGATCCTCAGAGCTTGGACTGCAGTGACTTCAGG

Table 2.11: Primers used for mycoplasm detection and cloning in this study
Fw, forward; rev, reverse.

2.5.4.2 Internal primers

Name	Sequence (5' to 3')	Tm	Cycle number	Fragment size
Pex11α, fw	CAGGCAACTGAGCAGAGCAT	55°C	35	431bp
Pex11α, rev	GCCAGAGGCCTAGTTTGTCC			
Pex11β, fw	CCTCTGGCGTTGTGGCCCTG	60°C	31	296bp
Pex11β, rev	CGCAGAGGTGCGCTGGAGTC			
Pex11γ, fw	ATGACCTGGCCATGTTTGTC	52°C	40	464bp
Pex11γ, rev	GGAGATGGTGCCCATGAGG			
Pex3, fw	CCTGGGCACGGTCCTTGGAGG	59°C	31	480bp
Pex3, rev	TCTGTCAGGCCATCTCCAAGTAGG			
Acox1, tv1, fw	GCGCATCCAGCCACAGCAGG	59°C	25	488bp
Acox1, tv1, rev	AGCGGCCAAGCACAGAGCCA			
GAPDH, fw	ACG ACC CCT TCA TTG ACC	50°C	25	589bp
GAPDH, rev	CCA GTG AGC TTC CCG TTC AGC			

Table 2.12: Primers used for semi-quantitative PCR in this study
Fw, forward; rev, reverse; Tm, melting temperature used; tv, transcription variant.

All primers were purchased at Eurofins MWG Operon (Ebersberg, Germany).

2.6 FREQUENTLY USED BUFFERS AND SOLUTIONS

All solutions were prepared with distilled water (ROpure infinity reverse osmosis water system; Barnstead, Dubuque, USA) if not indicated otherwise.

Blocking solution for immunofluorescence

- 1 % (w/v) BSA in PBS

Blocking solution for western blots

- 5 % (w/v) Milk powder in PBS

Fixative for immunofluorescence

- 4 % (w/v) para-Formaldehyde in PBS, pH 7.4

Cell culture medium for COS-7 and HepG2 cells

- DMEM, high glucose (4.5 g/l) with L-glutamine
- 10 % (v/v) FBS
- 100 U/mL Penicillin
- 100 µg/mL Streptomycin

Cell culture medium for CHO cells

- Ham's F-12 with L-glutamine
- 1.18 g/L Sodium bicarbonate
- 10 % (v/v) FBS
- 100 U/mL Penicillin
- 100 µg/mL Streptomycin

Cell culture medium for SH-S5Y5 cells

- DMEM, high glucose (4.5 g/L) with L-glutamine
- Ham's F-12 with L-glutamine
- Mix 1:1
- 15 % (v/v) FBS
- 100 U/mL Penicillin
- 100 µg/mL Streptomycin

Cell culture medium for serum-free growth of HepG2 cells

- DMEM, high glucose (4.5 g/L) with L-glutamine
- N1 serum supplement (1:100)
- 100 U/mL Penicillin
- 100 µg/mL Streptomycin

HBS – HEPES buffered saline, pH 7.15, for electroporation

- 5 g/L HEPES
- 8 g/L Sodium chloride
- 0.37 g/L Potassium chloride
- 0.01g/L Sodium phosphate dibasic
- 1.08 g/L D(+)Glucose

LB medium

- 2.5 % (w/v) LB-Broth Miller

LB plates

- 2.5 % (w/v) LB-Broth Miller
- 1 % (w/v) Agar

Lysisbuffer, pH 8.0 (radio-immunoprecipitation buffer)

- 25 mM Tris
- 50 mM Sodium chloride
- 0.5 % (w/v) Sodium deoxycholate
- 0.5 % (w/v) Triton X-100

Mounting medium for immunofluorescence

- 3 volumes Mowiol stock
- 1 volume n-propylgallat stock

Mowiol stock

- 12 g Mowiol 4-88
- 40 mL PBS, stir over night
- 20 mL Glycerol, stir over night
- Centrifuge 1 hour, 15.000 rpm, 4° C
- Sodium azide added to the supernatant

PBS – phosphate buffered saline, pH 7.35

- 140 mM Sodium chloride
- 2.5 mM Potassium chloride
- 6.5 mM Sodium phosphate dibasic
- 1.5 mM Potassium phosphate dibasic

Permeabilization for immunofluorescence

- 0.2 % (v/v) Triton X-100 in PBS

Permeabilization for immunofluorescence

- 1 mg/mL Digitonin stock solution
- 1:400 diluted in PBS

Peroxisome homogenization buffer, pH 7.4 (standard)

- 5 mM MOPS
- 250 mM Sucrose
- 1 mM EDTA
- (0.1 % (v/v) Ethanol)

n-propylgallate stock (anti-fading reagent)

- PBS
- 2.5 % (w/v) n-propylgallate
- 50 % (v/v) Glycerol

Protease inhibitor mix (final concentrations)

- 0.1 mM PMSF
- 0.01 mM FOY 305
- 0.25 % (v/v) Trasylol

SDS loading buffer (Laemmli, 1970)

- 60 mM Tris, pH 6.8
- 2 % (w/v) SDS
- 10 % (v/v) Glycerol
- 0.005 % (w/v) Bromophenol blue
- 20 mM DTT
- 5 % (v/v) β-mercaptoethanol (fresh)

SDS running buffer

- 25 mM Tris
- 190 mM Glycine
- 0.1 % (w/v) SDS

Semidry blotting buffer

- 48 mM Tris
- 39 mM Glycine
- 0.4 % (w/v) SDS
- 20 % (v/v) Methanol

Sudan Black solution

- 0.1 g in 100 mL 70 % Ethanol (0.1 %)
- Boil
- Cool to room temperature
- Filter

50x TAE – Tris-Acetate-EDTA, pH 8.0

- 40 mM Tris
- 20 mM Acetic acid
- 1 mM EDTA

TBS – Tris buffered saline

- 50 mM Tris, pH 7.5
- 150 mM Sodium chloride
- 1 mM EDTA

Tris buffer separation gel (pH 8.8)

- 2 M Tris (60.56 g in 250 mL water)

Tris buffer stacking gel (pH 6.8)

- 1 M Tris (30.28 g in 250 mL water)

Wash buffer I for immunoprecipitation

- PBS, pH 7.35
- 0.5 % (w/v) Sodium deoxycholate
- 0.5 % (w/v) Triton X-100

Wash buffer II for immunoprecipitation, pH 8.0

- 500 mM Sodium chloride
- 125 mM Tris
- 10 mM EDTA
- 0.5 % (w/v) Triton X-100

2.7 MAMMALIAN CELL LINES

2.7.1 Cell lines

Unless indicated otherwise, all cell lines were obtained from the American Type Culture Collection (ATCC, Rockville, MD, USA).

COS-7

- ATCC number: CRL-1651
- Organism: *Cercopithecus aethiops* (african green monkey)
- Tissue: kidney
- Morphology: adherent, fibroblast-like
- Medium: DMEM, high glucose

CHO-K1

- ATCC number: CCL-61
- Organism: *Cricetulus griseus* (Chinese hamster)
- Tissue: ovary
- Morphology: adherent, epithelial
- Medium: Ham's F-12 with L-glutamine

HepG2

- ATCC number: HB-8065
- Organism: *Homo sapiens* (human)
- Tissue: hepatocellular carcinoma
- Morphology: adherent, epithelial
- Medium: DMEM, high glucose

AR42J

- ATCC number: CRL-1492
- Organism: *Rattus norwegicus* (rat)
- Tissue: exocrine pancreatic tumour
- Morphology: adherent, epithelial
- Medium: DMEM, high glucose

SH-SY5Y cells

- ATCC number: CRL-2266
- Organism: *Homo sapiens* (human)
- Tissue: brain neuroblastoma cell line (derived from bone marrow metastasis)
- Morphology: mixed adherent and suspension, epithelial
- Medium: DMEM, high glucose and Ham's F-12 (1:1)

Pex19-deficient patient fibroblasts (ΔPex19)

- Source: G. Dodt (University of Tübingen, Germany); R. Wanders (AMC, Amsterdam, The Netherlands)
- Organism: *Homo sapiens* (human)
- Tissue: skin fibroblasts
- Morphology: adherent fibroblasts
- Medium: DMEM, high glucose

2.7.2 Stable cell lines

Name	Parent cell line	Construct	Reference
CHO-GFP-PTS1	CHO-K1	GFP-PTS1	(Islinger et al., 2007)
CHO-DsRed-PTS1	CHO-K1	DsRed-PTS1	This study
CHO-PMP70-YFP	CHO-K1	PMP70-YFP	This study
CHO-DsRed-ΔPex26	CHO-K1	DsRed-ΔPex26	This study
COS7-GFP-PTS1	COS-7	GFP-PTS1	(Koch et al., 2004)

Table 2.13: Overview of the stable cell lines used/generated in this study

2.8 CELL CULTURE

Mammalian cell lines were routinely cultured under sterile conditions using a laminar flow safety cabinet and kept at 37°C under a 5 % CO_2 atmosphere. All cell culture materials and solutions were sterilized by either filtration, heat inactivation (baking) or autoclaving prior to use. Unless indicated otherwise (2.8.9), culture media were supplemented with 10 % fetal bovine serum (FBS) to supply hormones, carrier proteins, attachment factors, amino acids, salts and trace elements essential for cell growth. To further avoid contamination of media and cell lines with bacteria, antibiotics were routinely added (100 U/mL penicillin, 100 µg/mL streptomycin). For continuation of cultures and biochemical experiments, cells were seeded in 100 mm cell culture dishes; to seed cells for immunofluorescence, 60 mm cell culture dishes containing 18 mm coverslips were used. A Neubauer counting chamber was used to determine the number of cells prior to seeding.

2.8.1 Cell passage

In order to guarantee optimal growth and provide cells for subsequent experiments, cells were routinely passaged twice a week. In between cell passages, cell culture medium was exchanged every 2 days to provide fresh nutrients and remove cellular waste products.

Protocol: After aspiration of cell culture medium, cells were washed once in PBS to remove any residual traces of culture medium. Next, 2mL of trypsin/EDTA solution (0.05 %

trypsin/0.02 % EDTA) were added and the cells were incubated at 37°C and 5 % CO_2 for 5-10 minutes to detach the adherent cells from the culture dish surface. At 37°C trypsin reaches its optimal activity, cleaving extracellular adhesion molecules (integrins) and cell-cell adhesions (cadherins). Furthermore, the chelator EDTA binds calcium – a necessary cofactor for both integrin and cadherin adhesions - which further impairs their integrity. The reaction was stopped by the addition of 10 mL of complete cell culture medium, as the included serum contains protease inhibitors. The detached cells were thoroughly resuspended, transferred to a 15 mL reaction tube and pelleted by centrifugation at 500g for 5 minutes. The cells were then resuspended and seeded in a ratio of 1:10 into a fresh cell culture dish containing 10 mL of complete cell culture medium.

For certain cell lines such as AR42J, SH-S5Y5 or HepG2 cells, an additional coating step of cell culture dishes and/or coverslips was routinely performed.

AR42J cells were seeded onto materials coated with the so-called matrigel to facilitate general attachment of the cells. Matrigel is an extracellular matrix extract of the murine Engelbreth-Holm-Swarm (EHS) tumour and was prepared according to Kleinmann (Kleinmann et al., 1981). For cell culture use, matrigel was sterilized by irradiation with 100 Gray and stocks were aliquoted into 2 mL fractions and stored at -20°C. Prior to use, the stock was diluted 1:5 in PBS. Coating with matrigel was performed for 5-10 minutes at room temperature and the surplus was collected again to be re-used.

HepG2 and SH-S5Y5 cells were routinely seeded onto coated glass coverslips for immunofluorescence experiments to enhance attachment and spreading of cells in order to improve morphology. In the case of HepG2 cells, coating of glass coverslips was performed using Collagen R solution (1:10 in dH_2O) for 5-10 minutes at room temperature while SH-S5Y5 cells were seeded onto Poly-L-lysine coated coverslips (5-10 minutes Poly-L-lysine, 3 times washed in dH_2O).

2.8.2 Generation of cell stocks

In order to generate back-up stocks of cell lines, early cell passages were regularly collected and stored in liquid nitrogen. The freezing medium was created by supplementing the appropriate complete cell culture medium (2.7.1) with FBS and DMSO to minimize the formation of water crystals upon freezing and thus cell rupture.

Protocol: Cells of a confluent 100 mm cell culture dish were trypsinized and pelleted by centrifugation (2.8.1). The cell pellet was then resuspended in freezing medium and the cell suspension was equally distributed over several 2mL cryo tubes. Aliquots were quickly frozen

at -80°C in a freezing unit to guarantee slow, gradual freezing to avoid a high mortality rate. After 24 hours, cells were transferred into liquid nitrogen for long time storage.

Freezing medium

- Cell culture medium
- 20 % (v/v) FBS
- 10 % (v/v) DMSO

To defreeze said cell stocks, cell aliquots were carefully de-frozen by gradually applying a small volume of pre-warmed, sterile complete cell culture medium on top of the frozen cell suspension. Thawed cells were transferred to a 15 mL reaction tube, pelleted by centrifugation and resuspended in fresh complete medium to remove any traces of DMSO. The cells were seeded into 100 mm cell culture dishes and cultivated at 37°C under a 5 % CO_2 atmosphere.

2.8.3 Stimulation of AR42J cells with dexamethasone

Stimulation of AR42J cells with the synthetic glucocorticoid dexamethasone leads to a profound rearrangement of cellular gene expression, cell morphology and cellular differentiation. As a result, all compartments of the secretory pathway are enlarged and the number of electron dense granule as well as the concentration and secretion of digestive enzymes increases (Logsdon et al., 1985; Swarovsky et al., 1988).

Protocol: To stimulate AR42J cells with dexamethasone, the cell culture medium was removed and fresh complete medium containing 10 nM (or 1 µM where indicated) of dexamethasone was added to the cells. Stimulated cells were incubated for 24–72 hours at 37°C and 5 % CO_2.

2.8.4 Mycoplasma detection

To guarantee optimal cell growth of cultured cells, contaminations with intracellular pathogens such as mycoplasms have to be avoided. Potential contamination was determined by either Hoechst staining or Mycoplasm PCR.

2.8.4.1 Hoechst staining

Hoechst 33528 is a DNA intercalating reagent. Upon mycoplasma contamination, not only cell nuclei, but also the rod-shaped bacteria will appear upon UV irradiation (excitation: 359 nm; emission: 461 nm).

Protocol: After cell passage (2.8.1), cells were seeded in 60 mm cell culture dishes containing 18 mm coverslips. After 24 hours, the cell culture medium was aspirated and the cells were washed twice in PBS to remove any residual traces of medium. Then, cells were fixed for 20 minutes at room temperature using 4 % para-Formaladehyde (pFA). Afterwards, cells were washed in PBS and stained with Hoechst 33258 (1:2000 in PBS) for 2 minutes at room temperature. Residual Hoechst solution was removed by extensive washing. Coverslips were shortly dipped in dH_2O before mounting onto microscopy slides using Mowiol solution. Mycoplasma contamination was examined by fluorescence microscopy.

2.8.4.2 Mycoplasm detection by polymerase chain reaction (PCR)

Mycoplasm detection by PCR (2.12.3) is facilitated by the usage of primer pairs that comprise DNA sequences present in the majority of mycoplasm species.

Protocol:

Reagents	Quantity
Template	1.0 µL
ThermoPol reaction buffer (10x)	5.0 µL
Primer GPO (50 pmol)	0.5 µL
Primer MGSO (50 pmol)	0.5 µL
dNTP's	2.5 µL
Taq DNA polymerase	1.0 µL
dH_2O	37.5 µL
Final volume	50 µL

Table 2.14: Mycoplasm PCR reaction mix

100 µL culture supernatant of cells grown for at least 2 days were collected and boiled at 95°C for 5 minutes to lyse cells and possible mycoplasms. After a quick centrifugation step to pellet debris, the supernatant was transferred into a new reaction tube to be used as the PCR template. PCR was performed according to the program indicated below. Routinely, contaminated cell culture supernatants and dH_2O were included as positive and negative controls, respectively.

PCR program		
Initial denaturation	5 minutes, 95°C	
Denaturation	30 seconds, 95°C	35 ×
Annealing	30 seconds, 55°C	
Elongation	1 minute, 72°C	
Final elongation	5 minutes, 72°C	

Table 2.15: PCR program

PCR samples were then subjected to 1 % agarose gel electrophoresis (2.12.5). Contaminated samples showed a band at 720 bp.

2.8.5 Transient transfection of mammalian cells

The term transfection describes the introduction of foreign DNA into a mammalian cell. A transient – i.e. temporary – transfection has to be discriminated from a stable (permanent) transfection. Depending on the cell line used and/or the desired quantity of transfected cells (transfection efficiency), several methods can be applied with different underlying mechanisms of DNA uptake and delivery.

One can distinguish between DNA uptake

- by endo- or phagocytosis (DEAE-Dextran, PEI, Turbofect)
- by fusion with the cell (Lipofection)
- by diffusion (electroporation)
- by microinjection
- by viral infection

In general, the transfection efficiency depends on the cell lines used and the respective reaction conditions (such as e.g. the concentration of transfection reagent and cell density).

2.8.5.1 Dietheylaminoethyl-(DEAE)-Dextran transfection

The polycation DEAE-Dextran adsorbs to the negatively charged DNA which is thus associated with the high molecular weight structure of dextran. This high molecular weight particle is then endocytosed by the target cells. To avoid subsequent degradation of the DNA within lysosomes, chloroquine is added to the cells which buffers acidic compartments and prevents the activation of acidic hydrolases. DEAE-Dextran was used to transfect plasmid DNA derived from Mini-Preps (2.12.13) to check for correct targeting of positive clones.

Protocol: One day prior to transfection, COS-7 cells were seeded onto glass 18 mm coverslips in a 12 well cell culture dish (1 coverslip per well). For transfection, 2 µL of plasmid DNA were mixed with 500 µL of serum-free DMEM and 3 µL of DEAE-Dextran polymer (50 mg/mL). Cells were washed twice in PBS, as residual serum traces could adsorb to DEAE-Dextran and mediate intracellular toxic effects. The mixture was added to one well of the cell culture plate and incubated for 1.5 hours at 37°C and 5 % CO_2. The DEAE-Dextran mixture

was then replaced by 2 mL of complete medium supplemented with 2 µL of chloroquine (60 mg/mL). The medium was changed again after 3-4 hours. Cells were fixed after 48 hours.

2.8.5.2 Electroporation

In the course of electroporation, the cell membrane is shortly permeabilized due to the electric current applied, thus allowing DNA to diffuse into the cell.

Protocol: Cells of a confluent 100 mm cell culture dish were trypsinized (2.8.1) and pelleted by centrifugation for 5 minutes at 500g. The cell pellet was washed once in 5 mL HEPES-buffered saline (HBS) buffer. Finally, the cell pellet was taken up in 1 mL of HBS before 500 µL cell suspension were mixed with 10 µg of plasmid DNA in a 4 mm electroporation cuvette. Electroporation was carried out at the parameters indicated below. Immediately after the electric pulse, 1 mL of complete cell culture medium was added to the cells to relieve electroporation stress. Cells were resuspended and seeded into cell culture dishes containing pre-warmed culture medium. Cells were fixed 24-48 hours after electroporation. Note that electroporation of AR42J cells was carried out in complete cell culture medium.

Cell line	Voltage	Capacitance	Resistance
AR42J	250V	1500µF	125Ω
CHO	230V	1500µF	125Ω
COS-7	230V	1500µF	125Ω
ΔPex19 fibroblasts	260V	1050µF	100Ω

Table 2.16: Electroporation conditions used

2.8.5.3 Lipofectamine

Lipofectamine transfection is mediated by the use of cationic lipids that contain a positively charged head group combined with up to two hydrocarbon chains. In a hydrophilic environment, a liposomal structure with a positive surface charge is formed. The negatively charged DNA adsorbs to the liposome and forms a complex that adheres to the cell membrane and can be endocytosed.

Protocol: One day prior to transfection, cells were seeded on 18 mm coverslips in 60 mm cell culture dishes. To perform Lipofectamine transfection, 3.2 µg of DNA were mixed with 200 µL of serum-free medium in one reaction tube, while 12 µL of Lipofectamine Transfection reagent were diluted in 200 µL of serum-free medium. Samples from both reaction tubes were pooled and incubated for 30 minutes at room temperature. Cells were washed with PBS and 2 mL of serum- and antibiotic-free medium were added. Finally, the transfection mixture was applied to the cells which were subsequently incubated for 5 hours at 37°C and 5 % CO_2. The

medium was then changed to complete medium and cells were incubated for 24-48 hours before further use.

2.8.5.4 Polyethyleneimine-(PEI)-transfection

The electron-dense PEI - an ethylene-imine-polymer - is a heavily branched, basic molecule whose amino groups are protonated in a hydrophilic environment. The negatively charged DNA backbone binds to the protonated amino groups and is taken up by cellular endocytosis. The high transfection efficiency of PEI transfection is mediated by the "proton sponge effect", as the amino groups of the PEI molecule possess a high buffer capacity in the physiological range. This results in an increased uptake of counter anions (e.g. chloride ions) into the acidic compartments (lysosomes, endosomes) which in turn leads to osmotic swelling and organelle rupture. Thus, DNA is released into the cytoplasm (Akinc et al., 2005).

Protocol: Prior to transfection, cells were seeded on coverslips in a 60 mm cell culture dish. For transfection, 15 µg of plasmid DNA were mixed with 750 µL of sterile 150 mM NaCl solution. In parallel, 100 µl of PEI working solution (0.9 mg/mL) were combined with 650 µL of NaCl solution. Both mixtures were incubated separately for 20 minutes at room temperature, before the PEI solution was added to the DNA mixture in a drop-wise fashion. The combined mixture was incubated for another 20 minutes at room temperature to allow the formation of DNA-PEI complexes. In the meanwhile, the cell culture medium was changed to 2.5 mL of complete medium and ultimately 500 µL of the PEI-DNA mixture was added to the cells. After 3-6 hours of incubation at 37°C and 5 % CO_2, cells were washed once with PBS and medium was exchanged to fresh complete medium. 24- 48 hours after transfection, cells were processed for further experiments.

2.8.5.5 Turbofect

The so-called TurboFect Transfection Reagent is a sterile solution of a cationic polymer in water. This polymer forms compact, stable, positively charged complexes with DNA that are taken up by the cell via endocytosis.

Protocol: One day prior to transfection, cells were seeded on 18 mm coverslips in 60 mm cell culture dishes. For transfection with Turbofect, 4 µg of plasmid DNA were diluted in 400 µL of serum-free medium before 6 µL of Turbofect Transfection Reagent were added. The solution was mixed by pipetting and incubated for 20 minutes at room temperature to allow the formation of DNA-Turbofect complexes. Meanwhile, cells were washed twice in PBS and covered in 3 mL of serum-free medium. At last, the Turbofect transfection mixture was added

drop-wise to the cells and the cells were incubated for 5 hours at 37°C and 5 % CO_2 before the medium was changed to regular complete medium. After 24-48 hours, cells were processed for further experiments.

2.8.6 Generation of stable cell lines

The stable, permanent insertion of a foreign DNA sequence into the cellular genome is referred to as a stable transfection. This procedure occurs naturally in only one of 10^4 cells and can be induced by selective pressure, such as the addition of the antibiotic G418 after transient transfection of a construct carrying the corresponding neomycin resistance marker. As the exact position of insertion into the cell genome occurs spontaneous and unselective, DNA sequences are inserted at different, differentially active sites, resulting in the generation of heterogeneously expressing cell lines. These need to be further subcloned to generate more homogenous cell lines. In line with this, instead of using high copy expression plasmids under the control of a viral CMV promoter, it is advantageous to use more moderate, mammalian expression vectors under the control of e.g. the murine ROSA26 promoter. Upon successful generation of stable cell lines, these can be cultured without the continuous application of selective pressure; however, cells then tend to lose the construct over time. Thus, the generation of early passage cell stocks is recommended. The stable CHO cell lines used in this study (2.7.2) were generated in co-operation with Prof. Dr. Georg Lüers (Universitätsklinikum Eppendorf, Hamburg, Germany).

Protocol: The process of successfully generating stable mammalian cell lines can be subdivided into 4 steps:

- transfection of mammalian cells
- selection in G418
- Selection/subcloning of cell clones
- Validation of plasmid expression

In order to introduce the desired plasmid into the cells, CHO cells were transfected by either lipofection (2.8.5.3) with 1-2 µg of DNA (in a 35 mm cell culture dish) or by electroporation of a 100 mm cell culture dish (2.8.5.2) with 5 µg of plasmid DNA. CHO cells transfected by lipofection were passaged into 100 mm cell culture dishes 24 hours after transfection (2.8.1). Depending on the transfection method used, the selection process was initiated 24 hours after electroporation or 48 hours after lipofection: the cell culture medium was exchanged for 10

mL of complete cell culture medium supplemented with G418 (1:100; Stock: 40 mg/mL). Selection occurred for 10 days in selection medium which was renewed every 2-3 days. After 10 days, surviving cell clones – appearing as visible, round, small cell agglomerates on the cell culture dish – were isolated: the cell culture medium was aspirated and the position of cell clones was marked by labelling with a pen on the cell culture dishes exterior. Selection rings – small metal rings dipped in silicone (ca. 10 mm interior diameter) – were adhered to encircle cell clones. Afterwards cells were covered in PBS and 20 µL of trypsin solution were added to the interior of the selection rings to detach the cell clones. After a short incubation period, 20 µL of cell culture medium were added into the selection ring to resuspend the cell clones. The various selected cell clones were then transferred to the wells of a 24 well cell culture plate in duplicate (1 clone distributed over 2 wells). The cells of one well served to subculture the clone, the other well contained a coverslip to assess the expression of the plasmid by microscopy. Cell clones were then cultured for 2-3 days at 37°C and 5 % CO_2. After 3 days, cell clones on coverslips were fixed for 20 minutes in 4 % pFA at room temperature and mounted on microscope slides. Plasmid expression was assessed by fluorescence microscopy. Several clones were screened for expression regarding the ratio of transfected cells, expression rate and heterogeneity. Cell clones displaying a homogenous, good expression rate of the fluorescent marker were further subcloned. Hence, the clones of the corresponding culture dish were trypsinized, seeded in a low cell density and subjected to another round of G418 selection.

2.8.7 Generation of hybridoma cells*/ in vivo* fusion assay

In order to study the potential fusion of peroxisomes in mammalian cells, an *in vivo* fusion assay was established based on mitochondrial fusion assays (Mattenberger et al., 2003; Niemann et al., 2005). The assay is based on the polytethyleneglykol-(PEG)-based fusion of differentially labelled stably transfected CHO cell lines (2.7.2) after co-cultivation of cells. Upon generation of hybridoma cells, further incubation at 37°C and 5 % CO_2 ensures intermixing of organelles and potential fusion of peroxisomes, resulting in the generation of "yellow" peroxisomes upon fluorescent marker mixing.

Protocol: In order to generate CHO hybridoma cells, differentially labelled CHO cell lines were co-cultured on 18 mm coverslips at a defined density of 1.6 x 10^6 cells/mL in 12 well cell culture dishes and cultivated overnight. After 24 hours, cycloheximide (10 mg/mL stock in dH_2O), an inhibitor of eukaryotic protein translation, was added to fresh complete medium in a final concentration of 50 µg/mL. After 30 minutes of incubation at 37°C, cells were fused on a drop of pre-warmed 50 % (w/v) PEG-6000 in PBS/glucose solution (1 g/L) for 2

minutes. PEG is a chemical inert, water soluble, non-toxic polymer. Highly hydrated, it extracts water out of the contact zone between biological membranes, thus forcing them into a close apposition which in turn generates elastic stress. The stress is subsequently released by hemifusion of the outer bilayers and the formation of fusion pores (Chernomordik et al., 2006). As protein diffusion is hampered by PEG, cells were washed extensively in PBS/glucose and kept in complete cell culture medium with cycloheximide until fixation or imaging.

PEG-6000 solution (50 % w/v)

- 10 g PEG-6000, autoclaved
- 10 mL PBS/glucose solution

2.8.8 Stimulation of peroxisomal fusion with peroxisomal metabolites

To assess if the percentage of interacting peroxisomes could be increased upon stimulating heterogeneity between interacting peroxisomes, CHO-GFP-PTS1 cells were stimulated with peroxisomal metabolites prior to the *in vivo* peroxisomal fusion assay.

Protocol: CHO-GFP-PTS1 cells were stimulated with either 10 µM arachidonic acid (AA) or 400 µM oleic acid (OA) 24 hours prior to the *in vivo* peroxisomal fusion assay (Schrader et al., 1998a; Listenberger et al., 2007). In another set, cells were pre-stimulated with 100 µM H_2O_2 (Schrader et al., 1999). After application of the *in vivo* peroxisomal fusion assay, cells were fixed at the indicated time points and processed for epifluorescence microscopy.

2.8.9 Screen for inducers of peroxisome tubulation and/or proliferation

One objective of this study was to characterize the effects of certain classes of stresses/compounds on peroxisome dynamics.

HepG2 and COS-7 cells were used as a model system to assess peroxisomal (oxidative) stress responses. As previously shown, the well-differentiated human hepatoblastoma cell line HepG2 has a very plastic peroxisome compartment, displaying small spherical (0.1-0.3 µm) and rod-shaped (0.3 µm) peroxisomes as well as elongated-tubular ones (up to 5 µm and more) (Schrader et al., 1994; Schrader et al., 1996a). Usually, 24 hours after seeding the majority of HepG2 cells grown under routine cell culture conditions (2.7.1) contain tubular peroxisomes (around 50 %), complicating the identification of external stimuli leading to peroxisome tubulation. However, the inherent formation of tubular peroxisomes can be almost completely inhibited by culturing under serum-free conditions (DMEM/N1), with

HepG2 cells still demonstrating healthy peroxisome morphology and numerical density. Induction of tubular peroxisomes is restored upon addition of 10 % FBS and growth factors, but also other inducers of tubulation were identified such as arachidonic acid, UV-C irradiation and H_2O_2 (Schrader et al., 1998a; Schrader et al., 1999). The serum-free HepG2 cell culture model was employed in this study to characterize a peroxisomal response to several ROS inducers which generate oxidative stress at different intracellular sites:

- The mitochondrial complex II inhibitor malonate: often used to induce striatal lesions to study ischemic stroke or Huntington's disease, malonate was shown to induce cell death via mitochondrial potential collapse in a ROS-dependent fashion (Fernandez-Gomez et al., 2005).
- the neurotoxin 6-hydroxydopamine (6-OHDA): 6-OHDA is a toxin, widely used to induce lesions in dopaminergic neurons due to generation of ROS (Blum et al., 2001; Bove et al., 2005b; Gomez-Lazaro et al., 2008).
- Heavy metals: ROS have been linked to the toxicity of transition metals by either involving Fenton-like chemistry (e.g. iron, copper) or depletion of glutathione and protein-bound sulfhydryls (nickel, cadmium) (Stohs & Bagchi, 1995).
- Others: the widely-used herbicide paraquat generates superoxide radical upon redox cycling *in vivo* (Bus & Gibson, 1982; Franco et al., 2010). Moreover, direct application of H_2O_2 was chosen to increase cellular oxidative stress (Schrader et al., 1999).

As a control to test reactivity of HepG2 cells, 10 % FCS or AA were added to the cells to induce peroxisome tubulation (Schrader et al., 1998a). Some ROS inducers were further tested in COS-7 cells under regular culture conditions.

In addition to an oxidative stress response, the effect of glucocorticoids on peroxisome dynamics was investigated by employing the rat AR42J model system using dexamethasone at physiological and pathophysiological conditions (2.8.3).

Protocol: Routinely cultured HepG2 cells were trypsinized (2.8.1) and seeded on coverslips in a 60 mm cell culture dish in serum-free DMEM/N1 at a defined density of 2 x 10^5 cells/mL as described previously (Schrader et al., 1998a; Schrader et al., 1999). After 4 hours of incubation at 37°C and 5 % CO_2 to allow attachment and recovery of the cells, different stimuli were applied (see Table 2.17 and 2.18). After application of stimuli, HepG2 cells were incubated overnight in DMEM/N1, until peroxisome elongation reached its maximum after 24 hours. COS-7 cells were seeded as described above (2.8.1).

Cells were fixed in 4 % pFA and processed for immunofluorescence (2.9.1) against peroxisomal markers (Bonekamp et al., 2011b). Induction of peroxisomal tubulation was examined by fluorescence microscopy (2.9.3); upon successful induction replication and statistical analysis was performed (2.9.8). Non-successful inducers were excluded from further studies.

Compound	Concentration	Time
Serum (FBS)	10 %	24 hours
Arachidonic acid (AA)	10 µM	24 hours
Palmitic acid (PA)	10 µM	24 hours

Table 2.17: Tubulation controls employed for the HepG2 assay.

Compound	Concentration	Time	Cell line
6-Hydroxydopamine	50 µM	3, 6, 12, 24 hours	SH-SY5Y
Copper	100 µM	24 hours	HepG2
Dexamethasone	10 nM, 1 µM	6, 24, 48, 72 hours	AR42J
Hydrogen peroxide	100 µM	24 hours	HepG2
Malonate	10 mM 50 mM 100 mM	1, 6, 12, 24 hours	HepG2 COS-7
Menadione	10 µM 30 µM	10, 30 minutes 6, 24 hours	HepG2 COS-7
Nickel	100 µM	24 hours	HepG2
Paraquat	5 µM 10 µM 25 µM 50 µM	6, 12, 24, 48 hours	HepG2 COS-7

Table 2.18: Stresses/compounds screened in this study.

2.8.10 Induction of peroxisome proliferation

Peroxisomes react to the application of certain extracellular stimuli with an increase in the number and size of peroxisomes as well as with the induction of peroxisomal enzymes, a term referred to as peroxisome proliferation (1.2.4). In mammals, peroxisome proliferators encompass fibrates, polyunsaturated fatty acids and hypolipidimic drugs that activate PPARα, especially in rodents (1.2.4) (Pyper et al., 2010). One objective of this study was to screen for stresses/compounds that affect peroxisome morphology (tubulation) and thus potentially induce peroxisome proliferation events. To compare the mechanisms of peroxisome tubulation to action of well-described proliferators, rodent AR42J cells (2.7.1) were treated with described peroxisomes proliferators such as bezafibrate and eicosatetraynoic acid.

2.8.10.1 Bezafibrate

Bezafibrate – like clofibrate and ciprofibrate – is an amphiphatic carboxylic acid that activates PPARα which regulates lipid metabolism and peroxisome proliferation.

Protocol: 7.24 mg of bezafibrate were dissolved in 50 µL of DMSO. Medium was then added to a final volume of 2 mL. The pH was adjusted to pH 7 if necessary. This 0.01 M stock was added to the cells in a 1:1000 dilution. Cells were incubated at 37°C and 5 % CO_2 for 4 days and fresh medium supplemented with bezafibrate was renewed daily.

2.8.10.2 Eicosatetraynoic acid (ETYA)

Polyunsaturated fatty acids (PUFAs) lead to a prominent peroxisome proliferation at physiological levels. ETYA is a non-metabolizable analogue of arachidonic acid that also activates PPARα.

Protocol: 5 mg of ETYA were dissolved in 1 mL DMSO, creating a 16.8 mM stock solution. To induce peroxisome proliferation, a dilution of 1:1000 was prepared in complete cell culture medium. The medium was renewed every day and new ETYA was added over a course of 3-4 days.

2.8.11 Detection of ROS generation using 2′,7′-dichlorodihydrofluorescein diacetate (2′,7′-dichlorofluorescein diacetate; H_2DCFDA)

2′,7′-dichlorofluorescein (DCF) and its derivatives are commonly used to fluorescently detect ROS generation. The different forms of DCF are non-fluorescent until the acetate groups are removed by intracellular esterases and oxidation by ROS occurs within the cell. Upon esterase cleavage of the lipophilic blocking groups, a charged form of the dye is generated that is retained within the cells. Oxidation of these probes and concomitant increase in fluorescence can be detected with a flow cytometer, a microplate reader or a fluorescence microscope, using excitation sources and filters appropriate for fluorescein. In this study, an assay using H_2DCFDA and a TECAN microplate reader was established according to Wang (Wang & Joseph, 1999).

Protocol: A stock of H_2DCFDA (10 mM) was prepared in DMSO and frozen at -20°C. One day prior to the experiment, cells were seeded in a black 96 well cell culture plate with transparent bottom at a density of 10^4 cells/well. Cell stressors (2.8.9) were added for the indicated time points. After incubation, the medium was carefully removed by decanting of the plate and the cells were washed once with PBS. 100 µL of DCF working solution (10 µM in PBS) were added to each well and the cells were incubated for 10 minutes at 37°C and 5 % CO_2 to allow cellular uptake of DCF. The DCF was removed carefully and cells were washed

again once with PBS to remove traces of extracellular DCF. The fluorescence measurement was performed in PBS using a TECAN M200 infinite plate reader (excitation: 485 nm; emission: 530 nm; 37°C). To assess the level of background fluorescence, unlabelled cells and DCF only controls were routinely included in the procedure. In order to ensure that only a few cells were lost during the decanting procedure, centrifugation steps can be added during the labelling procedure (2 minutes, 1300 rpm, table top centrifuge).

2.9 MICROSCOPIC TECHNIQUES

2.9.1 Immunofluorescence

The selective labelling of specific cellular structures using fluorescently-labelled antibodies is referred to as immunofluorescence. Sample preparation for immunofluorescence requires several careful steps: to preserve the cellular structures of interest, cells need to be quickly fixed. Commonly, formaldehydes (e.g. para-formaldehyde or glutaraldehyde) are used to fix cells by reversibly cross-linking primary amino groups in proteins with other nearby nitrogen atoms in other proteins or DNA. However, due to its strong autofluorescence, glutaraldehyde is more often used as a fixative in electron microscopy applications. Alternatively, alcohols and organic solvents can be used which basically dehydrate cells and precipitate proteins while removing lipids (thus simultaneously permeabilizing cell membranes). To enable antibody binding, cell membranes need to be permeabilized by the use of detergents such as Triton-X-100 or digitonin, however, the latter permeabilizes primarily the cell membrane while the peroxisomal membrane remains intact. As there is a high concentration of free aldehyde groups as well as potential epitopes within the cell's protein environment, unspecific antibody binding needs to be avoided by a blocking step (e.g. in bovine serum albumin). Finally, specific antibodies are used to detect the structures of interest. The antibody can be directly coupled to a fluorophore or be labelled in an additional incubation step with a fluorophore-coupled secondary antibody that is directed against the IgG species of the primary antibody (indirect immunofluorescence). For most applications, immunofluorescence against peroxisomal or mitochondrial markers was performed (Bonekamp et al., 2011b).

Protocol: Cells were washed twice in PBS to remove any traces of medium and were fixed for 20 minutes at room temperature in 4 % para-formaldehyde (pFA). Routinely, cells were permeabilized using 0.2 % Triton-X-100 (Tx100) for 10 minutes at room temperature; however, some applications required permeabilization by digitonin (1:400, 1 mg/mL stock) for 5 minutes at room temperature. Unspecific reactions were then blocked using 1 % BSA for 10 minutes at room temperature, followed by incubation with primary and secondary

antibodies for one hour each. Antibody dilutions (2.4) were routinely prepared in PBS and 30 µL were applied on top of the coverslip. Moreover, to avoid antibody evaporation and photobleaching, cells were kept in a humid, dark chamber during incubation. Between the different incubation steps, cells were thoroughly washed with PBS. At the end of the incubation period, cells were washed again in PBS, then carefully dipped in dH_2O to remove salt traces and mounted onto a microscope slide using Mowiol 4-88 as mounting medium. The mounting medium was supplemented with the anti-fading reagent n-propylgallate. Slides were dried and evaluated by fluorescence microscopy.

Note that for experiments requiring differential permeabilization pFA-fixed sets of cells were permeabilized using 0.2 % Tx100, digitonin and methanol (absolute, 5 minutes, room temperature).

2.9.2 Lipid droplet staining

The so-called lipid droplets are the main cellular organelles for the storage of neutral lipids. Previously thought to be inert, their dynamic formation and association with other subcellular organelles such as peroxisomes and the ER has gained considerable interest over the years (Guo et al., 2009). Upon increasing intracellular concentrations of neutral lipid, lipid droplets grow in size and number. The fat-soluble Sudan dyes are frequently employed to stain lipid droplets due their high affinity for fats.

Protocol: For Sudan Black staining of lipid droplets, cells were washed twice in PBS prior to fixation with 4 % pFA (30 minutes at room temperature). After removal of pFA, cells were washed shortly in dH_2O, followed by a short incubation in 50 % ethanol. The Sudan Black staining solution was applied (0.1 % in 70 % ethanol) and lipid droplet staining was performed for 30 minutes at room temperature. After removal of the staining solution, cells were washed in dH_2O and mounted for phase contrast microscopy.

2.9.3 Epifluorescence microscopy

Fluorescence microscopy is based on the principle that fluorophores absorb light of a specific wavelength and emit a fraction of the absorbed light as light of a higher wavelength. Using a combination of different filter sets, co-localization of proteins can be visualized. In epifluorescence microscopy the specimen is illuminated through the objective, using a high energy mercury lamp as a light source. Light of a specific wavelength is then applied onto the specimen by specific filter sets using a dichroic filter and excitation of the fluorophore ultimately leads to fluorescence. The thus emitted light is then collected by the objective and

reflected onto a dichroic mirror where it is focussed through an emission filter onto the ocular to be detected by the eye or a CCD camera.

Protocol: For morphological studies an inverted Olympus IX-81 microscope was used equipped with the appropriate filter combinations and a 100x objective (Plan-Neofluar, 100x/1.40 oil objective). Digital images were acquired with the F-View CCD camera and optimized for brightness and contrast using the Soft Imaging Software and Adobe Photoshop CS2.

2.9.4 Confocal microscopy

Using epifluorescence, the resolution within the z-plane is limited, resulting in the combination/intermixing of signals from different planes within the specimen. Confocal microscopy allows the collection of emission light from only one confocal plane. The Laser generated excitation light is focused onto one point of the specimen by the objective and the emitted light is focussed on a pinhole and detected by a series of photomultipliers. As the focal point and pinhole are in conjugated, so-called confocal, planes, scattered light of other areas/planes is repressed from detection. As only light of a specific point is detected, the specimen needs to be rastered line by line, creating a computer-generated image. By sequential scanning throughout the z-plane, 3 dimensional pictures can be obtained.

Protocol: Confocal images were obtained using a Zeiss LSM 510 Meta confocal setup (Carl Zeiss, Oberkochen, Germany) equipped with Plan-Apochromat 63x and 100x/1.4 oil objectives using the 488 and 561 laser lines, respectively. Images were selected and optimized for brightness and contrast using LSM Image Browser and Adobe Photoshop CS2 software.

2.9.5 Image deconvolution

In imaging, the term deconvolution refers to the process of removing optical distortion (e.g. blurring of signals) from microscopic images using a software algorithm, thus sharpening images. Image stacks of different focal planes are generated and an image is then sharpened by calculating the distortion of the optical system (described by the point spread function, PSF) and the subsequent removal of the equivalent blur from each image. To generate high resolution images of peroxisomal interactions, confocal microscopy in combination with image deconvolution was performed.

Protocol: After application of the *in vivo* peroxisomal fusion assay, cells were fixed and mounted for confocal microscopy using a Leica TCS SP2 AOBS confocal microscope (Leica, Wetzlar, Germany) equipped with a 100x oil objective (PlanApo 100x/1.40 oil objective). Using the 488 and 543 nm laser lines, z-stacks of hybridoma cells were generated with high

zoom setting (8x zoom) using the optimal number of slices suggested by the program (Leica Confocal Software). Oversaturation of signals was avoided by adjusting of respective photomultipliers. Image deconvolution was performed using Huygens Professional Software (Scientific Volume Imaging, Hilversum, The Netherlands). Using the 3D images generated by the program, interacting peroxisomes were assessed for co-localization of signals and mean distance between objects using the tools "co-localization parameters" and "distance to reference objects", respectively. For data analysis, the relative co-localization between green and red peroxisomes was determined to identify true interaction events (co-localization parameters). Subsequently, the distance from the centre of a mass to the nearest surface point (in µm) was determined of those events by using the tool "distance to reference object". 83 different interaction events from 15 different hybridoma cells were evaluated. For calculation of a mean distance between interacting peroxisomes, those events were selected that displayed at least a mutual signal co-localization of 20 % (relColocS: % of intersecting intensity relative to object intensity) and the resulting mean distance was evaluated using Microsoft Excel.

2.9.6 Live cell imaging

In addition to the static, structural characterisation of e.g. protein localization within cells and tissues, the investigation of dynamic cellular processes has become more and more essential in the last two decades, especially due to the high utilization of the green fluorescent protein (GFP) and its analogues. GFP vectors are powerful tools for live cell imaging, as they allow the easy genetic addition of a stable tag with inherent fluorescent properties to any protein of interest. The autofluorescent properties of GFP – isolated from the jellyfish *Aequoria victoria* – are a result of the spontaneous formation of the chromophoric group that is comprised of the side chains of three adjacent amino acids (Ser^{65} – Tyr^{66} – Gly^{67}). Live cell imaging applications include the characterization of cell migration, cell growth, mitosis, metabolic transport or even signal transduction events, however, the various processes differ dramatically in their kinetics, ranging from seconds to days. Thus, when e.g. investigating long time series, the imaging setup demands for maintenance of constant culture conditions (temperature, CO_2, humidity) and the correct focal point. Compromises have to be found regarding detector sensitivity, velocity of image acquisition, signal stability, z-resolution and sample protection.

Protocol: For live cell time-lapse imaging studies, the Zeiss LSM 510 Meta confocal microscope was equipped with a closed chamber (heating insert P) aerated with 5 % CO_2 that allowed the generation of stable culture conditions over the course of the experiment. Cells were seeded into 35 mm glass bottom dishes in complete culture medium without phenol red

to avoid quenching of fluorescent signals. In order to study the effect of ROS generation in shorter time frames in living cells, the genetically encoded photosensitizer KillerRed (Bulina et al., 2006a; Bulina et al., 2006b) was used. Variants of KillerRed targeted either to the cytoplasm, mitochondria or peroxisomes were transfected into COS-GFP cells one day prior to the experiment. To induce generation of free radicals, selected cells were illuminated with green fluorescent light using the mercury lamp and filter sets of the associated microscope. KillerRed bleaches were quickly upon activation and illumination was carried out for twice the duration of photobleaching, following the recommendation of Bulina et al (Bulina et al., 2006b). Time series were subsequently acquired using the 488 laser line and collecting images every minute for 30-60 minutes.

2.9.7 Spinning disk confocal microscopy

Most commonly, confocal high speed spinning disk systems are used to investigate fast processes within the cell such as calcium imaging in real-time, as they allow for a very high rate of image acquisition (up to 400 pictures/second) upon use of one laser line. The so-called Nipkow-systems contain two spinning disks: the first one is equipped with a large number of tiny lenses and located directly behind the laser (source of light) where it simultaneously – due to the high number of lenses – focuses the laser light onto many focal points of the specimen. The other, synchronized spinning disc – which contains thousands of simultaneously rotating pinholes – generates the confocal behaviour, as it collects the emission signal of the many focal points of the specimen in parallel. Basically, the spinning disk system is a confocal microscope acting on many focal points in parallel. In contrast to conventional confocal setups, the emitted light is not detected by a photomultiplier, but by a CCD camera which quickly and simultaneously detects the light of the many pinholes, reducing phototoxicity and photobleaching. However, due to the multiple image acquisition, photobleaching experiments cannot be carried out with a Nipkow system.

Protocol: To investigate peroxisomal fusion events, live cell imaging was performed using a spinning disk confocal system Andor Revolution XD (Advanced light microscope facility, IBMC, Porto under the supervision of Dr. Paula Sampaio) using the 488 and 561 laser lines, respectively. CHO cells were seeded into 35 mm glass bottom dishes in complete culture medium (Ham's F-12) and images were taken after hybridoma generation (2.8.7). Images were acquired from 5 different z-planes (0.5µm thickness) every 5 seconds for 200 frames.

2.9.8 Quantitative evaluation of peroxisome and mitochondrial dynamics

2.9.8.1 Evaluation of peroxisome and mitochondrial fusion in fixed cells

For studies on peroxisomal fusion, the degree of matrix and membrane marker exchange was determined by fluorescence microscopy. Therefore, either matrix or membrane labelled CHO cell lines (2.7.2) were subjected to the *in vivo* fusion assay (2.8.7), cultivated for 2, 4 and 6 hours, fixed and processed for fluorescence microscopy. Images of hybridoma cells were acquired and the total number of peroxisomes per hybridoma cell as well as the number of "yellow" (co-localization of signals) peroxisomes was determined using analySIS software, and the measuring tool "touch count". Fusion of mitochondria was determined under the same experimental conditions using Mito-GFP and Mito-DsRed. As mitochondrial fusion within a cell was already almost complete, the percentage of hybridoma cells with "yellow" mitochondria over the whole coverslip was determined.

2.9.8.2 Analysis of peroxisomal interactions

For quantitative image analysis after spinning disk confocal microscopy, the ImageJ software (v1.45a, NIH, MD, USA) was used. The number of either green or red peroxisomes per cell was determined using the PlugIn Particle counter. For analysis of peroxisomal interactions, Image5D stacks of time lapse images were generated and frame-by-frame analysis was performed for every z stack. Interactions – defined as the close apposition of two differentially labelled peroxisomes - and their dynamic behaviour were followed over the course of the experiment. The duration of the interactions, the number of peroxisomes involved and the number of re-engagements of the peroxisomes involved was assessed. In total, 425 interaction events from image stacks of 15 different hybridoma cells (n = 3) were analyzed. To analyze the kinetics of peroxisomal interactions, the duration of the interactions between individual peroxisomes and the duration of complete signal overlay was determined for every peroxisomal interaction evaluated (n = 903). The frequency of contacts lasting longer or equal than a certain duration was evaluated as a cumulative frequency plot against time using Microsoft Excel. Detailed mathematical analysis of the observed peroxisome interactions was performed by Dr. Fernão Vistelo de Abreu (University of Aveiro, Portugal) (8.1.1.1). Moreover, a simple computational model was developed to address the question whether the fraction of peroxisomes engaging in ATP driven motility has been optimized to promptly homogenize the peroxisomal population within a cell at a minimal energy expense.

To analyze the number of peroxisomal interactions after fatty acid or ROS stimulation (2.8.8), images of hybridoma cells were evaluated using ImageJ (tool: cell counter) and the number of

green and red peroxisomes was determined as well as the number of interacting/attaching peroxisomes (defined as “yellow” ones and those attached to each other). Data is taken from 3-4 independent experiments (10-15 cells/condition) and data analysis and presentation was performed using Microsoft Excel software. Data is presented as means +/- standard deviation (SD). An unpaired t-test was used to determine statistical differences between experimental groups. P-values < 0.05 are considered significant and P-values < 0.01 are considered highly significant.

2.9.8.3 Quantification of peroxisome morphology

For quantification of peroxisome morphology, peroxisomes were categorized as displaying either a spherical or rod-shaped or tubular morphology (Schrader et al., 1994; Schrader et al., 1996a). 100 cells per coverslip (2-4 coverslips per condition) were categorized accordingly and experiments were performed 2-3 times. Data analysis and presentation was performed using Microsoft Excel software. Data is presented as means +/- standard deviation (SD). An unpaired t-test was used to determine statistical differences between experimental groups. P-values < 0.05 are considered significant and P-values < 0.01 are considered highly significant.

2.10 BIOINFORMATIC SCREENING TOOLS

2.10.1 *In silico* determination of transmembrane domains

In the course of this study, the membrane topology of the peroxisomal biogenesis factor Pex11pβ was investigated. For initial determination of potential transmembrane domains the following databases/tools/servers were used to screen the protein sequence (UniProtKB: O96011, PX11B_HUMAN):

- UniProt: http://www.uniprot.org/
- SOSUI: http://bp.nuap.nagoya-u.ac.jp/sosui/
- Toppred tool, Mobyle@Pasteur: http://mobyle.pasteur.fr/cgi-bin/portal.py#welcome
- HMMTOP: http://www.enzim.hu/hmmtop/
- TMPred: http://www.ch.embnet.org/software/TMPRED_form.html
- TMHMM Server, v 2.0: http://www.cbs.dtu.dk/services/TMHMM/
- PredictProtein: http://www.predictprotein.org/
- Split 4.0 server: http://split.pmfst.hr/split/4/

For calculation of protein fragment size after proteinase K digest, peptide mass was calculated using PeptideMass (http://web.expasy.org/peptide_mass/).

2.10.2 *In silico* determination of potential phosphorylation sites

Up until now, only little is known about the potential phosphorylation of the mammalian peroxisomal biogenesis factor Pex11pβ. Strongest evidence was obtained for the Pex11 protein of the yeast *S. cerevisiae* (Knoblach & Rachubinski, 2010), however, the yeast and human proteins differ considerably. The following databases were used to screen for either phospho-sites within the human Pex11pβ sequence (UniProtKB: O96011, PX11B_HUMAN) or potential binding sites for kinases:

- KinasePhos 2.0: http://kinasephos2.mbc.nctu.edu.tw/index.html
- NetPhos 2.0: http://www.cbs.dtu.dk/services/NetPhos/
- DISPHOS: http://core.ist.temple.edu/pred/pred.html
- NetPhosK: http://www.cbs.dtu.dk/services/NetPhosK/
- Scansite MotifScan: http://scansite.mit.edu/motifscan_seq.phtml
- ScanProsite: http://expasy.org/tools/scanprosite/
- ELM: http://elm.eu.org/

Alignment of Pex11pβ protein sequences from different species was performed using the ClustalW2 tool (http://www.ebi.ac.uk/Tools/msa/clustalw2/).

2.11 BIOCHEMICAL METHODS

2.11.1 Preparation of peroxisome-enriched fractions

In order to isolate organelles from intact cells, they have to be released by homogenisation procedures. To guarantee the extraction of intact organelles, adequate buffer conditions and the use of protease inhibitors have to be ensured. The heterogeneous homogenate can be further separated by differential centrifugation which is based on the principle that particles in liquid medium migrate according to their density and sedimentation coefficient. Hence, cell nuclei and debris sediment relatively fast, while mitochondria, peroxisomes and microsomes only follow at higher velocities. The resulting fractions can be further purified using density gradient centrifugation.

Protocol: To prepare peroxisome-enriched fractions, cells of 4 confluent 100 mm cell culture dishes were washed twice with PBS before cells were scraped carefully from the dish surface in 1 mL of PBS using a rubber policeman. The combined cell suspensions of 4 cell culture

dishes were collected in a 15 mL reaction tube and pelleted by centrifugation using a table top centrifuge (500g; 5 minutes; room temperature). The supernatant was discarded, the cell pellet was resuspended in 1 mL of peroxisome homogenisation buffer supplemented with protease inhibitors and then transferred to a 2 mL reaction tube. Cells were subsequently homogenized using a 1 mL syringe equipped with a 26G needle. The resulting homogenate was centrifuged again at 500g for 5 minutes at 4°C. The supernatant was collected and the pellet was homogenized again in another 500 µL of peroxisome homogenisation buffer. Both supernatants were pooled and the resulting 500g pellet – containing cell debris and nuclei – was discarded. The 500g supernatant that contains cytosol and intact cell organelles was then centrifuged for 10 minutes at 2.000g at 4°C to pellet heavy mitochondria. Next, the resulting 2.000g supernatant fraction was transferred to a 50 mL Beckman centrifugation tube and centrifuged for 25 minutes at 4°C and 25.000g (Beckmann Avanti-J251). The final pellet contained mitochondria, peroxisomes and microsomes. The supernatant was discarded and the pellet was resuspended in 100 µL of peroxisome homogenisation buffer for further experiments.

Highly purified peroxisomal fractions were prepared as described previously and kindly provided by PD Dr. Markus Islinger (University of Aveiro, Portugal) (Völkl et al., 1996).

2.11.2 Preparation of cell lysates

In order to analyze the cellular protein content biochemically, cell lysates of various mammalian cell lines were routinely generated (e.g. to determine expression of a protein of interest).

Protocol: Cells of one confluent 100 mm cell culture dish were washed twice with PBS to remove any traces of medium. Next, 500 µL of lysis buffer (2.6) supplemented with protease inhibitors were added to the cells and the cells were scraped off the culture dish using a rubber policeman. Lysates were transferred to a 1.5 mL reaction tube and incubated for 20 minutes at 4°C with overhead rotation to guarantee complete rupture and lysis of cells and organelles. Subsequently, lysates were further homogenized using a 1 mL syringe equipped with a 26G needle to shred the liberated, denatured DNA. Finally, cell lysates were centrifuged for 15 minutes, at 4°C at 13.000rpm in a table-top centrifuge to pellet cell debris and DNA. The resulting supernatant was transferred into a new 1.5mL reaction tube.

2.11.3 Triton-X-100 (Tx100) extraction assay

To assess the Tx100-mediated removal of the peroxisomal membrane protein Pex11pβ from the peroxisomal membrane biochemically, a Tx100-based extraction assay was designed.

Protocol: COS-7 cells were transfected with myc-tagged variants of Pex11pβ prior to the experiment and seeded in 100 mm cell culture dishes. After the indicated time points, the cell culture medium was aspirated and cells were fixed using 4 % pFA for 20 minutes. Subsequently, cells were washed and 1.5-2 mL of 0.2 % Tx100 was added to the cells. After 10 minutes, the Tx100 supernatant was collected in a reaction tube and centrifuged for 15 minutes at 13.000 rpm and 4°C to remove cell debris. In parallel, the corresponding fixed COS-7 cells were lysed (2.11.2). The protein concentration of both Tx100 supernatant and cell lysate was determined (2.11.5) and sufficient amounts of protein were precipitated for downstream applications (2.11.4).

2.11.4 Protein precipitation

To remove traces of detergent and/or to concentrate the sample, protein precipitation was performed.

2.11.4.1 Methanol-Chloroform precipitation (Wessel & Flugge, 1984)

Protocol: 4 volumes of methanol p.a. were added to 1 volume of sample. The mixture was vortexed and 1 volume of chloroform was added. The sample was mixed again by vortexing, 3 volumes of dH_2O were added and centrifuged at 13.000 rpm for 3 minutes at room temperature in a table-top centrifuge. After centrifugation, two phases can be distinguished; the proteins accumulate as a white interphase between those. The upper watery phase was discarded, 3 volumes of methanol were added and the sample was centrifuged as indicated above after thorough mixing. A white protein pellet was formed which was dried at room temperature, taken up in Lämmli sample buffer after drying and boiled at 95°C for 5 minutes.

2.11.4.2 Trichloroacetic acid (TCA) precipitation

Protocol: 1 volume of 20 % TCA solution was added to 1 volume of protein and incubated for 30 minutes on ice. The mixture was then centrifuged for 15 minutes at 13.000 rpm and 4°C in a table-top centrifuge upon which a white protein pellet was formed. The supernatant was discarded and the pellet was washed twice with 1 mL of acetone, incubated for 5 minutes on ice and centrifuged again. Finally, the acetone supernatant was removed, the pellet was dried at room temperature and taken up in Lämmli sample buffer. To facilitate dissolution of the

protein pellet, the sample was incubated with shaking for 20 minutes at room temperature and then boiled at 95°C for 5 minutes.

2.11.5 Determination of protein concentration according to Bradford

The colorimetric determination of the protein concentration according to Bradford (Bradford, 1976) is based on the reaction of functional groups of proteins with a colour-forming reagent, in this case the blue acidic dye Coomassie Brilliant Blue, which binds unspecifically to cationic and unpolar, hydrophobic amino acid side chains. In an acidic protein environment, the absorption maximum of the dye shifts from 465 nm to 595 nm as the unprotonated, sulphated form of the dye is complexed and stabilized. The intensity of the resulting colour switch is proportional to the protein concentration and can thus be quantified by spectrophotometry.

Protocol: To generate a standard curve, defined amounts of standard (BSA, 1 mg/mL) were filled up to a final volume of 100 µL with 0.1 M NaOH in a 1.5 mL reaction tube. 2 µL of the sample were treated equally and standards as well as sample were supplemented with 1 mL Bradford reagent (1:5 in dH_2O). Samples were incubated for 15 minutes at room temperature and measured in a table top spectral photometer at 595 nm against a blank. Measurement was performed in duplicate.

2.11.6 One dimensional polyacrylamide gelelectrophoresis (SDS-PAGE)

The term electrophoresis is defined as the migration of charged particles in an electric field. Different charges and sizes of particles result in a different electrophoretic mobility. Using SDS-PAGE, proteins within a matrix of polyacrylamide are separated according to their size. The gel matrix is formed by chemical co-polymerisation of acrylamide monomers with a cross-linker (N, -N,-Methylenebisacrylamide, BIS). The polymerisation reaction is started due to a chain reaction initiated by the disintegration of peroxide sulphate ions. The generated radicals activate TEMED which initiates the cross link of the monomers. As oxygen leads to termination of the chain reaction, a vertical gel stand is used, excluding as much oxygen as possible. Due to slow ongoing polymerization, the gels are cast one day prior to use. The anionic detergent SDS is usually added to gel mixture, as it covers the auto-charge of proteins so that particles with a constant negative charge are formed which are solely separated according to their size. Upon sample preparation in Lämmli sample buffer tertiary and quarternary structures of proteins are dissolved by boiling. Reducing thiol compounds (e.g. DTT or 2-mercaptoethanol) break inter-protein disulfide bonds. Routinely, a standard discontinuous electrophoresis system according to Lämmli (Laemmli, 1970) was used that

combines a tightly meshed resolving and a loosely meshed stacking gel. The use of a stacking gel avoids protein aggregation, resulting in better band separation. A Tris-Cl/Tris-glycine buffer system was used: the pH of the stacking gel is close to the isoelectric point of the amino acid glycine, thus glycine migrates more slowly within the gel. The chloride ions on the other hand migrate very fast ("leading ion"). The applied proteins migrate between those. If an electric field is applied, all ions within this discontinuous system migrate with the same velocity. Consequently, as migration velocity is proportional to electrical field strength and mobility, an area of lower field strength is formed around the ions with higher mobility and vice versa. Due to the subsequent formation of an electrical field gradient along the protein ions, those form a stack of protein ions according to their mobility (the protein ions with the highest mobility directly follow the leading ion and so forth). Upon entering the more tightly meshed resolving gel, migration of proteins, but not glycine is hindered, leading to the formation of a homogenous buffer and a migration according to protein sizes.

Protocol:

	Stacking gel	**Separation gel**		
	5 %	7.5 %	12.5 %	15 %
30 % Polyacrylamide	1.66 mL	4.0 mL	6.67 mL	8.0 mL
2 M Tris pH 8.8	-	2.89 mL	2.89 mL	2.89 mL
1 M Tris pH 6.8	1.25 mL	-	-	-
20 % SDS	50.0 µL	80.0 µL	80.0 µL	80.0 µL
dH_2O	6.95 mL	8.89 mL	6.22 mL	4.89 mL
TEMED	10.0 µL	8.0 µL	8.0 µL	8.0 µL
10 % APS	80.0 µL	48.0 µL	48.0 µL	48.0 µL
Total volume	10.0 mL	16.0 mL	16.0 mL	16.0 mL

Table 2.19: Gel solutions for SDS-PAGE

Routinely, 12.5 % or 15 % polyacrylamide gels were cast. The various parts of the gel apparatus were cleaned with water and 70 % ethanol and assembled. The resolving gel was cast between the glass plates and covered with isopropanol to exclude oxygen during the polymerization reaction. When polymerization was complete, isopropanol was removed by decanting and the stacking gel was cast onto the resolving gel. Quickly, a comb was inserted to allow sample pocket formation. The fully polymerized gel was kept in a wet chamber at 4°C until use. Samples were taken up in Lämmli sample buffer, boiled for 5 minutes at 95°C or 20 minutes at 65°C, quickly centrifuged and loaded onto the gel. To determine protein size, a protein marker standard was included. Electrophoresis was performed in SDS Running Buffer at an initial voltage of 80 V and then at 120 V (400 mA, 100 W).

2.11.7 Immunoblotting

The term immuno- or western blotting refers to a transfer of proteins onto a carrier membrane followed by immnunodetection. Thus, proteins separated by SDS-PAGE are fixed. In electroblotting, the process is assisted by an electric field (Towbin et al., 1992). Routinely, a semi-dry blotting procedure according to Kyhse-Andersen (Kyhse-Andersen, 1984) was used. The blotting system is comprised of two plate electrodes in between which the blot sandwich - consisting of Whatman filters soaked in buffer, the polyacrylamide gel and the nitrocellulose membrane - is placed. Upon initiation of blotting, an electrical field is formed perpendicular to the gel layer and proteins migrate in the direction of the positively charged anode onto the membrane. SDS migrates faster than the proteins and is thus separated from those. Hydrophobic interactions between the proteins and the nitrocellulose membrane then lead to membrane adhesion of the proteins. This interaction is facilitated by the methanol-containing blotting buffer.

Protocol: Whatman filter papers and nitrocellulose membranes were cut to gel size and soaked in blotting buffer. The blot sandwich consisting of filters, gel and membrane was assembled onto the plate electrodes of the semi-dry blotting machine. Protein transfer occurred at 12 V (400 mA, 100 W) for 45 minutes.

2.11.8 Ponceau S staining

In order to control successful transfer of proteins after western blotting, a Ponceau S staining was performed. Ponceau S is a red diazo dye that binds reversibly to the positively charged amino groups of proteins that can be easily washed off the nitrocellulose membrane after detection.

Protocol: After western blotting, the nitrocellulose membrane was transferred into a plastic dish and covered in some millilitres of Ponceau S solution (0.1 % in 5 % acetic acid). After careful shaking, the protein pattern could be distinguished as pinkish-red bands on the nitrocellulose. If necessary, the membrane was cut into pieces along the band margins. The excess Ponceau S solution was recollected again for further use and the nitrocellulose membrane was washed with dH_2O to remove the stain.

2.11.9 Enhanced chemiluminescence (ECL) for detection of proteins

The transferred proteins of interest are selectively detected by an antibody-based immune reaction with a peroxidase-linked secondary antibody. Quantification of proteins occurs by the ECL reaction: the indirectly coupled peroxidase catalyses the oxidation of luminol which

is excited to a higher energy level (excited state). Upon return to the stationary state, photons are emitted (chemiluminescence) that blacken the light-sensitive ECL film. The reaction is enhanced by phenols in one of the two solutions.

Protocol: After transfer upon nitrocellulose and Ponceau staining, the membrane was incubated in a solution of 5 % skimmed milk (in PBS) for 1 hour at room temperature to block unspecific binding of the antibody. Primary antibody incubation was either performed for 3 hours at room temperature or over night at 4°C with overhead rotation. Residual traces of primary antibody were removed by washing with PBS. Next, the blot membrane was incubated with a peroxidase-coupled secondary antibody for 45 minutes at room temperature. After several more washing steps, the ECL solutions 1 and 2 were mixed (1:1) and incubated for 3 minutes with the blot membrane. Detection of signals was performed in a dark room on light sensitive films. Exposure times were adjusted depending on the strength of the signal.

2.11.10 Removal of antibodies from western blots (Stripping)

Stripping is the colloquial term used to describe the removal of primary and secondary antibodies from a western blot membrane which is necessary, if, for instance, one wants to investigate another protein of similar size on the same blot. The bound primary and secondary antibodies are denatured by the use of detergents and thiol compounds and subsequently removed by extensive washing.

Protocol:

Stripping buffer (final concentrations)

- 2 % SDS
- 62.5 mM Tris-HCl, pH 6.8
- 100 mM 2-mercaptoethanol

The nitrocellulose membrane was incubated in an excess of stripping buffer for 30 minutes at 60°C with shaking. Next, the stripped blot was washed twice in TBS-T for 10 minutes at room temperature and then re-blocked in skimmed milk (5 % in TBS-T).

2.11.11 Immunoprecipitation (IP)

Using a so-called immunoprecipitation, proteins can be isolated – *de facto* precipitated – from a complex protein mixture using specific antibodies against the protein itself or an epitope tag. In order to accelerate pelleting of the antibody-antigen complex which would normally require the optimal ratio between antigen and antibody to allow maximum complex

formation, a sepharose matrix covered with protein A (PAS) from *Staphylococcus aureus* is commonly used. Protein A binds specifically to the constant chains of IgG antibodies and in combination with heavy sepharose serves to pellet the protein of interest more easily. To reduce unspecific binding of PAS within the protein environment of a cell lysate, a so-called pre-clearing is performed in which PAS is added to the lysate and pelleted by centrifugation before the addition of the specific antibody. After immunoprecipation and pelleting of the sepharose beads, several washing steps are carried to remove unspecific contaminants.

2.11.11.1 Radio-immunoprecipitation to validate cycloheximide efficiency

To determine the validity of the cycloheximide mediated import block within our peroxisomal *in vivo* fusion assay, a pulse-chase assay was established. The term "pulse-chase" refers to experiments in which the transport/fate of proteins is investigated over time. First, protein synthesis is arrested by depriving cells of the essential amino acid methionine in methionine-free medium. After addition of the radioactively labelled methionine, translation is allowed to resume and a pool of newly synthesized, radio-labelled protein is generated. However, upon addition of cycloheximide, translation should still be terminated, thus no new, radioactive pool of protein is generated. The stable cell line CHO-GFP-PTS1 was used in this study and the IP was performed against GFP to assess efficient translation arrest.

Protocol: CHO-GFP-PTS1 cells were pre-incubated for 1 hour in methionine-free DMEM supplemented with 10 % FBS and were afterwards pulse-labelled for 2 and 4 hours in fresh medium containing [S^{35}]methionine (35 µCi) in the presence or absence of 50 µg/mL cycloheximide. Afterwards, cells were lysed in radio-immunoprecipitation buffer containing protease inhibitor mix and a pre-clearing with PAS was performed (3-6 hours) to minimize unspecific binding. Immunoprecipitation was performed with polyclonal anti-GFP antibody (1:666). To precipitate antigen-antibody complexes 20 µl of a 50% slurry of PAS was added to 500 µL of lysate and incubated with mixing overnight at 4°C. The beads were then pelleted, washed extensively with 3 x 1mL wash buffer 1 and 3 x 1 mL high salt wash buffer 2 (2.6). The immunoprecipitates were solubilized in Lämmli sample buffer, and subjected to 12.5 % SDS-PAGE. Phospho-images of dried gels were analyzed using a FLA-3000 phosphoimager and GelProAnalyzer 4.0 software.

2.11.11.2 Radio-immunoprecipitation to determine protein phosphorylation (*In vivo* phospholabelling)

To determine the phosphorylation status of the peroxisomal biogenesis factor Pex11pβ, *in vivo* phospholabelling against a YFP-tagged version of the protein was performed. APP-GFP and empty YFP-C1 vector served as positive and negative controls, respectively. The basic principle of the assay is as follows: cells expressing the above mentioned constructs are starved in phosphate-free Krebs-Ringer buffer and then pulse-labelled with an excess of the highly radioactive P^{32} orthophosphate that is subsequently equilibrated into cellular ATP/GTP pools and incorporated into proteins upon phosphorylation. Upon immunoprecipitation against the epitope tag, here GFP, the proteins of interest are pulled down and can be investigated for incorporation of radioactive phosphate after SDS-PAGE.

Protocol: 48 hours prior to the phospholabelling, COS-7 cells (2 × 100 mm cell culture dishes per condition) were transfected with the proteins of interest (APP-GFP, YFP-C1, YFP-Pex11β) by electroporation (2.8.5.2). In order to deplete intracellular phosphate pools, the cell culture medium was aspirated and the cells were washed 3 times in phosphate-free Krebs-Ringer buffer before 5 mL of Krebs-Ringer buffer were added to each dish. Cells were incubated at 37°C and 5 % CO_2 for 2 hours. Afterwards, cells were washed once and 2-3 mL of phosphate-free Krebs-Ringer buffer were added. Cells were then pulsed by the addition of 50 µCi/mL of P^{32} orthophosphate and incubated for 4 hours at 37°C with shaking. Subsequently, the radioactive buffer was removed and cells were washed once in washing buffer (20 mM HEPES, pH 7.4, 150 mM NaCl) before 500 µL of radio-immunoprecipitation buffer supplemented with protease inhibitor mix and phosphatase inhibitors (2 mM sodium orthovanadate, 50 mM sodium fluoride) was added to the cells. Cells were scraped off the culture dish and lysates of the 2 corresponding 100 mm cell culture dishes were pooled in a 2 mL reaction tube. Lysates were rotated 20 minutes at 4°C to guarantee complete cell and organelle lysis and then centrifuged for 15 minutes at maximum speed in a table top centrifuge. The supernatant was transferred into a new 1.5 mL reaction tube. For pre-clearing, 30 µL of PAS were added to the lysates and rotated at 4°C for at least 2 hours. To pellet the PAS beads, lysates were centrifuged for 2 minutes at 5.000 rpm in a table top centrifuge and the supernatant was transferred to a new reaction tube. 1.5 µL of polyclonal anti-GFP antibody were added to each of the samples, followed by further incubation with rotation at 4°C for more 30 minutes before 50 µL of PAS were added to the mixture. Incubation occurred overnight at 4°C with rotation. The next day, immunoprecipitates were pelleted by centrifugation at 5.000 rpm and 4°C in a table top centrifuge. PAS beads were washed twice

in IP washing buffers 1 and 2 to reduce unspecific binding and after a final spin at 5.000 rpm for 5 minutes, PAS beads were taken up in 30 µL of 3 x Lämmli sample buffer. The denatured proteins and antibodies are thus removed from the sepharose beads. Samples were boiled for 5 minutes at 95°C, shortly centrifuged to pellet beads and loaded onto a 12.5 % SDS gel. After SDS-PAGE, the gel was fixed and dried for 2-3 hours using a BioRad gel drying unit. The radioactive gel was exposed on a phospho-imaging screen for 2-3 days. Phospho-imaging was performed using a BioRad Molecular FX scanner.

Krebs-Ringer Buffer (phosphate-free)

- 118 mM sodium chloride
- 4.75 mM potassium chloride
- 1.2 mM magnesium chloride
- 0.26 mM calcium chloride
- 25 mM sodium bicarbonate

2.11.12 Proteinase K digest

Proteinase K (or endopeptidase K) is a highly reactive serine protease that was isolated from the fungus *Tritirachium album.* Interestingly, it is stable over a broad range of pH and temperature and various concentrations of buffer salts and detergents. Even in the presence of 0.1-0.5 % SDS it retains its activity, rendering it a useful tool for the inactivation of nucleases in DNA preparations and the determination of protein topology on (intra)cellular membranes. To determine membrane protein topology, protein samples and untreated controls are incubated with proteinase K. The parts of the protein that are accessible to the protease will be cleaved into fragments, while membrane protected parts will remain intact. The resulting changes in the size of detectable protein bands yield a certain pattern from which the protein topology can be concluded. As a control, samples will also be digested in the presence of detergents (or otherwise permeabilized membranes) which results in the complete digest of the protein.

Protocol: In this study, proteinase K digest was carried out on overexpressed peroxisomal membrane proteins, therefore two days prior to the experiment, cells were transfected to yield 4 confluent 100 mm cell culture dishes at the day of the experiment. Routinely, untransfected cells were included as controls to rule out any antibody artefacts. On the day of the experiment, peroxisome-enriched fractions were prepared out of the cells of 4 confluent 100

mm cell culture dishes to increase the concentration of the protein of interest (2.11.1). The crude peroxisome pellet was taken up in 100 µL of peroxisome homogenization buffer (Azevedo protocol) without the addition of protease inhibitors which would compromise further digest. A Bradford assay was performed to determine protein concentration (2.11.5) and for each condition, 3 samples were prepared: 60 µg of protein was transferred into a reaction tube, for the untreated control the sample was filled up to a volume of 50 µL with homogenisation buffer. Proteinase K was added to the other samples (25 µL of a 2 mg/mL stock) in the presence or absence of 1 % Tx100. Additionally, as an alternative to Tx100 permeabilization, peroxisomal membranes were ruptured by sonication (3 × 10 seconds, 100 W, on ice). The proteinase K digest was carried out for 30-45 minutes on ice and then stopped by the addition of PMSF (5 mM final concentration). All samples were brought to a volume of 100 µL with homogenisation buffer and a TCA precipitation was performed (2.11.4.2). Protein pellets were dissolved in 3x Lämmli sample buffer and run on 12.5-15 % polyacrylamide gels.

Peroxisome homogenisation buffer (Azevedo protocol)

- 20 mM MOPS-KOH pH 7.4
- 250 mM Sucrose
- 1 mM EDTA-NaOH pH 7.4

Proteinase K

- Stock: 2 mg/mL in 20 mM MOPS-KOH, pH 7.4

2.11.13 Carbonate treatment

To weaken and disrupt the ionic bonds/interactions and thus extract peripheral membrane proteins, solutions of extreme ionic strength or pH can be incubated with cellular membranes. In this study, peripheral membrane proteins were removed by a solution of 500 mM Na_2CO_3, pH 11.5 (Fujiki et al., 1982).

Protocol: To yield a sufficient amount of protein, cells were usually transfected to express the protein of interest and peroxisome-enriched fractions were prepared out of 8 confluent 100 mm cell culture dishes per condition. Routinely, also untransfected cells were used as controls. The crude peroxisome pellet was resuspended in 100 µL of peroxisome homogenization buffer (with protease inhibitor mix) and split into two samples (Control and

carbonate-treated fraction). The control sample was diluted 1:5 in peroxisome homogenisation buffer and the carbonate-treated fraction was diluted 1:5 in ice-cold sodium carbonate solution (500 mM Na_2CO_3, pH 11.5). Both fractions were incubated for 30 minutes on ice with gentle shaking every 5 minutes. The samples were centrifuged in an Optima LE-80K Ultracentrifuge (Ti 80 rotor; Beckman Coulter) at 50.000 rpm (223 000g) for 1 hour at 4ºC. The resulting pellet fractions correspond to the membrane fraction (containing integral membrane proteins) and – in the case of the carbonate-fraction – the supernatant contains the extracted peripheral membrane proteins. The pellet was resuspended in peroxisome homogenization buffer and protein concentrations of all fractions were determined (2.11.5) prior to SDS-PAGE (2.11.6) and immunoblotting (2.11.7).

2.12 MOLECULAR BIOLOGY TECHNIQUES

2.12.1 Extraction of total RNA from mammalian cell lines

Isolation of total RNA from mammalian cell lines was routinely performed to generate cDNA template for subsequent cloning purposes or to assess differences in the expression pattern of key peroxisomal biogenesis factors after stimulation.

2.12.1.1 RNA-extraction using RNeasy Mini Kit (Qiagen)

A commercially available RNA extraction kit (RNeasy Mini Kit, Qiagen) was regularly used to extract total RNA from human HepG2 cells for cloning purposes. The collected HepG2 cell pellets were resuspended in buffer containing guanidinium isothiocyanate and 2-mercaptoethanol that leads to a complete denaturation of the cell and organelle membranes, including the nucleus. 2-mercaptoethanol serves as an RNAse inhibitor. Subsequent homogenisation of the viscous solution with a 20G syringe needle guarantees shredding of genomic DNA and other cellular components, yielding a more homogenous solution to be applied to the extraction columns. The addition of ethanol improves the selective binding of the negatively charged RNA molecules to the positively charged silica matrix of the extraction column. Contaminants are removed in consecutive washing steps and the total RNA can be eluted.

Protocol: The cell pellet of 1.5 confluent 100 mm cell culture dishes was carefully resuspended in the supplied buffer (supplemented with 2-mercaptoethanol, according to the manufacturer's instructions) and homogenized using a syringe and a 20G needle. RNA extraction was carried out according to the manufacturer's instructions. RNA was eluted in 30

µL of the supplied RNAse-free water. After determination of RNA concentration (2.12.14), RNA was aliquoted and frozen at -80°C.

2.12.1.2 RNA extraction using TriFast (PeqLab, (Chomczynski & Sacchi, 1987))

The so-called TriFast reagent from PeqLab (or the analogous TriZol from Invitrogen) allows the simultaneous isolation of RNA, DNA and protein from cells and tissues of various origins (animal, plant, bacterial, yeast). The supplied TriFast solution contains the organic solvent phenol and guanidinium thiocyanate to lyse cellular membranes. Upon lysis, chloroform is added and after subsequent centrifugation the homogenate separates into three phases – the upper aqueous phase contains RNA, the white interphase DNA and the organic phase proteins. The upper RNA phase is then carefully transferred into a new reaction tube and RNA is precipitated using isopropanol. After washing and drying, the RNA pellet is resuspended in RNAse-free water. TriFast extraction was routinely used to extract RNA from AR42J cells to determine regulation of key peroxisomal biogenesis factors in subsequent semi-quantitative PCR (2.12.4).

Protocol: Cells of a confluent 60 mm cell culture dish were harvested by trypsinization (2.8.1) and pelleted by centrifugation in a 1.5 mL reaction tube. For homogenization, 500 µL of TriFast were added and the lysate was passed several times through the pipette tip before incubation for 5 minutes at room temperature to guarantee complete lysis. For phase separation, 100 µL of chloroform were added and the tube was shaken vigorously by hand for 15 seconds. After a further incubation step for 5 minutes at room temperature, homogenates were centrifuged for 15 minutes at 12.000g and 4°C in a table top centrifuge. The upper RNA phase was carefully transferred into a fresh 1.5 mL reaction tube. To facilitate RNA precipitation, 3 M sodium acetate, pH 4.5 was added to the RNA solution (1:10 of final volume) before 3 volumes of 100 % ethanol p.a. were added to one volume of the solution to precipitate RNA. The mixture was incubated at -20°C for at least 30 minutes and centrifuged for 15 minutes at 12.000g and 4°C upon which a faint RNA pellet is formed at the bottom of the tube. The pellet was washed twice in 500 µL of 75 % ethanol (in RNAse-free water) and then air-dried at room temperature. Usually, the RNA pellet was then resuspended in 30 µL of RNAse-free water and stored at -80°C until further use.

2.12.2 Reverse Transcription (cDNA synthesis)

To be used as template DNA for PCR applications, the extracted total RNA has to be transcribed into cDNA – i.e. DNA that is complementary to the mRNA sequence. In this study, a reverse transcriptase originating from the moloney-mouse-leukemia virus (MuLV RTase) was used. To initiate polymerization and to isolate the desired mRNA, a so-called OligodT primer – consisting of 15 thymidine nucleotides, hence the name - was employed which binds complementary to the poly-A-tail characteristic for the 3' end of mRNA.

Protocol:

Reagent	Volume
Total RNA	3.0 µg
OligodT primer (100 µM)	2.8 µL
dNTP's (10 mM each)	0.5 µL
10 × M-MuLV reverse transcription buffer	3.0 µL
RNAse Inhibitor (40 U/µL)	0.5 µL
M-MuLV reverse transcriptase (200 U/µL)	0.5 µL
RNAse-free water	x µL
Final volume	30 µL

Table 2.20: Reverse transcription

The reaction mixture was carefully pipetted on ice and well mixed. Next, an initial incubation at room temperature for 10 minutes was performed, followed by incubation at 42°C – the enzymes temperature optimum – for 90 minutes with shaking. Inactivation of the reverse transcriptase was carried out at 65°C for 20 minutes. The cDNA mixture was aliquoted on ice and stored at -20°C until further use.

2.12.3 Polymerase chain reaction (PCR)

Polymerase chain reaction (PCR) is a method to selectively amplify specific stretches of DNA. It is based on the intrinsic ability of DNA polymerases to duplicate DNA in the presence of short stretches of double-stranded (ds) DNA that contain a free OH group at their 3'end (primer). For PCR applications, sequence specific primers of 20-30 base pair length are used to amplify the desired region between the so-called *forward* and *reverse* primers. In addition to template DNA and primers, the reaction usually includes an adequate buffer solution, free nucleotides and $MgSO_4$ as an essential polymerase co-factor. The PCR reaction itself is comprised of several specific steps: the initial denaturation step at 94°C leads to dissolution of the DNA double helix into its single strands, the following annealing step allows *forward* and *reverse* primers to bind to the specific sequences in the corresponding DNA template strands. The annealing temperature is dependent on the melting temperature of

both primers and is usually chosen to lie 5-10 degrees below the aforementioned. Within the subsequent elongation phase, the thermostable DNA polymerase generates the PCR product from the primer pairs in 5'-3' direction. Elongation temperature is dependent on the temperature optimum of the polymerase used. Moreover, for cloning purposes in which the correct amplification of the DNA sequence is essential, it is beneficial to use a DNA polymerase that displays 3'-'5 exonuclease activity (proofreading). Each PCR cycle leads to a doubling of the desired sequence, by repetition of the three basic steps, a specific DNA fragment is further amplified.

Protocol: For cloning purposes, a proofreading polymerase of *Thermococcus kodakaraensi* was used, supplied as the so-called "KOD Hot Start Polymerase Kit" (Novagen). The polymerase action is initially inhibited by complexing with two monoclonal antibodies that block polymerase and exonuclease activity to minimize unspecific amplification. In the initial denaturation, the antibodies are inactivated and polymerase action can begin.

Reagent	**Volume**
Template cDNA	5.0 µL
Forward primer (100 pmol/µL)	0.5 µL
Reverse primer (100 pmol/µL)	0.5 µL
10 × KOD Hot Start DNA polymerase PCR buffer	5.0 µL
dNTP's (2 mM each)	5.0 µL
$MgSO_4$ (25 mM)	2.0 µL
KOD Hot Start DNA polymerase (1 U/µL)	1.0 µL
ddH_2O	x µL
Final volume	50 µL

Table 2.21: Standard PCR

The PCR reaction was pipetted on ice according to the protocol listed above before PCR was carried out under the following conditions:

PCR program		
Initial denaturation/activation of polymerase	94°C, 3 min	
denaturation	94°C, 30 sec	34 ×
annealing	55°C, 30 sec	
elongation	72°C, 60 sec	
Final elongation	72°C, 3 min	
cooling	4°C, ∞	

Table 2.22: Standard PCR program

2.12.4 Semi-quantitative PCR (SQ-PCR)

The classical PCR (2.12.3) is a highly qualitative method to strongly amplify even the smallest amount of template. The course of the PCR reaction can be roughly divided into three phases: the initial *lag phase* that is characterized by low template concentrations and suboptimal conditions regarding the ratio between template, primer and polymerase, the *exponential phase* in which there is a correlation between the concentrations of PCR product and template and the *plateau phase* in which the ratio between template, primer and enzyme is again suboptimal due to the high amount of amplified product, limited amount of primer and nucleotides and a possible instability of the enzyme. Thus, a correlation between expression level of the target mRNA – and hence the targets abundance as cDNA - and the PCR product can only be concluded from the exponential phase. The so-called semi-quantitative PCR aims at determining the relative expression levels of the mRNA of interest (e.g. after extracellular stimulation) in relation to appropriate controls within the exponential phase of the standard PCR reaction. In order to determine the exponential phase itself, samples of the PCR mix are manually collected after several cycles to be checked on an agarose gel. If a continuous increase in the amount of PCR product can be seen, it is possible to conclude cycles within the exponential phase. The manual approach is similar to the more sophisticated real-time quantitative PCR in which the amount of PCR product is measured by fluorescence after each cycle.

Protocol: In order to assess the expression level of key peroxisomal biogenesis factors after dexamethasone stimulation, specific internal primer sets were chosen by consulting the NCBI Primer Blast tool (http://www.ncbi.nlm.nih.gov/tools/primer-blast) and selected according to the following parameters: primer length between 18-25 bases (optimal: 21); the melting temperature (Tm) should fall between 57-65°C (optimal 60-62°C); the length of the amplification product between 200 and 500 bp (Marone et al., 2001). RNA isolation (2.12.1) and cDNA synthesis (2.12.2) were carried out as indicated above. It was extremely important to transcribe equal amounts of RNA and use equal amounts of cDNA to detect changes in expression. To first determine the exponential phase of the PCR, 10 µL of the various PCR reactions were collected within the standard PCR run (2.12.3) at the end of the elongation phase – for peroxisomal biogenesis factors sample collection was carried out starting at 24 cycles, for housekeeping genes such as GAPDH after 15 cycles. After determination of the optimal cycles for each template, the SQ-PCR was performed using the optimized annealing temperatures for each of the primer sets investigated. The PCR run was terminated after the determined cycle number (2.5.4.2) (within the exponential phase). Routinely, as controls

housekeeping genes were included. 10 µL of the samples were run on 1 % agarose gels and checked for changes in expression.

Reagent	Volume
cDNA	2.0 µL
Forward primer (10 µM)	1.0 µL
Reverse primer (10 µM)	1.0 µL
ThermoPol Taq reaction buffer (10 ×)	5.0 µL
dNTP's (10 mM each)	1.0 µL
Taq polymerase (5 U/µL)	0.5 µL
ddH_2O	x µL
Final volume	50 µL

Table 2.23: Semi-quantitative PCR

PCR program		
Initial denaturation	94°C, 5 min	
denaturation	94°C, 30 sec	40 ×
annealing	x °C, 30 sec	
elongation	72°C, 90 sec	
Final elongation	72°C, 5 min	
cooling	4°C, ∞	

Table 2.24: Semi-quantitative PCR program

2.12.5 Agarose gel electrophoresis

DNA can be electrophoretically separated, as the negatively charged sugar phosphate backbone migrates to the positive charged anode upon application of an electric field. Depending on their size, DNA fragments collide with the agarose gel matrix and are thus retained and slowed in their migration. Velocity of migration is therefore dependent on DNA fragment size, applied voltage, running buffer, agarose concentration and intercalating reagents. Routinely, horizontal midi gels were cast using Tris-acetate buffer to separate DNA fragments according to their size. Sample buffer included glycerol to increase density and the dyes bromphenol blue and xylenecyanol that enable visual verification of the migration progress. Ethidium bromide was routinely used to stain DNA; the organic dye intercalates with the heteroaromatic rings of the DNA due to its planar structure and can be excited by UV light to emit orange-yellow range fluorescence.

Protocol: Agarose concentration was chosen depending on fragment size and the adequate amount of agarose was dissolved in TAE buffer upon boiling in a microwave. The solution was allowed to cool down and ethidium bromide (0.5 µg/mL) was added. The gel was cast into a horizontal midi gel chamber prepared with combs to allow pocket formation. Sample buffer (6 times concentrated) was added to the DNA mixture and gels (midi) were run at 75 V and 400 mA for 30-60 minutes.

2.12.6 Restriction digest

Restriction enzymes (RE) are endonucleasese of bacterial origin that hydrolytically cleave the phospho-diester bond of the DNA backbone. The many restriction enzymes differ in their recognition sequence, their cleavage sequence and their organism of origin. For molecular biological applications, type II restriction enzymes are used that cleave within their recognition sequences which generates defined fragments that can be separated on an agarose gel. In most cases, the often palindromic recognition sequence spans 4-8 base pairs and cleavage can generate blunt or ends with an overhang (sticky ends). After incubation of the fragment to be cloned and the target vector under appropriate buffer conditions, complementary ends are generated which are used to ligate the sequences (preparative digest). To ensure correct orientation of the insert within a vector, most commonly fragments and vector are digested with two different restriction enzymes (double digest) either simultaneously or in consecutive reactions. In this study, consecutive restriction digest was performed and DNA was precipitated in between (2.12.7). Moreover, successful insertion of fragment into the vector can be verified by restriction digest in a smaller scale (analytical digest).

Protocol: For preparative digest, both insert and vector DNA were mixed with restriction enzyme under appropriate buffer conditions according to the protocol below. The digestion mix was incubated for at least 2 hours at 37°C and DNA was precipitated and dissolved in dH_2O before restriction digest with another enzyme.

Reagent	Volume
DNA	1-2 µg
Restriction enzyme I (10 U)	1.0 µL
Buffer (10 ×)	5.0 µL
dH_2O	x µL
Final volume	50 µL

Table 2.25: Preparative restriction enzyme digest

Reagent	Volume
DNA (Mini-prep)	2 µL
Restriction enzyme I (10 U)	0.2 µL
Buffer (10 ×)	2.0 µL
dH_2O	x µL
Final volume	20 µL

Table 2.26: Analytical restriction digest

2.12.7 DNA precipitation

DNA can be easily precipitated in the presence of ethanol or isopropanol.

Protocol: 2 volumes of 100 % ethanol were mixed with 1 volume of DNA mixture and incubated at –80°C at 30 minutes. To pellet DNA, centrifugation for 30 minutes at 17.000g and 4°C was performed. The supernatant was removed and the pellet was washed once in 50 µL 70 % ethanol. The DNA pellet was then dried and resuspended in an adequate amount of dH_2O.

2.12.8 Gel Extraction

PCR products and similar samples were extracted from the agarose gel for furter applications using commercially available gel extraction kits (Macherey-Nagel).

Protocol: The desired fragment was quickly cut out of the agarose gel using UV illumination and then boiled in buffer containing chaotropic salts to solubilise the gel matrix. Simultaneously, the buffer conditions created optimal conditions for DNA binding to the silica membrane of the columns. Upon application of the sample, agarose residues run through the column, while salts were washed away with ethanol-containing buffers. Finally, the DNA was eluted from the column. Gel extraction was carried out according to the manufacturer's instructions.

2.12.9 Dephosphorylation of vector DNA

To avoid false-positive clones after, dephosphorylation of the vector backbone was routinely performed using a so-called Antarctic Phosphatase. The phosphatase removes the free 5'phosphate from the vector backbone; therefore relegation of the vector is suppressed. The presence of 5'phosphates on the insert is sufficient for subsequent ligation.

Protocol: The eluted vector sample was mixed with Antarctic Phosphatase buffer (1:10 of volume) and 1 µL of Antarctic Phosphatase and incubated for 30 minutes at 37°C. Inactivation of the phosphatase occurred for 20 minutes at 65°C.

2.12.10 Ligation

To insert the desired DNA sequence into the target vector after restriction digest, the complementary ends are connected by the reaction of the enzyme ligase that creates a phosphodiester bond upon annealing of the sequences

Protocol: To increase the possibility of successful insertion, the insert is usually added in excess to the vector. As a guideline to determine the amount of fragment, the following formula can be used:

(10 ng *vector* × bp *fragment*)/bp *vector* = ng *fragment* (× 3, for 3:1 ratio insert-vector)

The ligation reaction was prepared according to the table below and either incubated for 1 hour at room temperature or overnight at 16°C. Routinely, controls with only cleaved vector were included.

Reagent	Volume
Insert DNA	x µg
Vector DNA	30 µg
T4 ligase buffer (10 ×)	3.0 µL
T4 ligase	1.0 µL
dH_2O	x µL
Final volume	30 µL

Table 2.27: Ligation reaction

2.12.11 Generation of chemically competent bacteria

To amplify DNA plasmids, bacterial strains that are competent for transformation are used. They have previously been modified by chemical or electrical procedures to allow easier uptake of plasmids.

Protocol: In order to generate chemically competent bacteria, 5 mL of an overnight culture of DH5α E-coli were added to 500 mL of LB medium and incubated at 37°C with shaking until an optical density of OD_{600nm} = 0.4 was achieved. Then the bacterial culture was incubated for 15 minutes on ice before pelleting at 3.000 rpm at 4°C in a Beckman Avanti centrifuge. The pellet was resuspended in 40 mL of ice-cold 0.1 M $CaCl_2$ and incubated for another 30 minutes on ice. After another centrifugation step, bacteria were resuspended in 20 mL of ice-cold 0.1 M $CaCl_2$ and 20 % (v/v) of glycerol were added. After 2 hour incubation on ice, competent bacteria were aliquoted, frozen in liquid nitrogen and transferred to -80°C for long-term storage.

2.12.12 Chemical transformation into competent bacteria

In order to transform bacteria, the DNA plasmid is incubated together with the competent bacteria. A subsequent heat shock at 42°C shortly permeabilizes the bacterial cell membrane and the plasmid can be taken up by diffusion. As the plasmid carries a bacterial origin of replication, it can be promoted and amplified in E. coli.

Protocol: 100 µL of competent E.coli (DH5α strain) were mixed with DNA (1 µL of plasmid DNA or total ligation mixture) and incubated on ice for 30 minutes. After a heat shock at 42°C for 90 seconds, 700 µL of LB medium were added to the cells and they were incubated for 1 hour at 37°C. Afterwards, cells were pelleted by centrifugation at 5.000 rpm for 3 minutes on a table top centrifuge and resuspended in 100 µL of LB medium before the

bacteria solution was plated on LB agar plates carrying the appropriate selection antibiotic. The plates were incubated overnight at 37°C.

2.12.13 Plasmid preparation in a small (mini prep) and large scale (maxi prep)

Plasmid DNA routinely needs to be amplified to e.g. check for the correct insertion of cloned inserts or for the transfection of mammalian cell lines. Plasmid preparation is initiated by overnight culture of bacteria that were transformed with the desired plasmid. Bacteria are pelleted and then resuspended in an EDTA containing buffer which destabilizes the bacterial cell walls upon chelating of Ca^{2+}. Subsequently, alkaline lysis of bacteria is performed buffer containing SDS and NaOH, as the anionic detergent removes phospholipids and protein components while the NaOH denatures genomic and plasmid DNA as well as protein. The following neutralization step in acidic potassium acetate buffer results in the formation of acetate containing complexes of proteins, DNA and cell debris. As potassium dodecylsulfate is less soluble than its sodium counterpart, it precipitates. In contrast to genomic DNA, the smaller plasmid DNA is not denatured as dramatically, thus renaturing upon neutralisation and staying in solution. In commercially available plasmid preparation kits, the supernatant is applied to an anion exchange matrix in which the negatively charged DNA interacts with the protonated DEAE-Dextran groups under low salt conditions. After washing steps in a high salt buffer to remove unspecific contaminants, plasmid DNA can be eluted. After elution, plasmid DNA is precipitated by the addition of isopropanol (and monovalent cations). The DNA can then be pelleted by high speed centrifugation. To remove salts and traces of isopropanol, the DNA pellet is washed with ethanol.

Protocol: Plasmid preparations in a large scale were carried out according to the manufacturer's instructions (Macherey-Nagel Kit). One day prior to the experiment, 200 mL of LB medium supplemented with the appropriate selection marker were inoculated with bacterial cultures (e.g. a 3 mL pre-culture or from glycerol stocks) and cultured at 37°C overnight.

Analogously, a Macherey-Nagel Mini Kit was used to perform pure mini-preps from 3-5 mL of bacterial cultures inoculated 1 day prior to use. Alternatively, a "dirty" mini-prep using self-made solutions was performed. After overnight incubation at 37°C in selection medium, most of the culture was transferred into a 1.5 mL reaction tube and bacteria were pelleted at 13.000 rpm for 30 seconds in a table top centrifuge. To increase DNA concentration, several more millilitres of culture can be pelleted again. The supernatant was discarded and the

bacterial pellets were resuspended in 300 µL of Solution I. Next, 300µL of Solution II were added and mixed by gently inverting the tube prior to a 5 minute incubation at room temperature. Neutralization was initiated by the addition of Solution III (ice cold) and the tube was gently turned again and incubated for another 5 minutes at room temperature. To pellet cell debris, centrifugation was carried out at 13.000 rpm at room temperature for 10 minutes in a table top centrifuge. To precipitate DNA, 600 µL of isopropanol were added to 800 µL of plasmid solution and vortexed well. DNA was pelleted by centrifugation at 13.000 rpm for 5 minutes at 4°C. Pellets were washed once in 500 µL of 70 % ethanol and final DNA pellets were dried at room temperature. Finally, DNA was dissolved in 50 µL of TE or dH_2O.

Solution I, pH 8.0, autoclave

- 50 mM Glucose
- 10 mM Tris
- 10 mM EDTA
- 100 µg/mL RNAse

Solution II

- 0.2 M Sodium hydroxide
- 1 % (w/v) SDS

Solution III

- 3 M Potassium acetate
- pH 4.8 with glacial acetic acid

2.12.14 Determination of nucleic acid concentration

For most applications, the exact amount of DNA or RNA needs to be determined. Photometric determination of nucleic acid concentration is carried out by measurement at 260 nm against a blank, as nucleic acids are capable to absorb UV light due to their aromatic rings. The absorption maxima of single-stranded nucleic acids are higher than those of double-stranded nucleic acids (hyperchromia). By approximation, 1 OD_{260nm} corresponds to 50 µg/mL of dsDNA, 40 µg/mL of ssDNA and 33 µg/mL of ssRNA. By determining the ratio OD_{260nm}/OD_{280nm} the purity of a preparation can be determined; a pure DNA preparation is supposed to have a ratio of 1.8 and a clean RNA preparation a ratio of 2.0. The advantage of the NanoDrop photometer is that it allows the usage of tiny quantities of 0.5-2 µL samples

without a cuvette. The sample is directly pipetted on a sample pedestal and as the apparatus is closed, a sample column is formed that is automatically adjusted for optimal path length and then measured photometrically.

Protocol: Using the Qubit fluorometer, samples were prepared according to the manufacturer's instructions using the kit "BR DNA assay" and "BR RNA assay", respectively.

For determination of nucleic acid concentration using NanoDrop, 1 µL of sample was loaded onto the sample pedestal and measured at 260 nm against a blank.

3 RESULTS

3.1 PEROXISOMAL DYNAMICS: DO MAMMALIAN PEROXISOMES FUSE?

Peroxisomes and mitochondria are both essential cellular organelles that fulfil a variety of metabolic functions, however, in recent years it became more and more obvious that they share an intricate relationship (Schrader & Yoon, 2007; Camoes et al., 2009; Ivashchenko et al., 2011). They cooperate on a metabolic level, e.g. in the β-oxidation of fatty acids, thermogenesis in brown adipose tissue and the scavenging of ROS, but also in antiviral defence (Binns et al., 2006; Schrader & Yoon, 2007; Bonekamp et al., 2009; Dixit et al., 2010; Bonekamp et al., 2011a). Moreover, both organelles were shown to be highly dynamic and thus prone to frequent changes in size and morphology. Interestingly, the organellar fission processes are mediated by key proteins shared between the organelles, such as the membrane receptors Mff, Fis1 and the large GTPase DLP1 (Delille et al., 2009; Schrader et al., 2011) (1.2.2). However, mitochondria are known to regulate their dynamics by frequent fusion events (for review, see Okamoto & Shaw, 2005; Hoppins et al., 2007)), while the existence of a peroxisomal fusion mechanism has only been indicated as part of peroxisome maturation in the yeast *Y. lipolytica* (Titorenko & Rachubinski, 2001a). The occurrence of fusion events between mature peroxisomes in mammalian cells, in a mechanism analogous to mitochondrial fusion, has been a matter of debate. Along the same line, it remains to be elucidated if proteins of the mitochondrial fusion machinery, like the ones of the fission machinery, are also shared with peroxisomes.

In the first part of this thesis, the contribution of peroxisome fusion to peroxisome dynamics in mammalian cells was investigated. Moreover, a dual localization of mitochondrial fusion proteins was addressed. The work presented in this section is the continuation of a diploma thesis (Bonekamp, 2007).

3.1.1 Establishing an *in vivo* fusion assay to study peroxisomal fusion

To examine peroxisomal fusion in mammalian cells, an *in vivo* cell fusion assay using Chinese Hamster Ovary (CHO) cells as a model system was established (Fig. 3.1 A, alternative figures adjusted to for colour-blind people can be found in the appendix (8.1.2)). CHO cells are frequently used for peroxisomal studies (Tsukamoto et al., 1990; Nashiro et al., 2011), as they contain a dynamic peroxisomal compartment. First, CHO cells were generated that stably express either a red (DsRed-PTS1) or a green (GFP-PTS1) fluorescent marker

protein targeted to the peroxisomal matrix which greatly facilitated the subsequent analysis of potential fusion events in comparison to transient transfection. In order to generate hybridoma cells, CHO-DsRed-PTS1 and CHO-GFP-PTS1 cells were mixed, co-cultivated at optimized cell densities, and cell fusion was initiated by the addition of PEG-6000 according to established assays for mitochondrial fusion (Mattenberger et al., 2003; Niemann et al., 2005). Hybridoma cells were then further incubated at 37°C to guarantee proper intermixing of organelles as well as potential fusion and mixing of peroxisomal matrix components. If mammalian peroxisomes are engaged in fusion events, similar to mitochondria, intermixing of red and green matrix markers would result in a co-localization of signals and thus, in "yellow" peroxisomes as illustrated in Fig. 3.1 A.

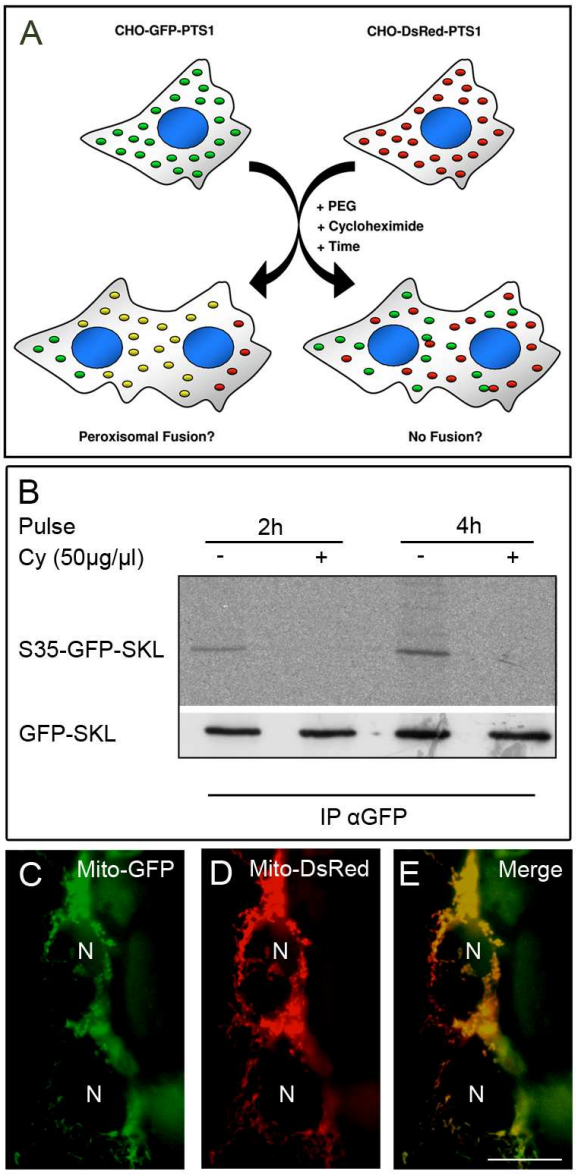

Fig. 3.1: Establishing a peroxisomal *in vivo* fusion assay.
(A) Principle of the peroxisomal *in vivo* fusion assay established in this study. CHO cell lines either stably expressing a matrix-targeted peroxisomal GFP (CHO-GFP-PTS1) or DsRed construct (CHO-DsRed-PTS1) were generated. To assess peroxisomal fusion, the cell lines were mixed and fused using PEG-6000. Hybridoma cells were incubated at 37° C in the presence of cycloheximide to avoid false positive events by peroxisomal protein import. The appearance of yellow peroxisomes (marker for co-localization) and peroxisomal dynamics were investigated by fluorescence microscopy and live cell imaging.
(B) Protein translation is efficiently blocked over the course of the observation period. Control (-) and cycloheximide (Cy, +)-blocked CHO-GFP-PTS1 cells were pulse labeled with S^{35}-methionine for 2 and 4 hours, respectively. Cell lysates were split and subjected to immunoprecipitation with anti-GFP. One set of samples was subjected to SDS-PAGE and autoradiographs were developed by PhosphoImaging (upper panel). As a loading control, the other set of samples was separated by SDS-PAGE, immunoblotted and incubated with anti-GFP (lower panel).
(C - E) Mitochondrial fusion in CHO cells. As a positive control, CHO-K1 cells were transiently transfected with Mito-GFP (C) and Mito-DsRed (D), respectively. Differentially labeled cells were subjected to the *in vivo* fusion assay. After 4 hours, cells were fixed and processed for fluorescence microscopy. Overlay of fluorescent signals from (C) and (D) is shown in (E). N, nucleus. Bar, 20µm.

To exclude false positive co-localization of GFP-PTS1 and DsRed-PTS1 signals due to peroxisomal import of the corresponding matrix marker, protein biosynthesis was inhibited

for the duration of the experiment by the addition of cycloheximide, a widely used inhibitor of eukaryotic protein translation. To validate the efficiency of the cycloheximide block, radio-immunoprecipitation of intracellular GFP-PTS1 was performed. The cells were pulse-labelled with S^{35}-methionine either in the presence or absence of cycloheximide and incubated at 37°C. Afterwards, cells were lysed and an immunoprecipitation with anti-GFP antibodies was performed. In the presence of cycloheximide no signal for radio-labelled – and thus newly synthesized – GFP-PTS1 was detected (Fig. 3.1 B, upper panel) indicating that protein biosynthesis (translation) was efficiently blocked. To ensure that the lack of GFP signal was not due to loading artefacts, fractions of the immunoprecpitation were immunoblotted using anti-GFP antibodies. Equal amounts of GFP were precipitated corresponding to the pre-existing GFP-PTS1 pool in the cycloheximide-containing fractions (Fig. 3.1 B, lower panel). Thus, *de novo* protein synthesis and consecutive peroxisomal import of fluorescent proteins was excluded under the chosen experimental conditions.

Finally, to verify the applicability of the *in vivo* fusion assay, mitochondrial fusion served as a positive control. CHO-K1 cells were transiently transfected with either matrix-targeted Mito-GFP or Mito-DsRED and subsequently fused with PEG-6000. After 4 hours, cells were fixed and analyzed by fluorescence microscopy (Fig. 3.1 C-E). Hybridoma cells displayed fusion of differentially labelled mitochondria and subsequent intermixing of mitochondrial matrix markers as reported in other studies (Mattenberger et al., 2003; Niemann et al., 2005), thus the *in vivo* fusion assay was successfully established.

3.1.2 The occurrence of yellow peroxisomes points to peroxisomal fusion events in CHO cells

Next, the potential fusion of mature peroxisomes in CHO cells was examined using the peroxisomal *in vivo* fusion assay. After generation of hybridomas, cells were fixed after 2-6 hours and analyzed for the occurrence of yellow peroxisomes and hence peroxisomal fusion by epifluorescence microscopy (Fig. 3.2 A-E).

A clear co-localization of GFP and DsRed fluorescence was observed in several areas of the hybridoma cells (Fig. 3.2 A-E, arrowheads). Depending on the ratio of green to red fluorescence, more orange to greenish overlays of peroxisomal signals were as well observed, but were more difficult to detect. Furthermore, several red and green peroxisomes in close vicinity to each other were also observed, apparently caught in some type of interaction (Fig. 3.2, asterisks).

To exclude the possibility that co-localization of fluorescence resulted from overlay of peroxisomal signals from different focal planes in epifluorescence, confocal microscopy was performed (Fig. 3.2 F-H). As mature, spherical peroxisomes are known to have a diameter of around 0.3-0.5 µm, a plane thickness of ≤ 0.37 µm was selected to ensure co-localization of signals from one confocal plane. Confocal microscopy confirmed a clear co-localization of the peroxisomal matrix marker proteins GFP-PTS1 and DsRed-PTS1 in a subset of peroxisomes of the CHO hybridoma cells (Fig. 3.2 H). These observations point to the existence of peroxisomal fusion in CHO hybridoma cells.

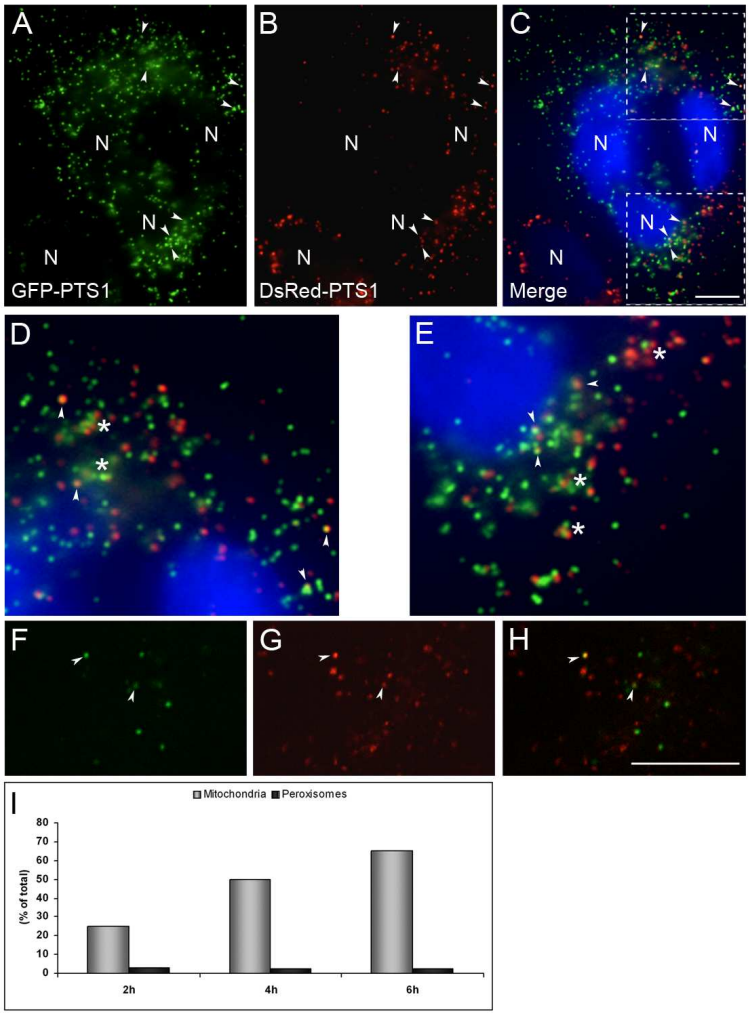

Fig. 3.2: Peroxisomal matrix signals co-localize in fixed cells.
CHO-GFP-PTS1 (A, F) and CHO-DsRed-PTS1 cells (B, G) were mixed and subjected to the peroxisomal *in vivo* fusion assay. Hybridoma cells were incubated for 4 hours, fixed and processed for epifluorescence (A – E) or confocal microscopy (F – H). Higher magnification images of the boxed regions in (C) are shown in (D) and (E). Arrowheads point to yellow peroxisomes. Asterisks highlight red and green peroxisomes engaged in intimate contacts.
(I) Quantitative analysis of mitochondrial and putative peroxisomal matrix intermixing (yellow organelles). CHO cell lines either transfected with differential mitochondrial or peroxisomal markers were subjected to the *in vivo* fusion assay. After the indicated time points, cells were fixed and processed for fluorescence microscopy. The percentage of yellow peroxisomes (% of total organelle number per hybridoma cell) at different time points of a representative experiment is shown. To assess mitochondrial fusion, the overall number of hybridoma cells with yellow mitochondria (full fusion) was determined. N, nucleus. Bars, 20µm.

Mitochondrial fusion has been shown to result in a thorough mixing of about 50 % of matrix signals after approx. 4 hours in *in vivo* fusion assays (Niemann et al., 2005). To similarly assess the extent of peroxisomal matrix interchange, statistical analysis of fusion events was performed (Fig. 3.2 I). The number of co-localizing peroxisomes ("yellow" peroxisomes) in regard to the total number of peroxisomes in a hybridoma cell at different time points (2-6 hours) after cell fusion was determined. An increase in co-localization of peroxisomal markers was not observed after extended time points (data not shown). Furthermore, omitting

cycloheximide in the assay did not alter co-localization events (data not shown). Fusion of mitochondria was determined under the same experimental conditions (Fig. 3.2 I). As mitochondrial fusion (Mito-GFP and Mito-DsRed overlap) was almost complete within hybridoma cells, the overall percentage of hybridoma cells with "yellow" mitochondria was determined. For peroxisomes, the degree of peroxisomal marker protein "intermixing" was around 2 % after 2 hours, and remained similar over time. In contrast to that, a constant increase of matrix intermixing (hybridoma cells with "yellow" mitochondria) was observed over time (Fig. 3.2 I).

In summary, contrary to previous indications in mammalian cells (Huybrechts et al., 2009), co-localization events between peroxisomes were detected under the chosen experimental conditions, pointing to the occurrence of peroxisomal fusion. However, though mitochondrial fusion appeared to be fast, time dependent and almost complete as expected, peroxisomal fusion was slow, time independent, less frequent and only visible in a subpopulation of peroxisomes. This questioned the exchange of matrix marker proteins between individual peroxisomes, at least by a complete mechanism analogous to mitochondria; therefore, fusion events were investigated using live cell imaging.

3.1.3 Live cell imaging reveals close peroxisomal contacts and vivid peroxisomal interactions without an exchange of matrix proteins

To clarify the question if peroxisomes fuse with each other and exchange matrix marker proteins, live cell imaging was performed 1-6 hours after hybridoma generation. The peroxisomal *in vivo* fusion assay was conducted and peroxisome interactions in hybridoma cells were observed using time-lapse spinning disk confocal microscopy. Images were captured every 5 seconds in 5 different confocal planes (0.5 µm) using the 488 and 561 laser lines, respectively. When monitoring the dynamic behaviour of differentially labelled peroxisomes (Fig. 3.3), it was observed that previously separated, single peroxisomes interacted with each other (Fig. 3.3, 0-50s arrowheads) and were engaged in transient and long term contacts. Moreover, the same peroxisomes were often observed to interact multiple times. This "re-engaging" behaviour remained restricted to the initially interacting peroxisomes, although other candidate peroxisomes for interaction were in close vicinity and abundant (Fig. 3.3). During these contacts the red and green fluorescent signals were observed to completely co-localize (Fig. 3.3, 60-65s), accounting for the observations made in fixed cells (Fig. 3.2). However, with proceeding observation time, the closely interacting

peroxisomes separated again into the initial, individual (red and green) peroxisomes without any detectable exchange of matrix markers (Fig. 3.3, 80s; see also Movies S1 and S2). Even with increased sensitivity (higher gain settings and exposure times), no exchange of matrix fluorescence was detected and the fluorescence signals of the separated organelles remained similar to the individual peroxisomes before interaction.

These findings indicate that while peroxisomes do not fully fuse to allow exchange of matrix marker proteins, differential peroxisomes are engaged in close, long-term interactions.

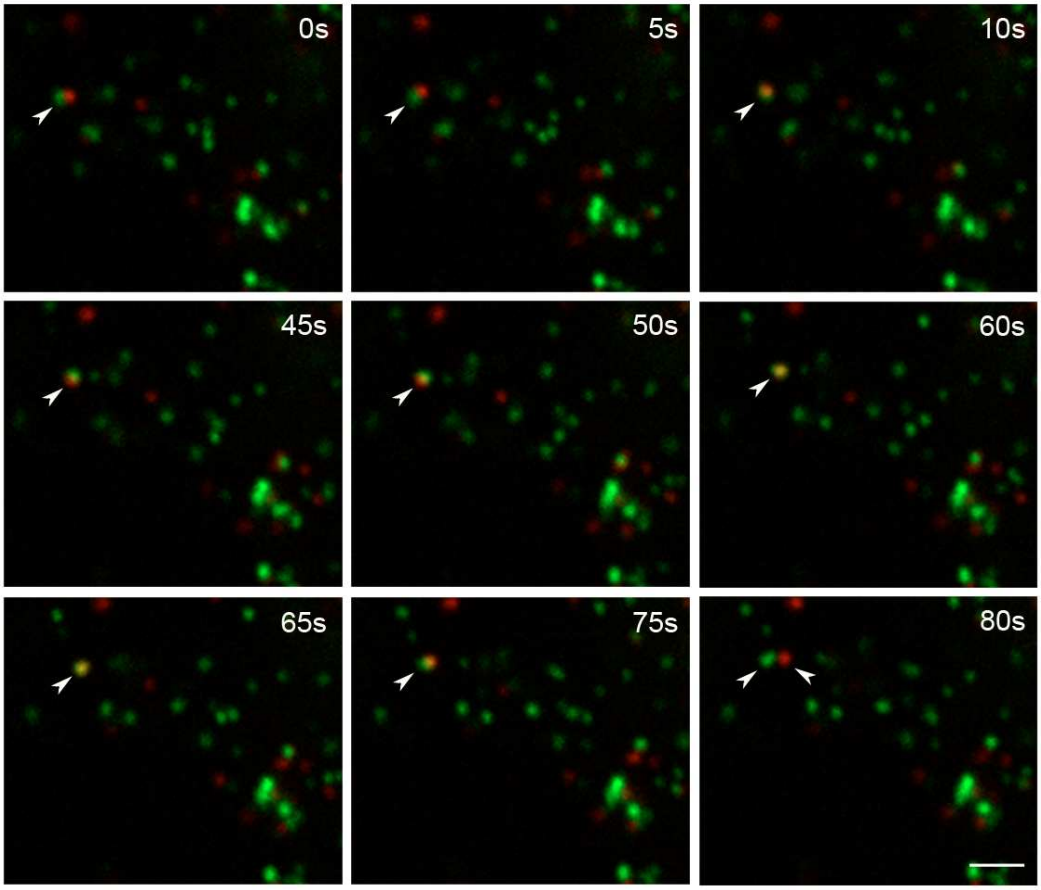

Fig. 3.3: Time-lapse confocal microscopy reveals that peroxisomes interact extensively, but do not exchange matrix proteins.
CHO-GFP-PTS1 and CHO-DsRed-PTS1 cells were subjected to the peroxisomal *in vivo* fusion assay. Hybridoma cells were allowed to recover for 30 minutes and were then analyzed by time-lapse confocal microscopy. Images were taken every 5 seconds using 488 and 561 laser lines, respectively (see also Movies S1 and S2). Arrows indicate interaction events. Note the close (60 – 65s), but transient (80s) overlap of differentially labelled peroxisomes. Bar, 5µm.

In order to confirm the observation of close, intimate contacts between individual peroxisomes at a higher resolution, image deconvolution was performed. After application of the *in vivo* peroxisomal fusion assay, cells were fixed and mounted for confocal microscopy using a Leica TCS SP2 AOBS confocal microscope equipped with a 100x objective. Using the 488 and 543 nm laser lines, z-stacks were generated of hybridoma cells (settings: 8x zoom) using the optimal number of slices suggested by the program (Leica Confocal Software). Oversaturation of signals was avoided by adjusting of respective PMTs. Image

deconvolution was performed using Huygens Professional Software, generating high resolution 3D images of peroxisomal interactions (Fig. 3.4).

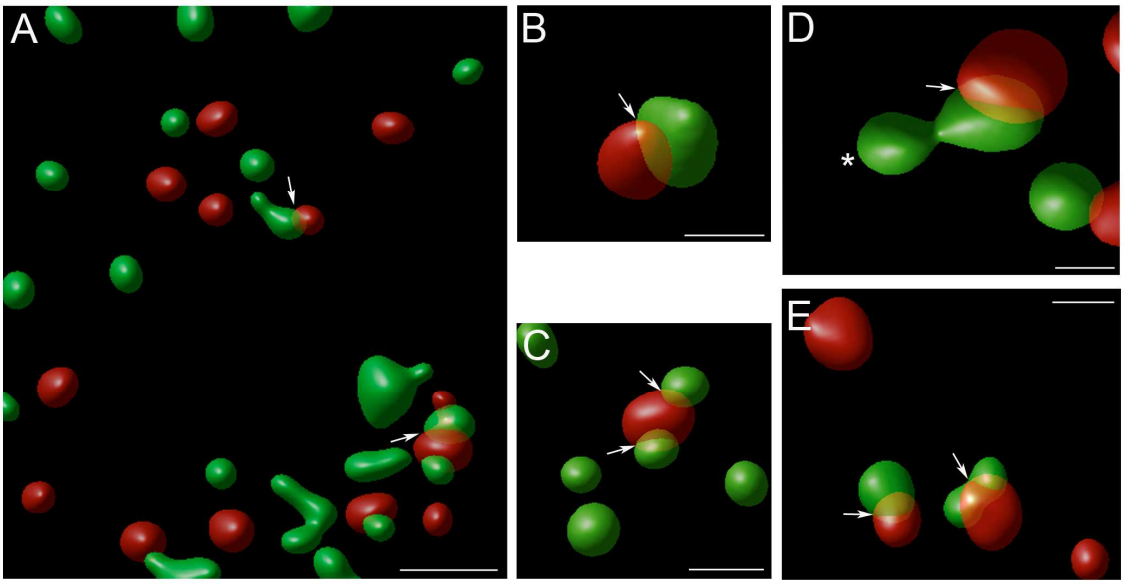

Fig. 3.4: High resolution images of peroxisomal interactions.
Differentially labelled CHO cell lines were subjected to the *in vivo* peroxisomal fusion assay and processed for confocal microscopy. Image deconvolution was performed using Huygens Professional software. A selection of peroxisomal interaction events is shown (A-E). Arrows highlight overlap of markers; a potential fission event is labelled by an asterisk. Note the close, intimate contacts between interacting peroxisomes. In (E, peroxisomes on the right) one peroxisome appears to embrace another (estimated co-localization of signals: approx. 50% (green) and 24% (red)). Data analysis revealed a mean distance between interacting peroxisomes of about 0.07 µm +/- 0.029 µm. As data evaluation only allowed for the calculation of distances between the centre of one mass to the nearest surface point (but not for the surface-to-surface distance), the actual distance is most probably even smaller. Bars, 1µm (A); 0.25µm (B); 0.5µm (C-E).

High resolution 3D images obtained by image deconvolution confirmed intimate contacts between interacting peroxisomes (Fig. 3.4). In some cases, the differentially labelled peroxisomes appeared to embrace each other (Fig. 3.4 E); this frequent appearance of lengthy and intimate contacts points to a physiological relevance of the observed peroxisomal interactions.

3.1.4 Transient peroxisomal interactions can potentially contribute to the homogenization of the peroxisomal compartment

In search for a physiological function of close peroxisome interactions, we used a simple computational model to address if peroxisome contacts could principally contribute to the distribution of e.g. metabolites, signals, or other “molecular information” and thus, to the homogenization of the peroxisomal compartment on a feasible timescale.

The majority of peroxisomes in mammalian cells was shown to perform Brownian like movements, reaching distances of $L<0.5$ µm after $\Delta t=2$ min (Rapp et al., 1996; Wiemer et al.,

1997; Schrader et al., 2000). For Brownian movements L varies with time as $L \sim (D\ \Delta t)^{1/2}$. Given a typical cell size of 50 µm, it can be concluded that the time required for these peroxisomes to travel from one side of the cell to the other would be of the order of $\Delta t \sim 2x10^4$ minutes, i.e. almost two weeks. For smaller cells of e.g. 15 µm widths, the time required would be of the order of one day. Thus, it can be concluded that the slow diffusion of peroxisomes may be irrelevant for physiological functions requiring peroxisome contacts. However, a small fraction of peroxisomes has been shown to use ATP driven, microtubule-dependent motility to move faster and more persistently (Rapp et al., 1996; Wiemer et al., 1997; Schrader et al., 2000). The existence of the aforementioned numerous and lengthy contacts suggests that, even with energy expenditure, peroxisomal interactions may confer a physiological advantage. Indeed, for mean velocities of around 0.2 µm/s, peroxisomes could cross the whole extent of the cell in 50/0.2 = 4 min.

One may wonder whether the fraction of peroxisomes engaging in ATP driven motility has been optimized to promptly homogenize the peroxisomal population within a cell at a minimal energy expense. In order to address this issue a simple computational model was developed (co-operation Dr. F. Vistelo de Abreu, University of Aveiro). In this model peroxisomes are viewed as small spheres with a diameter of d = 0.3µm, displaying two types of movements. One class of peroxisomes performs slow Brownian movements, with the velocity $v_{slow} = 0.024\,\mu m/s$ and changing onto another randomly chosen velocity direction every Δt=20s. The other class performs faster $v_{fast} = 0.24\,\mu m/s$ and more persistent movements (change direction every Δt=100s). These values agree with previous observations (Rapp et al., 1996; Wiemer et al., 1997; Schrader et al., 2000). For simplicity the intracellular space was modelled to correspond to two fused flat cells as a bidimensional square with a side length equal to 70µm. Reflecting boundary conditions were considered on the ends, keeping peroxisomal movements within the cell. Whenever peroxisomes collide, they bind and move together with the same averaged velocity. Then they unbind at a rate $p=0.05s^{-1}$. At the beginning of the simulation it was assumed that two disjoint peroxisomal subpopulations (red and green peroxisomes, on different sides as in Fig. 3.1 A) were present. Peroxisomes were then allowed to move and mix. The number of peroxisomes that contacted peroxisomes from the other cell, evolved according to $n(t) = n_0(1 - \exp(-t/\tau))$.

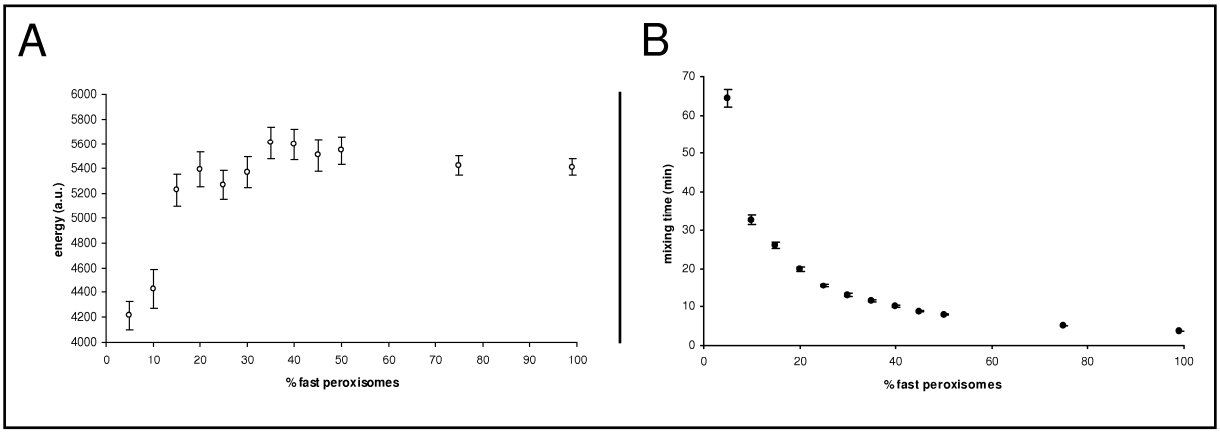

Fig. 3.5: Relation between energy consumption, fast moving peroxisomes and peroxisome interactions. (A) The average energy consumed (arbitrary units) measured by the number of moves by fast moving peroxisomes for time intervals Δt=0.1s. (B) The time required for 75% of the peroxisomes to have interacted with at least one peroxisome of the other fused cell, as a function of the percentage of fast moving (ATP driven) peroxisomes. Each point corresponds to results obtained from simulations on 100 different populations. Note the marked decrease in the energy spent between 10% and 15% of fast moving peroxisomes. Simultaneously, the time required for proper mixing of the populations is increasing.

Fitting these curves, τ, the characteristic mixing time, was measured. The number of moves required by fast moving (ATP driven) peroxisomes was also measured, until 75 % of the population contacted a peroxisome from the other peroxisomal population. This quantity is proportional to the energy cost involved to mix the population to that extent. Simulations were performed 100 times for each fraction of fast moving peroxisomes in the population. Characteristic mixing times and energy costs were averaged and standard errors calculated (Fig. 3.5). Results are consistent with the expectation that fast peroxisomes can efficiently mix the populations. Indeed, characteristic mixing times can be well below one hour with only a small fraction of fast peroxisomes participating actively in the diffusion. While the amount of time required for mixing diverges for small fractions of fast peroxisomes, a sharp decrease in the energy expenditure appears for small fractions (Fig. 3.5 A). This confirms the initial assumption that no prominent advantage for mixing would be achieved if all peroxisomes participated in fast and yet costly motility. Thus, it appears that an optimization may have occurred to quickly homogenize peroxisomal populations with the lowest energy costs. Interestingly, results are consistent with previous observations of ~15 % fast moving peroxisomes (Rapp et al., 1996; Wiemer et al., 1997; Schrader et al., 2000).

In conclusion, a combination of fast, ATP-driven movement of peroxisomes and subsequent formation of close contacts between individual peroxisomes might well contribute to a homogenization of the peroxisomal compartment in mammalian cells in the timescale of one

to several hours. The simple model obtained here is consistent with the degree of peroxisomal mixing in the cell fusion assay.

3.1.5 Transient peroxisomal interactions display a complex behaviour

Next, the interactions between differentially labelled peroxisomes were analyzed to determine their characteristics with focus on frequency, duration and number of peroxisomes involved. Determining the number of interacting (red and green) peroxisomes in each frame revealed that about 5-6 differentially labelled peroxisomes interact within a hybridoma cell, accounting for 1.5-2% of the total number of peroxisomes (up to 4 % when a similar interaction rate between peroxisomes labelled in the same colour is assumed). These observations are consistent with our findings in fixed cells (Fig. 3.2 I). For most of the time, the initial two peroxisomes only interact with each other, but other peroxisomes can join to take part in the interactions (mostly 2-3, but even up to 4 and more peroxisomes, Fig. 3.6 E). Within the course of the interaction, the individual peroxisomes interacting also separate again, only to re-engage in interactions; most frequently the same two peroxisomes come together again 1-3 times, but can also re-engage up to 8 times (Fig. 3.6 F). The majority of the peroxisomes, which are engaged in close contacts, stay attached to each other for a time span of about 5-40 seconds (Fig. 3.6 A), but some even up to 300 or 500 seconds. Thirty-five percent of those interactions result at some time point in an interaction that is tight enough for apparent co-localization of matrix signals ("overlay", see Fig. 3.6 C); the majority of those marker "overlay" events has a duration of about 5-15 seconds, but again single events last up to 100, 300 and even 500 seconds (Fig. 3.6 C).

For both cases, the frequency of events with a duration larger than a given value (the cumulative frequency distribution of contact duration) was analysed in more detail (Fig. 3.6 B, D) (co-operation Dr. F. Vistelo de Abreu, University of Aveiro). A marked difference can be observed on both distributions. The distribution of close contacts shows an exponential behaviour (Fig. 3.6 B), while the distribution of "overlay" contacts displays power law decay (Rhodes & Anderson, 1996; Viswanathan et al., 2002; Newman, 2005; Sornette, 2006; Clauset et al., 2009; James et al., 2011).

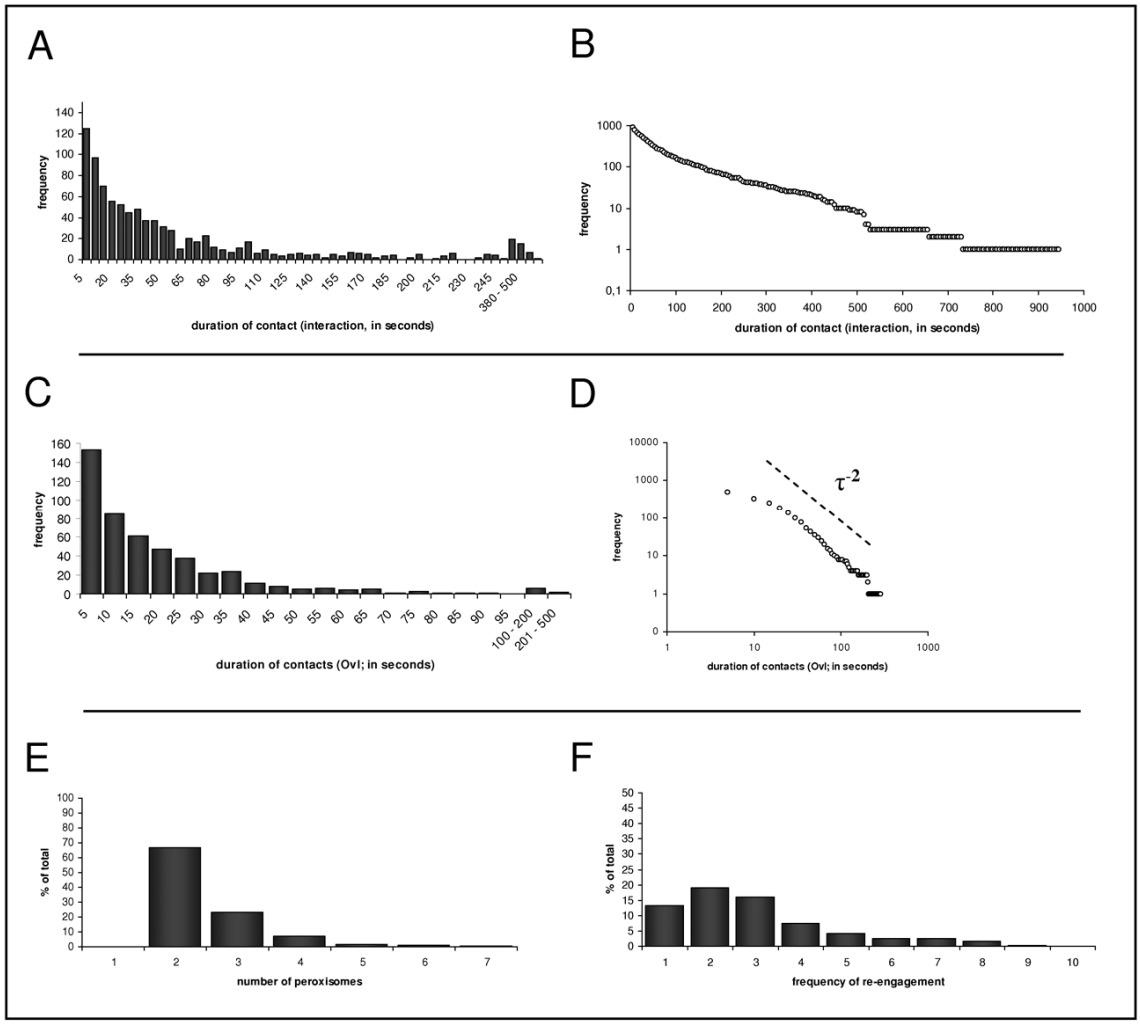

Fig. 3.6: Characteristics of peroxisomal interactions.
Image 5D stacks of time lapse images were generated and frame-by-frame analysis was performed for every z-stack. To analyze the kinetics of peroxisomal interactions, the duration of the interactions (A) (i.e. the time frame of intimate attachment between peroxisomes, see Fig. 3.3, 0s) and the duration of complete signal overlay (C) (Ovl, see Fig. 3.3, 60s) was determined for every peroxisomal interaction evaluated (n = 903). The frequency of contacts lasting longer or equal than a certain duration is represented as a cumulative frequency plot against time (in seconds) in (B) and (D). Data in (B) is expressed on a semi-logarithmic scale to highlight approximate exponential behaviour, while data in (D) is presented on a logarithmic scale to highlight power law behaviour. The mean number of peroxisomes involved in an interaction as well as the mean number of re-engagement between individual peroxisomes is presented in (E) and (F), respectively and expressed as relative frequency plot.

Power law behaviour has been extensively investigated in many biological areas (Rhodes & Anderson, 1996; Viswanathan et al., 2002; Newman, 2005; Sornette, 2006; Clauset et al., 2009; James et al., 2011), because it indicates the existence of intricate dynamics originating from diverse, and yet specific mechanisms. It has also been hypothesized that power laws could emerge from optimality principles e.g. in foraging (Viswanathan et al., 2002), although this remains controversial (James et al., 2011). Power law distributions have heavy tails, i.e. the number of events with lower frequencies – in our case, the number of long term contacts – is substantially larger than it could be expected from an exponential distribution,

corresponding to random events. We used the statistical methods described in (Clauset et al., 2009) and performed a goodness-of-fit test calculating a p-value of 0.89, which is greater than 0.1 and hence supports the hypothesis that the frequency distribution has power law decay (8.1.1.1). An estimate for the power law exponent $\alpha = -1.8 \pm 0.2$ on the cumulative frequency distribution of contact duration was obtained. In the Appendix, a simple model is provided that could explain the origin of this power law behaviour $\alpha = -2$. This model indicates that to account for this type of frequency dependency, it is necessary to assume that interactions between peroxisomes can span over a wide range of contact lifetimes, and it crucially depends on the contact interaction process. This is also consistent with the observation of an exponentially decaying distribution for the duration of close contacts (Fig. 3.6 B). In this case, in some events peroxisomes may not be interacting and consequently their consideration "smears" the power law decay behaviour. This also supports the idea that the power law behaviour observed indeed originates from intricate peroxisome interactions. Hence, this analysis strongly suggests that peroxisome interactions appear to be more diverse and complex than assumed.

3.1.6 Peroxisomal interactions: not be mistaken for fission

In some cases, where peroxisomes are engaged in close contacts of longer duration, their separation may easily be misinterpreted as peroxisomal fission, especially in live cell observations, where only one fluorescent peroxisomal marker is used. Peroxisomes multiply by processes of elongation, constriction and subsequent fission (Schrader & Fahimi, 2006; Schrader et al., 2011). However, true peroxisomal fission events have been rarely documented in live cells. Thus, the occurrence of peroxisomal fission was screened for in COS-7 cells overexpressing YFP-Pex11pβ by time-lapse spinning disk confocal microscopy (Fig. 3.7). Pex11pβ promotes an elongation of peroxisomes and subsequent DLP1-dependent fission into numerous small peroxisomes (Schrader et al., 1998b; Delille et al., 2010; Schrader et al., 2011) (1.2.2.1). During live cell imaging, peroxisomes in YFP-Pex11pβ expressing cells were observed to form tubular extensions and become elongated prior to fission. A daughter peroxisome often "pinches off" at the end of the tubule (Fig. 3.7, Movie S3). Elongated or tubular peroxisomes are also observed in mammalian cells under normal culture conditions (the degree of elongation may vary depending on cell type and growth conditions) (Schrader & Fahimi, 2006). Thus, it is likely that fission events in mammalian cells (in contrast to peroxisome interactions and separation) are accompanied by some degree of membrane

elongation prior to division. These findings have to be considered when analyzing peroxisomes in living cells.

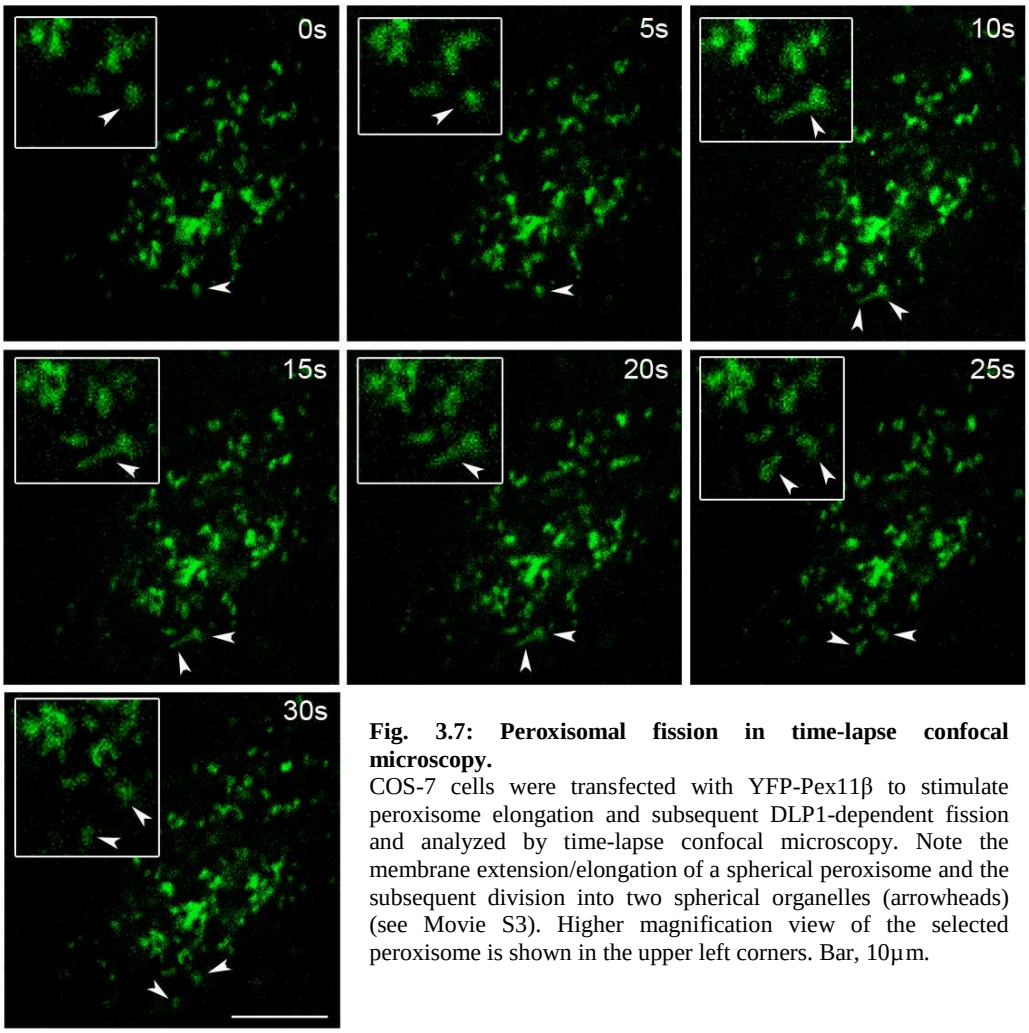

Fig. 3.7: Peroxisomal fission in time-lapse confocal microscopy.
COS-7 cells were transfected with YFP-Pex11β to stimulate peroxisome elongation and subsequent DLP1-dependent fission and analyzed by time-lapse confocal microscopy. Note the membrane extension/elongation of a spherical peroxisome and the subsequent division into two spherical organelles (arrowheads) (see Movie S3). Higher magnification view of the selected peroxisome is shown in the upper left corners. Bar, 10µm.

3.1.7 Peroxisomes do not exchange membrane proteins during peroxisome interaction

As there was no evidence for an exchange of matrix marker proteins during peroxisome interactions, it was subsequently investigated whether peroxisomal membrane marker proteins can redistribute upon interaction. To address this possibility, CHO cell lines stably transfected with peroxisomal membrane markers (PMP70-YFP and dPex26-mDsRed, respectively) were generated. The peroxisomal *in vivo* fusion assay was conducted with these cell lines and a possible exchange of membrane markers was determined by confocal microscopy (Fig. 3.8 A-C, higher magnifications shown in G). Peroxisomes in the hybridoma cells were thoroughly

mixed, with PMP70-YFP occasionally inducing the formation of peroxisomal aggregates, an observation made upon overexpression of membrane proteins (Fig. 3.8 A).

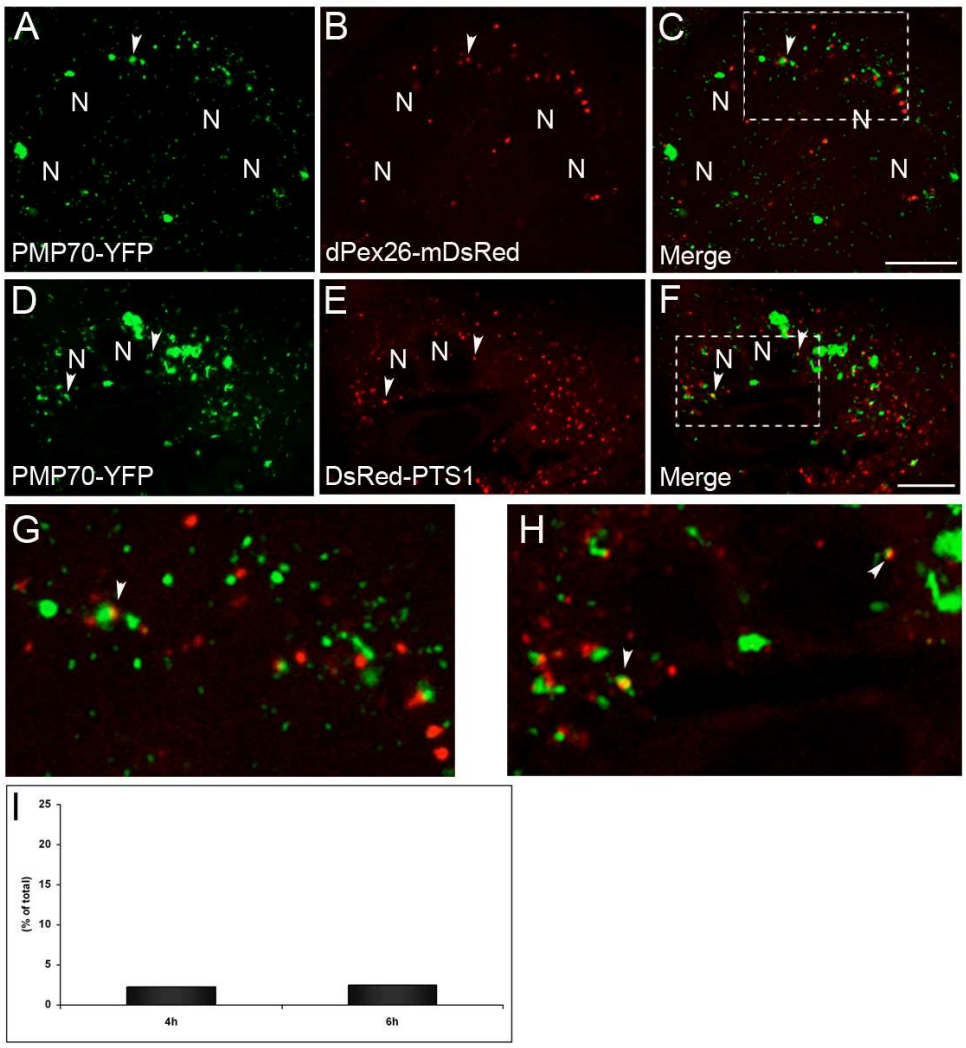

Fig. 3.8: Peroxisomes do not exchange membrane components.
CHO-K1 cells stably expressing the peroxisomal membrane markers PMP70-YFP (A) or DsRed-dPex26 (B) were subjected to the peroxisomal *in vivo* fusion assay and assayed for the exchange of membrane components (C). In a second set of experiments, CHO-PMP70-YFP (D) and CHO-DsRed-PTS1 cells (E) were fused. Overlay of signals is shown in (F). Higher magnification images of (C) and (F) are shown in (G) and (H), respectively. Arrowheads point to intimate interactions. (I) Quantitative analysis of putative peroxisomal membrane intermixing. The percentage of yellow organelles (% of total organelle number per hybridoma cell) at different time points of a representative experiment is shown. N, nucleus. Bars, 20µm.

Similar to the observations made with matrix marker proteins, a close interaction between differentially labelled peroxisomes and subsequent co-localization of membrane marker fluorescence was detected (Fig. 3.8, arrowheads). However, no constant increase in "yellow" peroxisomes was observed by statistical analysis (approx. 2 % at 4 and 6 hours after fusion, Fig. 3.8 I), indicating that there was no intermixing of membrane markers between peroxisomes over time. Furthermore, no exchange of membrane markers or membrane fusion

was observed, when peroxisomes were artificially clustered (Fig. 3.8 G) (Delille et al., 2010). Additionally, fusion experiments with PMP70-YFP were also conducted using the more homogenous matrix-labelled DsRed-PTS1 cell line (Fig. 3.8 D-F, higher magnifications shown in H). It was assumed that if membrane components would be exchanged, there would be an increase of YFP-signal on the red peroxisomes, but not vice versa. However, this experimental setup was consistent with our previous results. Thus, we conclude that despite vivid and complex interactions, mammalian peroxisomes do not fuse completely or exchange the matrix or membrane marker proteins tested in our experimental setup.

3.1.8 Peroxisomal interactions do not increase after fatty acid or H_2O_2 treatment

Peroxisomal interactions may facilitate the exchange of metabolites between different peroxisomal pools. To investigate, whether an increase in the heterogeneity between peroxisomal subpopulations would result in an enhanced frequency of peroxisomal interactions, CHO-GFP-PTS1 cells were pre-trated with different peroxisomal metabolites (oleic acid (OA), arachidonic acid (AA), H_2O_2) prior to fusion with non-stimulated CHO-DsRed-PTS1 cells. Successful application of fatty acids was monitored by an increase in the number and size of lipid droplets (Fig. 3.9 A, B). After the indicated time points, cells were fixed, processed for epifluorescence microscopy and assessed for the percentage of interacting peroxisomes (Fig. 3.9 C). Unlike before when determining the number of “fusing” peroxisomes (Fig. 3.2), for this experiment interacting, non-“yellow” peroxisomes were also included in the calculations, thus the number of interacting peroxisomes in control cells is higher than reported before and increased with time due to complete intermixing (Fig. 3.2 I). The slight increase in the number of interactions after AA treatment (after 1 hour) was not found for OA. H_2O_2 treatment resulted in an overall decrease of interactions, probably due to cellular oxidative stress. In general, no prominent increase in the percentage of interacting peroxisomes was detected between control and treated cells (Fig. 3.9 C). In addition, pre-treatment of the cells with peroxisome proliferators (bezafibrate, ETYA) did not alter the number of peroxisomal interactions (data not shown).

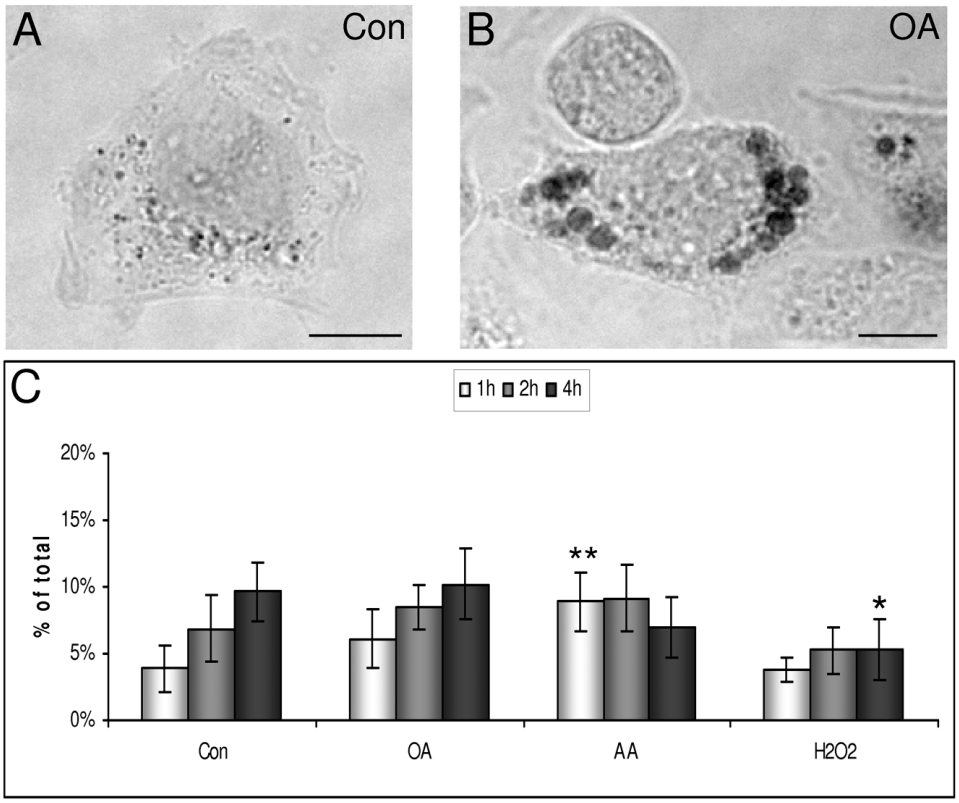

Fig. 3.9: Stimulation with peroxisomal metabolites does not result in an increase of peroxisomal interactions.
(A, B) Oleic acid (OA) leads to an increase in the size of lipid droplets in CHO cells. To verify successful stimulation of CHO cells, lipid droplet staining using Sudan Black was performed in control (A) and treated cells (B). Bars, 20µm.
(C) Statistical evaluation of peroxisomal interactions after stimulation. 24 hours prior to the *in vivo* fusion assay, CHO-GFP-PTS1 cells were stimulated with either OA, AA or H_2O_2 to increase heterogeneity between populations. After application of the *in vivo* peroxisomal fusion assay, cells were fixed at the indicated time points and processed for epifluorescence microscopy. Images of hybridoma cells were evaluated using ImageJ. The number of green and red peroxisomes as well as the number of interacting/attaching peroxisomes (defined as "yellow" ones and those attached to each other) was determined. Data evaluation was performed using Microsoft Excel and data is taken from 3-4 independent experiments (10-15 cells/condition each) and expressed as means +/- standard deviation (* $p< 0.05$; ** $p<0.01$, compared to control).

3.1.9 Mitochondrial fusion proteins do not localize to peroxisomes

Although above findings exclude the existence of a peroxisomal fusion in a manner similar to mitochondrial fusion, a dual localization of mitochondrial fusion proteins was still investigated. First of all, both organelles have been shown to share their key division components, such as the large GTPase DLP1 that mediates fission of both organelles after recruitment by the tail-anchored adaptor proteins Fis1 and Mff (Schrader et al., 2011). Moreover, though primarily described as mitochondrial, the outer membrane protein Mitofusin (Mfn) 2 was also localized to the ER where it controls ER morphology and its tethering to mitochondria (de Brito & Scorrano, 2008b; de Brito & Scorrano, 2009), while OPA1 was localized to lipid droplets (Pidoux et al., 2011). Thus, a potential peroxisomal

localization of the mitochondrial fusion proteins Mfn 1 and 2 – large GTPases that coordinate outer membrane fusion – and OPA1, a GTPase mediating inner membrane fusion was investigated.

3.1.9.1 The outer membrane fusion proteins Mfn 1 and 2 do not localize to peroxisomes

Myc-tagged variants of wild-type Mitofusin 1 and 2 were expressed in COS-7 cells stably expressing a GFP-PTS1 fusion protein, which is exclusively targeted to peroxisomes (Koch et al., 2004). As a positive control, GFP-Fis1 was expressed, a tail-anchored protein which is known to be targeted to both peroxisomes and mitochondria (Koch et al., 2005) (Fig. 3.10 B). Co-localization with peroxisomes was assessed by epifluorescence microscopy. While GFP-Fis1 showed a dual localization to both peroxisomes and mitochondria (Fig. 3.10 C), Myc-Mfn1 was exclusively targeted to mitochondria (Fig. 3.10 E, G).

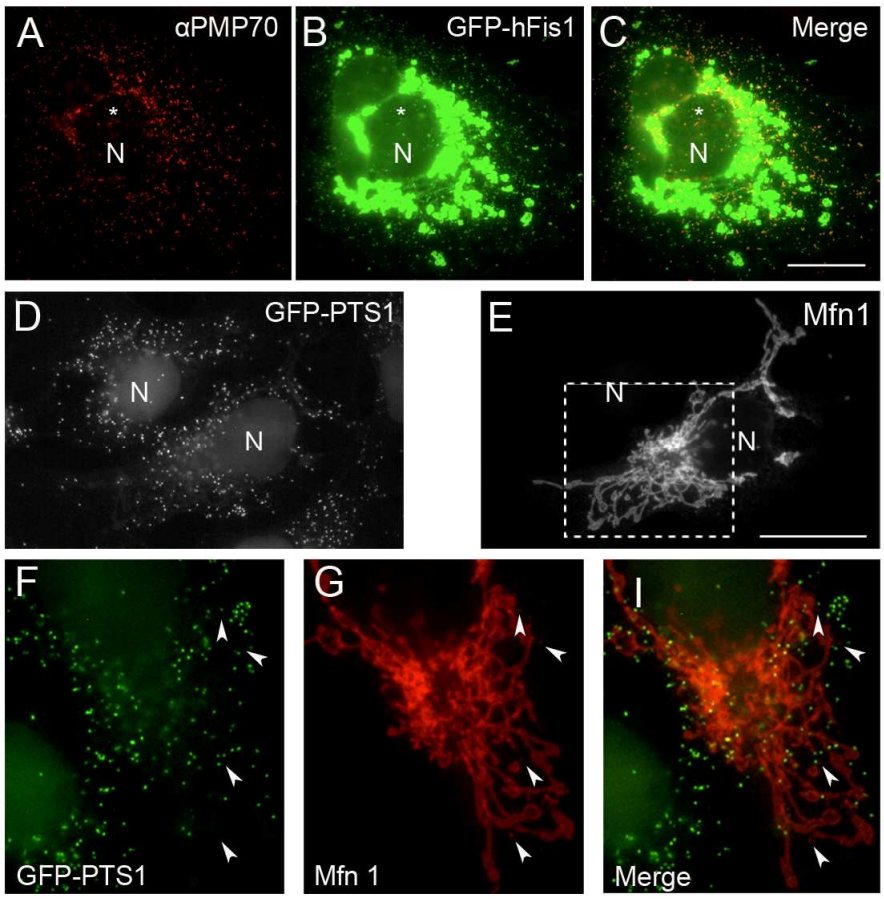

Fig. 3.10: The mitochondrial fusion protein Mfn1 does not localize to peroxisomes.
(A–C) Fis1 is dually targeted to peroxisomes and mitochondria. As a positive control, COS-7 cells were transfected with GFP-hFis1 (B) and processed for immunofluorescence with anti-PMP70 (A). (C) Overlay of (A, B). Note the localization of GFP-Fis1 at peroxisomes (asterisks) and clustering of mitochondria.
(D–G) Mfn1 does not localize to peroxisomes. COS-7 cells stably expressing GFP-PTS1 (D) were transfected with Mfn1-myc (E) and processed for immunofluorescence using anti-myc. Higher magnification image of the boxed area in (E) is shown in (F–H). Overlay (Merge) of (F, G) is shown in (H). Note that although small punctuate Mfn1 positive structures can be seen, there is no co-localization with peroxisomal markers (arrowheads).
N, nucleus. Bars, 20µm.

Similar observations were made upon overexpression of Mfn2 (data not shown). Alterations of mitochondrial morphology were observed upon overexpression of the mitofusins which are consistent with previous findings, as e.g. overexpression of Mfn 1 is known to cause perinuclear aggregation of mitochondria (Santel et al., 2003) (Fig. 3.10 E). Furthermore, activity-deficient variants of the mitofusins (Fig. 3.11) were expressed that are known to alter mitochondrial morphology resulting in their fragmentation and perinuclear clustering. However, peroxisomal morphology remained unaffected, indicating that mitofusins are not functionally relevant to maintain peroxisome morphology (Fig. 3.11).

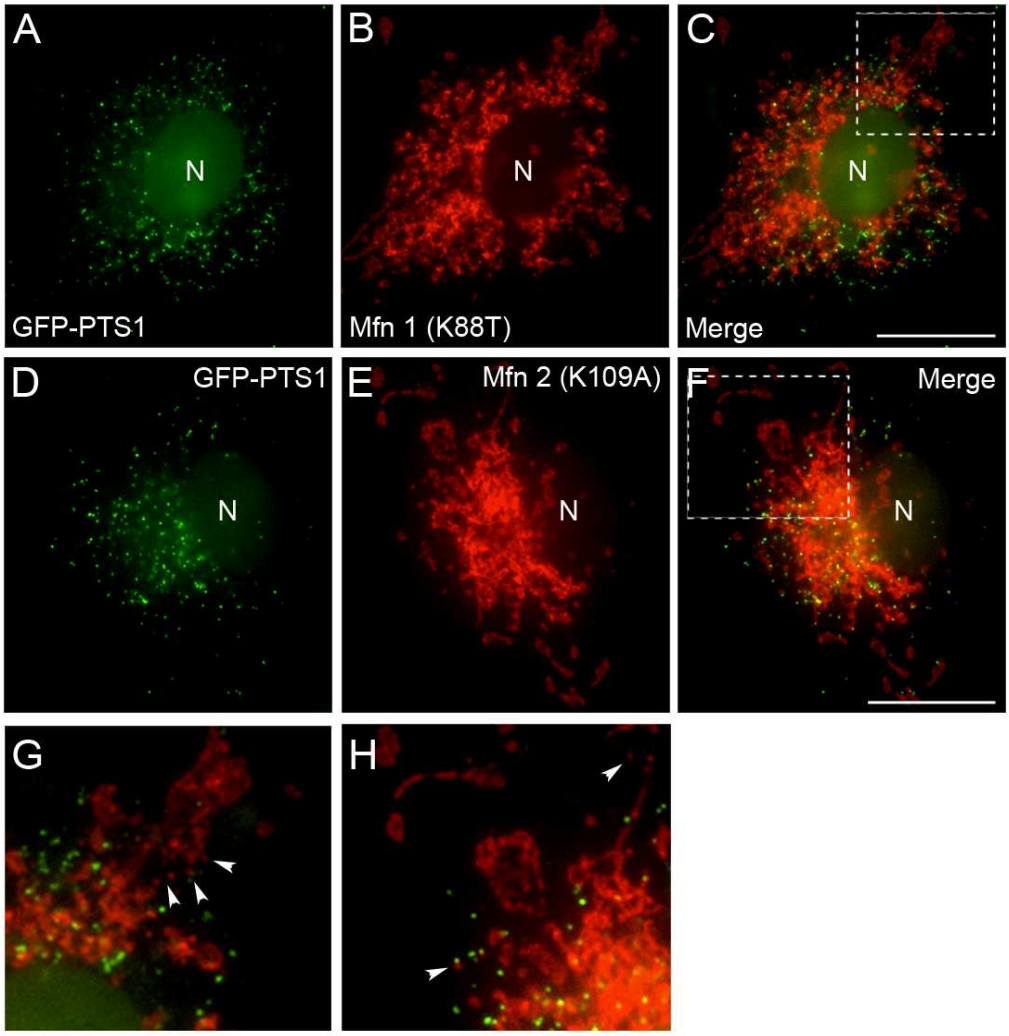

Fig. 3.11: Expression of activity-deficient mitofusin variants does not affect peroxisome morphology.
COS-7 cells stably expressing GFP-PTS1 (A, D) were transfected with activity-deficient variants of Mfn1 (K38T) (B) and Mfn2 (K109A) (E). After 24 hours, cells were processed for immunofluorescence using anti-myc antibodies. Overlays (Merge) of (A, B) and (D, E) are shown in (C) and (F). Higher magnification images of boxed areas in (C) and (F) are shown in (G) and (H). Asterisks highlight mitofusin-positive punctuate structures that do not co-localize with peroxisomal markers. Note that although mitochondria are prone to fragmentation upon overexpression of Mfn mutants, peroxisomal morphology remains unaffected. N, nucleus. Bars, 20µm.

Taken together, upon overexpression of wild-type and activity-deficient variants of both mammalian outer membrane fusion proteins no peroxisomal localization was detected.

Moreover, the mutant variants did not affect peroxisome morphology, thus neither Mfn1 nor Mfn2 are targeted to peroxisomes.

3.1.9.2 The inner mitochondrial membrane protein OPA1 is not targeted to peroxisomes

To study the localization of the inner mitochondrial membrane GTPase OPA1 in COS-7 cells, immunofluorescence microscopy using OPA1-specific antibodies was performed. Similar to above observations for Mfn1 and 2, no OPA1 signal was detected on peroxisomes, even when OPA1 signals appeared to be concentrated as spherical structures reminiscent of peroxisomes (Fig. 3.12 E, arrowheads). Using a specific OPA1 antibody, these findings were substantiated by immunoblotting, using highly purified peroxisomal and mitochondrial fractions (Fig. 3.12 F). While OPA1 was detected in the mitochondrial fractions, it appeared to be absent from highly purified peroxisomes (Fig. 3.12 F, PO).

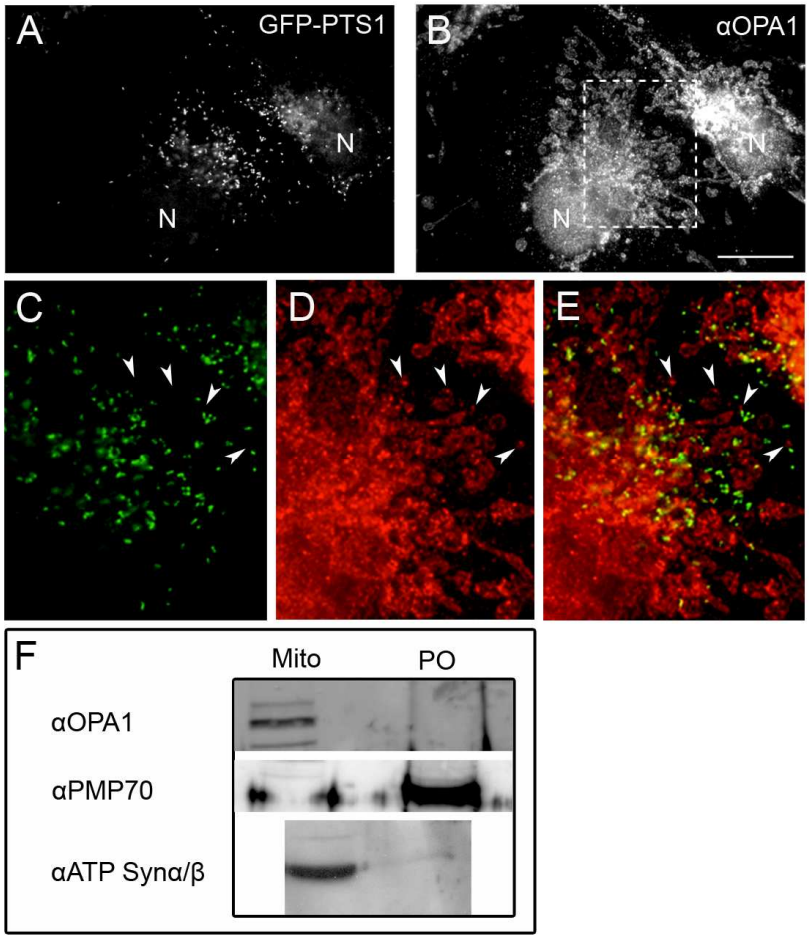

Fig. 3.12: The mitochondrial inner membrane fusion protein OPA1 does not localize to peroxisomes.
OPA1 is not a peroxisomal protein. (A–E) COS-7 cells stably expressing GFP-PTS1 (A) processed for immunofluorescence using anti-OPA1 (B). Higher magnification images of the boxed area in (B) are shown in (C–E). (E) Overlay (Merge) of (C, D). Note that some punctuate structures are positive for OPA1, but do not co-localize with the peroxisomal marker. N, nucleus. Bar, 20µm.
(F) Highly purified peroxisomes (PO) and mitochondria (Mito) were separated by 12.5% SDS-PAGE and immunoblotted using anti-OPA1, anti-PMP70 and anti-ATP synthase antibodies. Equal amounts of protein (50µg) were applied. Multiple OPA1 bands correspond to different splice variants.

As a conclusion, this study could clearly show for the first time that mitochondrial fusion proteins are not shared by mitochondria and peroxisomes, unlike their key fission machinery.

3.1.10 Summary

In the first part of this thesis, the contribution of peroxisomal fusion to organelles dynamics, analogous to mitochondrial fusion, was addressed systematically. An *in vivo* fusion assay was established based on hybridoma formation by cell fusion and, unlike what was observed in other studies (Huybrechts et al., 2009), a clear co-localization of matrix markers was detected in fixed cells. Although subsequent live cell studies excluded an exchange of matrix or membrane markers between individual peroxisomes, the existence of transient, vivid contacts between peroxisomes was demonstrated for the first time. Using computational modelling and mathematical analysis, transient peroxisome interactions were shown to follow a complex, non-random behaviour that might facilitate homegenization of the compartment. However, they do not appear to contribute to the exchange of fatty acids or H_2O2. Furthermore, computational analysis indicated for the first time that the contribution of microtubule-dependent peroxisome movement has evolved to represent the optimum between energy cost and organelle distribution. Finally, it was conclusively shown that mitochondria and peroxisomes do not share components of the fusion machinery, although the key fission proteins are shared by the two organelles.

3.2 REGULATION OF PEROXISOME DYNAMICS: CHARACTERIZATION OF THE PEROXISOMAL MEMBRANE PROTEIN PEX11B AND ITS N-TERMINAL DOMAIN

Peroxisomes are remarkably dynamic organelles which modulate their morphology and dynamics by a combination of membrane elongation and fission processes. Moreover, they travel long distances along microtubules and engage in vivid interaction as shown in the previous section (3.1). The key proteins mediating the dynamic growth and division of peroxisomes in mammals have been identified in recent years: prior to fission, the peroxisome membrane is elongated by the action of the Pex11 proteins (for review, see Schrader et al., 2011). Subsequently, the elongated tubule is constricted and divided by the large GTPase DLP1 that is recruited to the membrane by the tail-anchored proteins Mff and Fis1 (Delille et al., 2009; Otera et al., 2010; Schrader et al., 2011). While the latter components are shared with mitochondria, the mammalian membrane protein Pex11pβ is a constitutively expressed, uniquely peroxisomal protein that is placed in the centre of initiating and regulating peroxisomal growth and division in mammals (Schrader et al., 1998b; Schrader & Fahimi, 2006; Delille et al., 2010; Schrader et al., 2011). Only recently, Pex11pβ-mediated peroxisome proliferation was shown to follow a multi-step maturation process (Delille et al., 2010). Furthermore, the underlying mechanistic basis of the Pex11p-based membrane elongation was linked to the existence/action of a conserved amphipathic helix in the N-terminal domain of various Pex11 proteins from different species (Opalinski et al., 2011). Although the presence of this amphipathic helix is conserved from yeast to mammals, and its presence was confirmed in mammalian Pex11pβ, further characterization of the mammalian Pex11 family of proteins is required. For instance, it remains to be elucidate if the mere presence of Pex11pβ, and its amphipathic helix, is sufficient to promote and regulate peroxisome elongation. Furthermore, the regulation of Pex11p by phosphorylation or oligomerization has only been addressed in the yeast *S. cerevisiae* (Marshall et al., 1996; Knoblach & Rachubinski, 2010).

In the following part of this thesis, the regulation of peroxisome dynamics on the organelle level was investigated by characterizing the properties of human Pex11pβ, the key protein facilitating peroxisomal growth and division. Due to conflicting information *in silico* data, the topology of human Pex11pβ was determined in order to also conclusively define its crucial N-

terminal domain. Moreover, its regulation by phosphorylation and oligomerization was addressed.

3.2.1 Predicted positions of transmembrane domains within human Pex11pβ

Insight into the regulation of Pex11p proteins has been obtained from their domain structure, however, the mode of membrane association and the topology of the Pex11 proteins varies immensely across species, but also remained controversial in a single organism: *Sc*Pex11p was initially assumed to be an integral membrane protein, but re-defined as a peripheral protein (Erdmann & Blobel, 1995; Marshall et al., 1996; Schrader et al., 2011). Similarly, the topology and especially the position of the first transmembrane domain of human Pex11pβ remains elusive: using a variety of commonly used, online screening tools (Fig. 3.13, *in silico* screening), the position of the predicted transmembrane domains of human Pex11pβ was determined (Fig. 3.13). Notably, although generally assumed to carry two transmembrane domains (Abe & Fujiki, 1998; Schrader et al., 1998b), the majority of the algorithms used only detected a single transmembrane domain within human Pex11pβ. This information was also incorporated into widely used protein databases such as UniProtKB. As most algorithms only calculate the transmembrane domain at the extreme C-terminus, Pex11pβ was even identified as a tail-anchored protein in a large scale screen (Kalbfleisch et al., 2007). As indicated, the predicted position of the first transmembrane domain, if detected, also depended on the algorithm used (Fig. 3.13, TM1). As Pex11pβ plays a crucial role in the regulation of peroxisome dynamics, it extremely important to clarify its topology and the position of its transmembrane domains, also in order to conclusively define its essential N-terminal domain.

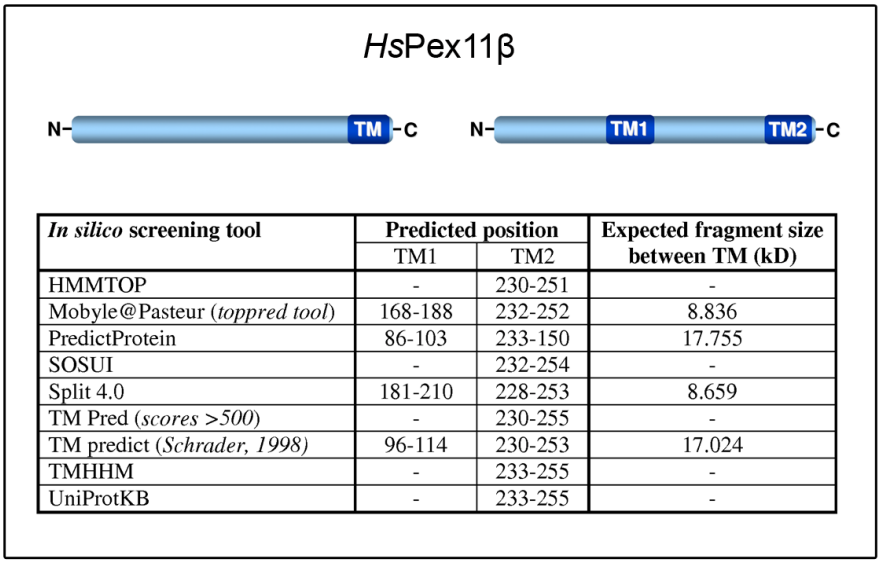

***In silico* screening tool**	**Predicted position**		**Expected fragment size between TM (kD)**
	TM1	TM2	
HMMTOP	-	230-251	-
Mobyle@Pasteur (*toppred tool*)	168-188	232-252	8.836
PredictProtein	86-103	233-150	17.755
SOSUI	-	232-254	-
Split 4.0	181-210	228-253	8.659
TM Pred (*scores >500*)	-	230-255	-
TM predict (*Schrader, 1998*)	96-114	230-253	17.024
TMHHM	-	233-255	-
UniProtKB	-	233-255	-

Fig. 3.13: Overview of the predicted positions of the transmembrane domains of human Pex11pβ.
Using the human sequence of Pex11pβ, a variety of *in silico* screening tools were applied to determine the position of the transmembrane domains. Based on the results, the expected size of the protein fragment between the two transmembrane domains was calculated using the tool PeptideMass counter.

3.2.2 Pex11pβ is removed from the peroxisomal membrane by Triton-X-100 treatment after formaldehyde fixation

To examine the characteristics of Pex11pβ in comparison to the other human isoforms, COS-7 cells were transfected with plasmids encoding myc-tagged version of Pex11pα, β and γ and differential permeabilization using either digitonin or Triton-X-100 (Tx100) was performed. In contrast to Tx100 which permeabilizes all cellular membranes, digitonin does not permeabilize peroxisomal membranes (Motley et al., 1994; Schrader et al., 1998b; Bonekamp et al., 2011b). To guarantee peroxisomal membrane integrity after digitonin permeabilization, untransfected COS-7 cells were either stained with an antibody against the cytosolic domain of the peroxisomal membrane protein PMP70 or the matrix protein acyl-CoA-oxidase (AOX) after differential permeabilization (Fig. 3.14 A-D). While PMP70 was readily detected under both conditions (Fig. 3.14 A, B), the peroxisomal matrix protein AOX only became accessible after membrane rupture with Tx100 (Fig. 3.14 C, D), verifying the efficiency of our differential permeabilization protocol. Interestingly, although one would assume the integral membrane protein Pex11pβ to be unaffected by Tx100 application after preceding fixation with 4 % pFA, the myc signal corresponding to Pex11pβ was lost upon Tx100 incubation and subsequent immunofluorescence (Fig. 3.14 H). In contrast to that, Tx100 incubation did not affect the localization of the other two Pex11 isoforms to this degree (Fig. 3.14 E-F, I-J). The observed Tx100 sensitivity might be indicative of incomplete cross-linking and subsequent removal of the protein (Goldenthal et al., 1985), however, fixation of proteins using pFA is catalyzed by chemical cross-linking of their lysine residues whose number is comparable between the three mammalian Pex11 isoforms. To address the removal of Pex11pβ from the peroxisomal membrane into the supernatant biochemically, COS-7 cells overexpressing myc-Pex11pβ were fixed in 4 % pFA and incubated with Tx100. As a control, PBS instead of the detergent was used after fixation. Tx100 and PBS supernatants were collected (Fig. 3.14 K, S) and the corresponding cells were lysed (Fig. 3.14 K, P). Equal amounts of protein of the supernatant and pellet fractions of PBS controls and Tx100-treated cells were subjected to SDS-PAGE and immunoblotting gainst the myc epitope (Fig. 3.14 K). In PBS-treated controls, a signal corresponding to Pex11pβ was observed in the pellet fraction, but not in the supernatant. Upon Tx100 incubation, however, only a small fraction of the protein still associated with the pellet and it was clearly extracted into the supernatant (Fig. 3.14 K). Nonetheless, signals corresponding to the pellet fractions remained weak under both conditions, which might indicate that epitope recognition is hampared by previous cross-linking of proteins with pFA. Interestingly, another band was clearly detected by the myc

antibody of around 55 kD size, corresponding to a dimeric form of myc-Pex11pβ (approximate molecular weight 28kD) (Fig. 3.14 K).

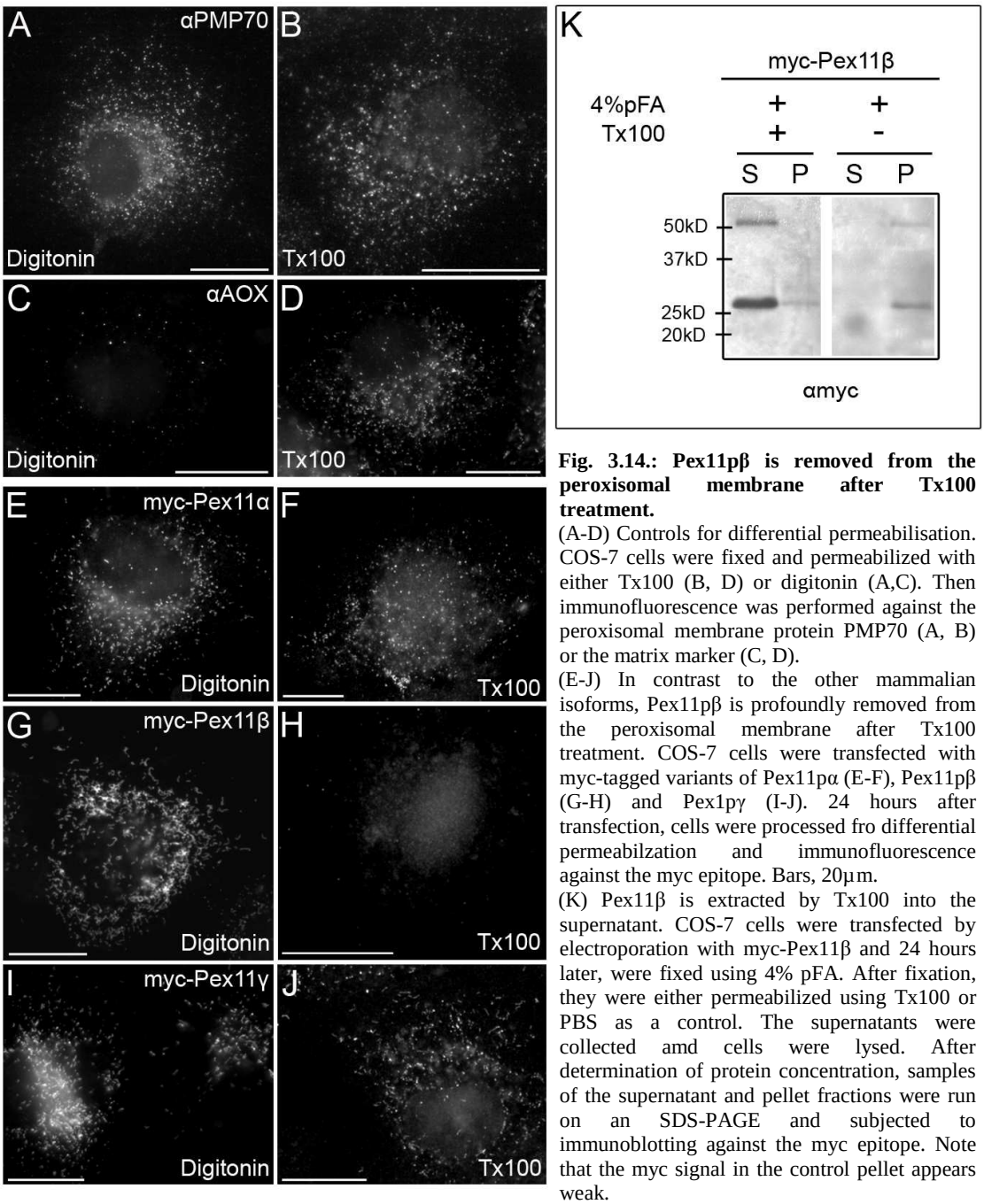

Fig. 3.14.: Pex11pβ is removed from the peroxisomal membrane after Tx100 treatment.
(A-D) Controls for differential permeabilisation. COS-7 cells were fixed and permeabilized with either Tx100 (B, D) or digitonin (A,C). Then immunofluorescence was performed against the peroxisomal membrane protein PMP70 (A, B) or the matrix marker (C, D).
(E-J) In contrast to the other mammalian isoforms, Pex11pβ is profoundly removed from the peroxisomal membrane after Tx100 treatment. COS-7 cells were transfected with myc-tagged variants of Pex11pα (E-F), Pex11pβ (G-H) and Pex1pγ (I-J). 24 hours after transfection, cells were processed fro differential permeabilzation and immunofluorescence against the myc epitope. Bars, 20µm.
(K) Pex11β is extracted by Tx100 into the supernatant. COS-7 cells were transfected by electroporation with myc-Pex11β and 24 hours later, were fixed using 4% pFA. After fixation, they were either permeabilized using Tx100 or PBS as a control. The supernatants were collected amd cells were lysed. After determination of protein concentration, samples of the supernatant and pellet fractions were run on an SDS-PAGE and subjected to immunoblotting against the myc epitope. Note that the myc signal in the control pellet appears weak.

In summary, these findings demonstrate that, unlike the other mammalian isoforms, Pex11pβ was removed from the peroxisomal membrane after Tx100 addition, even after fixation. This intrinsic characteristic of the protein enabled its simple simultaneous extraction and enrichment by a straightforward biochemical approach that allows for a side-by-side detection of monomeric and dimeric variants of the Pex11pβ. The established Tx100 extraction assay

was subsequently employed to investigate regulation of human Pex11pβ by oligomerization (3.2.11).

3.2.3 All human Pex11 isoforms behave like integral membrane proteins

Searching for an indication of why Pex11pβ is more Tx100-sensitive than the other mammalian isoforms, we compared the membrane association of the three mammalian Pex11 isoforms using carbonate extraction. COS-7 cells were transfected with myc-tagged variants of the human Pex11 isoforms and subjected to carbonate extraction at pH 11.5 (Fujiki et al., 1982). Equal amounts of pellet and supernatant samples from control and carbonate-treated peroxisome-enriched fractions were subjected to SDS-PAGE and immunoblotting against the myc-epitope. Detection of PMP70, a multi-membrane spanning protein of the peroxisomal membrane, was used as a control for integral association, while Pex19p served as a control for peripheral association. Although Pex19p is a PMP-binding chaperone shuttling between the cytosol and the peroxisomal membrane, it tightly associates with the peroxisomal membrane in the course of the PMP-import process by binding to the membrane receptor Pex3p, mimicking a transient peripheral association (1.1.5.2).

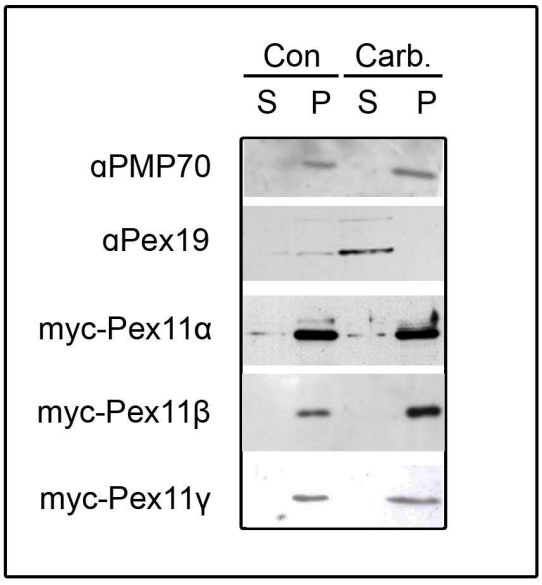

Fig. 3.15: All Pex11 isoforms behave like integral membrane proteins.
COS-7 cells were transfected with myc-tagged variants of the human Pex11 isoforms and subjected to carbonate extraction at pH 11.5. Protein concentration was determined and supernatant as well as pellet samples from control and carbonate treated fractions (60µg) were run on 12.5 % SDS-PAGE and subjected to immunoblotting against the myc epitope. To serve as a control for integral and peripheral proteins, PMP70 and Pex19p were used.

As expected for a multi-membrane spanning ABC transporter, PMP70 remained tightly associated with peroxisomal membrane in controls and carbonate-treated samples (Fig. 3.15, Con, Carb.). In the case of Pex19p, a faint, but clear signal was detected in the pellet fractions of controls, but not in the respective supernatant (Fig. 3.15). After carbonate treatment, a significant portion of Pex19p shifted into the supernatant, indicating that it was removed from the peroxisomal membrane and, at least transiently, behaved like a peripheral membrane

protein. However, none of the human Pex11 isoforms were removed from the peroxisomal membrane after carbonate treatment, indicating that all of them clearly behave like integral membrane proteins. Thus, membrane association as such does not provide an explanation for the Tx100-sensitivity of human Pex11pβ.

3.2.4 Characterization of a newly available Pex11pβ antibody

Up until now, conclusive determination of Pex11pβ topology was limited by the availability of adequate antibodies; however, a recently available antibody directed against a non-specified internal site of the human Pex11pβ protein now enabled further biochemical characterization.

Initially, detection of endogenous Pex11pβ was investigated in COS-7 and human HepG2 cells by indirect immunofluorescence with the Pex11pβ antibody after combined formaldehyde and methanol fixation. Pex11pβ immuno-staining revealed a very faint, spot-like intracellular signal, indicating that either epitope recognition was low or that steady-state Pex11pβ expression was below the detection threshold (data not shown). Thus, for further experiments characterizing Pex11pβ topology, overexpression of Pex11pβ was performed. For differential permeabilization, COS-7 cells were transfected with a myc-tagged variant of Pex11pβ prior to fixation and permeabilization with either Tx100, digitonin or methanol (Fig. 3.16). Cells were then processed for immunofluorescence against the myc epitope and Pex11pβ itself. To ensure peroxisomal membrane integrity upon digitonin application, immuno-staining against PMP70 and AOX was routinely included (see Fig. 3.14). After overexpression of Pex11pβ-myc and Tx100 incubation (Fig. 3.16 A-I), no clear signal corresponding to myc-Pex11pβ was observed using either antibody (Fig. 3.16 A-C), consistent with our previous observations regarding Pex11pβ Tx100 sensitivity (Fig. 3.14). Using digitonin, the C-terminal myc tag was readily recognized by the myc antibody, however, no signal corresponding to the Pex11pβ antibody was observed (Fig. 3.16 D-F) which indicates that the antibody epitope resided within the peroxisomal membrane and matrix and was thus not accessible to the antibody. Using combined fixation and membrane permeabilization by methanol, a Pex11pβ antibody signal readily co-localized with the myc signal (Fig. 3.16, G-I). Similar observations were made upon overexpression of YFP-Pex11pβ, a variant carrying a larger protein tag (Fig. 3.16, J-R). Interestingly, unlike the myc-tagged variant, YFP-Pex11pβ was not extracted from the peroxisomal membrane by Tx100, presumably due to its large protein tag (of equal size as Pex11pβ itself). The fusion tag introduces further lysine residues into the protein and might thus facilitate a more profound cross-linking to other proteins. Consequently, an overlay of YFP and Pex11pβ signals was

only observed upon peroxisomal membrane permeabilization by Tx100 and methanol (Fig. 3.16, L, R), but not after digitonin application (Fig. 3.16, O).

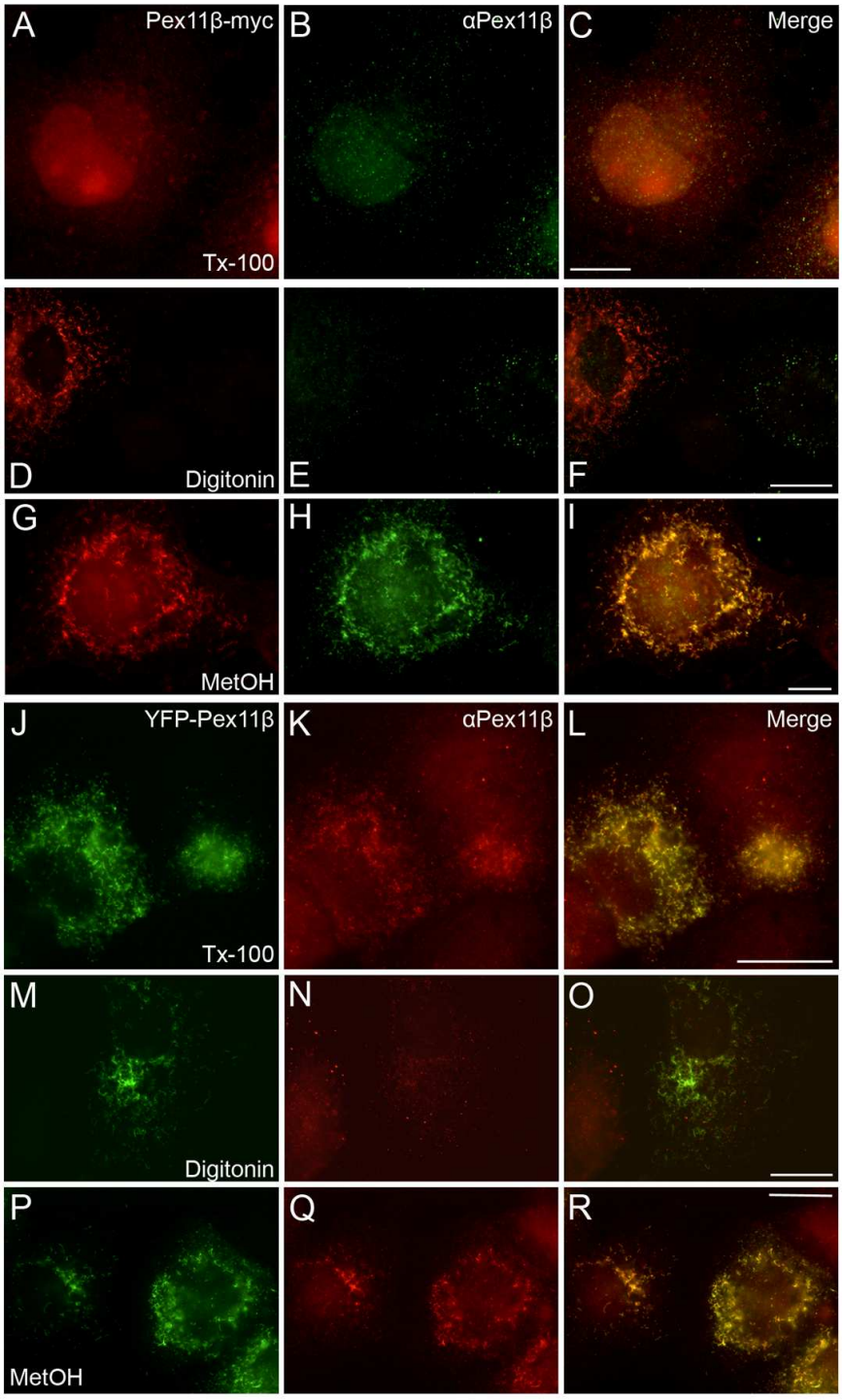

Fig. 3.16: The Pex11pβ antibody only recognizes its epitope after peroxisomal membrane permeabilization.
COS-7 cells were transfected with either Pex11β-myc (A-I) or YFP-Pex11β (J – R) and fixed after 24h. Membrane (and organelle membrane) permeabilization was achieved by incubating fixed cells with either 0.2 % Tx100 (A – C; J – L), 25µg/ml digitonin (D – F; M – O) or methanol (MetOH; G – I; P – R), before immunostaining against the myc epitope and an internal part of Pex11β (A – I) or Pex11β alone (J – R) was performed.
Note that Pex11β-myc is reomved from the peroxisomal membrane after Tx100 permeabilisation (A – C), while YFP-Pex11pβ is retained after fixation (J – L).
Bars, 20µm.

The observed recognition pattern after differential permeabilization indicates that the novel Pex11pβ antibody detects an epitope within the peroxisomal membrane or matrix; upon inquiry, the company confirmed that it was raised against a peptide sequence of the human protein comprised of amino acids 110 and 140 which rendered the antibody suitable for subsequent protease-protection assays.

3.2.5 Proteinase K digest of human Pex11pβ results in the formation of a 17 kD protease-protected fragment

The information on the position of the antibody epitope provided us with the opportunity to conclusively determine the position of the first transmembrane domain of human Pex11pβ. The localization of the epitope suggests the following scenarios: if Pex11pβ contains only one transmembrane domain at its very C-terminus (Fig. 3.17 A, upper panel), digest with the versatile serine protease proteinase K would result in an almost complete degradation of the protein (and the epitope), therefore no Pex11pβ signal would be detected upon immunoblotting. If a first transmembrane domain between amino acid positions 170 and 200 would be assumed (Fig. 3.13), the epitope would similarly be digested. On the other hand, if the first transmembrane domain lies approximately in the centre of the protein (positions aa 85-105), the antibody epitope would be rendered protected between the two transmembrane domains, resulting in the formation of a protein fragment of approximately 17kD upon proteinase K digest (Fig. 3.17 A, lower panel).

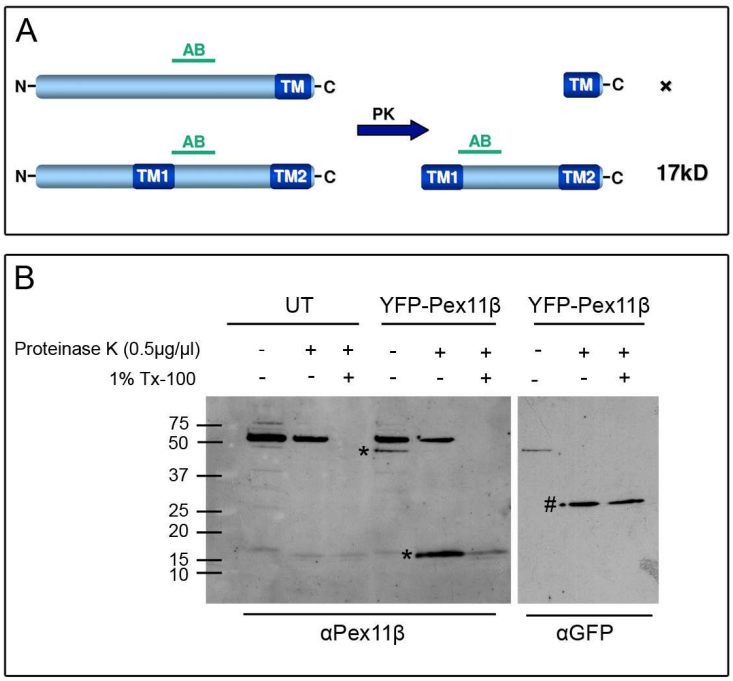

Fig. 3.17.: Protease protection assay of YFP-Pex11pβ.
(A) Scheme of assay, see text for details.
(B) COS-7 cells were transfected with YFP-Pex11β or mock transfected as a control (UT). 48 hours after transfection, peroxisome-enriched fractions were prepared and protein concentrations were determined. For protease K digest, 60 µg of protein were digested with protease K in the presence or absence of Tx100. Undigested controls were included. After 40 minutes, the reaction was stopped by the addition of PMSF and samples were precipitated by TCA. Samples were run on 12.5 % SDS-PAGE and immunoblotting was performed against Pex11pβ. As a loading control, the membrane was re-incubated with anti-GFP after membrane stripping. Asterisks indicate YFP-Pex11β band before and after digest.

For protease-protection assays, COS-7 cells were transfected with YFP-Pex11pβ and peroxisome-enriched fractions were generated. Untransfected cells were routinely included. Equal amounts of protein of were subjected to proteinase K digest for 40 minutes on ice (untreated controls, proteinase K addition in the presence and absence of Tx100), before the reaction was stopped with PMSF and protein was precipitated by TCA. Subsequently, protein samples subjected to SDS-PAGE and immunoblotting using the Pex11pβ antibody (Fig. 3.17,

B). Untransfected cells were routinely included as a control (Fig. 3.17, UT). After immunoblotting, the Pex11pβ antibody recognized an unspecific band in untransfected and transfected samples of around 60 kD, as indicated by the supplier. It also failed to detect a band corresponding to endogenous Pex11pβ (Fig. 3.17 B, UT), consistent with our previous observations. Upon overexpression of YFP-Pex11pβ, the expected band of around 56 kD size was observed in undigested, intact fractions, albeit weakly (Fig. 3.17 B, asterisk). After proteinase K addition to intact peroxisomes, a band shift occurred, yielding a detectable protein fragment of 16-18 kD size which was lost upon incubation with Tx100 (asterisks in Fig. 3.17 B). Interestingly, the YFP-fusion protein of YFP-Pex11pβ has proven to be resistent to proteinase K action, most probably due to the compact β-barrel structure of GFP and its analogues (Fig. 3.17 B, αGFP). Thus, it served as an excellent loading control upon re-incubation with anti-GFP antibody to ensure equal loading of lanes (Fig. 3.17 B, αGFP). In undigested controls, the YFP signal correlated with the previously observed Pex11pβ signal, while the YFP fusion tag was cleaved from Pex11pβ after proteinase K addition and remained resistent to its action (Fig. 3.17 B, #). Similar band intensities of YFP were detected with and without the addition of Tx100, verifying equal loading of lanes. Further incubation of nitrocellulose membranes with an AOX antibody routinely ensured integrity of the peroxisomal membrane before Tx100 addition (data not shown). Furthermore, similar results were obtained upon overexpression of the wild-type protein. The concentration of proteinase K used in this study was in line with experimental protocols employed in other peroxisomal studies (Pinto et al., 2009), but further protease-protection assays were performed using increasing concentrations of proteinase K (10µg/ml to 500µg/ml). The 17 kD fragment was already generated using lower concentrations of proteinase K (20µg/ml) (data not shown).

The results obtained by proteinase K digest are consistent with a predicted first transmembrane domain of Pex11pβ located approximately between amino acid positions 90 and 110 (Fig. 3.13) (PredictProtein; TM predict) (Schrader et al., 1998b).

In above experiments, specificity of the assay was ensured by addition of the detergent Tx100 and subsequent digest of the now accessible protein fragment, however, Pex11pβ was shown to be Tx100 sensitive. Thus, to address the question if the region between the two transmembrane domains extends into the peroxisomal matrix, protease-protection assays were performed using sonication as an alternative mode of membrane permeabilization.

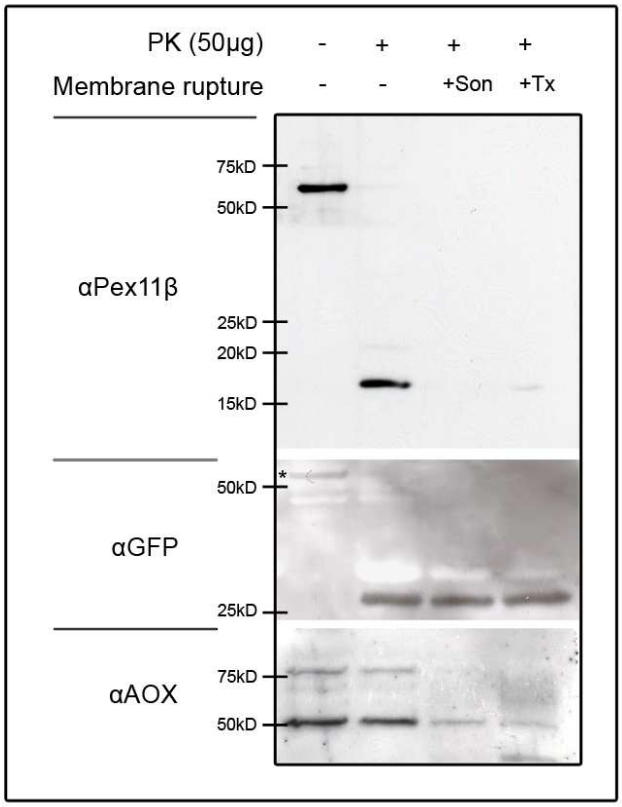

Fig. 3.18: The remaining Pex11pβ fragment is digested upon sonication.
COS-7 cells were transfected with YFP-Pex11β. 48 hours after transfection, peroxisome-enriched fractions were prepared and protein concentrations were determined. For proteinase K digest, 60 µg of protein were digested with proteinase K in the presence or absence of Tx100. Alternatively, fractions were sonicated (3 x 10 seconds, 100 W). Undigested controls were included. After 40 minutes, the reaction was stopped by the addition of PMSF and samples were precipitated by TCA. Samples were run on 12.5 % SDS-PAGE and immunoblotting was performed against Pex11pβ. As a loading control, the membrane was re-incubated with anti-GFP antibody. Successful membrane rupture was verified by incubation with an antibody against AOX, a peroxisomal matrix marker. Note that due to protein processing 3 bands corresponding to AOX are detected after immunoblotting (25, 50, 75 kD)

Disruption of peroxisomal membrane integrity by sonication and Tx100 addition was validated by monitoring AOX reactivity. After sonication or Tx100 treatment and subsequent proteinase K digest, a prominent decline in corresponding AOX signals was observed (Fig. 3.18, AOX), indicating successful membrane permeabilization. In line with our previous observations, proteinase K digest of intact peroxisomal membranes resulted in the generation of a 17kD protein fragment of YFP-Pex11pβ which disappeared upon sonication (Fig. 3.18, Pex11β). Detection of YFP again served as a loading control (Fig. 3.18, GFP)

These findings indicate that the regio between the two transmembrane domains of Pex11pβ extends into the peroxisomal matrix and becomes susceptible to protease digest upon sonication. Thus, finally, human Pex11pβ was conclusively shown to possess two transmembrane domains, the first of which is localized between amino acids 90 and 110; consequently its crucial N-terminal domain is defined to reach from amino acids 1-90.

3.2.6 In peroxisome-deficient cells, Pex11pβ is mistargeted to mitochondria

Mutations in the peroxins Pex3p, Pex16p and/or Pex19p which are essential for peroxisomal membrane biogenesis result in a complete absence of peroxisomal structures (1.1.5.2), resulting in severe pathophysiological conditions (1.1.4). Under those conditions, the ER was suggested to serve a default membrane for peroxisomal membrane proteins (1.2.1), thus the

targeting of human Pex11pβ was investigated in peroxisome-deficient ΔPex19 patient fibroblasts.

Pex11pβ-myc was co-transfected with a mitochondrial GFP construct (Mito-GFP) into ΔPex19 fibroblasts. After 24 hours, cells were fixed and processed for immunofluorescence against the myc epitope (Fig. 3.19)

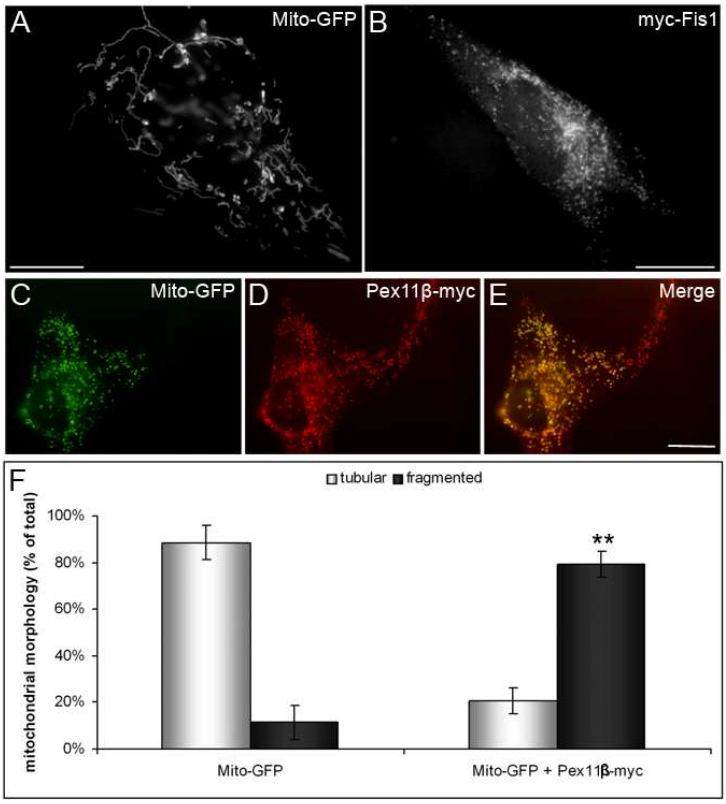

Fig. 3.19.: In ΔPEX19 cells, Pex11pβ mistargets to mitochondria and leads to their fragmentation.
(A, B) ΔPEX19 fibroblasts were transfected with either the mitochondrial matrix marker Mito-GFP (A) or myc-Fis1, a tail-anchored protein known to fragment mitochondria (B). Cells were fixed and in the case of (B) processed for immunofluorescence against the myc epitope.
(C-E) ΔPex19 fibroblasts were co-transfected with Mito-GFP and Pex11β-myc and processed for immunofluorescence against the myc epitope. Merge of signals is seen in (E). Bars, 20µm.
(F) For statistical analysis, ΔPex19 fibroblasts were either transfected with Mito-GFP alone or co-transfected with Mito-GFP and Pex11β-myc and processed for immunofluorescence. Mitochondrial morphology was assessed to be either tubular (A) or fragmented (B) and 100 cells/coverslip (2 coverslips/condition) were grouped accordingly. Data is shown as means +/- SD (** $p<0.01$ compared to control).

Interestingly, in the absence of peroxisomal membranes, Pex11β-myc was mislocalized to mitochondria, but not to the ER (Fig. 3.19 C-E). Moreover, contrary to its default role as membrane tubulator, mitochondrial mistargeting of Pex11pβ led to a prominent fragmentation of mitochondria reminiscent of e.g. overexpression of Fis1, a tail-anchored protein that is involved in recruiting DLP1 to mitochondria and peroxisomes (Fig. 3.19 B) (1.2.2.3). Mitochondrial morphology was assessed to be either tubular (A) or fragmented (B) and statistical analysis was performed. Statistical evaluation clearly revealed a highly significant increase in the number of fragmented mitochondria after Pex11pβ-myc overexpression and mistargeting.

3.2.7 Upon mistargeting to mitochondria Pex11pβ retains its Tx100 sensitivity and orientation

Contrary to its membrane elongating effects on peroxisomes, targeting of Pex11pβ to mitochondria led to their severe fragmentation; to address if its native characteristics and orientation were perturbed, Tx100 sensitivity and protein topology at the mitochondrial membrane were investigated.

N-terminally and C-terminally myc-tagged variants of Pex11pβ were transfected into ΔPex19 fibroblasts and processed for differential permeabilization using either digitonin or Tx100. Subsequently, cells were processed for indirect immunofluorescence against the myc epitope and evaluated by epifluorescence microscopy.

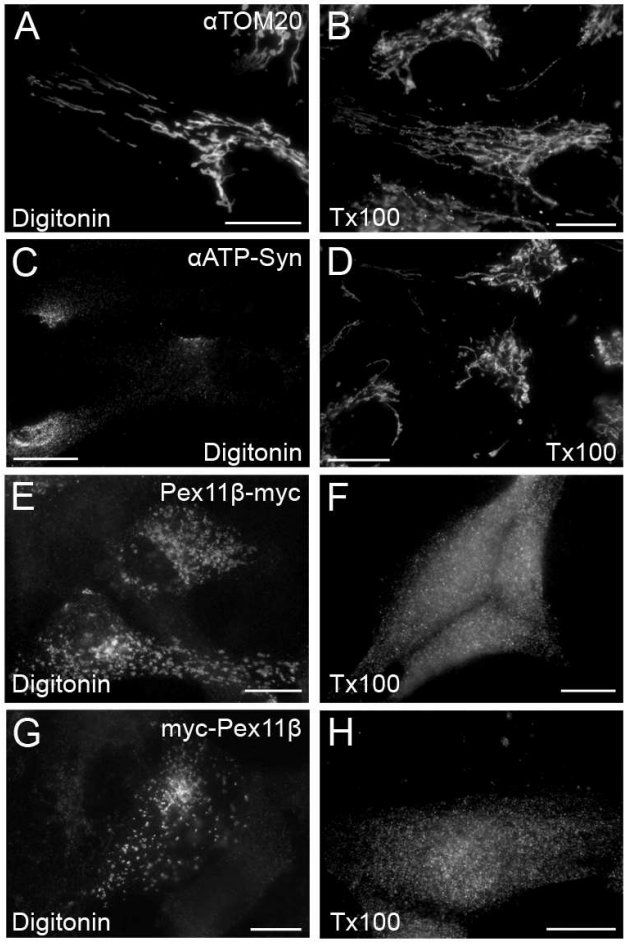

Fig. 3.20: Upon mistargeting to mitochondria, Pex11β retains its Tx100 sensitivity and both termini remain exposed to the cytosol.
(A-D) Permeabilization controls. ΔPex19 fibroblasts were fixed and processed for differential permeabilization using either digitonin (A, C) or Tx100 (B, D). Subsequently, they were stained either with antibodies against the outer membrane marker TOM20 (A, B) or the matrix localized portion of ATP-Synthase (αβ subunit) (C, D).
Bars, 20µm.
(E-H) Both termini of Pex11pβ are exposed to the cytosol. ΔPex19 fibroblasts were transfected with either N-terminally or C-terminally tagged Pex11β and processed for differential permeabilization and immunofluorescence 24 hours later.
Bars, 20µm.

To control differential permeabilization of mitochondrial membranes, immunofluorescence against the outer membrane protein TOM20 as well as the matrix-localized portion of ATP-Synthase (subunit αβ) was performed. As expected, TOM20 was readily detected under both conditions (Fig. 3.20 A,B), while ATP-Synthase reactivity was only provided upon mitochondrial membrane permeabilization with Tx100 (Fig. 3.20 D). Both, N-terminally and

C-terminally tagged variants of Pex11pβ were localized at the mitochondrial membrane after digitonin permeabilization, indicating that both termini extend to the cytosol (Fig. 3.20 E,G). Upon Tx100 addition, however, the Pex11pβ signal was reduced to the appearance of small spot-like structures throughout the cytosol (Fig. 3.20 F,H) that were not associated with mitochondria anymore. Hence, Pex11pβ retained its Tx100 sensitivity, although it was embedded in a different lipid environment. To address if Pex11pβ is inserted into the mitochondrial membrane in its native topology, Pex11pβ-myc was overexpressed in ΔPex19 fibroblasts and differential permeabilization and co-staining with the Pex11pβ antibody was performed.

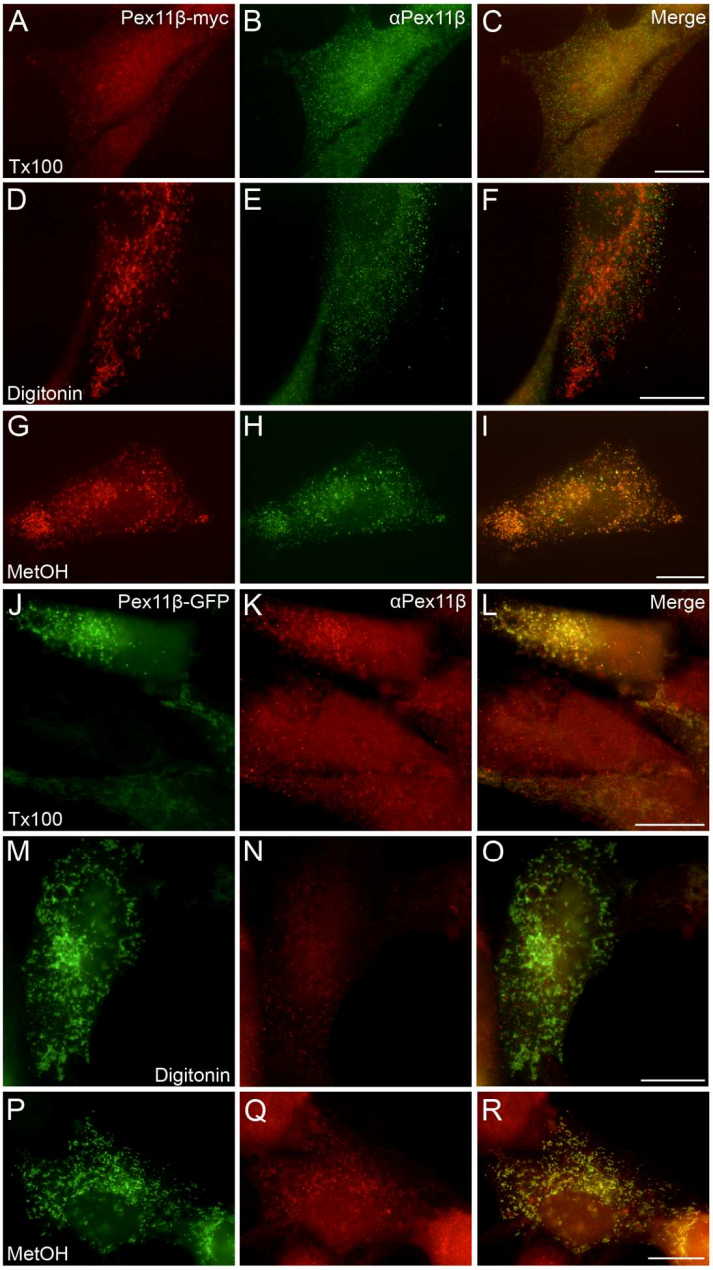

Fig. 3.21: Pex11pβ retains its topology upon mistargeting to mitochondria.
(A-I) ΔPex19 fibroblasts were transfected with Pex11pβ-myc, fixed after 24 hours and permeabilized using either Tx100 (A-C), digitonin (D-F) or methanol (G-I). Subsequently, they were co-stained with antibodies against the myc epitope (A, D, G) and Pex11pβ (B, E, H).
(J-R) In a similar approach, ΔPex19 fibroblasts were transfected with Pex11β-GFP before permeabilization using either Tx100 (J-L), digitonin (M-O) or methanol (P-R).
Subsequently, staining against Pex11pβ was performed (K, N, Q).
Bars, 20µm

Similar to the observations made in COS-7 (Fig. 3.16), upon mistargeting to mitochondria in ΔPex19 cells, the Tx100-sensitive Pex11pβ-myc was only recognized by the Pex11pβ antibody upon permeabilization of the mitochondrial membrane with methanol (Fig. 3.21 A-I). Overexpression of Pex11pβ-GFP which was not removed from (peroxisomal and) mitochondrial membranes by Tx100, and subsequent co-staining with the Pex11pβ antibody in ΔPex19 cells similarly revealed that antibody detection was only guaranteed after membrane rupture with either Tx100 or methanol (Fig. 3.21 J-R). As the Pex11pβ antibody recognition pattern after differential permeabilization mirrored the observations at the peroxisomal membrane, Pex11pβ was inserted in its proper orientation into the mitochondrial membrane in ΔPex19 cells. It has to be noted, however, that upon overexpression a fraction of the protein was detected in the cytosol, but never at the ER.

3.2.8 Pex11pβ targeting to mitochondria depends on its N-terminal domain

Upon overexpression of YFP-Pex11pβ in peroxisome-deficient ΔPex19 cells, hardly any mitochondrial localization of the fusion protein was observed, while Pex11pβ-GFP mistargeted efficiently to mitochondria, indicating that the N-terminal domain is important for mitochondrial targeting. To investigate this question, side-by-side overexpression of YFP-Pex11pβ, Pex11pβ-YFP and Pex11pβ-GFP in ΔPex19 fibroblasts and subsequent analysis by epifluorescence microscopy was performed. Overexpression of YFP-Pex11pβ led to a predominantly cytosolic localization of the protein (Fig. 3.22 B), while C-terminal tagging of Pex11pβ resulted in a clearly detectable mitochondrial localization (Fig. 3.22 C, D). Moreover, mitochondrial targeting of Pex11pβ was impaired upon deletion of the first 40 amino acids of the protein (ΔN40-Pex11pβ-myc) (Fig. 3.22 A).

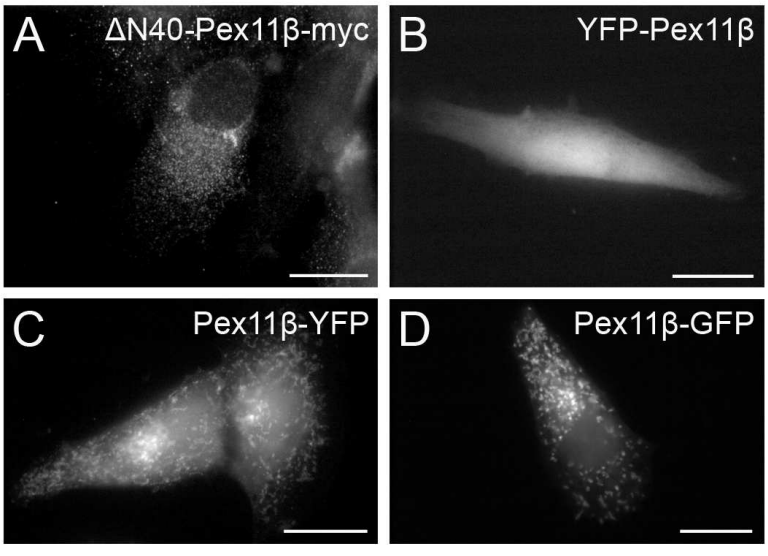

Fig. 3.22: The N-terminal domain of Pex11pβ mediates its mitochondrial targeting.
ΔPex19 fibroblasts were either transfected with a deletion mutant of Pex11β-myc lacking the first 40 aa (A), YFP-Pex11pβ (B), Pex11pβ-YFP (C) or Pex11pβ-GFP (D) and after 24 hours were fixed and processed for immunofluorescence. Note that although the protein is targeted to mitochondria in (C) and (D), there is some cytosolic signal. Bars, 20µm

These findings indicate that mitochondrial mistargeting of Pex11pβ is mediated by its N-terminal domain.

3.2.9 Post-translational regulation of human Pex11pβ: *In silico* phospho screening of mammalian Pex11β

In the previous section of this study, the often evoked N-terminal domain of Pex11pβ was defined to be comprised of amino acids 1-90. Although the membrane deforming capacity of Pex11 proteins was recently linked to the presence of an amphipathic helix within the N-terminus, only little is known about how the action of Pex11 proteins is further regulated by other post-translational mechanisms. For instance, phosphorylation of *Sc*Pex11p was only demonstrated in the yeast *S. cerevisiae* and shown to be crucial for its action (Knoblach & Rachubinski, 2010), therefore, the potential regulation of human Pex11pβ by phosphorylation was examined.

An initial *in silico* screen of Pex11pβ was performed using various databases that either calculate potential phosphorylation sites within the protein or screen for potential kinase binding sites (2.10.2). To gain insight into the selection of appropriate residues, screening results obtained with the validated S165/167 phospho-site of *Sc*Pex11p were used as a guideline where applicable. To further narrow down the number of potential phospho-sites, only multiple hits obtained by several screening tool were selected for further characterization (Fig. 3.23 A). Furthermore, a homology screen of various Pex11pβ protein sequences was performed and examined for conservation of phosphosites (Fig. 3.23 C). The positions of potential phospho-sites are indicated by red brackets in Fig. 3.23 C. Combining *in silico* screening results and protein homology of Pex11pβ, several conserved sites were identified at positions S11, S38, S70, S154, S160, S168 and T178 within the human protein. Their position within the protein overall architecture is depicted in Fig. 3.23 B (probable sites). However, due to the fact that no intra-peroxisomal kinases have been identified so far and our study was focused on the regulation of the protein's N-terminal domain, intra-peroxisomal phospho-sites were excluded for further analysis for the time being (Fig. 3.23 B, extraperoxisomal sites). Furthermore, the potential S70 site was excluded from further studies due to preliminary data indicating that deletion of the first 70 amino acid of Pex11pβ did not exercabate the effect of deletion of the first 40 amino acids (personal communication MJ. Cardoso). Thus, for a parallel approach, the potential N-terminal phospho-sites S11 and S38 were selected for the generation of phospho-mimicking "on" and "off" mutants (Fig. 3.23 B, selected sites).

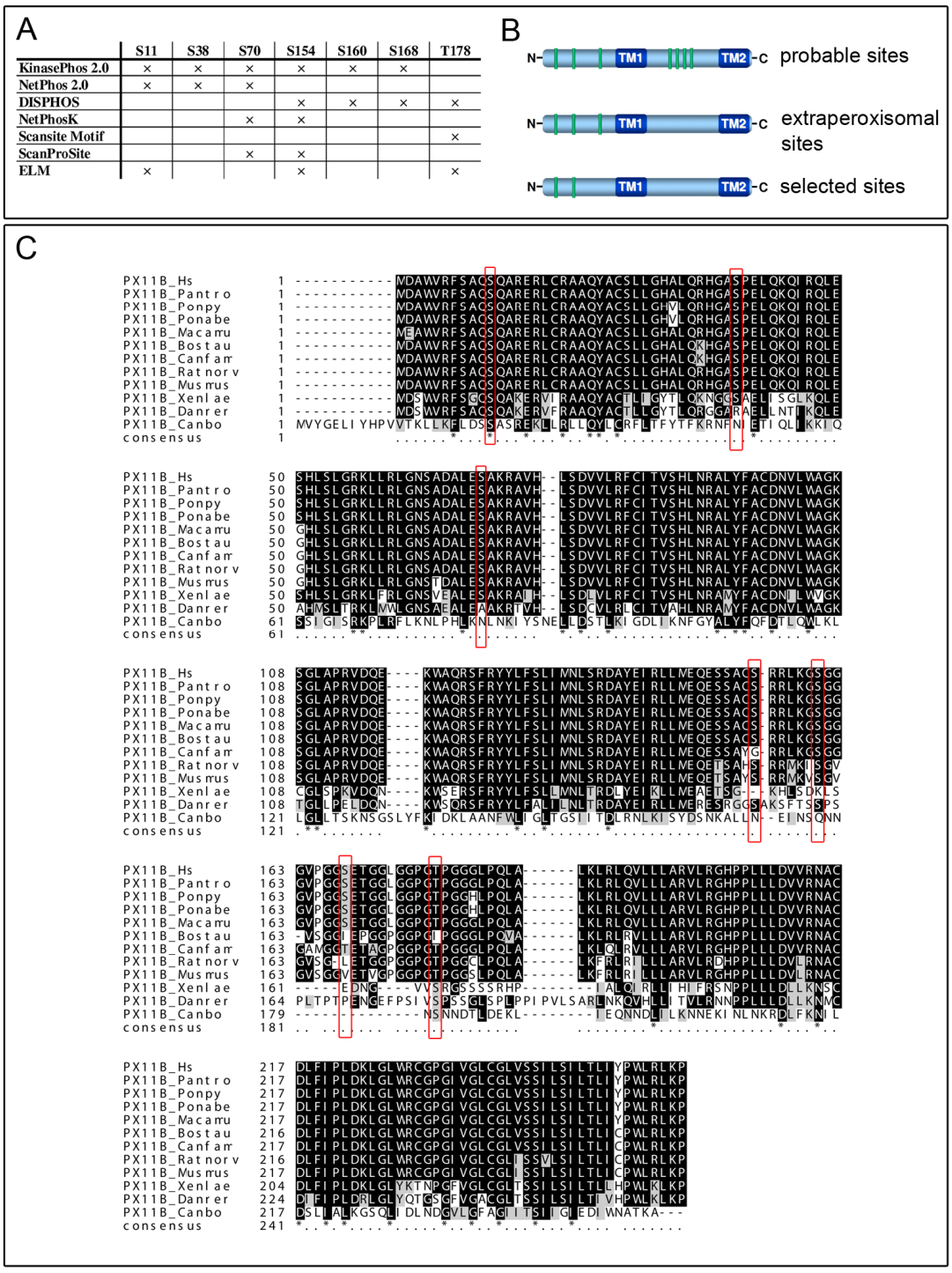

Fig. 3.23: Determination of potential phospho-sites within human Pex11pβ.
(A) Overview of multiple hits for different positions. Several online screening tools were used to determine potential phospho-sites in the sequence of human Pex11pβ. The various tools are plotted against the positions given.
(B) Scheme depicting phospho-sites chosen for subsequent studies. Based on the screening, several potential phosphosites were selected whose approx. location is indicated in the upper scheme (potential sites). Based on our findings regarding the topology of Pex11pβ, intraperoxisomal sites were excluded (Extraperoxisomal sites). Furthermore, based on studies regarding deletions of N-terminus, the sites listed on the bottom were chosen.
(C) Overview of conserved amino acids in Pex11pβ protein sequences across species. The potential phospho-sites are depicted in red brackets. Note that the one at position S11 is highly conserved.

3.2.10 Human Pex11pβ is not phosphorylated in COS-7 cells

To determine phosphorylation of human Pex11pβ, *in vivo* phospho-labelling of Pex11pβ was performed while phospho-mimicking "on" and "off" mutants of the S11 and S38 residues were generated in parallel (co-operation MJ. Cardoso).

For *in vivo* phospho-labelling, COS-7 cells overexpressing human YFP-Pex11pβ were starved in phosphate-free buffer and then incubated with P^{32}-orthophosphate for several hours, before the cells were lysed in the presence of protease and phosphatase inhibitors. Subsequently, immunoprecipitation against YFP was performed. Overexpression of YFP-Pex11pβ was chosen due to high transfection and precipitation rates. As negative and positive controls, YFP-C1 (empty vector) and human APP-GFP were included. APP, the amyloid precursor protein, is an integral membrane protein that functions as a cell surface receptor and performs physiological functions on the surface of neurons relevant to neurite growth, neuronal adhesion and axonogenesis. In the last decades, studies of APP and its proteolytic products have been mostly focused on its role as a producer of the toxic amyloid beta peptide associated with Alzheimer's disease. However, especially the C-terminal domain of APP has been shown to be extensively regulated by phosphorylation essential for its physiological function (Lee et al., 2003; Schettini et al., 2010).

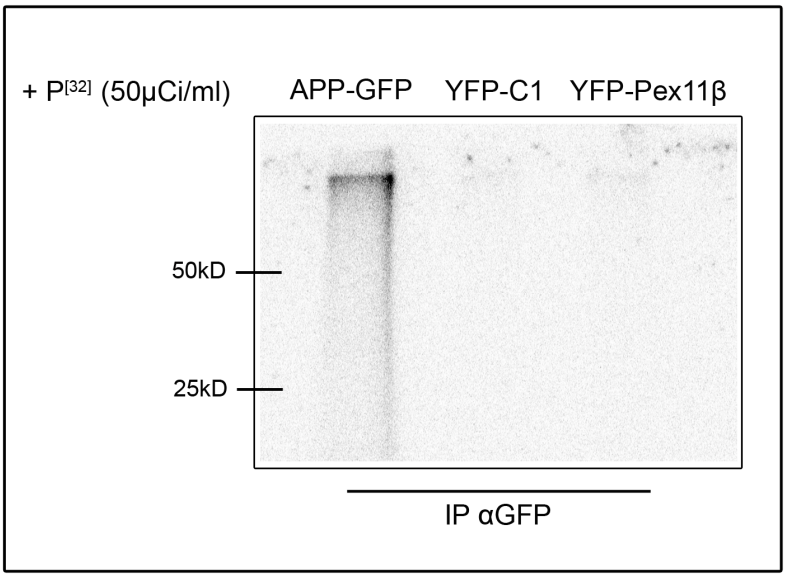

Fig. 3.24: YFP-Pex11pβ is not phosphorylated in COS-7 cells. COS-7 cells were transfected with either APP-GFP (100kD), YFP-C1 (28kD) or YFP-Pex11β (56kD). 24 hours later, *in vivo* phospholabelling was performed for 4 hours at 37°C before cells were lysed and immunoprecipitation against GFP was performed. Precipitated samples were run on 12.5 % SDS-PAGE , fixed and dried. The dried gel was exposed for 3 days on a phosphoimaging screen and evaluated using a BioRad Molecular FX imager.

Phosphorylated APP-GFP was successfully precipitated with the GFP antibody, resulting in the detection of a radio-labelled protein band of the expected size (Fig. 3.24). Furthermore, no signal corresponding to empty YFP vector was observed. Concerning YFP-Pex11pβ, no radio-labelled fraction of the protein was detected upon *in vivo* phospho-labelling, similar to the negative control, indicating that human Pex11pβ is not phosphorylated in COS-7 cells. Furthermore, no effect on peroxisome dynamics was observed upon expression of the selected

phospho-mimicking mutants of Pex11pβ when compared to wild-type, thus, phosphorylation does not appear to contribute to the regulation of Pex11pβ activity in mammals.

3.2.11 Pex11pβ-mediated peroxisome membrane elongation is regulated by homo-dimerization

Concerning the regulation of Pex11 protein activity, the action of Pex11p in *S. cerevisiae* was suggested to be regulated by homo-dimerization in a redox-dependent manner: a model was proposed in which *Sc*Pex11p actively acts as a monomer at the inner surface of the peroxisomal membrane and is oxidized upon maturation of peroxisomes to form inactive dimers in mature peroxisomes (Marshall et al., 1996). Human Pex11pβ was also shown to form homo-dimers, depending on its N-terminal domain (Li & Gould, 2003; Kobayashi et al., 2007; Koch et al., 2010). Deletion of the N-terminal domain abolishes membrane elongation (Kobayashi et al., 2007) (our unpublished results}, but it not clear if monomeric or dimeric Pex11pβ represents the active form in higher organisms. For instance, while the decline in Pex11pβ-based membrane elongation upon N-terminal deletion might only be linked to the deletion of the amphipathic helix (Kobayashi et al., 2007), our unpublished results indicated that deletion of the first 40 amino acids already diminished membrane elongation, although the amphipathic helix remained intact. As phosphorylation of Pex11pβ was excluded to contribute to regulate peroxisome dynamics at the organelle level, the dimerization of Pex11pβ was addressed.

Overexpression of Pex11pβ in mammalian cells was shown to profoundly induce the formation of elongated peroxisomal structures: already 5 hours after transfection, approximately 90 % of the transfected cells contained predominantly tubular peroxisomes. Subsequently, the number of elongated peroxisomes decreased to 60 % after 24 hours and 25 – 30 % after 72 hours, respectively (Schrader et al., 1998b) (Fig. 3.25 A). In order to correlate the described morphologies with the stochiometry of human Pex11pβ, we took advantage of the Tx100 extraction protocol established in this study (3.2.2) that allowed simultaneous cross-linking and enrichment of Pex11pβ. COS-7 cells were transfected with myc-Pex11pβ and the Tx100 extraction assay (2.11.3) was performed 5, 24 and 72 hours after transfection. Equal amounts of supernatant and pellet fractions of fixed COS-7 cells as well as unfixed lysates were subjected to SDS-PAGE and subsequent immunoblotting against the myc epitope (Fig. 3.25). While overall expression of myc-Pex11pβ remained low at early time points (L, 5h, 24h), detectable levels of Pex11pβ were successfully extracted into the supernatant. Interestingly, mostly dimeric forms of myc-Pex11pβ (approx. 56kD) were

detected 5 and 24 hours after transfection, coinciding with a predominantly tubular morphology of peroxisomes at these time points (Fig. 3.25 A). Note that, like before (3.2.2) monomeric Pex11pβ was also detected upon longer exposure, albeit at lower concentrations. 72 hours after transfection, monomeric Pex11pβ was primarily detected. Notably, upon overexpression of an N-terminally truncated version of Pex11pβ-myc lacking the first 40 amino acids (ΔN40-Pex11pβ-myc), peroxisomes maintained a predominantly spherical morphology 5 – 72 hours after transfection. After application of the Tx100 extraction assay and subsequent immunoblotting at the corresponding time points, dimer formation of Pex11pβ was impaired (personal communication S. Grille).

These findings indicate that, contrary to to *Sc*Pex11p, human Pex11pβ acts as a dimer to induce membrane tubulation, while monomeric might mirror an inactive state.

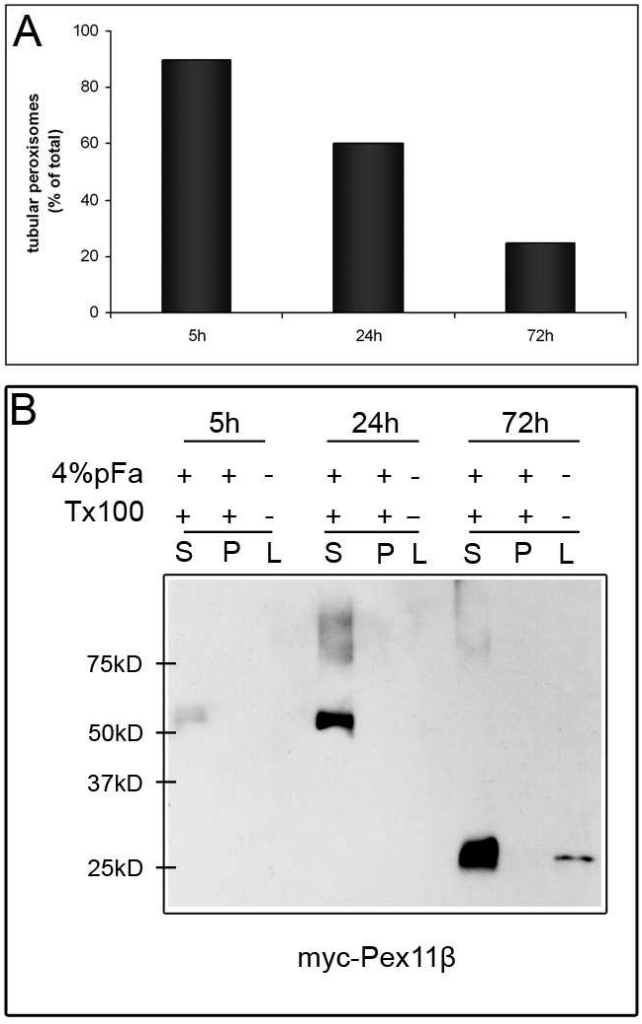

Fig. 3.25: Human Pex11pβ acts predominantly as a dimer at early time points.
(A) Induction of tubular peroxisomes after Pex11pβ expression. COS-7 cells were transfected by electroporation with myc-Pex11pβ and were fixed after 5, 24 and 72 hours, resp, and processed for immunofluorescence against peroxisomal markers. (adapted from (Schrader et al., 1998b).
(B) COS-7 cells were transfected by electroporation with myc-Pex11pβ and were fixed after 5, 24 and 72 hours, resp, using 4 % pFA. After fixation, they were permeabilized using 0.2% Tx100. The supernatants (S) were collected and cells (P) were lysed. Simultaneously, lysates (L) of non-fixed cells were prepared to verify expression of myc-Pex11pβ. After determination of protein concentration, samples of the supernatant and pellet fractions were run on an SDS-PAGE and subjected to immunoblotting against the myc epitope. Note that the myc signal in the control pellet is very difficult to detect. Similarly, myc-Pex11pβ detection in control lysates (L) is very faint at early time points, indicating expression of the protein is lower at early time points.

3.2.12 Summary

In the second part of this thesis, human Pex11pβ, a crucial protein regulating peroxisomal growth and division, was characterized biochemically in order to gain insight into the regulation of peroxisome dynamics on the organellar level. Using a newly available antibody directed against an internal part of the protein in combination with differential permeabilization and protease-protection assays, the first transmembrane domain of human Pex11pβ was conclusively localized to amino acid positions 90-110 for the first time. Consequently, the N-terminal domain of the protein was investigated in regard to its contribution to Pex11pβ regulation. *In vivo* phospho-labelling did not reveal phosphorylation of human Pex11pβ, but biochemical cross-linking and enrichment of Pex11pβ in time-course experiments linked its membrane-deforming activity to homo-dimerization. Deletion of the first 40 amino acids abolished the formation of elongated peroxisomal structures, concomitant with an impairment in dimer formation, although the amphipathic helix remained intact. Thus, human Pex11pβ is regulated in a different manner than its yeast counterpart. Moreover, human Pex11pβ was shown to mistarget to mitochondria in patient fibroblasts lacking any peroxisomal structures, an observation that might have further, underappreciated consequences for the severity of peroxisomal disorders.

3.3 IDENTIFICATION OF NOVEL STIMULI ALTERING PEROXISOME DYNAMICS

Peroxisomes have been known to be highly dynamic in regard to their morphology: in addition to spherical structures (the common textbook image), elongated, tubular peroxisomes as well as tubulo-reticular networks have been observed in electron and light microscopy (Gorgas, 1985; Gorgas, 1987; Yamamoto & Fahimi, 1987; Schrader et al., 2000; Schrader, 2001; Schrader & Fahimi, 2006). In mammalian cell culture models, peroxisome elongation was strongly induced upon direct manipulation of components of the peroxisomal growth and division machinery (e.g. by Pex11p overexpression or inhibition of DLP1, Fis1 or Mff) (Schrader et al., 1998b; Koch et al., 2003; Lingard & Trelease, 2006; Tanaka et al., 2006), but also stimulated under conditions of cellular growth and after the addition of growth factors and polyunsaturated fatty acids (PUFAs, e.g. arachidonic acid) (Schrader et al., 1996a; Schrader et al., 1998a). Moreover, a higher frequency of elongated peroxisomes was observed upon depolymerisation of microtubules and exposure of cells to UV irradiation and ROS (Schrader et al., 1996a; Schrader et al., 1996b; Schrader et al., 1999). However, the reception of those signals as well as their transduction onto the peroxisomal level mediating the stimulated formation of peroxisomal tubules remains unknown. Morphologically distinct types of peroxisomes have been described in different organs of mammalian organisms and cell types (Hicks & Fahimi, 1977; Gorgas, 1987; Yamamoto & Fahimi, 1987; Fahimi et al., 1993; Schrader et al., 1994; Litwin & Bilinska, 1995; Schrader et al., 1996a; Schrader et al., 2000), but mostly elongated structures have been linked to peroxisomal growth and division processes (1.2.2). Similarly, peroxisome elongation after UV irradiation was suggested to serve protective effect, as an increase in peroxisome numbers by growth and division might facilitate the scavenging of ROS and combat ROS-induced cell damage (Schrader et al., 1999). However, distinct peroxisomal structures induced upon stimulation might also be indicative of other specific functions: the formation of tubulo-reticular networks observed in lipid synthesizing epithelia was indicated to facilitate metabolic functions, e.g. by increasing the surface to volume ratio and generating a uniform distribution of proteins within the network (Gorgas, 1987; Kollatakudy et al., 1987; Schrader et al., 2000; Ribeiro et al., 2011). It has become clear in recent years that organelle morphology and dynamics are intricately linked to its function and thus, cellular homeostasis. In line with this, a lethal defect affecting peroxisomal and mitochondrial fission has been identified (Waterham et al., 2007). Moreover, alterations in peroxisome dynamics and perturbations of their number are linked to several

pathophyiological conditions such obesity, AOX1 deficiency and cancer (Chang et al., 1999; Lauer et al., 1999; Funato et al., 2006; Frederiks et al., 2010; Diano et al., 2011). Thus, it is extremely important to decipher the relationship between peroxisome morphology and function as well as to gain insight into the signal transduction mechanisms regulating organelle dynamics to potentially compensate disease phenotypes. .

The following section of this thesis aimed at characterizing a link between stimulated alterations of peroxisome dynamics and their potential function. Several different stimuli were grouped according to the nature of the stimulus and screened for a potential effect on peroxisome dynamics. Subsequent characterization of the response on the peroxisomal level enabled the characterization of a novel cell culture model to study the regulation of peroxisome dynamics.

3.3.1 6-hydroxydopamine induces DLP1-dependent fragmentation of mitochondria and apoptosis in SH-SY5Y neuroblastoma cells but has no effect on peroxisome dynamics

In the course of this study, the effects of 6-hydroxydopamine (6-OHDA) on mitochondrial morphology in neuronal SH-SY5Y cells were investigated (co-operation J. Jordan Bueso, University of Castilla-LaMancha, Spain). The neurotoxin 6-OHDA is an oxidative metabolite of dopamine that is widely used to generate experimental models of Parkinson's disease (Blum et al., 2001; Bove et al., 2005b). Although its mechanism of action remains a matter of debate, the generation of reactive oxygen species has been implicated (Galindo et al., 2003). It was observed that 6-OHDA induced a profound fragmentation of mitochondria that represented an early event of neuronal apoptosis, preceding the collapse of mitochondrial membrane potential and cytochrome c release (Gomez-Lazaro et al., 2008). Interestingly, the mitochondrial fragmentation was shown to be dependent of DLP1, the large GTPase mediating fission of mitochondria and peroxisomes. Therefore, the effect of 6-OHDA on peroxisomal morphology was investigated.

SH-SY5Y neuroblastoma cells transfected with a mitochondrial GFP construct were seeded on coverslips and treated with 50 µM 6-OHDA for 3 hours, a time point at which mitochondria were already profoundly fragmented. Cells were fixed and epifluorescence microscopy using antibodies against the peroxisomal membrane marker PMP70 was performed (Fig. 3.26 A-D).

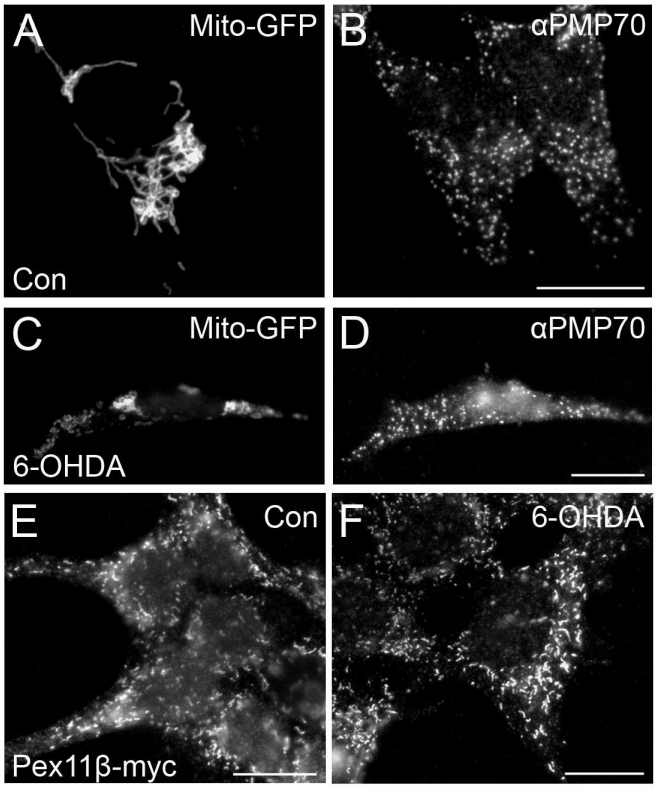

Fig. 3.26: 6-OHDA does not affect peroxisome dynamics.
(A-D) SH-SY5Y cells transfected with Mito-GFP (A, C) were either mock treated (A,B) or treated with 50 µM 6-OHDA for 3 hours and fixed with 4 % pFA. Subsequently cells were processed for immunofluorescence against the peroxisomal membrane protein PMP70 (B, D). (E-F) To facilitate detection of peroxisome fragmentation, SH-SY5Y cells were transfected with Pex11pβ-myc before treatment with 50 µM 6-OHDA (G). Cells were fixed and processed for immunofluorescence against the peroxisomal membrane protein PMP70 (F, G).
Bars, 20µm.

Whereas treatment with 50 µM 6-OHDA resulted in a clear fragmentation of mitochondria after 3 hours, no alterations of peroxisome dynamics were detected (Fig. 3.26 B, D). Peroxisomes retained their spherical morphology and no obvious increase in peroxisome number was observed. Even after prolonged incubation with 6-OHDA, no effect on peroxisome morphology was observed (data not shown). However, as detection of a potential fragmentation of already spherical peroxisomes proved difficult, SH-SY5Y cells were additionally transfected with the peroxisomal membrane tubulator Pex11pβ-myc prior to 6-OHDA treatment to induce a profound elongation/proliferation of peroxisomes and potentially determine a difference in the kinetics of subsequent division with and without 6-OHDA (Fig. 3. 26 E-F). Nonetheless, 6-OHDA treatment after Pex11pβ overexpression failed to induce any changes in peroxisomal morphology and number which would be expected if there was an induced fragmentation of peroxisome tubules (Fig. 3.26 F, G).

Taken together, these findings indicate that although 6-OHDA induced mitochondrial fragmentation in a DLP1-dependent manner, there was no effect on peroxisome morphology and dynamics. This suggests that although DLP1 is a shared component of both organelle fission machineries, the recruitment and/or regulation of DLP1 in response to specific stimuli is co-ordinated in an organelle-specific manner. Additionally, DLP1-mediated fragmentation after 6-OHDA application was shown to represent an early event in the onset of cellular apoptosis that precedes the collapse of mitochondrial membrane potential and cytochrome c

release (Gomez-Lazaro et al., 2008). Upon onset of cell death, peroxisomes maintained a predominantly spherical morphology, in line with previous observations (our unpublished results). Hence, the absence of tubular or more complex peroxisomal structures which to growth and division or a potential protective function might indicate that a "costly" induction of peroxisome tubulation was rendered unnecessary under apoptotic conditions in which cell death is imminent.

3.3.2 Alterations of peroxisome dynamics in response to oxidative stress

3.3.2.1 Overview of the model system employed to study alterations of peroxisome dynamics in response to oxidative stress

Peroxisomes in human HepG2 cells were shown to respond to UV irradiation and H_2O_2 treatment with profound peroxisomal tubulation, displaying a morphology reminiscent of the "beads-on-string" appearance associated with growth and division (Schrader et al., 1999). The observed phenotype was linked to oxidative stress, as pre-treatment with antioxidants reversed the response. Similarly, a dual response of peroxisomes to oxidative stress was characterized in plants, where plant peroxisomes were shown to respond to short-term oxidative stress (up to 2 hours) with the formation of small membrane protrusions called peroxules, while maintained oxidative stress initiated an analogous peroxisomal "bead-on-a-string" morphology (Sinclair et al., 2009). Peroxisomal tubulation after ROS exposure was suggested to represent a protective, morphological response, as an increase in the number and/or volume of peroxisomes might facilitate their ROS scavenging abilities. Interestingly, the formation of peroxules in plant cells was linked to the action of hydroxyl radicals and hydrogen peroxide (Sinclair et al., 2009), indicating that the nature of the stress signal is important. To analyze the importance of the nature, but also the intracellular source of oxidative stress leading to alterations of peroxisome dynamics, mammalian HepG2 and COS-7 cells were used as a model system (Fig. 3.27). In order to quantify a peroxisomal stress response, the induction of peroxisomal tubules was used as a read-out. Examples for a spherical (B, D) and tubular morphology (C, E) of the peroxisomes in the respective cell lines are given in Fig. 3.27 (B-E). To investigate the question if a general increase in cytosolic oxidative stress stimulates peroxisome tubulation, cells were treated with H_2O_2, the heavy metals copper and nickel (whose toxicity has been linked to ROS induction by Fenton-like chemistry or depletion of GSH) (Stohs & Bagchi, 1995) as well as paraquat (2.8.9). The toxicity of paraquat, one of the most widely used herbicides in the world, has been attributed to an enzymatically catalyzed one-electron redox cycling of the parent molecule, resulting in

generation of superoxide anions (Bus & Gibson, 1982). Its neurotoxic capacities have been linked to the development of Parkinson's disease (PD) which is further employed in toxin-induced PD models (Bove et al., 2005a; Franco et al., 2010). Additionally, the question was addressed if impairment of mitochondrial function affects peroxisome morphology and dynamics (Fig. 3.27 A, compartment-specific response). Therefore, cells were treated with inhibitors of the mitochondrial respiratory chain such as rotenone (complex I), malonate (complex II) and sodium azide (complex IV) (Chance et al., 1963; Schulz et al., 1997; Yoshikawa et al., 1998; Fei et al., 2000; Fernandez-Gomez et al., 2005). The existence of compartment-specific induction of tubular peroxisomes was further addressed by live cell imaging using variants of the photosensitizer KillerRed targeted to the cytosol, mitochondria and peroxisomes (Bulina et al., 2006a). The existence of peroxules in mammalian cells was additionally investigated in this set-up.

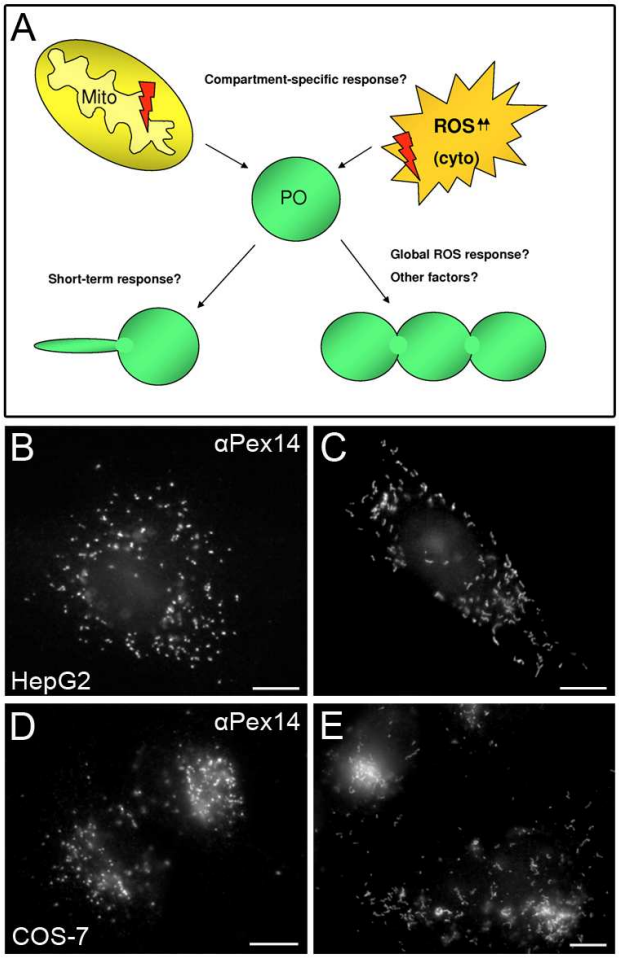

Fig. 3.27: Induction of tubular peroxisomes in mammalian cell lines.
(A) Scheme of the tubulation assay employed in this study. Peroxisomes (PO) have been shown to respond to oxidative stress with elongation, however, it is currently unclear if tubulation mirrors a global ROS response. Moreover, more factors leading to tubulation need to be identified. Furthermore, the existence of small membrane tubules (peroxules) after short-term stress has not been investigated in mammalian cells. It is also unclear if tubulation is induced differently depending if ROS are generated in the cytosol, mitochondria (Mito) or peroxisomes.
(B-E) Examples for peroxisome morphology in HepG2 (B, C) and COS-7 cells (D, E). HepG2 and COS-7 cells were seeded on coverslips, fixed and subjected to immunofluorescence against the peroxisomal membrane marker Pex14. In both cells, peroxisomal morphology can range from a more spherical (B, D) to a tubular morphology (C, E).
Bars, 20µm.

3.3.2.2 Screening for alterations of peroxisomes in response to oxidative stress

In order to screen for alterations of peroxisome dynamics after profound increase in cytosolic oxidative stress, HepG2 cells seeded on coverslips were treated with H_2O_2, the heavy metals

copper and nickel and paraquat. Stressors were applied in the indicated concentrations (Fig. 3.28 A). After 24 hours, cells were fixed and prepared for indirect immunofluorescence against the peroxisomal marker Pex14p before peroxisome morphology was assessed by epifluorescence microscopy. Peroxisome morphology was either defined as being spherical or tubular as described above.

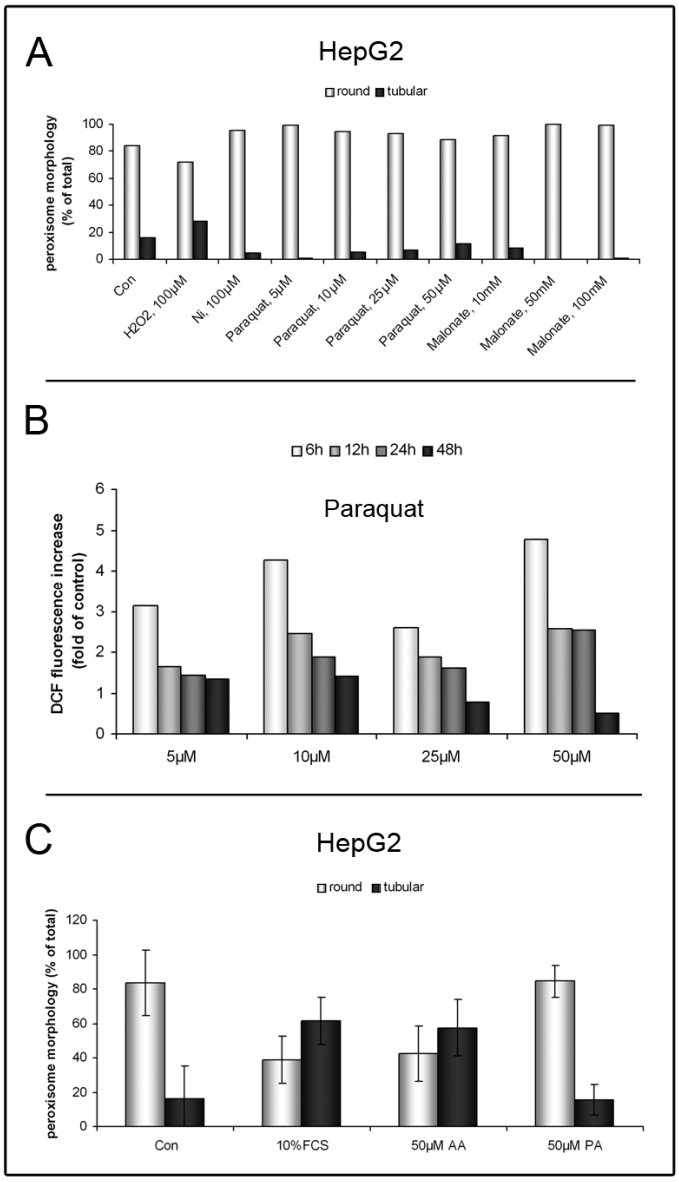

Fig. 3.28.: Screening for stressors affecting peroxisome dynamics.
(A) HepG2 were seeded on glass coverslips at a defined density of 2 x 10^5 cells/ml. 4 hours after seeding, the indicated stressors were applied at the indicated concentrations. After 24 hours, when peroxisome tubulation is described to reach its maximum (Schrader et al., 1998a; Schrader et al., 1999), cells were fixed and processed for epifluorescence microscopy. Peroxisome morphology was determined to be either spherical or tubular and data of representative experiments is shown.
(B) Paraquat induces a profound increase in oxidative stress in human HepG2 cells. HepG2 cells were seeded at a defined density of 10.000 cells/well in a black 96 well plate. The next day, cells were subjected to paraquat treatment at the indicated concentrations. After the indicated time points, cells were stained with 10 µM DCFDA and fluorescence intensity was measured using a TECAN fluorescence spectrometer. A minimum of 6 wells was measured per conditions. A representative experiment for paraquat treatment is shown.
(C) HepG2 cells respond to serum and fatty acid addition with elongation. In order to control the plasticity of peroxisomes in HepG2 cells, 4 hours after seeding, cells grown in serum-free medium were treated with 10 % serum as well as arachidonic acid (AA) and palmitic acid (PA) as described before (Schrader et al., 1998a). The next day, cells were fixed and processed for epifluorescence microscopy. Peroxisome morphology was determined to be either spherical or tubular. Data is shown as means +/- SD and taken from 3 independent experiments.

Although peroxisomes in HepG2 cells responded to the addition of H_2O_2 with a slight increase in the number of tubular peroxisomes (Fig. 3.28 A), treatment with nickel, copper or paraquat did not result in a significant elongation of the peroxisomal compartment. Similar results were obtained in COS-7 cells (data not shown). To verify a successful induction of oxidative stress, an increase of DCF fluorescence intensity after application of stressors was measured (2.8.11); as a representative example, induction of oxidative stress after paraquat

application is shown in Fig. 3.28 B. In HepG2 cells, a profound increase of DCF fluorescence was measured after 6 hours of paraquat exposure (up to 3-5 fold of control, depending on the concentration of paraquat used) that was diminished after longer incubation (1.5-2 fold after 12 hours). After prolonged time points (24 and 48 hours) the measured fluorescence intensity decreased to levels around control or even below control in the case of higher paraquat concentrations. This might be explained by the fact that cell metabolism and growth were already severely affected by paraquat treatment, resulting in a diminished growth rate when compared to control cells. Hence, the cell-density-dependent ratio of DCF fluorescence in regard to controls decreased below 1-fold. Similar observations were made with the other stressors. To rule out the possibility that the plasticity of peroxisomes as such was diminished or impaired in the HepG2 cells used, e.g. due to changing culture conditions, HepG2 cells (grown under serum-free conditions in this model system (2.8.9)) were stimulated with 10 % FCS and the fatty acids arachidonic acid (AA) and palmitic acid (PA) as described before (Schrader et al., 1998a). Although application of ROS stressors did not lead to any peroxisome tubulation, stimulation with serum and AA induced a profound tubulation when compared to controls (Fig. 3.28 C), indicating that the dynamics of the peroxisomal compartment were not impaired as such.

In a different set of experiments, the effect of mitochondrially-derived oxidative stress on peroxisome morphology was assessed. However, using different concentrations of malonate, an inhibitor of complex II of the mitochondrial electron transfer chain, no induction of peroxisome tubulation was observed in HepG2 cells (Fig. 3.28 A). In a parallel study, similar observations were made using rotenone and sodium azide (inhibitors of complex I and IV, respectively) in COS-7 cells (master thesis S. Pinho, co-supervisor N. Bonekamp): while both compounds led to a slight increase in oxidative stress (quantified by DCF measurement), sodium azide failed to induce profound peroxisome tubulation while rotenone treatment led to the formation of elongated peroxisomes. However, this observation was subsequently linked to its microtubule-depolymerising effects and not to oxidative stress or impairment of mitochondrial function. Interestingly, an induction of tubular peroxisomes was observed upon treatment with L-buthionine sulfoximine (BSO), a compound that changes cellular redox state by irreversibly inhibiting the rate-limiting enzyme of GSH synthesis (Griffith & Meister, 1979).

While HepG2 cells responded to external growth factor stimulation, but also to UV irradiation, with an elongation of the compartment, induction of cytosolic oxidative stress did not result in significant alterations of peroxisome dynamics. Furthermore, inhibition of the

mitochondrial electron transfer chain and subsequent ROS generation did not alter peroxisome morphology. Hence, these stimuli were excluded from further studies analyzing the molecular basis of peroxisome elongation. These findings indicate that mammalian peroxisomes do not respond to oxidative stress with a generalized, morphological ROS reponse, but that other factors contribute to modulate peroxisome morphology. For instance, while UV irradiation increases intracellular oxidative stress, it might trigger the activation of additional signalling cascades contributing to the observed peroxisome elongation. Moreover, the observations made after exposure to BSO suggest that alterations of peroxisome morphology might be more closely linked to changes in the cellular redox-state, but not a global increase in oxidative stress.

3.3.2.3 Compartment-specific activation of KillerRed does not induce peroxules or peroxisomal tubules

A possible compartment-specific effect of ROS increase on peroxisome dynamics was further investigated by live cell imaging using KillerRed. KillerRed is a phototoxic dimeric red fluorescent GFP-like protein that exceeds the phototoxic properties of any GFP protein by at least 1.000 fold (Bulina et al., 2006a; Bulina et al., 2006b). Being genetically encoded, it can either be fused to any protein or be targeted to any organelle of choice, where the fusion protein will produce primarily superoxide radicals upon green light activation. To examine an effect of compartment-specific ROS induction on peroxisome dynamics, KillerRed constructs targeted to either the cytosol (KillerRed-C) or mitochondria (KillerRed-Mito) were obtained. Additionally, the existence of small peroxisomal protrusions (peroxules) that are formed upon induction of short-term oxidative stress (up to 2 hours) in plant cells (Sinclair et al., 2009) was investigated in this set-up by determining alterations in peroxisome dynamics 30 – 90 minutes after KillerRed activation. COS-7-GFP-PTS1 cells, chosen because of their plastic peroxisomal compartment and their easy manipulation, were transfected with either KillerRed-C or KillerRed-Mito and subjected to live cell imaging using a Zeiss LSM 510 Meta confocal microscope equipped with a PECON chamber 24 hours later. According to the protocol (Bulina et al., 2006b), single cells expressing KillerRed were chosen and focused quickly in the centre of the image window. Exposure to green fluorescent light was kept to a minimum to avoid premature photobleaching. Using the 488 laser line, an image was taken of peroxisomal GFP-PTS1 prior to bleaching, then KillerRed activation was performed using the green fluorescent light of the mercury lamp. As expected, there was a profound photobleaching of KillerRed upon green light illumination and, in line with the manufacturer's instructions, cells were irradiated for twice as along as required for

photobleaching to ensure a reliable phototoxic effect (Bulina et al., 2006b). After photobleaching, images were taken every 60 seconds for 30-90 minutes using the 488 and 561 laser lines. Although KillerRed-C as well as KillerRed-Mito was clearly targeted to the respective compartments (Fig. 3.29, pre-bleach), and there was a successful photobleaching of KillerRed consistent with its activation and induction of oxidative stress, no changes in peroxisome morphology – including the formation of smaller tubules – were observed in live cell imaging. Even after longer time periods, there was no generation of tubular peroxisomes (Fig. 3.29), indicating that increased levels of both cytosolic and mitochondrial oxidative stress do not effect peroxisome dynamics.

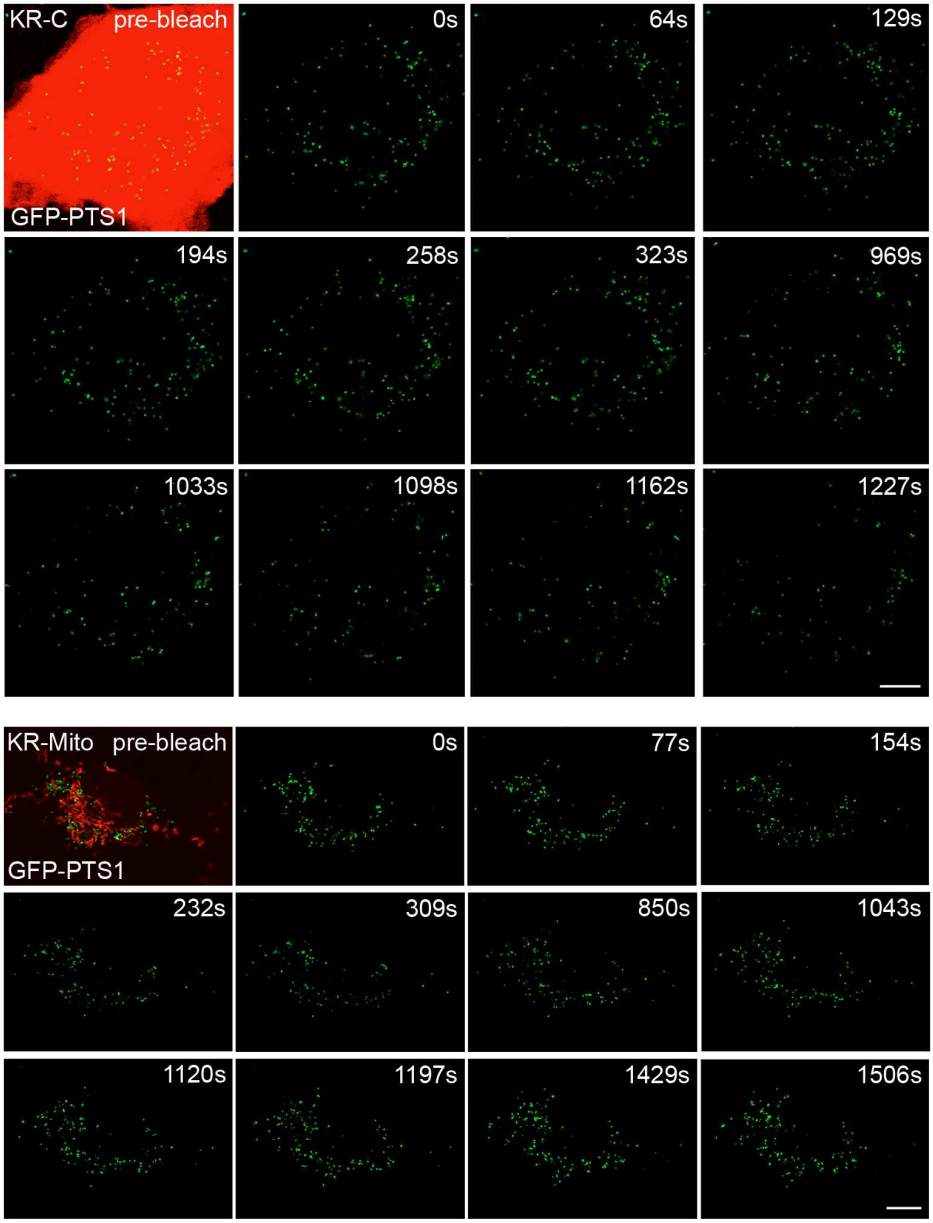

Fig. 3.29: Activation of KillerRed targeted to the cytosol or mitochondria does not alter peroxisome dynamics.
COS-7-GFP-PTS1 cells were transfected with either KillerRed-C (upper panel) or KillerRed-Mito (lower panel). 24 hours later, cells were subjected to live cell imaging using a LSM 510 Meta confocal microscope. Before activation of KillerRed images of single cells were taken (Pre-bleach). After photobleaching of KillerRed, images were collected every 60 seconds for 30-90 minutes.
Bars, 20µm.

In another set of experiments, the effect of an increase in intra-peroxisomal oxidative stress on peroxisome dynamics was examined. Therefore, a peroxisomally-targeted variant of KillerRed was generated by fusion of a C-terminal fragment of AOX to the C-terminus of KillerRed (KR-PO, Fig. 3.30, A-C). To ensure proper targeting, KR-PO was transfected into COS-7-GFP-PTS1 cells and co-localization of signals was observed by epifluorescence microscopy (Fig. 3.30, C). Note that in some cells, a cytosolic signal of KR-PO was observed, indicating a slower targeting of the construct into peroxisomes which is consistent with findings made in a recent study (Ivashchenko et al., 2011). For live cell imaging and activation of KR-PO, the construct was transfected into COS-7-GFP-PTS1 cells and subjected to the imaging procedure described above. Single cells displaying a clearly peroxisomal morphology were chosen.

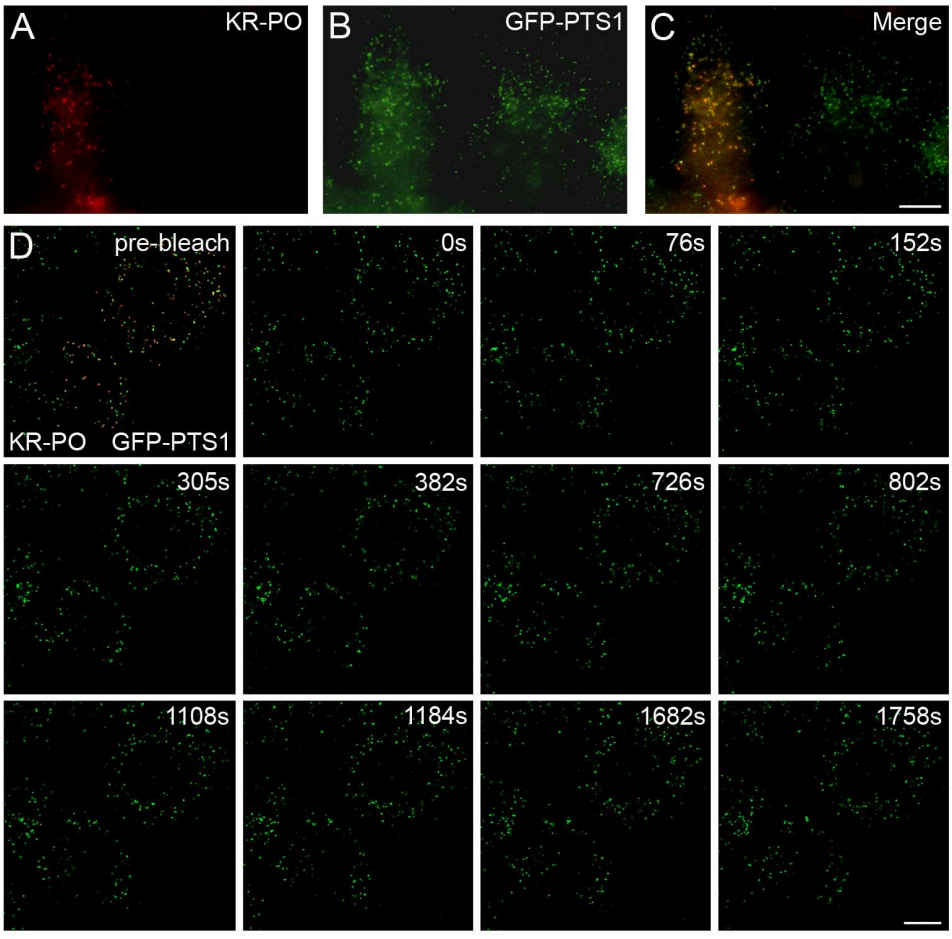

Fig. 3.30: Activation of peroxisomal KillerRed does not affect peroxisome dynamics. (A-C) COS-7-GFP-PTS1 (B) cells were transfected with KillerRed-PO (KR-PO, A). 24 hours later, cells were fixed and mounted for epifluorescence microscopy. Merge of signal is shown in C. (D) KR-PO was transfected into COS-7-GFP-PTS1 cells. 24 hours later, cells were subjected to live cell imaging using a LSM 510 Meta confocal microscope. Before activation of KillerRed images of single cells were taken (Pre-bleach). After photobleaching of KillerRed, images were collected every 60 seconds for 30-90 minutes. Bars, 20µm.

Similar to the observation made with the cytosolic or mitochondrial variant, activation of the peroxisomally-targeted KillerRed variant did not result in any, not even short-term, changes in peroxisome morphology (Fig. 3.30, D) which maintained a primarily spherical appearance.

Thus, the observations made in live cell upon activation of the photosensitizer KillerRed targeted to the cytosol, mitochondria or peroxisomes support the aforementioned results obtained in fixed cells after treatment with oxidative stressors and inhibitors of the mitochondrial electron transfer chain. Moreover, small protrusions of peroxisomes, similar to the peroxules in the plant system, were never seen in this study.

In summary, no peroxisomal oxidative stress response coinciding with a profound alteration in peroxisome dynamics occurred in the mammalian system; however, additional signals might contribute to mediate a morphological response. Furthermore, peroxisomal characteristics other than dynamics may be affected by oxidative stress.

3.3.3 Dexamethasone treatment leads to an elongation of peroxisomes in AR42J cells

While screening for external stimuli affecting peroxisome dynamics, the effect of the synthetic glucocorticoid dexamethasone on peroxisome morphology was tested in rodent AR42J cells. AR42J cells were originally derived from a rat pancreatic tumour following exposure to azaserine (Longnecker et al., 1979) and have been used as a model system for granule formation and pancreatic exocrine secretion (Swarovsky et al., 1988). Treatment with the synthetic glucocorticoid dexamethasone induces the differentiation of AR42J cells into exocrine, acinar-like cells and the *de novo* formation of electron-opaque secretory granules, which contain the major pancreatic zymogens (Logsdon et al., 1985; Logsdon et al., 1987; Swarovsky et al., 1988). For instance, secretory differentiation markers such as chymotrypsinogen and amylase show a profound induction in regard to their mRNA and synthesis rates (Scheele, 1993).

To determine potential changes in peroxisome morphology, AR42J cells were seeded on coverslips and the next day, cells were induced using either 10 nM or 1 µM dexamethasone, a more pathophysiological concentration (Du et al., 2009). The cell culture medium was exchanged using fresh dexamethasone every day. Untreated controls and treated cells were fixed after 6, 24, 48 and 72 hours and processed for immunofluorescence against the peroxisomal membrane protein Pex14p. Routinely, co-staining with the secretory granule marker chymotrypsin was included as a positive control in order to verify successful induction of zymogen granules which are profoundly induced upon glucorticoid induced secretory differentiation (see above).

Peroxisome morphology was examined by confocal microscopy. Peroxisomes in AR42J cells usually display a small, spherical appearance (Fig. 3.31, A), however, upon prolonged

treatment with dexamethasone more elongated structures became prominent within the cells (e.g. Fig. 3.31, E, F, K). Moreover, the overall number of cells with tubular peroxisomes increased. These observations were made after 24, 48 and 72 hours of treatment, but not after 6 hours (Fig. 3.31. A-C). Furthermore, using a higher concentration of dexamethasone, the overall number of cells with tubular peroxisomes increased as well as the degree of tubulation within single cells, indicating a dose-dependent effect of dexamethasone. To substantiate these observations, statistical analysis was performed.

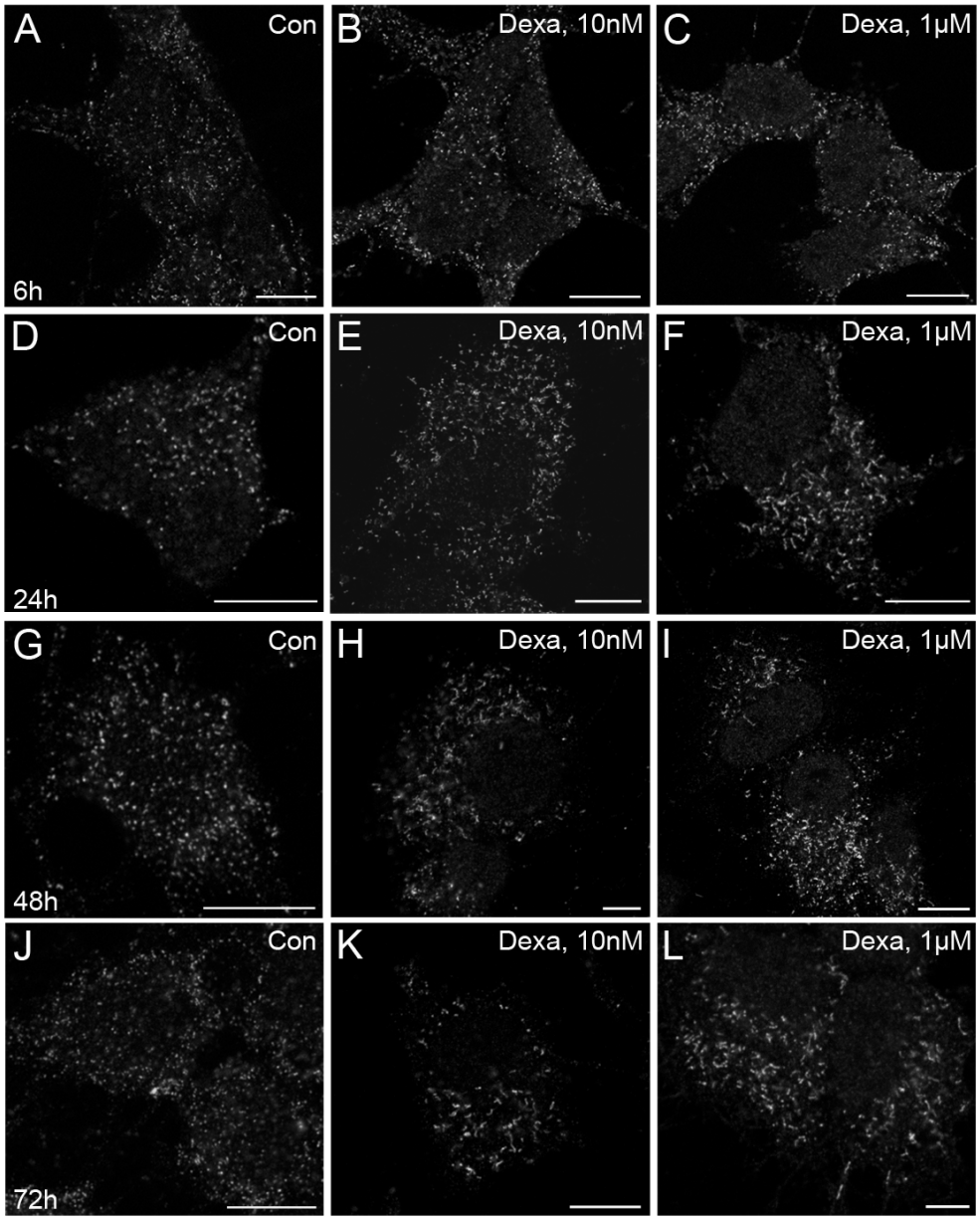

Fig. 3.31.: Dexamethasone induces peroxisome tubulation in AR42J cells.
AR42J cells were seeded on glass coverslips and were subsequently induced with either 10nM (B, E, H, K) or 1µM dexamethasone (C, F, I, L) after 24 hours. Untreated controls (A, D, G, J) and treated cells were fixed after 6, 24, 48 and 72 hours and processed for immunofluorescence against the peroxisomal marker protein Pex14. Changes in peroxisome morphology were assessed by confocal microscopy.
Bars, 10µm, except for H and L, 5µm.

For statistical analysis, untreated controls and induced AR42J cells were processed for immunofluorescence and epifluorescence microscopy as described above and peroxisome morphology was either determined to be spherical (e.g. Fig. 3.31 A) or tubular (Fig. 3.31 E) and grouped accordingly.

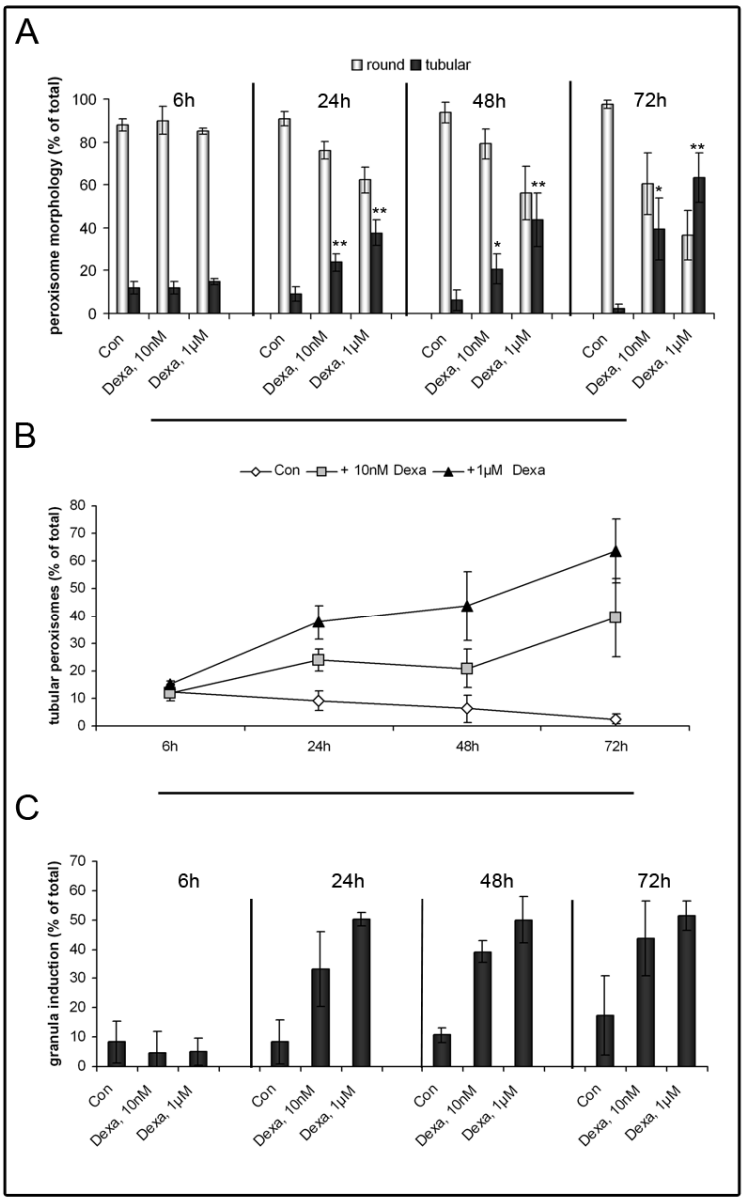

Fig. 3.32: Dexamethasone induces peroxisome elongation in a dose-dependent manner.
(A) For statistical analysis, untreated controls and dexamethasone-induced AR42J cells were processed immunofluorescence against Pex14p and chymotrypsin as described. Peroxisome morphology was either determined to be round/spherical or tubular and 100 cells per coverslip were counted. Per experimental condition, 2 coverslips were analyzed and data is presented from 4 independent experiments as means +/- SD (*, $p<0.05$; **, $p<0.01$ when compared to controls).
(B) Distribution of tubular peroxisomes after dexamethasone treatment over time. The percentage of tubular peroxisomes determined above was plotted against the different time points.
(C) Secretory granules are successfully induced upon dexamethasone treatment. As a control, untreated controls and dexamethasone-treated AR42J cells were processed for immunofluorescence against the granule marker chmyotrypsin after the indicated time points. For statistical analysis, 100 cells/coverslips were counted. Data is presented as means +/- S.D. and derived from 3 independent experiments.

While 6 hour treatment of AR42J cells with both concentrations of dexamethasone did not result in a profound change in peroxisome morphology (Fig. 3.32 A, 6 hours), prolonged incubation with dexamethasone for 24, 48 and 72 hours clearly induced a significant increase in the number of tubular peroxisomes when compared to respective controls. The difference between controls and treated cells became more prominent over time, as peroxisomes in control cells were observed to acquire a smaller, more spherical morphology with increased culture time (and cell density). Application of the higher dexamethasone concentration (1 µM) further increased the

percentage of tubular peroxisomes, indicating a dose-dependent effect of dexamethasone on peroxisome dynamics.

Plotting of the percentage of tubular peroxisomes over time (Fig. 3.32 B) revealed a clear trend for peroxisome tubulation: peroxisomes in untreated controls reached their peak tubular morphology 6 hours after induction (and 24 hours after seeding) after which the number of tubular structures steadily decreased to reach a minimum after 72 hours. Upon treatment with 10 nM dexamethasone, however, the percentage of tubular peroxisomes increased after 24 hours of induction and - after reaching a slight plateau after 48 hours – increased even further to reach a maximum at 72 hours after induction. A steady and even more dramatic continuous increase in the percentage of tubular peroxisomes was observed at the higher concentration of 1 µM dexamethasone. Successful stimulation with dexamethasone was verified by examining the induction of zymogen granules in AR42J cells. Controls and treated cells were processed for immunofluorescence against the granule marker chymotrypsin and analyzed by epifluorescence microscopy (Fig. 3.32 C). Stimulation with dexamethasone led to a re-arrangement of the secretory compartment in AR42J cells concomitant with an increase in chymotrypsin-positive granular structures after 24 – 72 hours. Still, it must be noted that not all cells displaying tubular peroxisomes also contained granular structures, indicating two uncoupled processes.

These findings indicate that dexamethasone induces the formation of tubular peroxisomes in a dose-dependent manner that is uncoupled from granule induction. Moreover, continuous application of dexamethasone seems to provide a constant stimulus for peroxisome tubulation, most probably inhibiting subsequent fission, as no obvious increase in the number of spherical peroxisomes was observed.

3.3.4 One-time stimulation with dexamethasone is sufficient to induce peroxisome elongation

Above findings indicate that application of dexamethasone provided a continuous stimulus for peroxisome elongation that did not result in an apparent subsequent fission of the tubuli which would be reminiscent of peroxisome proliferation. Thus, it was interesting to analyze if removal of dexamethasone after initial stimulation would lead to a breakdown of the tubules by fission and thus, an increase in peroxisome numbers. AR42J cells were seeded on coverslips and treated with 10 nM dexamethasone as described. Dexamethasone was then removed either 24 or 48 hours after initial stimulation and cells were thoroughly washed

before regular culture medium was applied. Upon shift to normal medium, cells were incubated for another 48 or 24 hours, respectively. 72 hours after initial induction, cells were fixed and processed for epifluorescence microscopy. Untreated controls as well as continuously treated AR42J cells were included as negative or positive controls. For statistical analysis, peroxisome morphology was assessed to be either spherical or tubular and cells were grouped accordingly. The results are shown in Fig. 3.33:

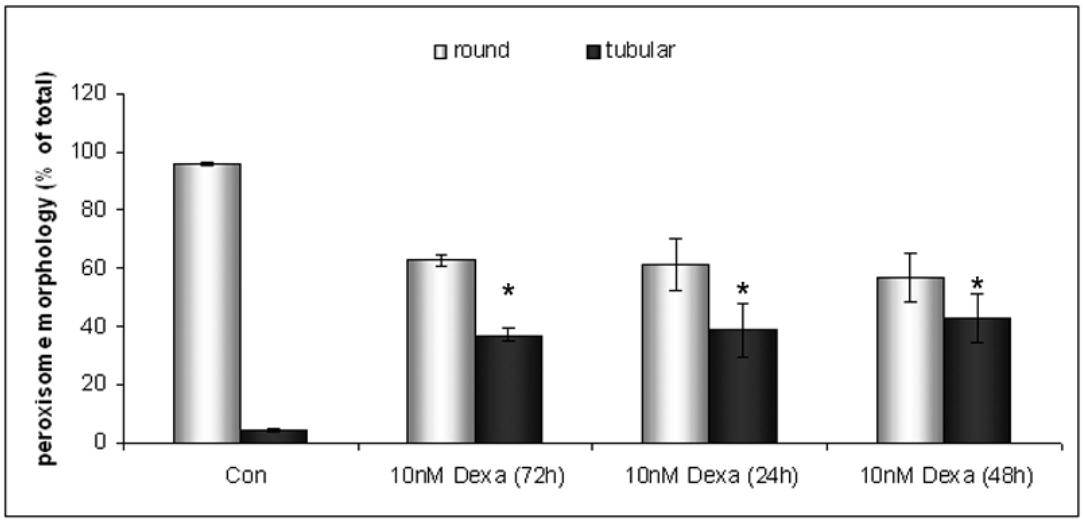

Fig. 3.33: Initial dexamethasone treatment is sufficient to maintain elongated peroxisomes.
AR42J cells were seeded on coverslips and treated with 10nM dexamethasone. Dexamethasone was removed after either 24 or 48 hours after stimulation and cells were thoroughly washed before they were shifted to regular culture medium. Then, cells were incubated for another 48 or 24 hours, respectively. 72 hours after initial induction cells were fixed and processed for epifluorescence microscopy. Untreated controls as well as continuously treated AR42J cells were included as negative or positive controls. For statistical analysis, peroxisome morphology was assessed to be either spherical or tubular and 100 cells/coverslip (2 coverslips/condition) were analyzed accordingly. Data is shown as means +/- SD and derived from 3 independent experiments. (*, $p<0.05$; when compared to untreated controls).

Consistent with the observations made before, the large majority of untreated control cells contained spherical peroxisomes 72 hours after mock stimulation (Fig. 3.33, Con), whereas treatment with dexamethasone resulted in a significant increase in the number of tubular peroxisomes (Fig. 3.33, 10 nM Dexa, 72h). Surprisingly, removal of dexamethasone after either 24 or 48 hours and subsequent cultivation without further stimulation still led to a profound increase in the number of tubular peroxisomes after 72 hours, very similar to what was observed for continuous stimulation (Fig. 3.32).

These findings indicate that even shorter application of dexamethasone treatment is sufficient to exert its downstream events on the peroxisomal level, most likely involving effects on the peroxisomal growth and division machinery.

3.3.5 The observed changes in peroxisome morphology after dexamethasone treatment are reminiscent of the phenotype of Pex11pβ overexpression

The previous findings characterized a novel effect of dexamethasone on the formation of tubular peroxisomes in rodent AR42J cells. The formation of tubular peroxisomes displaying a "beads-on-a-string"-like morphology was shown to be indicative of the early steps of peroxisomal growth and division (Schrader & Fahimi, 2006), a process in which the Pex11 family of proteins was shown to be key mediators of membrane elongation processes (Schrader et al., 2011). Thus, the overall morphology of peroxisomes after dexamethasone stimulation was compared to an overexpression phenotype of the three mammalian Pex11 isoforms in AR42J cells. AR42J cells were transfected with myc-tagged variants of the human Pex11 isoforms, Pex11pα, Pex11pβ and Pex11pγ. After 24 hours cells were fixed and processed for immunofluorescence against the myc epitope and the peroxisomal membrane marker PMP70 to ensure proper targeting. Confocal images were acquired using a Zeiss LSM 510 Meta confocal setup (Fig. 3.34). Upon overexpression, all three isoforms were successfully targeted to peroxisomes (Fig. 3.34, C, F and I). While overexpression of myc-Pex11pα did not result in the formation of tubular peroxisomes (Fig. 3.34 A-C), expression of the ubiquitously expressed Pex11pβ isoform (Fig. 3.34 D-F) led to a prominent elongation of the peroxisome compartment, reminiscent of the phenotype observed after dexamethasone stimulation. Expression of the Pex11pγ variant resulted in some elongation of peroxisomes, albeit not as strong as the observed Pex11pβ phenotype (Fig. 3.34 G-I).

As there was a striking similarity between the observed peroxisome morphology after dexamethasone treatment and overexpression of Pex11pβ, our results point to a relationship between dexamethasone-induced peroxisome elongation and the regulation of the mammalian Pex11 proteins. Therefore, they were selected as prime candidates to investigate the downstream effects of dexamethasone on a peroxisomal level.

3.3.6 Pex11α and Pex11β are induced upon dexamethasone treatment

To gain insight into the effects of dexamethasone on the regulation of the three mammalian Pex11 isoforms, uniquely peroxisomal regulators of peroxisomal growth and division, their expression pattern was assassed by semi-quantitative RT-PCR (SQ-PCR).

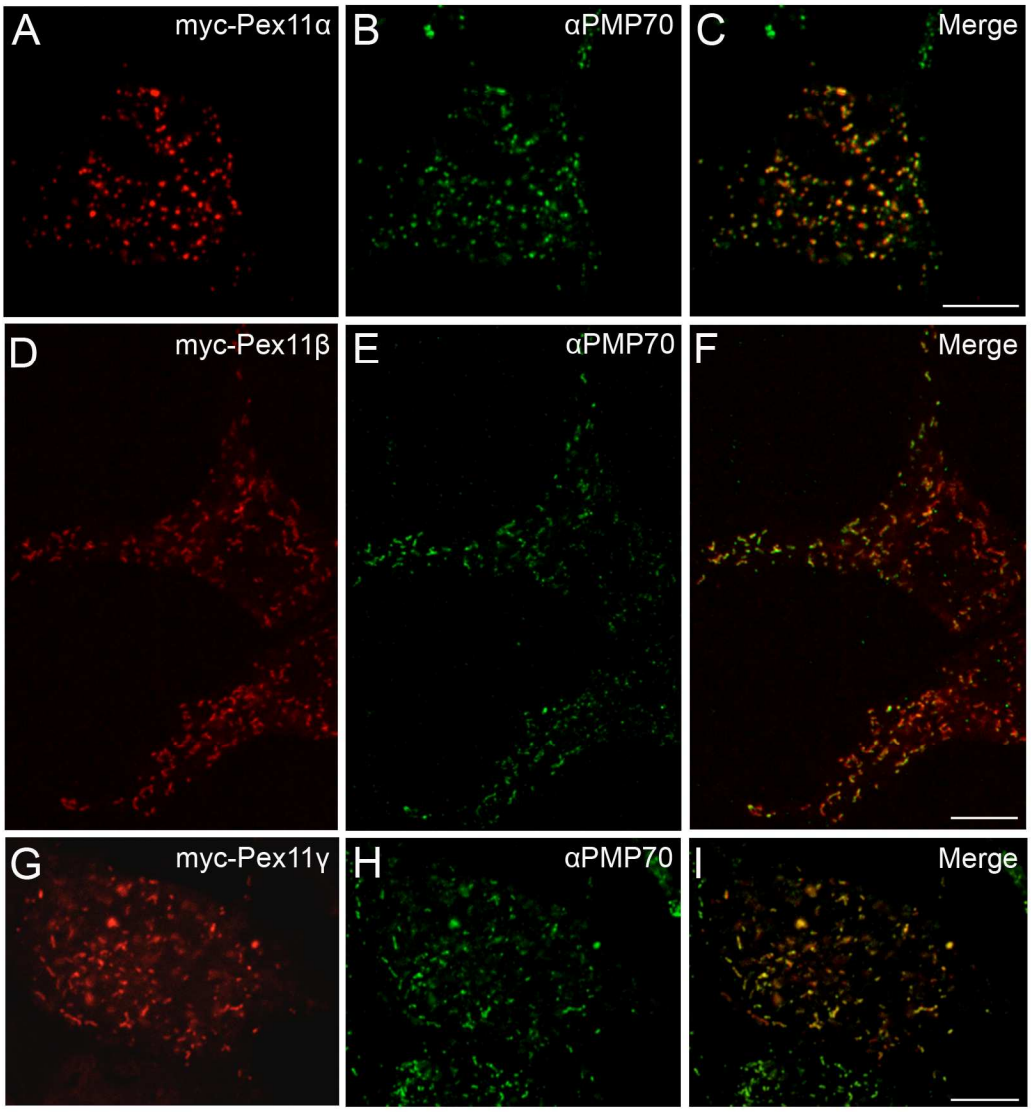

Fig. 3.34: Overexpression of the three human isoforms of Pex11 in AR42J cells.
AR42J cells were transfected with myc-tagged variants of the 3 human isoforms of Pex11, Pex11pα (A-C), Pex11pβ (D-F) and Pex11pγ (G-I). After 24 hours, cells were fixed and processed for immunofluorescence against the myc epitope (A, D, G) and the peroxisomal membrane protein PMP70 (B, E, H). Images were taken using a LSM 510 Meta confocal microscope. Merge of signals is shown in C, F and I, respectively.
Bars, 20µm.

Rodent AR42J cells were treated with 10 nM (+) or 1 µM (++) dexamethasone for 24, 48 and 72 hours. Untreated cells (-) as well as induced ones were harvested, total RNA was extracted and transcribed into cDNA. Semi-quantitative RT-PCR was subsequently performed using specific primer pairs for the three rat Pex11 isoforms, while AOX and GAPDH served as a internal controls (Fig. 3.35). The PCR reaction was stopped after pre-determined cycle numbers (2.5.4.2) to ensure that the reaction was still in its exponential phase and reliable conclusions in regard to initial copy numbers could be made.

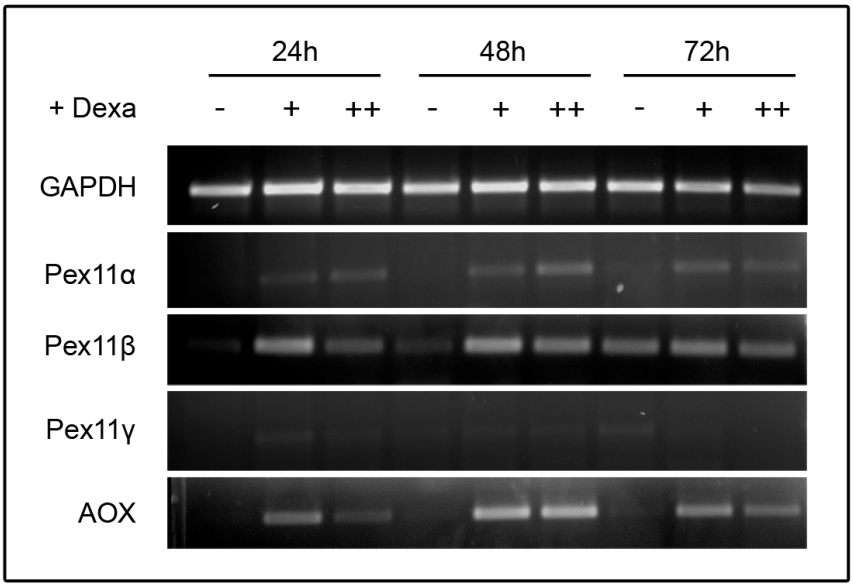

Fig. 3.35: Pex11α and Pex11β are induced by dexamethasone treatment. Rodent AR42J cells were treated with 10 nM (+) or 1 µM (++) dexamethasone for 24, 48 and 72 hours. Untreated cells (-) as well as induced ones were harvested, total RNA was extracted and transcribed into cDNA. Semi-quantitative RT-PCR was subsequently performed using specific primers for the 3 Pex11 isoforms, AOX and GAPDH as a loading control. Samples were then run on 1% agarose gels.

Detection of the housekeeping gene GAPDH revealed that its expression was not affected by stimulation with dexamethasone (Fig. 3.35), thus serving as an adequate normalization control. In regard to the Pex11 isoforms, there was a clear induction of Pex11α after 24, 48 and 72 hours of treatment: in non-treated controls faint, barely visible bands appeared under the conditions chosen which became clearly detectable using both dexamethasone concentrations chosen. In untreated controls, a signal for Pex11β was observed, in line with its ubiquitous, consistent expression in all tissues. Interestingly, although Pex11β is usually regarded as a non-inducible Pex11 isoform, since it is not induced upon treatment with classical PPARα-dependent proliferators (1.2.4), Pex11β levels were increased after dexamethasone stimulation for 24 and 48 hours when compared to controls. After 72 hours, no significant difference between control and stimulated Pex11β expression levels was observed. The third Pex11 isoform, Pex11γ was barely detected at all under the conditions chosen, thus only contributing marginally to the regulation of peroxisome morphology in AR42J cells. The induction of the peroxisomal key enzyme AOX mirrored the expression pattern of Pex11α, as it was induced after all the time points investigated. Interestingly, both, AOX and Pex11α. are induced by the action of the nuclear transcription factor PPARα (1.2.4), thus their induction pattern was very much reminiscent of peroxisome proliferation induced by e.g. fibrates.

To verify these findings on a protein level, peroxisome-enriched fractions of controls and dexamethasone treated samples (10 nM and 1 µM) were prepared and subjected to SDS-PAGE and immunoblotting against AOX and Pex11pβ. Detection of actin levels was used as a loading control (Fig. 3.36).

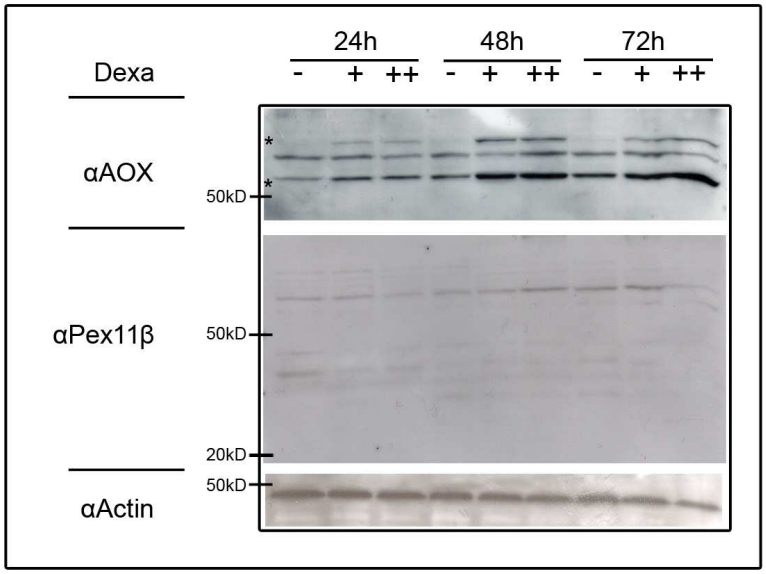

Fig. 3.36: AOX induction is reflected on the protein level.
AR42J cells were treated with no (-), 10 nM (+) or 1 µM (++) dexamethasone for 24, 48 and 72 hours. Cells were harvested and peroxisome-enriched fractions were generated before equal amounts of protein were subjected to SDS-PAGE and immunoblotting against the peroxisomal markers AOX and Pex11pβ as well as actin as a loading control.
Asterisks in the upper panel indicated the respective AOX bands at around 50 and 75 kD.

Whereas signals corresponding to AOX were only faintly detected under control conditions at all time points (Fig. 3.36, asterisks), there was a prominent increase in AOX protein levels after dexamethasone treatment, similar to the induction pattern observed by semi-quantitative PCR. Equal loading was ensured by detection of actin signals. In regard to Pex11pβ, several slight bands were observed at higher molecular weights; however, none of those corresponded to its approximate protein size of 28 kD. While this might also indicate that the overall expression levels of Pex11pβ remained below the detection threshold, it is more likely that the Pex11pβ antibody, which was raised against a peptide of the human protein, does not cross-react with the rat protein as indicated on its datasheet. In line with this, no clear antibody signal corresponding to Pex11pβ was detected after indirect immunofluorescence of control and dexamethasone-treated AR42J cells.

In conclusion, dexamethasone treatment induced PPARα-inducible peroxisomal enzymes like AOX, a pattern indicative of peroxisome proliferation. Notably, not only the inducible Pex11α isoform was up-regulated on a transcriptional level, but also Pex11β which is not induced by classical PPARα-dependent proliferators. Although both Pex11 isoforms were shown to be up-regulated and thus able to contribute to the observed alterations of peroxisome morphology, only Pex11pβ induced a profound tubulation of peroxisomes (1.2.2.1) (Fig. 3.35), similar to what was observed after dexamethasone addition.

3.3.7 AR42J cells do not respond to bezafibrate with peroxisome proliferation

Although several stimuli have been identified that lead to peroxisome proliferation and/or elongation, signal transduction events linked to changes in peroxisome dynamics are largely limited to the activation of PPARα in rodents. Upon binding of ligands – such as fatty acids and fibrates – PPARα forms heterodimers with RXR receptors, enabling them to bind to PPREs (1.2.4). As a result, there is a significant increase in peroxisome number as well as an induction in fatty acid β-oxidation enzymes such as AOX. The mechanism of transcriptional up-regulation via PPARα/PPRE is largely similar to induction by glucocorticoids. Furthermore, the response elements share large similarity, although Pex11β was never shown to be regulated by PPARα. In order to exclude that the observations made upon dexamethasone treatment represent merely an unspecific effect, AR42J cells were treated with bezafibrate, a well-known inducer of PPARα. Bezafibrate was renewed every day. For morphological and statistical analysis, untreated controls and treated cells were fixed after 24, 48, 72 and 96 hours and processed for epifluorescence microscopy (Fig. 3.37 A-C). Peroxisome morphology was determined to either be spherical or tubular and statistical analysis was performed. In contrast to the observations made for dexamethasone, peroxisomes retained their primarily spherical morphology and tubular peroxisomes were seldom observed (Fig. 3.37 B). Statistical analysis further indicated that bezafibrate failed to induce peroxisome tubulation in contrast to dexamethasone. Moreover, no obvious increase in peroxisome number was noticed. To compare the peroxisomal induction profiles of bezafibrate and dexamethasone, semi-quantitative RT-PCR was performed. AR42J cells were treated with bezafibrate for 96 hours, total RNA was extracted and cDNA was transcribed. Semi-quantitative RT-PCR was performed using primers against the rat Pex11 isoforms as well as AOX and GAPDH as controls. Surprisingly, while detected levels of the loading control GAPDH or the constitutively expressed Pex11β largely remained the same, no induction of either Pex11α or AOX was determined, unlike what was consistently shown for bezafibrate treatment in rodent hepatocytes. Similar observations were made upon treatment with ETYA, a analogue of arachidonic acid shown to activate PPARα (data not shown). An induction of AOX was further not detected by immunoblotting (Fig. 3.37 C).

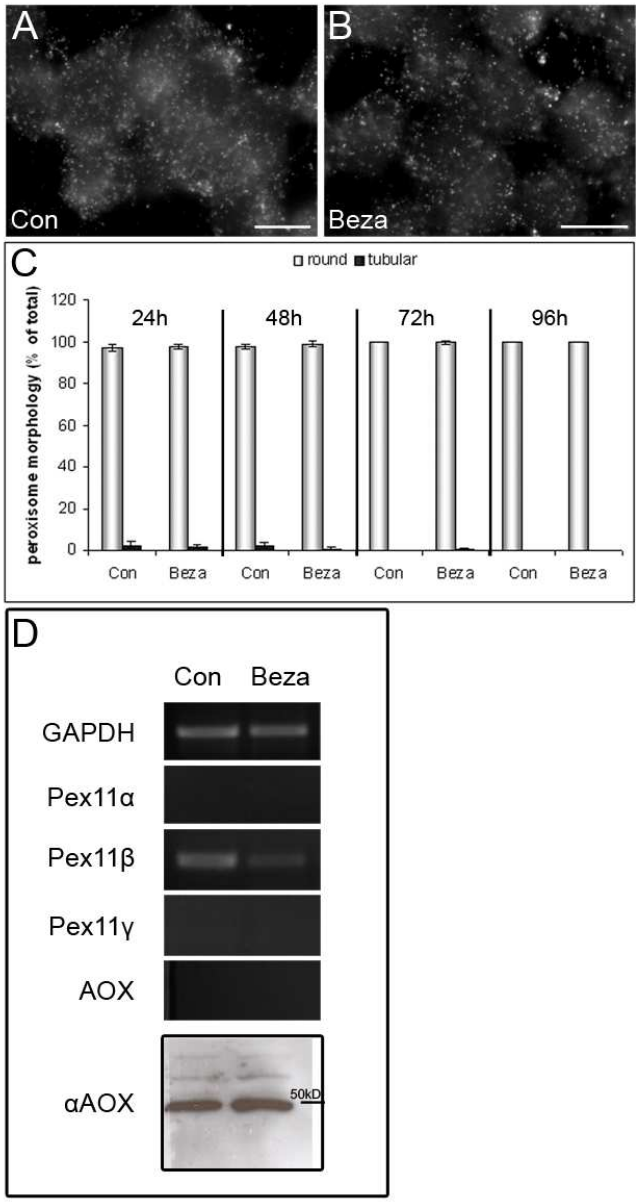

Fig. 3.37: Bezafibrate does not induce peroxisome proliferation in rodent AR42J cells.
(A-C) AR42J cells were either mock treated (Con) or treated with bezafibrate for 24, 48, 72 or 96 hours. Cells were fixed and processed for immunofluorescence against the peroxisomal marker Pex14. For statistical analysis, peroxisome morphology was either assessed to be spherical or tubular. 100 cells/coverslip were counted accordingly (2 coverslips/condition) and data is shown as means +/- SD.
Bars, 20µm.
(D) Expression profiles of bezafibrate treated AR42J cells.
AR42J cells were treated with bezafibrate for 96 hours, total RNA was extracted and cDNA was transcribed. Semi-quantitative RT-PCR was performed using primers against the Pex11 isoforms as well as AOX and GAPDH as controls. To validate findings on a protein level, peroxisome-enriched fractions of controls and bezafibrate treated samples were prepared and subjected to SDS-PAGE and immunoblotting against AOX.

Thus, our findings indicate that rodent pancreatic AR42J cells do not respond to bezafibrate treatment in a manner similar to rat hepatocytes. However, they responded prominently to dexamethasone treatment which points to two uncoupled processes regulating peroxisome proliferation/dynamics

3.3.8 Summary

In the final part of this thesis, stimuli altering peroxisome dynamics were screened for to delineate the relationship between peroxisome morphology and function, but also to establish a mammalian cell culture model to investigate signal transduction regulating peroxisome

dynamics. Although the neurotoxin 6-OHDA led to the fragmentation of mitochondria in a DLP1-dependent manner, no effect on peroxisome dynamics was observed which maintained a primarily spherical morphology. Induction of cytosolic oxidative stress, inhibition of the mitochondrial respiratory chain as well as the compartment-specific generation of superoxide radical using the genetically-encoded photosensitizer KillerRed did not result in any short or long-term alterations of peroxisome dynamics. Thus, previously observed alterations of peroxisome morphology (e.g after UV irradiation) might not be exclusively linked to the induction of oxidative stress, but to other factors such as the intra- or extracellular origin of the signal, cellular redox-state or other signalling pathways. In contrast to that, addition of dexamethasone to rodent pancreatic AR42J cells significantly elongated peroxisomal membranes in a dose-dependent manner. Notably, peroxisomes maintained their tubulated morphology without subsequent peroxisome fission, even after removal of the external stimulus. Dexamethasone action was linked to an induction of Pex11α and the PPARα-independent proliferator Pex11β by SQ-PCR by a potentially PPARα-independent mechanism. The classical peroxisome proliferator bezafibrate did not elicit any proliferative response in rodent pancreatic AR42J cells, contrary to rodent hepatocytes, which indicated the cell line to be a non-responder. The rodent AR42J cell line thus has high potential to serve as a highly reliable model system to study stimulus-induced alterations of peroxisome dynamics (without a large-scale manipulation of the peroxisomal growth and division machinery by e.g. overexpression of Pex11p).

4 DISCUSSION: TOWARDS AN UNDERSTANDING OF PEROXISOME DYNAMICS IN MAMMALIAN CELLS

Peroxisomes are ubiquitous, dynamic cell organelles that play a key role in numerous metabolic processes such as the α- and β-oxidation of fatty acids, the biosynthesis of plasmalogens and bile acids as well as the metabolism of ROS (van den Bosch et al., 1992; Wanders & Waterham, 2006b; Bonekamp et al., 2009; Bonekamp et al., 2011a; Fransen et al., 2011) (1.1.2). Moreover, novel biological functions continue to emerge, such their involvement in antiviral signalling (Dixit et al., 2010). Interestingly, many of the above mentioned functions are performed in co-operation with mitochondria (Schrader & Yoon, 2007; Bonekamp et al., 2009; Camoes et al., 2009; Dixit et al., 2010; Ivashchenko et al., 2011) (1.3). Peroxisomes and mitochondria also share components of their fission machinery and evidence has even been provided for a vesicular trafficking pathway between the two organelles (Neuspiel et al., 2008; Delille et al., 2009; Braschi et al., 2010; Schrader et al., 2011), indicating that the organelles share a much closer interrelationship than previously appreciated (Schrader & Yoon, 2007; Camoes et al., 2009). As a result of the essential contribution of peroxisomes to cellular homeostasis, disturbances of their functions and biogenesis lead to severe disorders (Steinberg et al., 2006; Wanders & Waterham, 2006a) (1.1.4). Originally, peroxisomes were thought to be autonomous organelles like mitochondria that multiply solely by growth and division from pre-existing organelles (Lazarow & Fujiki, 1985; Schrader & Fahimi, 2006), however, they were also observed to arise *de novo* from the ER under special conditions (Hoepfner et al., 2005; Kim et al., 2006; Hettema & Motley, 2009; Nagotu et al., 2010). The contribution of both processes under wild-type conditions in different species remains a matter of debate (Motley & Hettema, 2007; Hettema & Motley, 2009; van der Zand et al., 2010). In mammalian cells, peroxisome growth and division was shown to follow a well-defined sequence of morphological alterations: initial membrane elongation of the compartment is carried out by the key peroxisomal membrane protein Pex11pβ, whereas the combined action of the tail-anchored proteins Mff and Fis1 as well as the large GTPase DLP1 mediates final fission into smaller, spherical organelles (Koch et al., 2003; Li & Gould, 2003; Koch et al., 2005; Gandre-Babbe & van der Bliek, 2008; Otera et al., 2010; Schrader et al., 2011). While the key components of the fission machinery are shared with mitochondria (1.2.2), Pex11 proteins are uniquely peroxisomal and are, up until now, the only proteins identified to mediate peroxisome multiplication/proliferation in mammals which places them in the centre of regulating peroxisome dynamics. Proteins of the

Pex11 family have been identified across species for several years (Erdmann & Blobel, 1995; Marshall et al., 1995; Abe & Fujiki, 1998; Abe et al., 1998; Schrader et al., 1998b; Li et al., 2002a; Thoms & Erdmann, 2005; Lingard & Trelease, 2006; Schrader et al., 2011), but only recently the contribution of Pex11pβ to a multi-step maturation process of peroxisomal growth and division has been characterized (Delille et al., 2010). Moreover, studies on *P. chrysogenum* Pex11p have defined the importance of an N-terminal amphipathic helix in mediating membrane tubulation (Opalinski et al., 2011). In order to fulfil their multiple functions, peroxisomes are known to adjust their enzyme content, but also their number and morphology. For instance, UV irradiation, ROS, fatty acids and growth factors were previously shown to induce peroxisome elongation in mammalian cell culture models (Schrader et al., 1998a; Schrader et al., 1999). Moreover, treatment of rodents with hypolipidemic compounds such as fibrates not only leads to an increase in peroxisome number, but also an induction of enzymes involved in fatty acid β-oxidation (Hess et al., 1965; Lazarow & De Duve, 1976). The latter response was linked to the action of the nuclear receptor PPARα and the subsequent induction of its target genes (Issemann & Green, 1990; Pyper et al., 2010), such as the inducible Pex11 isoform Pex11pα (Abe et al., 1998). However, so far, regulation of peroxisome proliferation on a the molecular level remains largely limited to PPARα action, although several studies point to the existence of PPARα- and Pex11pα-independent mechanisms (Li et al., 2002a; Bagattin et al., 2010). (Gorgas, 1987; Kollatakudy et al., 1987; Schrader et al., 2000; Ribeiro et al., 2011). It has become clear in recent years that organelle morphology and dynamics are intricately linked to function and thus, human well-being. In line with this, a lethal defect affecting peroxisomal and mitochondrial fission has been identified (Waterham et al., 2007). Moreover, alterations in peroxisome dynamics and perturbations of their number are linked to several pathophyiological conditions such obesity, AOX1 deficiency and cancer (Chang et al., 1999; Lauer et al., 1999; Funato et al., 2006; Frederiks et al., 2010; Diano et al., 2011), therefore controlled manipulation of peroxisome proliferation (and morphology) might provide an interesting therapeutic target counteracting pathophysiological defects.

Thus, the aim of this thesis was to gain insight into the processes contributing to and regulating peroxisome dynamics in mammalian cells, both on a transcriptional and a post-translational level. These issues will be the focus of future research.

4.1 PEROXISOMAL DYNAMICS: DO MAMMALIAN PEROXISOMES FUSE?

4.1.1 Unlike mitochondria, mature mammalian peroxisomes do not exchange matrix or membrane components

Both mitochondria and peroxisomes are known to co-operate extensively in regard to metabolic activity and have also been shown to share key components of their fission machinery (Schrader & Yoon, 2007; Camoes et al., 2009). Moreover, both are very dynamic organelles prone to frequent changes in number and size, however, mitochondria fuse with one another to exchange matrix and membrane components (for review, see Okamoto & Shaw, 2005; Bereiter-Hahn & Jendrach, 2010; Westermann, 2010). In addition to complete fusion of mitochondrial networks, a transient mitochondrial fusion was only recently described upon which mitochondria interact in shorter time intervals to exchange soluble IMS and matrix components (Liu et al., 2009). Mitochondrial fusion itself is a stepwise process involving the sequential fusion of the outer and inner mitochondrial membranes which is mediated by the concerted action of the GTPases Mitofusin 1 and 2 (Mfn) and OPA1 (optic atrophy protein) 1 (for review, see Okamoto & Shaw, 2005; Zorzano et al., 2010). Mfn1 and Mfn2 are outer mitochondrial membrane proteins that were identified to be homologues of the Drosophila fuzzy onions (Fzo) protein (Hales & Fuller, 1997; Santel & Fuller, 2001; Chen et al., 2003; Eura et al., 2003; Santel et al., 2003). Human Mfns share a 63 % sequence identity as well as the same functional domains and they can interact in a homotypic and heterotypic fashion (Griffin et al., 2006; Zorzano et al., 2010). Fusion of the mitochondrial outer membrane is thought to occur by tethering of individual mitochondria upon Mfn1 dimerization that is followed by a GTP-dependent docking step. The inner mitochondrial membrane protein OPA1 (Mgm1p in yeast) controls mitochondrial inner membrane fusion as well as cristae remodelling (Cipolat et al., 2004; Chen et al., 2005; Song et al., 2007). It exists in eight splice variants in humans and is regulated by post-transcriptional and post-translational mechanisms (Delettre et al., 2000; Delettre et al., 2001; Olichon et al., 2007).

The question if peroxisomes engage in analogous fusion events, resulting in extensive intermixing of matrix and membrane components, remained a matter of debate. One of the aims of this study was to systematically investigate the existence of a potential peroxisomal fusion in mammalian cells and to determine if mitochondrial fusion proteins – similar to the fission machinery – are also shared by peroxisomes.

In order to investigate the existence of fusion of mature peroxisomes in CHO cells systematically, an *in vivo* fusion assay was established that included the application of cycloheximide, a well-known inhibitor of eukaryotic protein translation, to avoid false-positive signals due to peroxisomal import of the corresponding, newly synthesized marker proteins. Monitoring of mitochondrial fusion served as a positive control (Fig. 3.1). The assay is based on the co-cultivation of CHO cells stably expressing either a red or a green fluorescent protein targeted to peroxisomes and subsequent hybridoma formation by cell fusion. DsRed-PTS1 and GFP-PTS1 fusion proteins served as markers for the peroxisomal matrix (Fig. 3.2), whereas PMP70-YFP and dPex26-mDsRed represented peroxisomal membrane markers (Fig. 3.8). Successful shut-down of protein biosynthesis was verified by pulse-chase labelling with S^{35}-methionine (Fig. 3.1). In contrast to previous findings in CHO cells (Huybrechts et al., 2009), yellow peroxisomes were clearly observed in time course experiments with fixed cells by epifluorescence and confocal microscopy (Fig. 3.2). In contrast to mitochondrial fusion, however, which was fast, time dependent and almost complete, intermixing of peroxisomal matrix and membrane markers appeared to be slow, independent of time, less frequent and only visible in a subpopulation of peroxisomes (Fig. 3.2, Fig. 3.8). In depth-analyses of these observations by live cell imaging revealed that individual red and green peroxisomes were engaged in vivid interactions, but did not fuse. However, individual peroxisomes formed close contacts, which resulted in complete co-localisation of signals, and thus the “yellow” colour which accounted for the observations made in fixed cells (Fig. 3.3.; Fig. 3.4). Nonetheless, the observed interaction was only transient and individual red and green peroxisomes remained their entities after separation. No exchange or mixing of labelled matrix marker proteins was detected (even after increasing gain settings and exposure times). The same was true for red and green peroxisomal membrane marker proteins. These observations strongly indicate that, unlike mitochondria, individual peroxisomes in mammalian CHO cells do not fuse in a way which allows an exchange or mixing of matrix or membrane proteins. Our observations are in line with other findings made for mature peroxisomes in yeasts, plants and mammals (Arimura et al., 2004; Motley & Hettema, 2007; Huybrechts et al., 2009). In the yeast *S. cerevisiae* no overlap or mixing between the peroxisomal matrix markers GFP-PTS1 and HcRed-PTS1 was detected in a mating assay (Motley & Hettema, 2007), challenging the idea that mature yeast peroxisomes fuse *in vivo*. Similar to our observations, the formation of some yellow peroxisomes indicated the occurrence of peroxisomal fusion in plants, which did not result in a transition to a uniform colour of peroxisomes, even 1 day after photoconversion of the

marker used (Kaede-PTS1) (Arimura et al., 2004). Another study in mammalian CHO cells employed the HaloTag technology which enabled the differential labelling of peroxisomes and thus the generation of different peroxisome populations. Subsequent generation of hybridoma cells and epifluorescence microscopy revealed that peroxisomes containing newly imported matrix and membrane proteins do not mix their matrix content with pre-existing peroxisomes, as – in contrast to our observations - no spatial overlap of combined matrix signals was ever detected in this experimental setup (Huybrechts et al., 2009). Thus, "true" peroxisomal fusion processes remain limited to the multi-step peroxisome maturation process in the yeast *Y. lipolytica* (Titorenko & Rachubinski, 2000; Titorenko & Rachubinski, 2001a). However, none of the aforementioned studies ever addressed the formation of close contacts and vivid interactions between individual peroxisomes. Thus, a new dynamic behaviour contributing to peroxisome dynamics was characterized in the present study (see below). In terms of peroxisome dynamics, there are certain caveats that have to be considered. As peroxisomes are frequently observed to interact, but then come apart again as individual organelles, these observations could also be misinterpreted as peroxisomal fission events, especially when only one peroxisomal marker (e. g. GFP-PTS1) is used (Fig. 3.7).

In parallel, a peroxisomal localization of the mitochondrial fusion proteins Mfn1 and 2 as well as OPA1 was investigated, some of which were recently shown to be targeted to multiple subcellular organelles: Mfn2, for example, was localized to the ER (de Brito & Scorrano, 2008a) while OPA1 was recently identified at lipid droplets where it regulates adrenergic control of lipolysis (Pidoux et al., 2011). To determine the localization of mitofusins to peroxisomes, overexpression studies were performed in COS-7 cells stably transfected with a peroxisomal GFP-PTS1 and co-localization of markers was assessed by epifluorescence microscopy. However, wild type versions of Mfn1 and Mfn2 were not targeted to peroxisomes (Fig. 3.10). Moreover, expression of activity-deficient mutants of Mfn1 and Mfn2 did neither localize to peroxisomes nor resulted in any morphological changes of peroxisomes, whereas mitochondrial morphology shifted to a perinuclear aggregation as reported (Fig. 3.11) (Chen et al., 2003; Santel et al., 2003; Koshiba et al., 2004). Expression of Mfn2variants in which amino acid exchange in their C-terminal part leads to neutral/hydrophobic (Mfn2-IYFFT) or polar/basic (Mfn2-RRD) characteristics and thus, mistargeting to the ER (Rojo et al., 2002), still did not result in a peroxisomal localization. It was assumed that if mitofusins possess any peroxisomal targeting potential, they would be detectable at peroxisomes after experimental mistargeting. Moreover, OPA1 was also not observed at peroxisomes by immunofluorescence and immunoblotting of highly purified

peroxisomes (Fig. 3.12). Consequently, key mitochondrial fusion proteins (Mfn1, Mfn2 or OPA1) fail to localize to peroxisomes, unlike components of the fission machinery.

4.1.2 Transient and complex peroxisomal interactions: a new dynamic behaviour of mammalian peroxisomes

Despite the lack of evidence for an exchange or mixing of matrix content or membrane proteins between individual spherical peroxisomes, the organelles were observed to engage in vivid interactions (Fig. 3.3, Movie S1 and S2). In some cases, peroxisomes moved along linear tracks prior to their interaction as reported before (Schrader et al., 2000). By applying a simple computational model, evidence was provided that a combination of fast, ATP-driven movement of peroxisomes and subsequent formation of close contacts between individual peroxisomes can principally contribute to the homogenization (intermixing) of the peroxisomal compartment on a timescale of one to several hours (Fig. 3.5), e.g. to distribute metabolites, signals, or other "molecular information". This model also offers an explanation for the previous observation that only ~15 % of peroxisomes in mammalian cells are engaged in fast, microtubule dependent, long range movements (Rapp et al., 1996; Wiemer et al., 1997; Schrader et al., 2000). Apparently, no prominent advantage for homogenization or intermixing is achieved if all peroxisomes would participate in fast and yet energy consuming and costly motility. This may reflect an optimization process for rapid homogenization of peroxisome populations at the lowest energy costs.

Frame by frame analysis revealed that individual peroxisomes were engaged in several transient and long term contacts (approximately 2 % of differentially labelled peroxisomes at all times), and remained in close association for about 5-40 seconds (Fig. 3.6). However, some peroxisomes also stayed attached to one another for extended periods of time (up to 500 seconds). Moreover, individual peroxisomes also re-engaged in contacts, although there was a surplus of other potential peroxisomal interaction partners in the close vicinity. Thus, these interactions are not likely to be random events. Detailed analysis of the duration of interaction events indicated that the distribution of long term contacts displays power law behaviour (Rhodes & Anderson, 1996; Viswanathan et al., 2002; Newman, 2005; Sornette, 2006; Clauset et al., 2009; James et al., 2011) (Fig. 3.6). Power law distributions are defined to have heavy tails, as the number of events with higher values, in this case, the number of long term contacts, is substantially larger than could be expected from an exponential distribution (which would indicate random events). Power law distributions in biological processes are

indicative of the existence of intricate dynamics originating from diverse, and yet specific mechanisms. Hence, our analysis strongly suggests that peroxisome interactions appear to be more diverse and complex than assumed.

Regarding a possible physiological function of the observed interactions, it was surmised that the close apposition of peroxisomes may favour an exchange of metabolites and metabolic cross-talk. The interactions could as well contribute to the degradation of ROS or H_2O_2. As peroxisomes are very heterogeneous in regard to density, protein composition and import competence between species as well as within the same cell (Heinemann & Just, 1992; Luers et al., 1993; Islinger et al., 2007; Wiese et al., 2007; Islinger et al., 2010), an exchange of metabolic information might be required. To prevent release and escape of components from individual peroxisomes, a close interaction might also be beneficial. In search for a physiological function of transient peroxisomal interactions, it was therefore investigated whether an increase in the heterogeneity between peroxisomal subpopulations would result in an enhanced frequency of peroxisomal interactions. However, pre-treatment of CHO-GFP-PTS1 cells with peroxisomal metabolites such as fatty acids and H_2O_2 prior to fusion with non-stimulated CHO-DsRed-PTS1 cells did not result in a prominent increase of peroxisomal interactions (Fig. 3.9). Similar results were obtained after pre-treatment with peroxisome proliferators or after treatment of both cell lines prior to and after the formation of hybridoma cells. Thus, it is unlikely that the close apposition of peroxisomes favours an exchange of metabolites such as fatty acids or H_2O_2. However, peroxisomes contribute to a variety of metabolic processes (1.1.2); an exchange of other metabolites or lipids therefore cannot be rigorously excluded. Alternatively, the interactions might be part of a signalling system to sense the state and/or distribution of the peroxisomal population in the cell. This might be especially important in mammalian cells, where a large number of peroxisomes has to be co-ordinately distributed in a relatively large cytoplasmic volume. It is striking that shortly after hybridoma formation, the red and green peroxisome populations acquire a uniform, intermixed distribution within the cell. Microtubule-driven fast movements of peroxisomes and transient contacts might thus contribute to equilibrate peroxisome pools throughout the cell. In line with this, the formation of small groups (or functional units) of peroxisomes has been observed, e.g. in conjunction with lipid droplets (Novikoff & Shin, 1964) or in HepG2 cells after a phase of peroxisome multiplication when the cells become more confluent and differentiated (Stier et al., 1998).

4.1.3 Peroxisomal versus mitochondrial dynamics

Despite the fact that mitochondria and peroxisomes utilize the same basic molecular machinery for organelle fission (Schrader et al., 2011), the findings presented here further stress the point that peroxisomal dynamics are regulated in manner different and distinct from mitochondria. In general, mitochondria engage in frequent fission and fusion processes that enable the repartitioning of lipids, proteins and mtDNA throughout the cells and are furthermore distributed throughout the cell by microtubule-dependent movements, thus ensuring mitochondrial homeostasis (Nakada et al., 2001; Ono et al., 2001; Li et al., 2004) (Fig. 4.1). Transient mitochondrial fusion events were suggested to serve as a quick re-stocking mechanism for mitochondria in this regard (Liu et al., 2009). Moreover, the regulated formation of elongated structures/networks by shifting the balance to mitochondrial fusion was recently shown to prevent mitochondria from autophagosomal destruction upon nutrient starvation and represent a mitochondrial stress response (Tondera et al., 2009; Gomes et al., 2011; Rambold et al., 2011a; Rambold et al., 2011b). In terms of peroxisomal dynamics, an analogous balanced fusion/fission equilibrium regulating peroxisome dynamics can be excluded, but it should be noted that the observations presented here account for mature, spherical peroxisomes. Thus, the fusion of pre-peroxisomal structures or vesicles, e.g. during the formation or maturation of peroxisomes (Titorenko & Rachubinski, 2001a) cannot be excluded. Furthermore, in cultured cells and tissues, more complex reticular networks of peroxisomes have occasionally been described which appear to be engaged in vivid interactions (Schrader et al., 2000; Schrader & Fahimi, 2006). Hence, it cannot be rigorously excluded, that under more specific metabolic, environmental or developmental conditions peroxisomes fuse to form more complex reticular structures to fulfil special metabolic functions more efficiently. Nevertheless, the formation of reticular peroxisomes is unlikely to involve key components of mitochondrial fusion in contrast to what was recently shown for mitochondrial networks (Tondera et al., 2009; Gomes et al., 2011). Furthermore, in contrast to mitochondria, stress- or stimulus-induced elongation of mature peroxisomes (Schrader & Fahimi, 2006) is not mediated by a fusion of peroxisomes, but by processes of membrane deformation and elongation (Fig. 4.1). Additionally, our findings on the existence of transient and complex peroxisomal interactions add a new and interesting twist to peroxisomal dynamics, as they might contribute to an exchange a certain type of “molecular” information or as part of a signalling system to sense the state and/or distribution of the peroxisomal population in the cell (Fig. 4.1). Still, the physiological significance of the inter-peroxisomal

contacts requires further investigation. Furthermore, peroxisomes may arise *de novo* from the ER (Nagotu et al., 2010) which has not been observed for mitochondria.

However, similar to mitochondria, peroxisomes move along microtubule tracks, share key fission components with mitochondria, and are engaged in transient and long term contacts (Fig. 4.1).

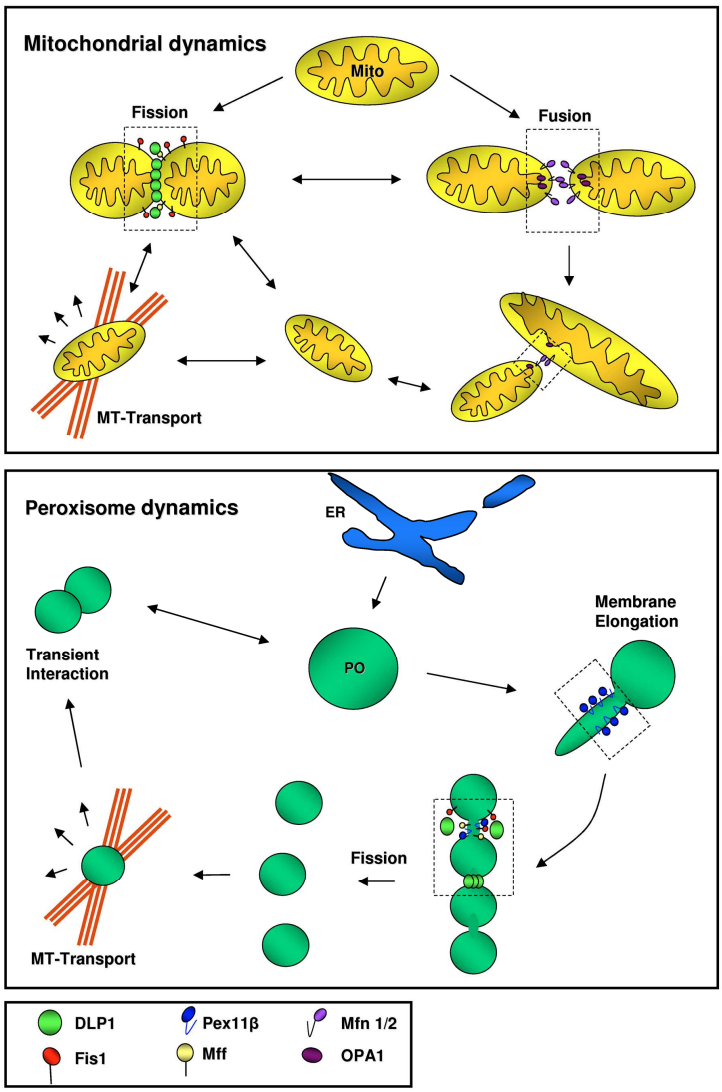

Fig. 4.1: Comparison of mitochondrial and peroxisomal dynamics.
Mitochondrial dynamics (upper panel) are regulated by a combination of frequent fusion and fission events that serve to homogenize the compartment. Mitochondrial fission is mediated by the action of Mff (yellow), Fis1 (red) and DLP1 (green), while fusion is concerted by the action of mitofusins (Mfn, purple) and OPA1 (violet). Note that fused mitochondria might further interact and fuse to form mitochondrial networks (lower right corner). Transport of mitochondria throughout the cell is facilitated by microtubule-dependent movements. Note that individual mitochondria continuously engage in cycles of fusion and fission. Peroxisomal dynamics (lower panel) are regulated by peroxisomal growth and division: unlike mitochondria, formation of tubular peroxisomal structures is facilitated by inherent membrane elongation mediated by Pex11pβ (blue). After constriction, fission into smaller organelles is carried out by the same machinery as mitochondrial fission. Long-range transport of peroxisomes is also mediated by the microtubule cytoskeleton. Unlike mitochondria, peroxisomes do not fuse and do not share the mitochondrial fusion proteins. However, they may engage in transient interactions that might, in combination with long-range transport, homogenize the compartment. Furthermore, peroxisomes arise *de novo* under special conditions, unlike mitochondria.

4.2 REGULATION OF PEROXISOME DYNAMICS: CHARACTERIZATION OF MAMMALIAN PEX11B AND ITS N-TERMINAL DOMAIN

The ubiquitously expressed Pex11pβ has been known to mediate elongation of the peroxisomal membrane prior to constriction and final fission into smaller, spherical peroxisomes in mammalian cells (Schrader et al., 1998b), placing this uniquely peroxisomal protein in the centre of regulating peroxisomal dynamics. Recently, Pex11pβ-mediated peroxisome proliferation was shown to follow a multistep-maturation process (Delille et al., 2010). The mechanistic basis of the membrane elongating properties of Pex11 proteins across species have now been linked to the existence/action of a conserved amphipathic helix in the protein's N-terminus (Opalinski et al., 2011). Although the presence of the amphipathic helix and thus the basic molecular mechanism of Pex11p-mediated peroxisomal membrane elongation appear to be conserved from yeast to mammals, it remains to be elucidated if the presence of the most conspicuous amphipathic helix within the human Pex11pβ isoforms is sufficient to induce peroxisomal membrane elongation. Furthermore, the regulation of Pex11pβ activity by post-translational mechanisms such as oligomerization or phosphorylation needs to be determined.

4.2.1 Human Pex11pβ – one integral membrane protein modulating the morphology of two organelles

Insight into the regulation of Pex11pβ in mammals has been obtained from its basic domain structure: its very short C-terminal tail was implied to facilitate interaction with the tail-anchored protein Fis1 which participates in the assembly of the final fission complex (1.2.2.3) (Kobayashi et al., 2007; Koch et al., 2010). Furthermore, Pex11pβ was shown to form homo-oligomers and hetero-oligomers with the mammalian gamma isoform (Li & Gould, 2003; Kobayashi et al., 2007; Koch et al., 2010). Its homo-oligomerization capacity is dependent on the presence of its N-terminal domain (aa 1-85) (Kobayashi et al., 2007), a region that also comprises the most conspicuous amphipathic helix (aa 45-75) within human Pex11pβ (Opalinski et al., 2011) (Fig. 4.2). The mode of membrane association and the topology of Pex11 proteins, however, may vary greatly across species (Schrader et al., 2011); for instance, *S. cerevisiae* Pex11p was initially characterized as a integral peroxisomal membrane protein (Erdmann & Blobel, 1995), but depending on the degree of peroxisome purification was then

re-defined as a peripherally associated protein of the peroxisomal membrane (Marshall et al., 1995; Marshall et al., 1996). Similarly, although both termini of Pex11pβ were shown to protrude into the cytosol by *in silico* studies and differential permeabilization (Abe & Fujiki, 1998; Schrader et al., 1998b), the exact position of the first transmembrane domain – and thus the definition of the crucial N-terminal domain – remained elusive due to the limited availability of suitable antibodies. In line with this, the predicted position of the first transmembrane domain within human Pex11pβ varies greatly, depending on the *in silico* search algorithm used (Fig. 3.13).

In the present study, a newly available, commercial Pex11pβ antibody was characterized to determine the topology of the human protein. Endogenous Pex11pβ was only recognized weakly, thus further analyses on its topology were carried out after overexpression of either myc or YFP-tagged variants of Pex11pβ that were previously shown to be functional (Schrader et al., 1998b; Delille et al., 2010). Differential permeabilization (using Tx100, methanol or digitonin) and subsequent immunostaining against Pex11pβ indicated that the antibody epitope was located within the peroxisomal membrane or matrix (Fig. 3.16) Personal communication with the supplier revealed that the antibody recognizes a stretch of amino acids located between amino acid positions 110 and 140 which enabled us to determine protein topology as well as the position of the first transmembrane domain by a protease-protection assay (Fig. 3.17). After proteinase K digest of YFP-Pex11pβ at intact peroxisomal membranes and subsequent immunoblotting with the Pex11pβ antibody, a protease-resistent fragment of approximately 17kD was detected. The molecular weight was consistent with the predicted fragment size obtained when the first transmembrane domain of Pex11pβ was located between amino acids 90 and 110 (Fig. 3.13) (PredictProtein: aa 86 – 103; TMPredict: aa 96 – 114) (Schrader et al., 1998b). The protease-resistant fragment was digested by proteinase K upon membrane permeabilization with either Tx100 or sonication (Fig. 3.17 B, Fig. 3.18), indicating an intra-peroxisomal localization of the region between the two transmembrane domains of Pex11pβ. Similar observations were made upon overexpression of the untagged wild-type Pex11pβ and lower concentrations of proteinase K (data not shown). Most of the protease-protection assays were carried out using YFP-Pex11pβ; as the YFP-fusion protein tag itself was not digested by the action of proteinase K, most probably due to its very compact β-barrel structure, it served as an excellent loading control in our assay (Fig. 3.17 B), while membrane integrity of peroxisomes was monitored by the detection of AOX signals (Fig. 3.18). Thus, the position of the first transmembrane domain of human Pex11pβ

was localized to amino acid positions 90 – 110. Consequently, the often evoked soluble N-terminal domain of human Pex11pβ is comprised of amino acids 1-90.

In another set of experiments, the targeting of human Pex11pβ was examined in patient fibroblasts devoid of Pex19p. Pex19p is a multifunctional protein, serving as a chaperone as well as an import-receptor for newly synthesized PMPs in the cytosol that directs PMPs to the peroxisomal membrane where it is tethered via interaction with Pex3p (Fransen et al., 2001; Fransen et al., 2004; Jones et al., 2004; Shibata et al., 2004) (1.1.5.2). In the ΔPex19 patient fibroblasts, peroxisomal membrane biogenesis is impaired and peroxisomal structures are completely absent. Upon co-expression of myc-tagged Pex11pβ with a mitochondrial GFP in ΔPex19 patient fibroblasts, a clear mistargeting of Pex11pβ to mitochondria was observed where it significantly induced mitochondrial fragmentation (Fig. 3.19). The mitochondrial phenotype was reminiscent of Fis1 overexpression (which leads to mitochondrial fragmentation) (1.2.2.3) (Fig. 3.19 B), however, no ER localization of myc-Pex11pβ was ever observed. In order to address if the induced mitochondrial fragmentation was a result of improper/incorrect insertion of Pex11pβ into the mitochondrial membrane, the topology of mitochondrial Pex11pβ was assessed by using N- and C-terminally myc-tagged variants of the protein, differential permeabilization and subsequent immunostaining against the myc epitope (Fig. 3.20). Consistent with the observations made at the peroxisomal membrane, both termini of Pex11pβ were accessible after digitonin treatment, while the protein remained sensitive to Tx100. In parallel, protein topology at the mitochondrial membrane was further examined using the Pex11pβ antibody after differential permeabilization with Tx100, methanol or digitonin (Fig. 3.21). Similar to our previous findings at the peroxisomal membrane, Pex11pβ signals were only detected upon membrane rupture, indicating that Pex11pβ retained its proper topology (at least to some degree) despite its mistargeting to a different organelle membrane. Still, it has to be noted that in addition to its mitochondrial localization, a cytosolic Pex11pβ signal was detected after overexpression of GFP-tagged variants (Fig. 3.22). Mitochondrial targeting of Pex11pβ itself was inhibited by either deletion of the first 40 amino acids or N-terminal tagging of the protein with YFP (Fig. 3.22), i.e. that a potential mitochondrial targeting signal might reside within the protein's N-terminus. However, no classical mitochondrial targeting signal was identified by common screening tools. Insertion of Pex11pβ into the mitochondrial membrane might also be facilitated by its potential default recognition by the mitochondrial tail-anchored protein import machinery: Pex11pβ was wrongly identified as a tail-anchored protein in a large scale screen due to its extreme C-terminal transmembrane domain (Kalbfleisch et al., 2007), but the determination of its protein

topology at the mitochondrial membrane exclude the possibility that Pex11pβ behaves like a tail-anchored protein (Fig. 3.21). Furthermore, C-terminal tagging of tail-anchored proteins usually interferes with their proper targeting, but mitochondrial targeting of Pex11pβ was not affected in our case (Fig. 3.22). Thus, mitochondrial mistargeting of Pex11pβ in peroxisome-deficient patient fibroblasts appears to be mediated by an unidentified or unspecific mechanism. Intriguingly, contrary to its default role as a tubulator of peroxisomal membranes, Pex11pβ led to a profound fragmentation of mitochondrial membranes in peroxisome-deficient cells. As Pex11pβ was shown to interact with Fis1 (Kobayashi et al., 2007; Koch et al., 2010) which recruits the large GTPase DLP1 to peroxisomes and mitochondria, Pex11pβ-induced fragmentation of mitochondria might be mediated by a DLP1-dependent mechanism. In line with this, mitochondrial morphology upon mistargeting of Pex11pβ resembled Fis1 overexpression (Fig. 3.19). Alternatively, as Pex11pβ maintained its proper protein topology, differences in organellar lipid compositions might account for the observed phenotype. The action of *P. chrysogenum* Pex11p and its amphipathic helix was shown to depend on membrane lipid composition, since addition of a peptide comprising the most conspicuous amphipathic helix only led to liposome tubulation upon incubation with negatively charged small unilamellar vesicles (SUV) that had a lipid content similar to the peroxisome membrane. Neutral SUVs similar to the plasma membrane composition, however, remained spherical (Opalinski et al., 2011). Nonetheless, the lipid composition of peroxisomes in *P. pastoris* (used in above study) shares some similarity to the mitochondrial membrane (Wriessnegger et al., 2007): PC and PE are the major constituents of both membranes, with smaller but similar amounts of PS. The mitochondrial membrane naturally contains a higher amount of CL, which was also identified to be a true component of the peroxisomal membrane (Schneiter et al., 1999; Wriessnegger et al., 2007), whereas the peroxisomal membranes contain more PI (almost twice the amount). Nevertheless, it is interesting to note that targeting of Pex11pβ to a different lipid environment within the mitochondrial membrane did not only result in a “non-elongation” as observed for the artificial neutral SUVs (Opalinski et al., 2011), but to a severe fragmentation of mitochondria, a phenotype frequently associated with pathological conditions as e.g. apoptosis (Sheridan & Martin, 2010).

Interestingly, upon expression of Pex11pβ in peroxisome-deficient patient fibroblasts, no ER association was ever observed. Studies on the potential mistargeting of peroxisomal proteins in conditions where peroxisomal membrane biogenesis is impaired (PBDs; 1.1.4) often remain focused on the ER, as peroxisome-deficient cell lines lacking Pex3p, Pex16p or

Pex19p are capable of forming peroxisomes *de novo* from the ER upon re-introduction of the missing gene (Matsuzono et al., 1999; South & Gould, 1999; Muntau et al., 2000; Toro et al., 2009). In addition to that, d*e novo* formation of peroxisomes from the ER was also observed in yeast (Hoepfner et al., 2005; Kragt et al., 2005; Tam et al., 2005; Haan et al., 2006), while several peroxisomal proteins (such as plant ascorbate peroxidase, Pex16p or *Sc*Pex15p) travel to the ER in yeast, plants and mammals (Elgersma et al., 1997; Mullen et al., 1999; Kim et al., 2006; van der Zand et al., 2010). Thus, the notion was established that the ER serves as a default membrane accommodating peroxisomal proteins in peroxisome-deficient cell lines. In contrast to that, our observations on the mitochondrial targeting of Pex11pβ in peroxisome-deficient cells support the idea that mitochondria provide the preferred membrane environment for PMPs in mammals under peroxisome-deficient conditions. In line with this, the mammalian tail-anchored protein Pex26p was targeted to mitochondria after mutation of its peroxisomal targeting signal, while an ER association was hardly ever observed (Halbach et al., 2006). Furthermore, truncated versions of Pex3p, Pex14p and PMP70 were also shown to be mistargeted to mitochondria in human fibroblasts (Soukupova et al., 1999; Sacksteder et al., 2000). Interestingly, Pex3p targeted artificially to mitochondria also enabled *de novo* formation of peroxisomes from mitochondria instead of the ER (Rucktaschel et al., 2010). A preferential mistargeting of peroxisomal proteins to mitochondria in the absence of functional peroxisomes in mammalian cells might be an underappreciated factor when characterizing the pathophysiological implications of PBDs. While the characterization of PBD severity is naturally focused on peroxisome function or the lack thereof, endogenous peroxisomal proteins might be mistargeted to mitochondria and affect their morphology and function, a side effect observed in this study. Thus, mitochondrial mistargeting of peroxisomal proteins might contribute to the phenotypes and severity of peroxisomal disorders. Nonetheless, it has to be taken into account that the observations presented here were based on overexpression studies, i.e. that intracellular Pex11pβ concentrations clearly exceeded the endogenous levels of peroxisomal proteins in PBD patients several fold, however, its mitochondrial mistargeting potential has been clearly established.

Our findings further strengthen the notion that in mammals, mitochondria serve a default membrane for peroxisomal membrane proteins in the absence of functional peroxisomes (Soukupova et al., 1999; Sacksteder et al., 2000; Halbach et al., 2006; Rucktaschel et al., 2010) with potential consequences for patient pathology.

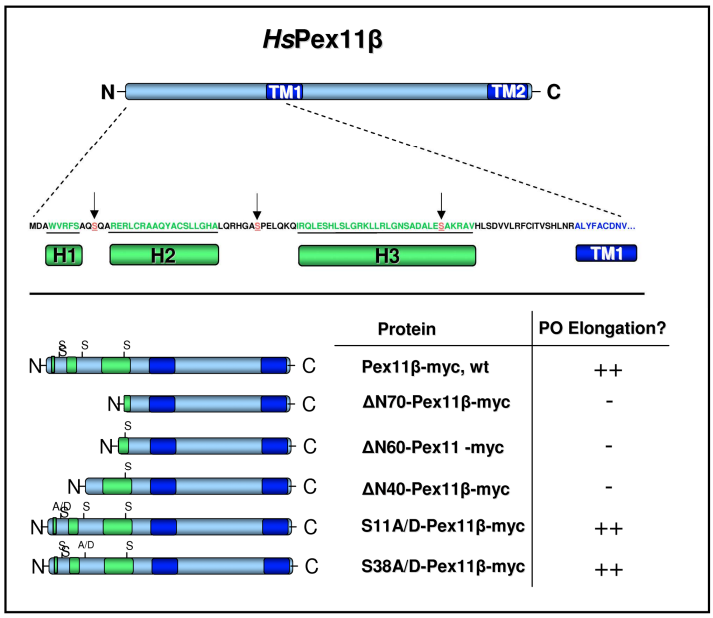

Fig. 4.2: Overview of the structure of human Pex11pβ and its N-terminal domain.
Overview of the position of transmembrane domains within human Pex11pβ (dark blue) and the amino acid sequence of its N-terminal domain. The positions of potential amphipathic helices are highlighted in green (taken from Opalinski, 2011). An overview of the different deletion mutants of Pex11pβ generated in our lab and their effect on peroxisome membrane elongation is given in the lower panel (our unpublished results).

4.2.2 Regulation of human Pex11pβ by oligomerization, but not phosphorylation

The presence of the most conspicuous amphipathic helix within *P. chrysogenum* Pex11p was shown to be sufficient to induce membrane elongation *in vitro* and *in vivo* upon expression in *H. polymorpha* (Opalinski et al., 2011). However, deletion of the first 40 amino acids of human Pex11pβ already abolished its membrane elongating capacity, although the predicted amphipathic helix remains intact (our unpublished results, Fig. 4.2). In line with previous findings (Kobayashi et al., 2007), further deletion of the first 60 and 70 N-terminal amino acids of Pex11pβ, also spanning the amphipathic region, inhibited peroxisomal membrane elongation, but did not exacerbate the phenotype of the Δ40 mutant (our unpublished results). Thus, it can be concluded that the mere presence of an amphipathic helix within human Pex11pβ is not sufficient to induce peroxisomal membrane elongation, indicating that the action of the protein is regulated by additional mechanisms. This part of the thesis aimed at investigating the regulation of human Pex11pβ by phosphorylation and oligomerization.

Up until now, evidence on a post-translational regulation of Pex11 proteins remained largely limited to studies in *S. cerevisiae* in which both phosphorylation and oligomerization of Pex11p was described: using *in silico* screening and subsequent *in vivo* phospho-labelling, *Sc*Pex11p was shown to be phosphorylated at a serine residue (S165/167) in the central part of the protein. Expression of phospho-mimicking mutants generated either a hyper-proliferative phenotype (“On”, S165/167D) or resulted in the formation of only a few clustered peroxisomes (“Off”, S165/167A) (Knoblach & Rachubinski, 2010). The

phosphorylation of *Sc*Pex11p was further determined to be dependent on the action of the kinase Pho85p which was previously identified (in combination with the cofactor pcl1) to potentially phosphorylate *Sc*Pex11p in a global analysis of protein phosphorylation in baker's yeast (Ptacek et al., 2005; Knoblach & Rachubinski, 2010). Only indirect evidence has been provided on a potential phosphorylation of Pex11pβ at a Y126 residue by a large scale screen using phospho-tyrosine antibodies in human tumour tissue (Rikova et al., 2007); however, this residue is positioned within the peroxisomal matrix and so far, no intra-peroxisomal regulation by kinases has been described. To determine a potential phosphorylation of human Pex11pβ, initially, *in silico* screening of human Pex11pβ was performed using databases that calculate potential phosphorylation sites (e.g. NetPhos 2.0, also used for the study on *Sc*Pex11p) and those that screen for potential kinase binding sites (e.g. KinasePhos 2.0) (Fig. 3.23 A). To gain insight into the applicability of the screening tools, values obtained for the confirmed *Sc*Pex11p S165/167 residue were used as a reference (probability of 0.995 using NetPhos 2.0). To narrow down the number of potential phospho-sites, we selected those identified by multiple screening tools which were also conserved among species (Fig. 3.23 A,C). Furthermore, as this study focused on the regulation of the N-terminal domain of Pex11pβ, intra-peroxisomal sites were excluded. Thus, the potential phosphorylation sites at positions S11, S38 and S70 were chosen for further studies. As deletion of the first 70 amino acids of Pex11pβ did not exacerbate the inhibition of elongation observed upon deletion of the first 40 amino acids (our unpublished results), phospho-mimicking mutants of the positions S11 and S38 were generated (co-operation with MJ Cardoso). In parallel, *in vivo* phospho-labelling and subsequent immunoprecipitation was performed using the YFP-tagged variant of Pex11pβ (Fig. 3.24). Empty YFP vector and the phosphoprotein APP-GFP were included as negative and positive controls, respectively. Although a radioactive signal was readily detected for the APP variant, consistent with its native regulation by phosphorylation (Lee et al., 2003; Schettini et al., 2010), no signal corresponding to YFP-Pex11pβ was discernable, indicating that it is not phosphorylated in human cells. Prominent elongation of peroxisomal membranes was confirmed by epifluorescence, indicating that the protein readily mediated elongation at the time points investigated. As overexpression of APP-GFP itself was sufficient to detect protein phosphorylation, it was surmised that the same would be applicable for Pex11pβ. Nonetheless, it cannot be excluded that phosphorylation of human Pex11pβ might only occur after very specific stimuli or that phosphorylation in humans is not linked to its membrane elongation capacity.

In regard to the regulation of Pex11p by oligomerization in *S. cerevisiae*, it is assumed to be regulated by dimerization in a redox-dependent manner (Marshall et al., 1996). After protein cross-linking and subsequent immunodetection, *Sc*Pex11p was shown to form monomers and dimers. Dimeric complexes of *Sc*Pex11p appeared to be more dominant in fractions representing mature peroxisomes. As protein dimerization was inhibited after mutation of a N-terminal cysteine residue, the authors proposed a model in which *Sc*Pex11p actively acts as a monomer at the inner surface of the peroxisomal membrane. Due to the increasing oxidative metabolism in mature peroxisomes, *Sc*Pex11p is then oxidized, leading to the formation of disulfide bridges and thus the formation of (inactive) dimeric forms of *Sc*Pex11p. (Marshall et al., 1996). As the human protein is also known to form homo-oligomers (Li & Gould, 2003; Kabeya et al., 2005; Kobayashi et al., 2007; Koch et al., 2010) which appear to be essential for peroxisomal membrane elongation (Kobayashi et al., 2007) (our unpublished results}, it remained unclear if monomeric Pex11pβ represents the active form in higher organisms. One of the aims of this study was to investigate the regulation of Pex11pβ by oligomerization. In order to do so, we took advantage of the fact that human myc-Pex11pβ, unlike the other mammalian Pex11 isoforms, was extracted from the peroxisomal membrane by Tx100 after protein-crosslinking with 4 % pFA (Fig. 3.14). Interestingly, the addition of a YFP-tag to the protein retained its localization at the peroxisomal membrane (Fig. 3.16 J-L). Although the Tx100 sensitivity of Pex11pβ was noticed before (Schrader et al., 1998b), this was the first time that its extraction into the supernatant was addressed by a biochemical approach. After immunoblotting of Tx100-treated fractions (Fig. 3.14), a prominent signal corresponding to myc-Pex11pβ was detected in the Tx100 supernatant fraction (Fig. 3.14 K). The respective pellet signal remained rather weak. The removal of membrane proteins after Tx100 addition was usually linked to incomplete protein-crosslinking by pFA (Goldenthal et al., 1985). Fixation of proteins by pFA is based on chemical crosslinking of their lysine residues, however, the overall number of lysine residues within the three mammalian Pex11 isoforms is similar. As Pex11pβ was the only isoforms removed from the peroxisomal membrane after Tx100 addition (Fig. 3.14), other factors must account for its behaviour. Alternatively, the non-ionic detergent Tx100 has long been indicated to interact with both amphiphilic proteins and unfixed lipids (Goldenthal et al., 1985). Furthermore, sequence similarities between *Sc*Pex11p and the ligand-binding domain of PPARs have been indicated, pointing to lipid-binding capabilities of *Sc*Pex11p (Barnett et al., 2000) which might facilitate interactions with Tx100. Additionally, the peroxisomal import receptor Pex3p similarly was also shown to contain α-helical structures capable of binding membrane lipids (Pinto et al., 2009). Thus, it is

tempting to assume that due to its amphiphilic, lipid-binding properties, Pex11pβ is able to interact with the non-ionic detergent Tx100 and is therefore extracted from permeabilized membranes. As the protein was shown to form predominantly homo-oligomers (Li & Gould, 2003; Kobayashi et al., 2007; Koch et al., 2010), protein cross-linking by pFA most probably led to the formation of Pex11pβ oligomers that share the same characteristic behaviour. The fact that the YFP variant of Pex11pβ remained situated at the peroxisomal membrane might be explained by the addition of the larger tag – of equal size as Pex11pβ itself – that led to the introduction of further lysine residues which facilitate a more potent cross-linking, also to other proteins. Using the Tx100 extraction assay, in addition to monomeric myc-Pex11pβ, another band was detected at the twofold molecular weight (Fig. 3.14), most probably representing a cross-linked, dimeric form of myc-Pex11pβ. As the Tx100 extraction assay established in this study provided a simple method of simultaneously cross-linking and enriching Pex11pβ, it was applied to determine the monomer/dimer ratio of human Pex11pβ at different time points: overexpression of myc-tagged variants of Pex11pβ was shown to initiate a prominent elongation of peroxisomes as soon as 5 hours after transfection (approx. 90 % tubular peroxisomes). After 24 hours, the majority of peroxisomes remains tubular, but diminishes after 48-72 hours due to subsequent fission of the newly-formed organelles (Schrader et al., 1998b). The distribution of monomeric and dimeric forms of myc-Pex11pβ was determined 5, 24 and 72 hours after transfection using the Tx100 extraction protocol and immunoblotting against the myc epitope (Fig. 3.25). Interestingly, in contrast to the findings in the yeast *S. cerevisiae*, dimeric forms of Pex11pβ were more prominent at the early time points corresponding to ongoing and profound peroxisome elongation. Thus, dimerization of human Pex11pβ appears to modulate protein activity. The observation that deletion of the first 40 amino acids of human Pex11pβ already diminished peroxisomal membrane elongation, although the predicted amphipathic helix of the protein remained intact, strongly indicated that those residues are necessary for the dimerization of the protein. Indeed, upon overexpression of the ΔN40 variant of Pex11β-myc, formation of Pex11pβ dimers was abolished (personal communication S. Grille).

In summary, our findings indicate that in mammalian cells, peroxisome dynamics at the organelle level are not merely regulated by the presence of amphipathic helix within the N-terminus of Pex11pβ, but that dimerization of the protein is required to exert its membrane deforming activity.

4.3 NOVEL STIMULI ALTERING PEROXISOME DYNAMICS

It has been pointed out that peroxisomes are highly dynamic subcellular organelles displaying a large plasticity, as not only spherical but also tubular structures as well as tubulo-reticular structures have been observed in ultrastructural and light microscopy studies (Yamamoto & Fahimi, 1987; Schrader et al., 1994; Schrader et al., 2000). In cell culture models, elongated peroxisomes have further been shown to be induced by stimulation with defined growth factors, PUFAs, microtubule depolymerisation, UV irradiation and exposure to H_2O_2 (Schrader et al., 1996a; Schrader et al., 1998a; Schrader et al., 1999). Similarly, peroxisome elongation/proliferation can be induced in plants after stress e.g. upon wounding, pathogen attack, osmotic stress or excess light (Lopez-Huertas et al., 2000; Desikan et al., 2001; del Rio et al., 2002; del Rio et al., 2006). In addition to that, the fast, transcription-independent formation of small peroxisomal tubules after ROS exposure was suggested to serve as a quick response to oxidative stress (Sinclair et al., 2009); thus it became more and more clear in recent years that peroxisome morphology is very closely linked to organelle function. Modulations of mitochondrial shape were shown to influence cellular functions such as calcium signalling and apoptosis (Westermann, 2010; Otera & Mihara, 2011), similarly, alterations and adaptations of peroxisome morphology and dynamics are also essential for cellular homeostasis. Along the same line, a lethal defect in peroxisome and mitochondrial fission was identified (Waterham et al., 2007). Peroxisome elongation as such represents an early step of peroxisomal growth and division to proliferate peroxisomes according to cellular needs (Wiemer et al., 1997; Schrader & Fahimi, 2006; Schrader et al., 2011); however, more complex peroxisomal structures such as elongated tubules or tubulo-reticular networks may also contribute and/or facilitate other peroxisomal functions (e.g. in metabolism, membrane signalling or stress response). In line with this, the formation of elongated peroxisomes is induced after UV irradiation or viral stimulation (Schrader et al., 1999; Dixit et al., 2010). However, detailed characterization of the link between peroxisome morphology and dynamics and the corresponding cellular function is required. Moreover, insight into reception of extracellular stimuli and their transduction onto the peroxisomal level remains is still limited.

4.3.1 Peroxisomes and neuronal apoptosis: no need for elongation at the point of no return?

Using the SH-SY5Y neuroblastoma cell line, the effects of the neurotoxin 6-hydroxydopamine (6-OHDA) on mitochondria and peroxisomes were investigated (co-

operation J. Jordan Bueso, University of Castilla-LaMancha, Spain). 6-OHDA, an oxidative metabolite of dopamine, is commonly used to generate experimental models of Parkinson's disease and its action has been linked to the increased generation of ROS (Blum et al., 2001; Bach et al., 2003; Galindo et al., 2003; Bove et al., 2005a). Exposure of SH-SY5Y cells to 6-OHDA led to a profound fragmentation of mitochondria which was very similar to the morphology observed after overexpression of Fis1, a protein involved in DLP1 recruitment. Mitochondrial fragmentation occurred rapidly (within 15 minutes after treatment) and could be observed in the majority of treated cells after 3 hours (Gomez-Lazaro et al., 2008). The effect of 6-OHDA on mitochondria was linked to ROS generation, as the use of "aged" 6-OHDA (from which ROS had been liberated by auto-oxidation) as well as the combined use of antioxidants prevented mitochondrial fragmentation. Interestingly, mitochondrial fragmentation seemed to be an early event in apoptosis, preceding the collapse of mitochondrial membrane potential and cytochrome c release, and was shown to be dependent on the action of DLP1 by silencing experiments. However, peroxisome morphology and dynamics remained unaffected by 6-OHDA treatment at time points when mitochondria were already drastically fragmented, but also after longer exposure (Fig. 3.26; Fig. 4.3). As an induction of a potential peroxisome fragmentation was difficult to detect, cells were additionally transfected with Pex11pβ-myc prior to 6-OHDA treatment to induce a profound tubulation of the peroxisomal membrane. Nevertheless, no effect of 6-OHDA on peroxisomes (fragmentation) was observed. (Fig. 3.26). Thus, the application of the ROS-inducing 6-OHDA stress did not exert any alteration of peroxisome morphology, unlike what was previously reported after UV irradiation and H_2O_2 exposure in HepG2 cells (Schrader et al., 1999). UV irradiation-induced peroxisome tubulation was linked to oxidative stress and suggested to mediate a protective response, e.g. by increasing the number of peroxisomes to counteract the effects of oxidative damage. As 6-OHDA action rapidly induced an apoptotic response, it might be concluded that a potential "rescue" mechanism corresponding to peroxisome elongation becomes obsolete under conditions where controlled cell death is already initiated. It is further interesting to note that while DLP1 is a shared component of both peroxisomes and mitochondria, DLP1-mediated effects of 6-OHDA are translated onto the organelle level in a differing manner. The proteins involved in the membrane recruitment of DLP1, the tail-anchored proteins Mff and Fis1, are also shared by both organelles, therefore differences in the regulation of the fission complex at mitochondria and peroxisomes are probably mediated by additional factors or mechanisms. In line with this, MiD49 and MiD51/MIEF have recently been identified as new components modulating DLP1

activity at mitochondria, but not peroxisomes (Palmer et al., 2011; Zhao et al., 2011) (our unpublished results). DLP1 was further shown to be influenced by post-translational modifications such as phosphorylation, sumoylation and ubiquitination (Chang & Blackstone, 2010), however, studies on the effects of those modifications have been limited to mitochondria. Future research needs to aim at determining potential effects on peroxisome dynamics, but nonetheless our results already indicate that mitochondrial and peroxisome dynamics are regulated in a differing manner.

4.3.2 Stress-induced peroxisomal elongation: the nature of the signal is the key

To further address the existence of general response of peroxisomes to an increase in oxidative stress, alterations of peroxisome dynamics were assessed after application of various ROS inducing compounds for longer time points (24 hours) in mammalian cells (Fig. 3.28). HepG2 and COS-7 cells were treated with various ROS-inducing components (leading to initiation of ROS production in the cytosol and mitochondria) and alterations of peroxisome morphology were determined by epifluorescence microscopy. While peroxisomes elongated profoundly after stimulation with fatty acids and serum in a control experiment (Schrader et al., 1998a) (Fig. 3.28 C), none of the applied oxidative stimuli induced a significant increase in the number of tubular peroxisomes (Fig. 3.28 A), in contrast to what was reported before after UV irradiation and H_2O_2 exposure (Schrader et al., 1999). Successful generation of oxidative stress after application of insults was confirmed by measuring an increase in DCF fluorescence (Fig. 3.28 B). Additionally, the existence of a short-term response to oxidative stress was examined. In plants, a dual response of peroxisomes to oxidative stress was observed, since short-term stress (up to 2 hours) initiated the formation of small membrane protrusions (“peroxules”), whereas longer stress periods led to the formation of the full peroxisomal “bead-on-a-string” morphology indicative of peroxisome proliferation that was also observed after UV irradiation (Schrader et al., 1999; Sinclair et al., 2009). A compartment-specific, short-term ROS response was investigated by the use of the genetically-encoded photosensitizer KillerRed (Bulina et al., 2006a; Bulina et al., 2006b). KillerRed is a phototoxic red fluorescent protein that is activated upon green light exposure, resulting in the generation of predominantly superoxide radical (Bulina et al., 2006a; Bulina et al., 2006b). KillerRed variants targeted to the cytosol, mitochondria and peroxisomes were overexpressed in COS-GFP-PTS1 cells and effects of their activation on

peroxisome morphology were assessed by live cell imaging (Figs. 3.29; 3.30). This set-up served a two-fold purpose: first, live cell imaging after KillerRed activation as such enabled us to determine if small, peroxisomal extensions were also formed in mammalian cells after 30-90 minutes, while the organelle-specific targeting of KillerRed variants served to validate a compartment-specific ROS response of peroxisomes, e.g. to determine if a sharp increase in mitochondrial stress leads to a rapid peroxisome elongation as a potential rescue or complementation mechanism. However, in this experimental setup, activation of none of the expressed variants led to any peroxisome elongation (Fig. 3.29; 3.30). This is in line with findings from our group on the effect of mitochondrial ROS generation (induced upon inhibition of the electron transfer chain) on peroxisome morphology in COS-7 cells in which no ROS-mediated elongation of peroxisomes was observed (Master thesis, S. Pinho; Co-supervisor: N. Bonekamp). Interestingly, the complex I inhibitor rotenone was demonstrated to have a dramatic microtubule-depolymerizing effect which initiated peroxisome elongation, in line with previous findings on the contribution of the microtubule cytoskeleton to peroxisome dynamics (Schrader et al., 1996a; Schrader et al., 1996b). Notably, treatment with L-buthionine sulfoximine (BSO), a compound inhibiting GSH repletion and thus modulating intracellular redox-state (Griffith & Meister, 1979), stimulated a significant increase in the percentage of tubular peroxisomes. Interestingly, a recent study has investigated the intra-peroxisomal redox balance in response to several stimuli using a reduction-oxidation sensitive GFP variant (roGFP) (Ivashchenko et al., 2011). Ratiometric measurements of its excitation maxima (representing reduced and oxidized states) allowed the determination of organellar redox-state after targeting of roGFP variants to either the cytosol, mitochondria and peroxisomes at steady-state conditions and after insults. Perturbations in peroxisomal function, e.g. in catalase-deficient fibroblasts, strongly affected mitochondrial redox-state. Additionally, KillerRed variants targeted to the cytosol, mitochondria and peroxisomes were used in combination with roGFP. Similar to our observations, KillerRed-PO displayed slower peroxisomal targeting kinetics (Fig. 3.30). In line with our findings, KillerRed activation in the three subcellular compartments did not modulate peroxisomal morphology, however, the peroxisomal redox state was shown to be affected, albeit only by upon intra-peroxisomal oxidative stress. Mitochondrial redox state on the other hand remained largely sensitive to changes within peroxisomes, suggesting an inter-organellar cross-talk mechanism (Ivashchenko et al., 2011). These findings indicate that a compartment-specific peroxisomal response to (oxidative) stress might rather be based on “detection” of organellar redox-state without a concomitant alteration of peroxisome morphology. Large scale alterations of

peroxisome morphology such as a prominent elongation might only be induced under very specific conditions. Interestingly, Ivashchenko et al also demonstrated that the peroxisomal redox state as such was largely influenced by cell culture conditions and passage number of the cells which strongly affected the experimental results and accounted for contradictory findings (Yano et al., 2010; Ivashchenko et al., 2011). Hence, this leaves us with the possibility that the steady-state intra-peroxisomal redox state differed between the present and previous studies (Schrader et al., 1999). Moreover, it is possible that the signal mediating a peroxisomal response to UV irradiation as such was not only linked to an increase in oxidative stress, but potentially also to the activation of other signalling pathways. For, instance the UV irradiation pulse applied (UV-C, 254 nm) (Schrader et al., 1999) affects DNA integrity, therefore the numerous cellular pathways activated as a DNA damage response might contribute to the observed phenotype (Lagerwerf et al., 2011). Interestingly, DNA damage has been shown to trigger autophagy (Rodriguez-Rocha et al., 2011), thus, an elongated peroxisome morphology might serve to protect peroxisomes from autophagosomal destruction as has been described for mitochondria (Gomes et al., 2011; Rambold et al., 2011a). Peroxisomes might then be protected and capable of supplying metabolites and lipids to counteract cellular damage.

The findings presented in this study indicate that the nature of stress signals is essential in modulating peroxisome dynamics. While a global increase in oxidative stress did not affect peroxisome morphology , changes in cellular redox state did (Fig. 4.3). Moreover, application of stressors might affect intra-peroxisomal redox-state without any visible change in peroxisome dynamics (Ivashchenko et al., 2011). Thus, the UV-induced tubulation of peroxisomes might not be linked as much to a large scale increase in oxidative stress as to other factors, such as UV-related cellular damage and damage signalling.

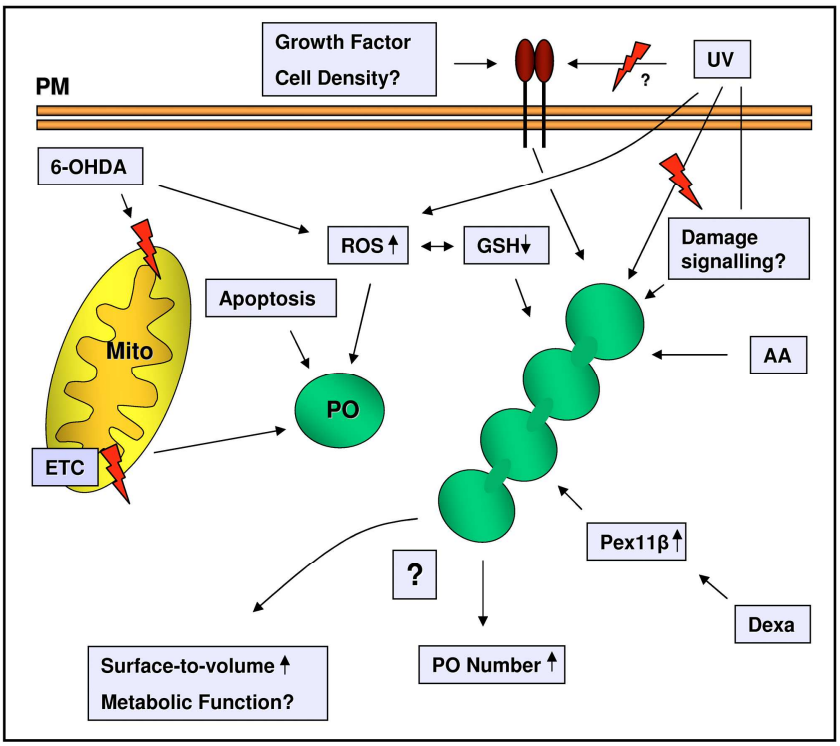

Fig. 4.3: Overview of the different extra- and intracellular stimuli and their effect on peroxisome dynamics.
Note that induction of cytosolic or mitochondrial (Mito) oxidative stress does not affect peroxisome dynamics, while UV irradiation, low cell density, growth factor and PUFA stimulation leads to a tubulation of peroxisomes. To facilitate this, membrane receptors and intracellular (damage) signalling might contribute to exert a peroxisomal response. Dexamethasone (Dexa) treatment induces peroxisome elongation which is linked to the regulation of Pex11β while 6-OHDA addition did not affect peroxisomal, but mitochondrial dynamics. Note that tubulation of peroxisomes might indicate peroxisomal growth and division to increase peroxisome numbers or mediate a metabolic function by e.g. increasing the surface-to-volume ratio.

4.3.3 The effect of the glucocorticoid dexamethasone on peroxisome proliferation: a defined physiological cell culture model to study peroxisome dynamics

Although several external stimuli leading to alterations of peroxisome dynamics and/or the induction of peroxisome proliferation have been characterized, knowledge regarding their molecular reception and subsequent signal transduction is still limited. In mammals, insight into the regulation of peroxisomal proliferation remains largely restricted to the activation of the nuclear receptor PPARα and its target genes in rodent animal models after feeding of peroxisome proliferators (1.2.4). Moreover, manipulation of peroxisome dynamics in cell culture is usually achieved by a “global” modulation of proteins involved in peroxisome growth and division processes, e.g. after overexpression of Pex11pβ. On a related note, for some of the signals inducing a profound tubulation of peroxisomes in mammalian cells, such as addition of serum or cell density (Schrader et al., 1994; Schrader et al., 1996a; Schrader et al., 1998a), an exact stimulus affecting peroxisome dynamics can hardly be defined, as numerous cellular pathways are affected. Hence, the characterization of a cell culture model is

desirable which allows to reliably monitor alterations of peroxisome dynamics after application of a defined, well-characterized stimulus.

In this study, we took advantage of an AR42J cell culture model that is usually employed to study the differentiation of pancreatic acinar cells and the biogenesis of zymogen granules (Swarovsky et al., 1988; Faust et al., 2008; Borta et al., 2010). Stimulation of AR42J cells which are derived from rat exocrine pancreatic tumour cells, with glucocorticoids such as dexamethasone was shown to lead to the coupled induction of exocrine proteins and a profound remodelling of intracellular compartments involved in the secretory pathway (Logsdon et al., 1985; Logsdon et al., 1987; Swarovsky et al., 1988). For instance, secretory differentiation markers such as chymotrypsinogen and amylase show a profound induction in regard to their mRNA and synthesis rates and the formation of zymogen granules is induced (Scheele, 1993). The AR42J cell culture model has been established in our lab (Faust et al., 2008; Borta et al., 2010) and was thus used here to study the effects of dexamethasone, a synthetic fluorinated glucocorticoid, on peroxisome dynamics. AR42J cells were treated with either 10 nM dexamethasone, a concentration used to stimulate differentiation of AR42J cells, or 1 µM of the compound, representing a more pathophysiological concentration (Du et al., 2009). Induction was carried out for 6-72 hours with fresh dexamethasone and peroxisome morphology as well as induction of chymotrypsinogen (a zymogen granule marker) was assessed by epifluorescence microscopy. As described before, a significant increase of zymogen granules/chymotrypsinogen was observed (Fig. 3.32 C), verifying successful dexamethasone action, but interestingly dexamethasone treatment also resulted in a significant, dose-dependent tubulation of peroxisomes (Fig. 3.31; 3.32; 4.3). Untreated controls displayed the pattern of peroxisome morphology after seeding as described for mammalian cells (Schrader et al., 1994; Schrader et al., 1996a), i.e. an increase in tubular forms 24 hours after seeding (and here 6 hours after induction) with a subsequent increase in spherical forms reminiscent of fission. In contrast to that application of dexamethasone provided a time- and dose-dependent stimulus for continuous peroxisome elongation (Fig. 3.32 B). Although induction of tubular peroxisomes mirrored the kinetics of zymogen granule formation, it is important to note that not all cells with tubular peroxisomes also displayed granular structures, insinuating that both processes are not necessarily coupled. Interestingly, also singular addition of dexamethasone and subsequent removal of the stimulus was sufficient to induce peroxisome tubulation, even 48 hours after removal of dexamethasone (Fig. 3.33). As the observed peroxisome morphology after dexamethasone treatment largely mimicked the morphology of peroxisomes observed after overexpression of Pex11pβ (Fig.

3.34), further analysis aimed at investigating changes in the induction profile of the three rat Pex11 isoforms by a semi-quantitative PCR approach (SQ-PCR) (Fig. 3.35). AR42J cells were stimulated with dexamethasone (10 nM and 1 µM) for 24, 48 and 72 hours and the induction of Pex11α, Pex11β and Pex11γ was assessed in comparison to the housekeeping gene GAPDH by SQ-PCR. The peroxisomal key enzyme AOX was included as a control for peroxisome proliferation. Compared to the stable expression of GAPDH, AOX was clearly induced after dexamethasone treatment. This induction pattern was mirrored at the protein level (Fig. 3.31) and is indicative of peroxisome proliferation. Pex11α, the inducible isoform (Abe et al., 1998), was similarly expressed and was only clearly detected after dexamethasone induction, mirroring the pattern of AOX induction. In contrast to that, clear signals corresponding to Pex11β were seen in controls at every time point investigated, in line with its constitutive expression in all tissues. However, Pex11β was also induced 24 and 48 hours after treatment with dexamethasone when compared to controls (Fig. 3.31). The Pex11pβ antibody failed to recognize the rat protein upon immunoblotting, thus induction of Pex11pβ was not verified on the protein level. Nonetheless, as the induction of AOX on the protein level followed the pattern observed on the mRNA level (Fig. 3.31), the observations made by SQPCR were reliable. Comparison between Pex11β levels in control cells at different time points revealed it to be induced after 72 hours (96 hours after seeding) when compared to the 24 and 48 hour expression levels. This might be due to a potential “normal” induction of Pex11β in the course of cell growth and differentiation. While Pex11α and Pex11β were clearly induced by dexamethasone addition, Pex11γ signals remained barely detectable throughout the experiment and were thus concluded to play a minor role in regulating dexamethasone-induced alterations of peroxisome morphology. Altogether, the rat AR42J cell line was established as a valuable cell culture model to study alterations of peroxisome dynamics and their regulation. In contrast to other stimuli, e.g. serum addition, the initial signal leading to peroxisome elongation was corresponded to one well-defined external stimulus, the glucocorticoid dexamethasone. The results obtained here were also highly reproducible. Moreover, dexamethasone addition was directly linked to the activation of key components of the peroxisomal growth and division machinery, Pex11α and Pex11β. However, as peroxisome tubulation is initiated upon expression of Pex11pβ and Pex11pγ, but not Pex11pα (Fig. 3.34), the peroxisomal phenotype of dexamethasone addition is most probably linked to Pex11β induction. Interestingly, although Pex11β is not induced by PPARα-mediated peroxisome proliferator acting on rat hepatocytes, its expression was stimulated by dexamethasone, thus a novel mechanism of PPARα-independent regulation of

peroxisome dynamics was identified in this study. Dexamethasone-induced peroxisomal elongation thus provides an easy, amenable and highly reproducible cell culture model to assess changes in the expression profile of peroxisomal genes involved in the regulation of peroxisome dynamics by e.g. large scale expression profiling. It might also contribute to the identification of novel components regulating peroxisome dynamics and offers a more straightforward approach to study regulation of peroxisome abundance when compared to fibrate-induced peroxisome proliferation in rodents.

The molecular action of glucocorticoids has so far been linked to several mechanisms: glucocorticoid activities can be divided into genomic effects, mediated by the cytosolic glucocorticoid receptor alpha (cGCR) and other non-genomic effects (Pratt, 1998; Almawi & Melemedjian, 2002; Adcock & Lane, 2003; Wikstrom, 2003; Buttgereit et al., 2004; Buttgereit et al., 2005; Stahn et al., 2007). In the classical mode of action, the unligated cGCR, a member of the steroid hormone receptor family, resides in the cytoplasm as a multiprotein complex including heat shock proteins, immunophilins, chaperones (such as Src) and several kinases of the MAPK family (Pratt, 1998; Almawi & Melemedjian, 2002; Wikstrom, 2003). The cGCR itself contains 3 key domains, the N-terminal transactivation domain, a DNA-binding zinc finger domain and a ligand binding domain (Wikstrom, 2003). Glucocorticoids can pass the plasma membrane due to their lipophilic structure and are able to bind the receptor which in turn leads to dissociation of the cCGR complex, homo-dimerization of the receptor and its translocation into the nucleus occurs where it binds specific DNA binding sites (glucocorticoid response elements, GREs) (Almawi & Melemedjian, 2002). In line with their use as anti-inflammatory drugs, GREs induce anti-inflammatory proteins, but also genes for gluconeogenesis. In addition to this positive regulation of GREs (“transactivation”), there is also negative regulation (“transrepression”) of negative GREs, inhibiting e.g. transcription of interleukin-1 (Falkenstein et al., 2000). Moreover, apart from direct GRE binding, the activated GC/GCR complex can also interact with other transcription factors or compete with other nuclear co-activators, leading to a transrepression of genes (Reily et al., 2006; Stahn et al., 2007) In terms of the genomic effects of cGCR action, the activation, translocation and binding to GREs takes about 30 minutes, while changes on the cellular or tissue level become apparent after hours or days (Stahn et al., 2007). Other non-genomic effects are thought to occur by a direct effect of the lipophilic GCs on biological membranes (e.g. by intercalation with the mitochondrial membrane) (Buttgereit & Scheffold, 2002; Buttgereit et al., 2004), downstream effects of the release of the cGCR complex via e.g. release of MAPK and activation of a potential membrane-bound GCR

(Gametchu et al., 1999; Croxtall et al., 2000; Buttgereit et al., 2004). Up until now, there is only limited information on the role of glucocorticoid action on peroxisome function and/or dynamics. However, dexamethasone was shown to regulate the expression of PPARα in rat hepatocytes (Rao & Subbarao, 1997; Plant et al., 1998; Lawrence et al., 2001). Most of these studies were carried out in rat hepatocytes to not only determine the contribution of glucocorticoids to peroxisome proliferation, but also to determine the basis of the cell proliferation and tumour growth observed in rodents upon feeding with peroxisome proliferators. It was also demonstrated that the addition of glucocorticoids during culturing of primary rat hepatocytes was necessary to maintain PPARα expression and thus responsiveness to peroxisome proliferators (Mitchell et al., 1984). Upon addition of peroxisome proliferators, electron microscopy and morphometric analysis then revealed in increase in the fractional volume of peroxisomes. However, dexamethasone application alone was not sufficient to induce the expression of the peroxisome marker PMP70 in mice (Lawrence et al., 2001). Our observations on the induction of Pex11α and Pex11β indicate a genomic effect of dexamethasone on peroxisome dynamics; however, the exact molecular regulation requires further analysis. The induction of AOX and Pex11α, both of which are regulated by PPARα, might indicate that dexamethasone induces PPARα which in turn activates transcription of its targets. To analyze a potential contribution of PPARα stimulation to the observed phenotype, AR42J cells were treated with bezafibrate, a potent inducer of PPARα-mediated peroxisome proliferation in rat hepatocytes. It was surmised that if dexamethasone effects stem from indirect consequences of PPARα activation, the observed morphology and induction pattern in AR42J cells would be similar. However, no effect on peroxisome elongation or proliferation was observed (Fig. 3.37 A-C). Furthermore, no induction of AOX or Pex11α – PPARα target genes – was detected (Fig. 3.37 D), indicating AR42J cells of rodent pancreatic origin only respond weakly to bezafibrate, unlike rat hepatocytes. Similar results were obtained using ETYA, another peroxisome proliferating drug (data not shown). This might be due to a low expression of PPARα in AR42J cells which actually contain features of both exocrine and endocrine pancreas. In line with this, though primarily endocrine pancreas was investigated, PPARα expression was indicated to be low in pancreatic tissue, while the glucocorticoid receptor was moderately expressed (Bookout et al., 2006). As our findings indicate AR42J cells to be low responders to bezafibrate and thus the action of PPARα, we concluded dexamethasone-induced peroxisome elongation is regulated independently. Notably, peroxisomes maintained their tubular morphology, even after removal of the dexamethasone stimulus, indicating that initial stimulation was sufficient to

activate the downstream signal transduction onto the molecular and then peroxisomal level. The maintained peroxisome elongation after glucocorticoid stimulation was not indicative of growth and division processes upon which peroxisomal tubules subsequently would be divided. Interestingly, elongation of the peroxisomal membrane and formation of complex structures have been linked to metabolic processes such lipid synthesis or penicillin production (Kollatakudy et al., 1987; Kabeya et al., 2005; Kiel et al., 2005b) and were suggested to facilitate a metabolic function of peroxisomes by generating a uniform biochemical distribution of proteins, increasing the surface to volume ratio and exchanging metabolites (Schrader & Fahimi, 2006). Thus, continuous membrane elongation after dexamethasone stimulation might represent a specific peroxisome morphology indicative of a metabolic function instead of an growth and division process. As glucocorticoids have vast anti-inflammatory capacities (Buttgereit et al., 2004; Stahn et al., 2007), a shift of peroxisomal dynamics to a more tubulated structure might modulate the anti-inflammatory response, by e.g. a stimulation peroxisomal breakdown of the inflammatory mediators leukotriene or prostaglandin as well as arachidonic acid (AA). In line with this, application of AA also induced elongated peroxisomes (Schrader et al., 1998a).

Thus, rat pancreatic AR42J cells have a high potential to serve as a model system for dexamethasone-induced peroxisomal elongation (Fig. 4.3). It provides an amenable system to easily assess changes in the expression profile of peroxisomal genes involved in the regulation of peroxisome dynamics after application of a well-defined stimulus. Future studies using large scale expression profiling in this system might contribute to the identification of novel components regulating peroxisome morphology and dynamics.

4.4 FUTURE PERSPECTIVES

In the present study, processes contributing to the modulations of peroxisome dynamics in mammalian cells were investigated. Although a complete fusion process of mature peroxisomes was ruled out to modulate peroxisome dynamics, peroxisomes were shown to engage in transient, but complex interactions. Future studies need to determine the physiological significance of the observed peroxisomal contacts. As peroxisomes are further known to interact extensively with other organelles such as the ER or mitochondria, the existence of complex interactions of peroxisomes with those organelles might also be addressed by live cell imaging studies and subsequent mathematical evaluation. Furthermore, membrane fusion processes might still be involved in the formation of more complex peroxisomal structures such as tubulo-reticular networks. Thus, it is desirable to establish a

model system to induce a higher frequency of reticular peroxisomes in order to characterize the generation of peroxisomal networks.

The regulation of peroxisome dynamics on the organellar level was addressed by characterizing the central peroxisomal biogenesis factor Pex11pβ. Upon mistargeting of human Pex11pβ to mitochondria in peroxisome-deficient cells, mitochondria were fragmented; however, the molecular basis of the observed fragmentation remains to be elucidated. Although *in vivo* phospho-labelling experiments indicated that Pex11pβ was not phosphorylated in mammalian cells, it cannot be strictly excluded that the protein is phosphorylated at very specific time points and/or after very particular stimuli. Moreover, phosphorylation in mammalian cells might be required for other downstream purposes, such as initiation of fission. Time-course experiments and subsequent detection of phosphorylation using non-radioactive methods such as phospho-amino acid specific antibodies might help to elucidate this question. Dimerization of human Pex11pβ was shown to be crucial to mediate its membrane deforming activity. It might be interesting to address if human Pex11pβ can be regulated in a redox-dependent manner, similar to the yeast *Sc*Pex11p. In order to do so, conspicuous cysteine residues within Pex11pβ need to be identified. Site-directed mutagenesis and subsequent expression studies might facilitate screening for a potential impairment of Pex11pβ-membrane elongation. Furthermore, redox western blotting techniques might additionally provide insight into a potential redox-regulation of Pex11pβ, especially after stress conditions and also after manipulation of the cellular redox state.

Finally, dexamethasone was identified as a novel stimulus inducing profound peroxisomal membrane tubulation. In this respect, the now established AR42J cell culture model provides a highly reproducible system in which peroxisome elongation can be induced upon application of a very defined stimulus. The cell model might form an elegant basis for large scale expression profiling to gain insight into peroxisome-related signal transduction of glucocorticoids, but also to screen for other yet unidentified regulators of peroxisome proliferation. The genomic effects of the glucocorticoid cascade in comparison to non-genomic effects might also be characterized on the peroxisomal level. Reporter studies using Pex11 promoter regions will help to determine the mode of genomic activation. A potential non-genomic effect via MAPK activation or downstream signalling and its contribution to the glucocorticoid-induced membrane elongation can be addressed by pharmacological studies using specific inhibitors. The suggestions outlined here will help to gain further insight in the regulation of peroxisome proliferation and dynamics.

5 SUMMARY

Peroxisomes are ubiquitous subcellular organelles involved in a variety of important metabolic processes. Recently, it became obvious that many of those functions are carried out in co-operation with mitochondria. The essential role of peroxisomes for human health is exemplified by the severe phenotype of peroxisomal disorders. Furthermore, peroxisomes are highly dynamic, adjusting their protein content, morphology and number in response to cellular needs. In recent years, peroxisome dynamics and their proper regulation were closely linked to organelle function and thus, human well-being. In line with this, a patient with a lethal defect in mitochondrial and peroxisomal fission was identified. Peroxisome dynamics are regulated by growth and division of the organelle, however, peroxisomes can also arise *de novo* from the ER under special conditions. In mammalian cells, peroxisomal growth and division follows a well-defined sequence of morphological alterations. Initial membrane elongation is carried out by the key peroxisomal membrane protein Pex11pβ, while final scission into smaller organelles is achieved by the combined action of the membrane adaptors Mff and Fis1 as well as the large GTPase DLP1. Interestingly, the key components of the peroxisomal fission machinery are shared with mitochondria; however the occurrence of peroxisomal fusion analogous to mitochondria remains a matter of debate. Although several external stimuli were identified to alter peroxisome dynamics, detailed information on their reception and transduction onto the peroxisomal level is limited. Thus, the aim of this study was to gain a deeper understanding of the processes contributing to and regulating peroxisome dynamics in mammalian cells. This thesis contains three parts: in the first section, the contribution of peroxisomal fusion, analogous to mitochondria, to organelle dynamics was addressed. In the second part, the regulation of peroxisome dynamics at the organelle itself was investigated by characterizing post-translational mechanisms modulating the action of Pex11pβ, the key mediator of peroxisome elongation/proliferation in mammalian cells. In the final part, different groups of external stimuli were characterized in regard to their capacity to alter peroxisome dynamics in order to study the regulation of peroxisome dynamics on a transcriptional level in mammalian cell culture.

To investigate fusion of mature peroxisomes in mammalian CHO cells, an *in vivo* fusion assay was established based on hybridoma formation by cell fusion using cell lines stably expressing GFP- or DsRed-derived peroxisomal matrix and membrane markers. Fluorescence microscopy in time course experiments of fixed cells revealed a merge of different peroxisomal markers in fused cells, pointing to a certain degree of peroxisomal fusion. Although subsequent live cell imaging indicated that peroxisomes did not exchange matrix or

membrane markers, the existence of transient, vivid interactions between individual peroxisomes was characterized for the first time. Interacting peroxisomes were shown to be tightly associated, accounting for the marker overlay observed in fixed cells. Using computational modelling and mathematical analysis, transient peroxisome interactions were shown to follow a complex, non-random behaviour that has the potential to facilitate the homogenization of the heterogeneous peroxisomal compartment. Pre-treatment with peroxisomal substrates indicated that transient, peroxisomal interactions do not contribute to the exchange of fatty acids or H_2O_2, but might facilitate the exchange of other peroxisomal metabolites or be part of a signaling system to sense the state and/or distribution of the peroxisomal population in the cell. Furthermore, for the first time, computational analysis provided an explanation why only 15 % of the peroxisome population is engaged in long-range microtubule-dependent movement. Additionally, evidence was provided that mitochondrial fusion proteins do not localize to peroxisomes, indicating that peroxisome dynamics in mammalian cells are regulated in a distinct manner.

To gain insight into the modulation of peroxisome dynamics at the organelle itself, Pex11pβ was characterized biochemically. Differential permeabilization and protease-protection assays in combination with a newly available commercial antibody localized the position of its first transmembrane domain to the amino acid positions 90 – 110. Subsequently, the contribution of the N-terminal domain to the regulation of human Pex11pβ activity was addressed. Deletion of the first 40 amino acids abolished Pex11pβ-membrane elongation, although the essential amphipathic helix within the protein remained intact. Biochemical cross-linking and enrichment of Pex11pβ in time-course experiments linked its homo-dimerization to its activity which was diminished upon N-terminal deletion. *In vivo* phospho-labelling did not indicate phosphorylation of Pex11pβ in a manner similar to its *S. cerevisiae* orthologue. Thus, Pex11 proteins in yeast and mammals appear to be regulated in an opposite manner. Furthermore, overexpression of Pex11pβ in peroxisome-deficient patient fibroblasts resulted in its mistargeting to mitochondria where an excessive fragmentation was induced. This further emphasizes that mitochondria, but not the ER, serve a default membrane for peroxisomal membrane proteins in the absence of peroxisomes in mammals. Potential disturbances of mitochondrial function might thus contribute to the clinical severity of peroxisome disorders.

In the final part of this thesis, external stimuli altering peroxisomal dynamics were characterized to establish a more physiological and amenable cell culture model to investigate the transcriptional regulation of peroxisome dynamics in mammalian cells. Application of the

neurotoxin 6-OHDA in SH-S5Y5 neuroblastoma cells did not affect peroxisome dynamics, but led to a profound DLP1-dependent fragmentation of mitochondria. Though DLP1 is a shared component of both organelles, mitochondrial and peroxisomal dynamics further appear to be regulated in a distinct manner. Using a variety of compounds inducing cytosolic and mitochondrial oxidative stress, no morphological alterations of peroxisomes were observed. KillerRed-based induction of ROS in different compartments produced similar results in living cells. Thus, other factors besides the induction of oxidative stress, such as e.g. the intracellular or extracellular origin of the signal, alterations of cellular redox-state or yet unidentified signalling pathways might contribute to induce the alterations of peroxisome dynamics observed before. Addition of the glucocorticoid dexamethasone to rat pancreatic AR42J cells resulted in a profound, continuous elongation of peroxisomes. Notably, peroxisomes maintained their tubular morphology even after removal of the stimulus. Continuous peroxisome tubulation might be linked to cell differentiation or a metabolic function. Dexamethasone application induced Pex11β (and Pex11α) on a transcriptional level by a potentially PPARα-independent mechanism. Thus, dexamethasone-induced peroxisome elongation in AR42J cells has a high potential to serve as a more physiological model to study the regulation of peroxisome dynamics in mammalian cells. Future studies using expression profiling after dexamethasone stimulation in order to identify novel components and/or molecular mechanisms regulating peroxisome dynamics have been initiated.

6 ZUSAMMENFASSUNG

Peroxisomen sind ubiquitäre Zellorganellen, die an einer Vielzahl wichtiger metabolischer Prozesse beteiligt sind. Viele dieser Funktionen werden in enger Kooperation mit Mitochondrien ausgeführt. Da Peroxisomen für die Gesundheit und Entwicklung des Menschen essentiell sind, führen peroxisomale Dysfunktionen zu schwerwiegenden Erkrankungen. Des Weiteren sind Peroxisomen sehr dynamische Zellorganellen, die ihre Proteinkomposition, Morphologie und Anzahl an die zellulären Anforderungen anpassen. Kürzlich wurde ein Patient mit einem letalen Defekt der mitochondrialen und peroxisomalen Teilung identifiziert; daraus wird ersichtlich, dass der korrekte Ablauf dynamischer peroxisomaler Prozesse eng mit der Funktion der Organelle verknüpft ist und somit ebenfalls essentiell für die menschliche Gesundheit ist. Die Dynamik der Peroxisomen als solche wird durch Wachstums- und Teilungsprozesse reguliert, jedoch können Peroxisomen unter bestimmten Bedingungen auch *de novo* aus dem ER gebildet werden. In Säugerzellen geht der peroxisomale Wachstums- und Teilungsprozess mit einer Reihe klarer morphologischer Veränderungen der Organelle einher: eine initiale Elongation der peroxisomalen Membran wird durch das peroxisomale Membranprotein Pex11pβ vermittelt, während die Durchschnürung der peroxisomalen Tubuli in kleinere Organellen durch die Membranadaptoren Mff, Fis1 sowie die GTPase DLP1 erfolgt. Interessanterweise sind letztere Proteine auch an der Teilung von Mitochondrien beteiligt. Die Frage, ob ausgereifte Peroxisomen, ähnlich wie Mitochondrien, miteinander fusionieren, blieb umstritten. Es wurden außerdem diverse externe Stimuli identifiziert, die die peroxisomale Dynamik verändern, jedoch sind die Mechanismen ihrer Rezeption und der Signaltransduktion auf die Ebene der Organelle weithin unbekannt. Die vorliegende Studie zielte daher darauf ab, Einblicke in Prozesse zu gewinnen, die an der Dynamik der Peroxisomen beteiligt sind und zu ihrer Regulation beitragen. Diese Dissertation besteht aus drei Teilen: im ersten Teil wurde die Existenz einer Fusion ausgereifter Peroxisomen, analog zur mitochondrialen Fusion, untersucht. Im zweiten Teil dieser Arbeit wurde die Regulation von Pex11pβ, des Schlüsselproteins der peroxisomalen Biogenese in Säugerzellen, durch post-translationale Mechanismen untersucht, um Einblicke in die Regulation der peroxisomalen Dynamik auf der Ebene der Organelle selbst zu gewinnen. Im dritten Teil dieser Studie wurden verschiedene Gruppen von Stimuli im Hinblick auf ihren Effekt auf das peroxisomale Kompartiment charakterisiert, um die Regulation der peroxisomalen Dynamik auf transkriptioneller Ebene in Säugerzellkulturmodellen zu untersuchen.

Um die Fusion ausgereifter Peroxisomen in Säugerzellen zu untersuchen, wurde ein *in vivo* Fusionsassay in CHO-Säugerzellen etabliert. Dieser beruhte auf der Kokultivierung stabiler Zelllinien, die GFP- oder DsRed-basierte peroxisomale Matrix- oder Membranmarker exprimierten, und der anschließenden Generierung von Hybridomzellen durch Zellfusion. Eine Überlappung der unterschiedlichen peroxisomalen Marker wurde fluoreszenzmikroskopisch in zu verschiedenen Zeitpunkten fixierten Zellen festgestellt, was zunächst auf einen gewissen Grad peroxisomaler Fusionen hinwies. Weitere Studien in lebenden Zellen zeigten jedoch, dass kein Austausch peroxisomaler Marker stattfand. Allerdings wurde erstmals die Existenz transienter peroxisomaler Interaktionen charakterisiert. Interagierende Peroxisomen gingen dabei enge Kontakte ein, die für die beobachtete Überlappung von peroxisomalen Markern in fixierten Zellen verantwortlich waren. Computer-basiertes *Modelling* und mathematische Analyse ergaben, dass transiente peroxisomale Interaktionen einem komplexen, nicht-zufälligen Verhaltensmuster folgten, welches potentiell zu einer Homogenisierung des peroxisomalen Kompartiments beitragen könnte. Vorstimulation der Zellen mit peroxisomalen Substraten wies darauf hin, dass Fettsäuren und H_2O_2 nicht ausgetauscht wurden, jedoch könnten transiente peroxisomale Interaktionen dem Austausch anderer peroxisomaler Metabolite dienen oder Teil eines Signalsystems z. B. zur Feststellung der Verteilung der Peroxisomenpopulation sein. Erstmals konnte außerdem erklärt werden, warum nur ein bestimmter Anteil von Peroxisomen (15 %) mikrotubuliabhängig bewegt wird. Zusätzlich wurde erstmals nachgewiesen, dass mitochondriale Fusionsproteine nicht peroxisomal lokalisiert sind, welches daraufhin weist, dass die Dynamik der Peroxisomen durch eigene, charakteristische Prozesse reguliert wird.

Um die Regulationsmechanismen der peroxisomalen Dynamik an der Organelle selbst zu untersuchen, wurde das zentrale Membranprotein Pex11pβ biochemisch charakterisiert. Differentielle Permeabilisierung und *protease-protection assays* ermöglichten in Kombination mit einem seit kurzem erhältlichen Antikörper die Lokalisation der ersten Transmembrandomäne von Pex11pβ zwischen den Aminosäurepositionen 90 und 110. Im Anschluss wurde die Bedeutung der N-terminalen Domäne von Pex11pβ für die Regulation der Proteinaktivität untersucht: die Deletion der ersten 40 Aminosäuren des Proteins inhibierte bereits die Pex11pβ-induzierte Elongation peroxisomaler Membranen, obwohl die für die Membrandeformation essentielle amphipathische Helix intakt blieb. Durch chemisches *Cross-linking* und eine Anreicherung von Pex11pβ nach unterschiedlichen Expressionszeitpunkten konnte festgestellt werden, dass eine Homodimerisierung des Proteins mit seiner membrandeformierenden Aktivität einhergeht. Diese wiederum war

abhängig von der N-terminalen Domäne von Pex11pβ. Im Gegensatz zum orthologen Protein in *S. cerevisiae*, wiesen *in vivo phospho-labelling*-Experimente nicht auf eine Phosphorylierung von Pex11pβ in Säugerzellen hin. Daher scheinen die Pex11-Proteine in Säuger- und Hefezellen gegensätzlich reguliert zu werden. Eine Überexpresssion von Pex11pβ in peroxisomendefizienten Patientenfibroblasten führte außerdem zu einer Fehllokalisation des Proteins an Mitochondrien, wo es eine exzessive mitochondriale Fragmentierung verursachte. Diese Beobachtung unterstreicht, dass in Säugerzellen Mitochondrien anstatt des ER als alternatives Membrankompartiment für peroxisomale Proteine dienen, wenn keine Peroxisomen vorhanden sind. Daraus resultierende Effekte auf die Dynamik und Funktion der Mitochondrien könnten zum klinischen Phänotyp peroxisomaler Erkrankungen beitragen.

Im letzten Teil dieser Arbeit wurden externe Stimuli charakterisiert, die die peroxisomale Dynamik beeinflussen, um ein eher physiologisches Säugerzellkulturmodel zu etablieren, welches die Untersuchung der Regulation dynamischer peroxisomaler Prozesse ermöglicht. Die Behandlung von SH-S5Y5 Neuroblastomzellen mit dem Neurotoxin 6-OHDA hatte keinen Einfluss auf die peroxisomale Dynamik, resultierte allerdings in einer prominenten DLP1-abhängigen Fragmentierung der Mitochondrien. Obwohl DLP1 eine Komponente beider Organellen ist, werden demnach die mitochondriale und peroxisomale Dynamik unterschiedlich reguliert. Des weiteren wurde eine Reihe verschiedener Komponenten, die zytosolischen und mitochondrialen oxidativen Stress auslösen, appliziert, diese führten allerdings nicht zu einer Veränderung des peroxisomalen Kompartiments in Säugerzellen. KillerRed-basierte Induktion von oxidativem Stress in verschiedenen Kompartimenten führte zu ähnlichen Resultaten in lebenden Zellen. Dies weist darauf hin, dass andere Faktoren als oxidativer Stress allein, wie z. B. der extra- oder intrazelluläre Ursprung des Signals, eine Veränderung des zellulären Redox-Gleichgewichts oder andere, bisher unidentifizierte Signaltransduktionsmechanismen, dazu beitragen, eine Veränderung der peroxisomalen Dynamik, wie in früheren Studien beobachtet, auszulösen. Die Behandlung von AR42J Zellen, einer Rattenzelllinie pankreatischen Ursprungs, mit dem synthetischen Glukokortikoid Dexamethason führte zu einer prominenten, kontinuierlichen Elongation von Peroxisomen. Interessanterweise wurde die tubuläre Morphologie der Peroxisomen auch aufrechterhalten, wenn der externe Stimulus entfernt wurde. Die kontinuierliche peroxisomale Tubulation könnte mit der Differenzierung der Zellen verknüpft sein oder auf eine bestimmte metabolische Funktion hinweisen. Dexamethasonbehandlung führte außerdem zu einer transkriptionellen Induktion von Pex11β (and Pex11α) durch einen potentiell PPARα-

unabhängigen Mechanismus. Daher hat das hier etablierte Modell der Dexamethason-induzierten peroxisomalen Elongation großes Potenzial, als eher physiologisches Säugerzellkulturmodell zur Untersuchung der Regulation peroxisomaler Dynamik zu dienen. Weitere Studien wurden bereits initiiert, um Veränderungen des Expressionsprofils peroxisomaler Proteine nach Dexamethason-Stimulation zu untersuchen. Diese dienen dazu, neue Komponenten und/oder molekulare Mechanismen aufzuklären, die die Dynamik der Peroxisomen regulieren.

7 REFERENCES

Abe, I & Fujiki, Y (1998). "cDNA cloning and characterization of a constitutively expressed isoform of the human peroxin Pex11p." *Biochem Biophys Res Commun* 252(2): 529-533.

Abe, I, Okumoto, K, Tamura, S & Fujiki, Y (1998). "Clofibrate-inducible, 28-kDa peroxisomal integral membrane protein is encoded by PEX11." *FEBS Lett* 431(3): 468-472.

Adcock, IM & Lane, SJ (2003). "Corticosteroid-insensitive asthma: molecular mechanisms." *J Endocrinol* 178(3): 347-355.

Agrawal, G, Joshi, S & Subramani, S (2011). "Cell-free sorting of peroxisomal membrane proteins from the endoplasmic reticulum." *Proc Natl Acad Sci U S A* 108(22): 9113-9118.

Ahlemeyer, B, Gottwald, M & Baumgart-Vogt, E (2012). "Deletion of a single allele of the Pex11beta gene is sufficient to cause oxidative stress, delayed differentiation and neuronal death in mouse brain." *Dis Model Mech* 5(1): 125-140.

Aitchison, JD, Murray, WW & Rachubinski, RA (1991). "The carboxyl-terminal tripeptide Ala-Lys-Ile is essential for targeting Candida tropicalis trifunctional enzyme to yeast peroxisomes." *J Biol Chem* 266(34): 23197-23203.

Akinc, A, Thomas, M, Klibanov, AM & Langer, R (2005). "Exploring polyethylenimine-mediated DNA transfection and the proton sponge hypothesis." *J Gene Med* 7(5): 657-663.

Aksam, EB, Koek, A, Kiel, JA, Jourdan, S, Veenhuis, M & van der Klei, IJ (2007). "A peroxisomal lon protease and peroxisome degradation by autophagy play key roles in vitality of Hansenula polymorpha cells." *Autophagy* 3(2): 96-105.

Almawi, WY & Melemedjian, OK (2002). "Molecular mechanisms of glucocorticoid antiproliferative effects: antagonism of transcription factor activity by glucocorticoid receptor." *J Leukoc Biol* 71(1): 9-15.

Anand, P, Kwak, Y, Simha, R & Donaldson, RP (2009). "Hydrogen peroxide induced oxidation of peroxisomal malate synthase and catalase." *Arch Biochem Biophys* 491(1-2): 25-31.

Angermuller, S, Bruder, G, Volkl, A, Wesch, H & Fahimi, HD (1987). "Localization of xanthine oxidase in crystalline cores of peroxisomes. A cytochemical and biochemical study." *Eur J Cell Biol* 45(1): 137-144.

Antonenkov, V, Grunau, S, Ohlmeier, S & Hiltunen, K (2009). "Peroxisomes are oxidative organelles." *Antioxid Redox Signal*.

Antonenkov, VD, Grunau, S, Ohlmeier, S & Hiltunen, JK (2010). "Peroxisomes are oxidative organelles." *Antioxid Redox Signal* 13(4): 525-537.

Arimura, S, Yamamoto, J, Aida, GP, Nakazono, M & Tsutsumi, N (2004). "Frequent fusion and fission of plant mitochondria with unequal nucleoid distribution." *Proc Natl Acad Sci U S A* 101(20): 7805-7808.

Ashrafian, H, Docherty, L, Leo, V, Towlson, C, Neilan, M, Steeples, V, Lygate, CA, Hough, T, Townsend, S, Williams, D, Wells, S, Norris, D, Glyn-Jones, S, Land, J, Barbaric, I, Lalanne, Z, Denny, P, Szumska, D, Bhattacharya, S, Griffin, JL, Hargreaves, I,

Fernandez-Fuentes, N, Cheeseman, M, Watkins, H & Dear, TN (2010). "A mutation in the mitochondrial fission gene Dnm1l leads to cardiomyopathy." *PLoS Genet* 6(6): e1001000.

Bach, D, Pich, S, Soriano, FX, Vega, N, Baumgartner, B, Oriola, J, Daugaard, JR, Lloberas, J, Camps, M, Zierath, JR, Rabasa-Lhoret, R, Wallberg-Henriksson, H, Laville, M, Palacin, M, Vidal, H, Rivera, F, Brand, M & Zorzano, A (2003). "Mitofusin-2 determines mitochondrial network architecture and mitochondrial metabolism. A novel regulatory mechanism altered in obesity." *J Biol Chem* 278(19): 17190-17197.

Baerends, RJ, Faber, KN, Kiel, JA, van der Klei, IJ, Harder, W & Veenhuis, M (2000). "Sorting and function of peroxisomal membrane proteins." *FEMS Microbiol Rev* 24(3): 291-301.

Baerends, RJ, Rasmussen, SW, Hilbrands, RE, van der Heide, M, Faber, KN, Reuvekamp, PT, Kiel, JA, Cregg, JM, van der Klei, IJ & Veenhuis, M (1996). "The Hansenula polymorpha PER9 gene encodes a peroxisomal membrane protein essential for peroxisome assembly and integrity." *J Biol Chem* 271(15): 8887-8894.

Baes, M & Aubourg, P (2009). "Peroxisomes, myelination, and axonal integrity in the CNS." *Neuroscientist* 15(4): 367-379.

Bagattin, A, Hugendubler, L & Mueller, E (2010). "Transcriptional coactivator PGC-1alpha promotes peroxisomal remodeling and biogenesis." *Proc Natl Acad Sci U S A* 107(47): 20376-20381.

Barnett, P, Tabak, HF & Hettema, EH (2000). "Nuclear receptors arose from pre-existing protein modules during evolution." *Trends Biochem Sci* 25(5): 227-228.

Baumgart, E, Schad, A, Volkl, A & Fahimi, HD (1997). "Detection of mRNAs encoding peroxisomal proteins by non-radioactive in situ hybridization with digoxigenin-labelled cRNAs." *Histochem Cell Biol* 108(4-5): 371-379.

Baumgart, E, Vanhorebeek, I, Grabenbauer, M, Borgers, M, Declercq, PE, Fahimi, HD & Baes, M (2001). "Mitochondrial alterations caused by defective peroxisomal biogenesis in a mouse model for Zellweger syndrome (PEX5 knockout mouse)." *Am J Pathol* 159(4): 1477-1494.

Baumgart, E, Volkl, A, Pill, J & Fahimi, HD (1990). "Proliferation of peroxisomes without simultaneous induction of the peroxisomal fatty acid beta-oxidation." *FEBS Lett.* 264(1): 5-9.

Baumgartner, U, Hamilton, B, Piskacek, M, Ruis, H & Rottensteiner, H (1999). "Functional analysis of the Zn(2)Cys(6) transcription factors Oaf1p and Pip2p. Different roles in fatty acid induction of beta-oxidation in Saccharomyces cerevisiae." *J Biol Chem.* 274(32): 22208-22216.

Beier, K, Volkl, A, Hashimoto, T & Fahimi, HD (1988). "Selective induction of peroxisomal enzymes by the hypolipidemic drug bezafibrate. Detection of modulations by automatic image analysis in conjunction with immunoelectron microscopy and immunoblotting." *Eur J Cell Biol* 46(3): 383-393.

Bentley, P, Calder, I, Elcombe, C, Grasso, P, Stringer, D & Wiegand, HJ (1993). "Hepatic peroxisome proliferation in rodents and its significance for humans." *Food Chem Toxicol.* 31(11): 857-907.

Bereiter-Hahn, J & Jendrach, M (2010). "Mitochondrial dynamics." *Int Rev Cell Mol Biol* 284: 1-65.

Bharti, P, Schliebs, W, Schievelbusch, T, Neuhaus, A, David, C, Kock, K, Herrmann, C, Meyer, HE, Wiese, S, Warscheid, B, Theiss, C & Erdmann, R (2011). "PEX14 is required for microtubule-based peroxisome motility in human cells." *J Cell Sci* 124(Pt 10): 1759-1768.

Binns, D, Januszewski, T, Chen, Y, Hill, J, Markin, VS, Zhao, Y, Gilpin, C, Chapman, KD, Anderson, RG & Goodman, JM (2006). "An intimate collaboration between peroxisomes and lipid bodies." *J Cell Biol.* 173(5): 719-731.

Bleazard, W, McCaffery, JM, King, EJ, Bale, S, Mozdy, A, Tieu, Q, Nunnari, J & Shaw, JM (1999). "The dynamin-related GTPase Dnm1 regulates mitochondrial fission in yeast." *Nat Cell Biol* 1(5): 298-304.

Blum, D, Torch, S, Lambeng, N, Nissou, M, Benabid, AL, Sadoul, R & Verna, JM (2001). "Molecular pathways involved in the neurotoxicity of 6-OHDA, dopamine and MPTP: contribution to the apoptotic theory in Parkinson's disease." *Prog Neurobiol* 65(2): 135-172.

Bonekamp, NA (2007). "Untersuchungen zur Fusion von Peroxisomen in Säugerzellen" *Institut für klinische Zytobiologie und Zytopathologie Philipps-Universität Marburg* Marburg, Germany Diplomarbeit

Bonekamp, NA, Fahimi, HD & Schrader, M (2011a). "Oxidative stress in peroxisomes". *Principles of Free Radical Biomedicine*. Pantopoulos, K and Shipper, H, Nova Science Publishers Inc. (in press).

Bonekamp, NA, Islinger, M, Gomez-Lazaro, M & Schrader, M (2011b). "Cytochemical detection of peroxisomes and mitochondria". *Cell Imaging Techniques: Methods and Protocols*. Roth, J and Taatjes, D, Springer Science + Business Media. Methods in Molecular Biology Series**:** (in press).

Bonekamp, NA, Volkl, A, Fahimi, HD & Schrader, M (2009). "Reactive oxygen species and peroxisomes: struggling for balance." *Biofactors* 35(4): 346-355.

Bonekamp, NA, Vormund, K, Jacob, R & Schrader, M (2010). "Dynamin-like protein 1 at the Golgi complex: a novel component of the sorting/targeting machinery en route to the plasma membrane." *Exp Cell Res* 316(20): 3454-3467.

Bookout, AL, Jeong, Y, Downes, M, Yu, RT, Evans, RM & Mangelsdorf, DJ (2006). "Anatomical profiling of nuclear receptor expression reveals a hierarchical transcriptional network." *Cell* 126(4): 789-799.

Borta, H, Aroso, M, Rinn, C, Gomez-Lazaro, M, Vitorino, R, Zeuschner, D, Grabenbauer, M, Amado, F & Schrader, M (2010). "Analysis of low abundance membrane-associated proteins from rat pancreatic zymogen granules." *J Proteome Res* 9(10): 4927-4939.

Bove, J, Prou, D, Perier, C & Przedborski, S (2005a). "Toxin-induced models of Parkinson's disease." *NeuroRx* 2(3): 484-494.

Bove, J, Serrats, J, Mengod, G, Cortes, R, Tolosa, E & Marin, C (2005b). "Neuroprotection induced by the adenosine A2A antagonist CSC in the 6-OHDA rat model of parkinsonism: effect on the activity of striatal output pathways." *Exp Brain Res* 165(3): 362-374.

Boveris, A, Oshino, N & Chance, B (1972). "The cellular production of hydrogen peroxide." *Biochem J* 128(3): 617-630.

Bradford, MM (1976). "A rapid and sensitive method for the quantitation of microgram quantities of protein utilizing the principle of protein-dye binding." *Anal Biochem* 72: 248-254.

Braschi, E, Goyon, V, Zunino, R, Mohanty, A, Xu, L & McBride, HM (2010). "Vps35 mediates vesicle transport between the mitochondria and peroxisomes." *Curr Biol* 20(14): 1310-1315.

Brites, P, Waterham, HR & Wanders, RJ (2004). "Functions and biosynthesis of plasmalogens in health and disease." *Biochim Biophys Acta.* 1636(2-3): 219-231.

Brocard, C, Kragler, F, Simon, MM, Schuster, T & Hartig, A (1994). "The tetratricopeptide repeat-domain of the PAS10 protein of Saccharomyces cerevisiae is essential for binding the peroxisomal targeting signal-SKL." *Biochem Biophys Res Commun* 204(3): 1016-1022.

Brocard, CB, Boucher, KK, Jedeszko, C, Kim, PK & Walton, PA (2005). "Requirement for microtubules and dynein motors in the earliest stages of peroxisome biogenesis." *Traffic.* 6(5): 386-395.

Brosius, U & Gartner, J (2002). "Cellular and molecular aspects of Zellweger syndrome and other peroxisome biogenesis disorders." *Cell Mol Life Sci* 59(6): 1058-1069.

Brown, LA & Baker, A (2003). "Peroxisome biogenesis and the role of protein import." *J.Cell Mol.Med.* 7(4): 388-400.

Brown, LA & Baker, A (2008). "Shuttles and cycles: transport of proteins into the peroxisome matrix (Review)." *Mol Membr Biol* 25(5): 363-375.

Brown, TW, Titorenko, VI & Rachubinski, RA (2000). "Mutants of the Yarrowia lipolytica PEX23 gene encoding an integral peroxisomal membrane peroxin mislocalize matrix proteins and accumulate vesicles containing peroxisomal matrix and membrane proteins." *Mol Biol Cell.* 11(1): 141-152.

Bulina, ME, Chudakov, DM, Britanova, OV, Yanushevich, YG, Staroverov, DB, Chepurnykh, TV, Merzlyak, EM, Shkrob, MA, Lukyanov, S & Lukyanov, KA (2006a). "A genetically encoded photosensitizer." *Nat Biotechnol* 24(1): 95-99.

Bulina, ME, Lukyanov, KA, Britanova, OV, Onichtchouk, D, Lukyanov, S & Chudakov, DM (2006b). "Chromophore-assisted light inactivation (CALI) using the phototoxic fluorescent protein KillerRed." *Nat Protoc* 1(2): 947-953.

Bus, JS & Gibson, JE (1982). "Mechanisms of superoxide radical-mediated toxicity." *J Toxicol Clin Toxicol* 19(6-7): 689-697.

Buttgereit, F, Saag, KG, Cutolo, M, da Silva, JA & Bijlsma, JW (2005). "The molecular basis for the effectiveness, toxicity, and resistance to glucocorticoids: focus on the treatment of rheumatoid arthritis." *Scand J Rheumatol* 34(1): 14-21.

Buttgereit, F & Scheffold, A (2002). "Rapid glucocorticoid effects on immune cells." *Steroids* 67(6): 529-534.

Buttgereit, F, Straub, RH, Wehling, M & Burmester, GR (2004). "Glucocorticoids in the treatment of rheumatic diseases: an update on the mechanisms of action." *Arthritis Rheum* 50(11): 3408-3417.

Camoes, F, Bonekamp, NA, Delille, HK & Schrader, M (2009). "Organelle dynamics and dysfunction: A closer link between peroxisomes and mitochondria." *J Inherit Metab Dis* 32(2): 163-180.

Casteels, M, Foulon, V, Mannaerts, GP & Van Veldhoven, PP (2003). "Alpha-oxidation of 3-methyl-substituted fatty acids and its thiamine dependence." *Eur J Biochem* 270(8): 1619-1627.

Castillo, MC, Sandalio, LM, Del Rio, LA & Leon, J (2008). "Peroxisome proliferation, wound-activated responses and expression of peroxisome-associated genes are cross-regulated but uncoupled in Arabidopsis thaliana." *Plant Cell Environ* 31(4): 492-505.

Cepinska, MN, Veenhuis, M, van der Klei, IJ & Nagotu, S (2011). "Peroxisome fission is associated with reorganization of specific membrane proteins." *Traffic* 12(7): 925-937.

Chance, B, Williams, GR & Hollunger, G (1963). "Inhibition of electron and energy transfer in mitochondria. I. Effects of Amytal, thiopental, rotenone, progesterone, and methylene glycol." *J Biol Chem* 238: 418-431.

Chang, CC, South, S, Warren, D, Jones, J, Moser, AB, Moser, HW & Gould, SJ (1999). "Metabolic control of peroxisome abundance." *J Cell Sci* 112(Pt 10): 1579-1590.

Chang, CR & Blackstone, C (2010). "Dynamic regulation of mitochondrial fission through modification of the dynamin-related protein Drp1." *Ann N Y Acad Sci* 1201: 34-39.

Chang, CR, Manlandro, CM, Arnoult, D, Stadler, J, Posey, AE, Hill, RB & Blackstone, C (2010). "A lethal de novo mutation in the middle domain of the dynamin-related GTPase Drp1 impairs higher order assembly and mitochondrial division." *J Biol Chem* 285(42): 32494-32503.

Chang, J, Mast, FD, Fagarasanu, A, Rachubinski, DA, Eitzen, GA, Dacks, JB & Rachubinski, RA (2009). "Pex3 peroxisome biogenesis proteins function in peroxisome inheritance as class V myosin receptors." *J Cell Biol* 187(2): 233-246.

Chen, H, Chomyn, A & Chan, DC (2005). "Disruption of fusion results in mitochondrial heterogeneity and dysfunction." *J Biol Chem* 280(28): 26185-26192.

Chen, H, Detmer, SA, Ewald, AJ, Griffin, EE, Fraser, SE & Chan, DC (2003). "Mitofusins Mfn1 and Mfn2 coordinately regulate mitochondrial fusion and are essential for embryonic development." *J Cell Biol* 160(2): 189-200.

Chernomordik, LV, Zimmerberg, J & Kozlov, MM (2006). "Membranes of the world unite!" *J Cell Biol* 175(2): 201-207.

Chomczynski, P & Sacchi, N (1987). "Single-step method of RNA isolation by acid guanidinium thiocyanate-phenol-chloroform extraction." *Anal Biochem* 162(1): 156-159.

Cimini, A, Benedetti, E, D'Angelo, B, Cristiano, L, Falone, S, Di Loreto, S, Amicarelli, F & Ceru, MP (2009). "Neuronal response of peroxisomal and peroxisome-related proteins to chronic and acute Abeta injury." *Curr Alzheimer Res* 6(3): 238-251.

Cipolat, S, Martins de Brito, O, Dal Zilio, B & Scorrano, L (2004). "OPA1 requires mitofusin 1 to promote mitochondrial fusion." *Proc Natl Acad Sci U S A* 101(45): 15927-15932.

Clauset, A, Shalizi, CR & Newman, MEJ (2009). "Power-Law Distributions in Empirical Data " *SIAM Rev* 51(4): pp. 661-703.

Cooper, TG & Beevers, H (1969). "Beta oxidation in glyoxysomes from castor bean endosperm." *J Biol Chem* 244(13): 3514-3520.

Costa-Rodrigues, J, Carvalho, AF, Gouveia, AM, Fransen, M, Sa-Miranda, C & Azevedo, JE (2004). "The N terminus of the peroxisomal cycling receptor, Pex5p, is required for redirecting the peroxisome-associated peroxin back to the cytosol." *J.Biol.Chem.* 279(45): 46573-46579.

Croxtall, JD, Choudhury, Q & Flower, RJ (2000). "Glucocorticoids act within minutes to inhibit recruitment of signalling factors to activated EGF receptors through a receptor-dependent, transcription-independent mechanism." *Br J Pharmacol* 130(2): 289-298.

Dammai, V & Subramani, S (2001). "The human peroxisomal targeting signal receptor, Pex5p, is translocated into the peroxisomal matrix and recycled to the cytosol." *Cell* 105(2): 187-196.

Danpure, CJ (2005). "Molecular etiology of primary hyperoxaluria type 1: new directions for treatment." *Am J Nephrol.* 25(3): 303-310.

Danpure, CJ (2006). "Primary hyperoxaluria type 1: AGT mistargeting highlights the fundamental differences between the peroxisomal and mitochondrial protein import pathways." *Biochim Biophys Acta* 1763(12): 1776-1784.

de Brito, OM & Scorrano, L (2008a). "Mitofusin 2 tethers endoplasmic reticulum to mitochondria." *Nature* 456(7222): 605-610.

de Brito, OM & Scorrano, L (2008b). "Mitofusin 2: a mitochondria-shaping protein with signaling roles beyond fusion." *Antioxid Redox Signal* 10(3): 621-633.

de Brito, OM & Scorrano, L (2009). "Mitofusin-2 regulates mitochondrial and endoplasmic reticulum morphology and tethering: the role of Ras." *Mitochondrion* 9(3): 222-226.

De Duve, C & Baudhuin, P (1966). "Peroxisomes (microbodies and related particles)." *Physiol Rev* 46(2): 323-357.

del Rio, LA, Corpas, FJ, Sandalio, LM, Palma, JM, Gomez, M & Barroso, JB (2002). "Reactive oxygen species, antioxidant systems and nitric oxide in peroxisomes." *J Exp Bot.* 53(372): 1255-1272.

del Rio, LA, Sandalio, LM, Corpas, FJ, Palma, JM & Barroso, JB (2006). "Reactive oxygen species and reactive nitrogen species in peroxisomes. Production, scavenging, and role in cell signaling." *Plant Physiol* 141(2): 330-335.

Delettre, C, Griffoin, JM, Kaplan, J, Dollfus, H, Lorenz, B, Faivre, L, Lenaers, G, Belenguer, P & Hamel, CP (2001). "Mutation spectrum and splicing variants in the OPA1 gene." *Hum Genet* 109(6): 584-591.

Delettre, C, Lenaers, G, Griffoin, JM, Gigarel, N, Lorenzo, C, Belenguer, P, Pelloquin, L, Grosgeorge, J, Turc-Carel, C, Perret, E, Astarie-Dequeker, C, Lasquellec, L, Arnaud, B, Ducommun, B, Kaplan, J & Hamel, CP (2000). "Nuclear gene OPA1, encoding a mitochondrial dynamin-related protein, is mutated in dominant optic atrophy." *Nat Genet* 26(2): 207-210.

Delille, HK, Agricola, B, Guimaraes, SC, Borta, H, Luers, GH, Fransen, M & Schrader, M (2010). "Pex11pbeta-mediated growth and division of mammalian peroxisomes follows a maturation pathway." *J Cell Sci* 123(Pt 16): 2750-2762.

Delille, HK, Alves, R & Schrader, M (2009). "Biogenesis of peroxisomes and mitochondria: linked by division." *Histochem Cell Biol* 131(4): 441-446.

Delille, HK & Schrader, M (2008). "Targeting of hFis1 to peroxisomes is mediated by Pex19p." *J Biol Chem* 283(45): 31107-31115.

Desikan, R, S, AH-M, Hancock, JT & Neill, SJ (2001). "Regulation of the Arabidopsis transcriptome by oxidative stress." *Plant Physiol.* 127(1): 159-172.

Dhaunsi, GS, Gulati, S, Singh, AK, Orak, JK, Asayama, K & Singh, I (1992). "Demonstration of Cu-Zn superoxide dismutase in rat liver peroxisomes. Biochemical and immunochemical evidence." *J Biol Chem* 267(10): 6870-6873.

Diano, S, Liu, ZW, Jeong, JK, Dietrich, MO, Ruan, HB, Kim, E, Suyama, S, Kelly, K, Gyengesi, E, Arbiser, JL, Belsham, DD, Sarruf, DA, Schwartz, MW, Bennett, AM, Shanabrough, M, Mobbs, CV, Yang, X, Gao, XB & Horvath, TL (2011). "Peroxisome proliferation-associated control of reactive oxygen species sets melanocortin tone and feeding in diet-induced obesity." *Nat Med* 17(9): 1121-1127.

Distel, B, Erdmann, R, Gould, SJ, Blobel, G, Crane, DI, Cregg, JM, Dodt, G, Fujiki, Y, Goodman, JM, Just, WW, Kiel, JA, Kunau, WH, Lazarow, PB, Mannaerts, GP, Moser, HW, Osumi, T, Rachubinski, RA, Roscher, A, Subramani, S, Tabak, HF, Tsukamoto, T, Valle, D, van der Klei, I, van Veldhoven, PP & Veenhuis, M (1996). "A unified nomenclature for peroxisome biogenesis factors." *J Cell Biol* 135(1): 1-3.

Dixit, E, Boulant, S, Zhang, Y, Lee, AS, Odendall, C, Shum, B, Hacohen, N, Chen, ZJ, Whelan, SP, Fransen, M, Nibert, ML, Superti-Furga, G & Kagan, JC (2010). "Peroxisomes are signaling platforms for antiviral innate immunity." *Cell* 141(4): 668-681.

Dodt, G, Warren, D, Becker, E, Rehling, P & Gould, SJ (2001). "Domain mapping of human PEX5 reveals functional and structural similarities to Saccharomyces cerevisiae Pex18p and Pex21p." *J Biol Chem* 276(45): 41769-41781.

Dohm, JA, Lee, SJ, Hardwick, JM, Hill, RB & Gittis, AG (2004). "Cytosolic domain of the human mitochondrial fission protein fis1 adopts a TPR fold." *Proteins* 54(1): 153-156.

Drin, G & Antonny, B (2010). "Amphipathic helices and membrane curvature." *FEBS Lett* 584(9): 1840-1847.

Du, J, Wang, Y, Hunter, R, Wei, Y, Blumenthal, R, Falke, C, Khairova, R, Zhou, R, Yuan, P, Machado-Vieira, R, McEwen, BS & Manji, HK (2009). "Dynamic regulation of mitochondrial function by glucocorticoids." *Proc Natl Acad Sci U S A* 106(9): 3543-3548.

Dunn, WA, Jr., Cregg, JM, Kiel, JA, van der Klei, IJ, Oku, M, Sakai, Y, Sibirny, AA, Stasyk, OV & Veenhuis, M (2005). "Pexophagy: the selective autophagy of peroxisomes." *Autophagy* 1(2): 75-83.

Einerhand, AW, Kos, WT, Distel, B & Tabak, HF (1993). "Characterization of a transcriptional control element involved in proliferation of peroxisomes in yeast in response to oleate." *Eur J Biochem.* 214(1): 323-331.

Einwachter, H, Sowinski, S, Kunau, WH & Schliebs, W (2001). "Yarrowia lipolytica Pex20p, Saccharomyces cerevisiae Pex18p/Pex21p and mammalian Pex5pL fulfil a common function in the early steps of the peroxisomal PTS2 import pathway." *EMBO Rep* 2(11): 1035-1039.

Eitzen, GA, Szilard, RK & Rachubinski, RA (1997). "Enlarged peroxisomes are present in oleic acid-grown Yarrowia lipolytica overexpressing the PEX16 gene encoding an intraperoxisomal peripheral membrane peroxin." *J Cell Biol.* 137(6): 1265-1278.

Elgersma, Y, Kwast, L, van den Berg, M, Snyder, WB, Distel, B, Subramani, S & Tabak, HF (1997). "Overexpression of Pex15p, a phosphorylated peroxisomal integral membrane protein required for peroxisome assembly in S.cerevisiae, causes proliferation of the endoplasmic reticulum membrane." *Embo J* 16(24): 7326-7341.

Elgersma, Y, Vos, A, van den Berg, M, van Roermund, CW, van der Sluijs, P, Distel, B & Tabak, HF (1996). "Analysis of the carboxyl-terminal peroxisomal targeting signal 1 in a homologous context in Saccharomyces cerevisiae." *J Biol Chem* 271(42): 26375-26382.

Elsner, M, Gehrmann, W & Lenzen, S (2011). "Peroxisome-generated hydrogen peroxide as important mediator of lipotoxicity in insulin-producing cells." *Diabetes* 60(1): 200-208.

Engerson, TD, McKelvey, TG, Rhyne, DB, Boggio, EB, Snyder, SJ & Jones, HP (1987). "Conversion of xanthine dehydrogenase to oxidase in ischemic rat tissues." *J Clin Invest* 79(6): 1564-1570.

Erdmann, R & Blobel, G (1995). "Giant peroxisomes in oleic acid-induced Saccharomyces cerevisiae lacking the peroxisomal membrane protein Pmp27p." *J Cell Biol* 128(4): 509-523.

Erdmann, R & Schliebs, W (2005). "Opinion: Peroxisomal matrix protein import: the transient pore model." *Nat Rev Mol Cell Biol* 6(9): 738-742.

Escano, CS, Juvvadi, PR, Jin, FJ, Takahashi, T, Koyama, Y, Yamashita, S, Maruyama, J & Kitamoto, K (2009). "Disruption of the Aopex11-1 gene involved in peroxisome proliferation leads to impaired Woronin body formation in Aspergillus oryzae." *Eukaryot Cell* 8(3): 296-305.

Eura, Y, Ishihara, N, Yokota, S & Mihara, K (2003). "Two mitofusin proteins, mammalian homologues of FZO, with distinct functions are both required for mitochondrial fusion." *J Biochem* 134(3): 333-344.

Fagarasanu, A, Fagarasanu, M, Eitzen, GA, Aitchison, JD & Rachubinski, RA (2006). "The Peroxisomal Membrane Protein Inp2p Is the Peroxisome-Specific Receptor for the Myosin V Motor Myo2p of Saccharomyces cerevisiae." *Dev Cell.* 10(5): 587-600.

Fagarasanu, A, Mast, FD, Knoblach, B & Rachubinski, RA (2010). "Molecular mechanisms of organelle inheritance: lessons from peroxisomes in yeast." *Nat Rev Mol Cell Biol* 11(9): 644-654.

Fagarasanu, M, Fagarasanu, A, Tam, YY, Aitchison, JD & Rachubinski, RA (2005). "Inp1p is a peroxisomal membrane protein required for peroxisome inheritance in Saccharomyces cerevisiae." *J Cell Biol* 169(5): 765-775.

Fahimi, HD (1968). "Cytochemical localization of peroxidase activity in rat hepatic microbodies (peroxisomes)." *J Histochem Cytochem* 16(8): 547-550.

Fahimi, HD (1969). "Cytochemical localization of peroxidatic activity of catalase in rat hepatic microbodies (peroxisomes)." *J Cell Biol.* 43(2): 275-288.

Fahimi, HD, Baumgart, E & Volkl, A (1993). "Ultrastructural aspects of the biogenesis of peroxisomes in rat liver." *Biochimie.* 75(3-4): 201-208.

Fahimi, HD & Cajaraville, MP (1995). "Induction of peroxisome proliferation by some environmental pollutants and chemicals in animal tissues.". *Cell Biology in Environmental Toxicology*. Cajaraville, MP. Bilbo, University of Basque Country Press Service**:** 221-255.

Fahimi, HD, E. Baumgart (1992). "Chapter 9. Cell Organelles, Peroxisomes ". Boca Raton, *CRC Press*.

Fahimi, HD, Reinicke, A, Sujatta, M, Yokota, S, Ozel, M, Hartig, F & Stegmeier, K (1982). "The short- and long-term effects of bezafibrate in the rat." *Ann N Y Acad Sci* 386: 111-135.

Falkenstein, E, Norman, AW & Wehling, M (2000). "Mannheim classification of nongenomically initiated (rapid) steroid action(s)." *J Clin Endocrinol Metab* 85(5): 2072-2075.

Fang, Y, Morrell, JC, Jones, JM & Gould, SJ (2004). "PEX3 functions as a PEX19 docking factor in the import of class I peroxisomal membrane proteins." *J Cell Biol* 164(6): 863-875. Epub 2004 Mar 2008.

Farre, JC & Subramani, S (2004). "Peroxisome turnover by micropexophagy: an autophagy-related process." *Trends Cell Biol.* 14(9): 515-523.

Faust, F, Gomez-Lazaro, M, Borta, H, Agricola, B & Schrader, M (2008). "Rab8 is involved in zymogen granule formation in pancreatic acinar AR42J cells." *Traffic.* 9(6): 964-979.

Faust, PL, Banka, D, Siriratsivawong, R, Ng, VG & Wikander, TM (2005). "Peroxisome biogenesis disorders: the role of peroxisomes and metabolic dysfunction in developing brain." *J Inherit Metab Dis* 28(3): 369-383.

Fei, MJ, Yamashita, E, Inoue, N, Yao, M, Yamaguchi, H, Tsukihara, T, Shinzawa-Itoh, K, Nakashima, R & Yoshikawa, S (2000). "X-ray structure of azide-bound fully oxidized cytochrome c oxidase from bovine heart at 2.9 A resolution." *Acta Crystallogr D Biol Crystallogr* 56(Pt 5): 529-535.

Feige, JN, Gelman, L, Michalik, L, Desvergne, B & Wahli, W (2006). "From molecular action to physiological outputs: Peroxisome proliferator-activated receptors are nuclear receptors at the crossroads of key cellular functions." *Prog Lipid Res.* 45(2): 120-159.

Ferdinandusse, S, Denis, S, Dacremont, G & Wanders, RJ (2009). "Toxicity of peroxisomal C27-bile acid intermediates." *Mol Genet Metab* 96(3): 121-128.

Ferdinandusse, S, Meissner, T, Wanders, RJ & Mayatepek, E (2002). "Identification of the peroxisomal beta-oxidation enzymes involved in the degradation of leukotrienes." *Biochem Biophys Res Commun* 293(1): 269-273.

Ferdinandusse, S, Mulders, J, L, IJ, Denis, S, Dacremont, G, Waterham, HR & Wanders, RJ (1999). "Molecular cloning and expression of human carnitine octanoyltransferase: evidence for its role in the peroxisomal beta-oxidation of branched-chain fatty acids." *Biochem Biophys Res Commun* 263(1): 213-218.

Fernandez-Gomez, FJ, Galindo, MF, Gomez-Lazaro, M, Yuste, VJ, Comella, JX, Aguirre, N & Jordan, J (2005). "Malonate induces cell death via mitochondrial potential collapse and delayed swelling through an ROS-dependent pathway." *Br J Pharmacol* 144(4): 528-537.

Fidaleo, M (2010). "Peroxisomes and peroxisomal disorders: the main facts." *Exp Toxicol Pathol* 62(6): 615-625.

Filipits, M, Simon, MM, Rapatz, W, Hamilton, B & Ruis, H (1993). "A Saccharomyces cerevisiae upstream activating sequence mediates induction of peroxisome proliferation by fatty acids." *Gene.* 132(1): 49-55.

Fourcade, S, Lopez-Erauskin, J, Galino, J, Duval, C, Naudi, A, Jove, M, Kemp, S, Villarroya, F, Ferrer, I, Pamplona, R, Portero-Otin, M & Pujol, A (2008). "Early oxidative damage underlying neurodegeneration in X-adrenoleukodystrophy." *Hum Mol Genet* 17(12): 1762-1773.

Franco, R, Li, S, Rodriguez-Rocha, H, Burns, M & Panayiotidis, MI (2010). "Molecular mechanisms of pesticide-induced neurotoxicity: Relevance to Parkinson's disease." *Chem Biol Interact* 188(2): 289-300.

Fransen, M, Nordgren, M, Wang, B & Apanasets, O (2011). "Role of peroxisomes in ROS/RNS-metabolism: Implications for human disease." *Biochim Biophys Acta*.

Fransen, M, Vastiau, I, Brees, C, Brys, V, Mannaerts, GP & Van Veldhoven, PP (2004). "Potential role for Pex19p in assembly of PTS-receptor docking complexes." *J.Biol.Chem.* 279(13): 12615-12624.

Fransen, M, Vastiau, I, Brees, C, Brys, V, Mannaerts, GP & Van Veldhoven, PP (2005). "Analysis of human Pex19p's domain structure by pentapeptide scanning mutagenesis." *J.Mol.Biol.* 346(5): 1275-1286.

Fransen, M, Wylin, T, Brees, C, Mannaerts, GP & Van Veldhoven, PP (2001). "Human pex19p binds peroxisomal integral membrane proteins at regions distinct from their sorting sequences." *Mol.Cell Biol.* 21(13): 4413-4424.

Frederiks, WM, Bosch, KS, Hoeben, KA, van Marle, J & Langbein, S (2010). "Renal cell carcinoma and oxidative stress: The lack of peroxisomes." *Acta Histochem* 112(4): 364-371.

Fujiki, Y, Hubbard, AL, Fowler, S & Lazarow, PB (1982). "Isolation of intracellular membranes by means of sodium carbonate treatment: application to endoplasmic reticulum." *J Cell Biol* 93(1): 97-102.

Fujiki, Y, Matsuzono, Y, Matsuzaki, T & Fransen, M (2006). "Import of peroxisomal membrane proteins: The interplay of Pex3p- and Pex19p-mediated interactions." *Biochim Biophys Acta* 1763(12): 1639-1646.

Fujimoto, M, Arimura, S, Mano, S, Kondo, M, Saito, C, Ueda, T, Nakazono, M, Nakano, A, Nishimura, M & Tsutsumi, N (2009). "Arabidopsis dynamin-related proteins DRP3A and DRP3B are functionally redundant in mitochondrial fission, but have distinct roles in peroxisomal fission." *Plant J* 58(3): 388-400.

Fujimura, S, Nakagawa, T, Ito, T, Matsufuji, Y, Miyaji, T & Tomizuka, N (2007). "Peroxisomal metabolism is regulated by an oxygen-recognition system through organelle crosstalk between the mitochondria and peroxisomes." *Yeast* 24(7): 589-597.

Funato, M, Shimozawa, N, Nagase, T, Takemoto, Y, Suzuki, Y, Imamura, Y, Matsumoto, T, Tsukamoto, T, Kojidani, T, Osumi, T, Fukao, T & Kondo, N (2006). "Aberrant peroxisome morphology in peroxisomal beta-oxidation enzyme deficiencies." *Brain Dev* 28(5): 287-292.

Galindo, MF, Jordan, J, Gonzalez-Garcia, C & Cena, V (2003). "Chromaffin cell death induced by 6-hydroxydopamine is independent of mitochondrial swelling and caspase activation." *J Neurochem* 84(5): 1066-1073.

Gametchu, B, Chen, F, Sackey, F, Powell, C & Watson, CS (1999). "Plasma membrane-resident glucocorticoid receptors in rodent lymphoma and human leukemia models." *Steroids* 64(1-2): 107-119.

Gandre-Babbe, S & van der Bliek, AM (2008). "The Novel Tail-anchored Membrane Protein Mff Controls Mitochondrial and Peroxisomal Fission in Mammalian Cells." *Mol Biol Cell* 19(6): 2402-2412.

Gariot, P, Barrat, E, Mejean, L, Pointel, JP, Drouin, P & Debry, G (1983). "Fenofibrate and human liver. Lack of proliferation of peroxisomes." *Arch Toxicol* 53(2): 151-163.

Gehrmann, W, Elsner, M & Lenzen, S (2010). "Role of metabolically generated reactive oxygen species for lipotoxicity in pancreatic beta-cells." *Diabetes Obes Metab* 12 Suppl 2: 149-158.

Geuze, HJ, Murk, JL, Stroobants, AK, Griffith, JM, Kleijmeer, MJ, Koster, AJ, Verkleij, AJ, Distel, B & Tabak, HF (2003). "Involvement of the endoplasmic reticulum in peroxisome formation." *Mol Biol Cell* 14(7): 2900-2907.

Ghaedi, K, Honsho, M, Shimozawa, N, Suzuki, Y, Kondo, N & Fujiki, Y (2000a). "PEX3 is the causal gene responsible for peroxisome membrane assembly-defective Zellweger syndrome of complementation group G." *Am J Hum Genet* 67(4): 976-981.

Ghaedi, K, Tamura, S, Okumoto, K, Matsuzono, Y & Fujiki, Y (2000b). "The peroxin pex3p initiates membrane assembly in peroxisome biogenesis." *Mol Biol Cell* 11(6): 2085-2102.

Girzalsky, W, Hoffmann, LS, Schemenewitz, A, Nolte, A, Kunau, WH & Erdmann, R (2006). "Pex19p-dependent targeting of Pex17p, a peripheral component of the peroxisomal protein import machinery." *J Biol Chem* 281(28): 19417-19425.

Glover, JR, Andrews, DW & Rachubinski, RA (1994). "Saccharomyces cerevisiae peroxisomal thiolase is imported as a dimer." *Proc Natl Acad Sci U S A* 91(22): 10541-10545.

Goldenthal, KL, Hedman, K, Chen, JW, August, JT & Willingham, MC (1985). "Postfixation detergent treatment for immunofluorescence suppresses localization of some integral membrane proteins." *J Histochem Cytochem* 33(8): 813-820.

Goldfischer, S, Moore, CL, Johnson, AB, Spiro, AJ, Valsamis, MP, Wisniewski, HK, Ritch, RH, Norton, WT, Rapin, I & Gartner, LM (1973). "Peroxisomal and mitochondrial defects in the cerebro-hepato-renal syndrome." *Science* 182(107): 62-64.

Goldman, BM & Blobel, G (1978). "Biogenesis of peroxisomes: intracellular site of synthesis of catalase and uricase." *Proc Natl Acad Sci U S A.* 75(10): 5066-5070.

Gomes, LC, Benedetto, GD & Scorrano, L (2011). "During autophagy mitochondria elongate, are spared from degradation and sustain cell viability." *Nat Cell Biol* 13(5): 589-598.

Gomez-Lazaro, M, Bonekamp, NA, Galindo, MF, Jordan, J & Schrader, M (2008). "6-Hydroxydopamine (6-OHDA) induces Drp1-dependent mitochondrial fragmentation in SH-SY5Y cells." *Free Radic.Biol.Med.* 44(11): 1960-1969.

Goodman, JM, Maher, J, Silver, PA, Pacifico, A & Sanders, D (1986). "The membrane proteins of the methanol-induced peroxisome of Candida boidinii. Initial characterization and generation of monoclonal antibodies." *J Biol Chem* 261(7): 3464-3468.

Gorgas, K (1985). "Serial section analysis of mouse hepatic peroxisomes." *Anat Embryol (Berl)* 172(1): 21-32.

Gorgas, K (1987). "Morphogenesis of peroxisomes in lipid synthesizing epithelia". *Peroxisomes in Biology and Medecine*. Fahimi, HD and Sies, H. Berlin, Heidelberg, Springer-Verlag**:** 3-17.

Gorgas, K, Teigler, A, Komljenovic, D & Just, WW (2006). "The ether lipid-deficient mouse: tracking down plasmalogen functions." *Biochim Biophys Acta* 1763(12): 1511-1526.

Gotte, K, Girzalsky, W, Linkert, M, Baumgart, E, Kammerer, S, Kunau, WH & Erdmann, R (1998). "Pex19p, a farnesylated protein essential for peroxisome biogenesis." *Mol.Cell Biol.* 18(1): 616-628.

Gould, SG, Keller, GA & Subramani, S (1987). "Identification of a peroxisomal targeting signal at the carboxy terminus of firefly luciferase." *J Cell Biol* 105(6 Pt 2): 2923-2931.

Gould, SJ, Keller, GA, Hosken, N, Wilkinson, J & Subramani, S (1989). "A conserved tripeptide sorts proteins to peroxisomes." *J.Cell Biol.* 108(5): 1657-1664.

Gould, SJ & Valle, D (2000). "Peroxisome biogenesis disorders: genetics and cell biology." *Trends Genet.* 16(8): 340-345.

Gouveia, AM, Guimaraes, CP, Oliveira, ME, Sa-Miranda, C & Azevedo, JE (2003). "Insertion of Pex5p into the peroxisomal membrane is cargo protein-dependent." *J Biol Chem* 278(7): 4389-4392.

Griffin, EE, Detmer, SA & Chan, DC (2006). "Molecular mechanism of mitochondrial membrane fusion." *Biochim Biophys Acta* 1763(5-6): 482-489.

Griffith, OW & Meister, A (1979). "Potent and specific inhibition of glutathione synthesis by buthionine sulfoximine (S-n-butyl homocysteine sulfoximine)." *J Biol Chem* 254(16): 7558-7560.

Grou, CP, Carvalho, AF, Pinto, MP, Alencastre, IS, Rodrigues, TA, Freitas, MO, Francisco, T, Sa-Miranda, C & Azevedo, JE (2009a). "The peroxisomal protein import machinery--a case report of transient ubiquitination with a new flavor." *Cell Mol Life Sci* 66(2): 254-262.

Grou, CP, Carvalho, AF, Pinto, MP, Huybrechts, SJ, Sa-Miranda, C, Fransen, M & Azevedo, JE (2009b). "Properties of the ubiquitin-pex5p thiol ester conjugate." *J Biol Chem* 284(16): 10504-10513.

Grou, CP, Carvalho, AF, Pinto, MP, Wiese, S, Piechura, H, Meyer, HE, Warscheid, B, Sa-Miranda, C & Azevedo, JE (2008). "Members of the E2D (UbcH5) family mediate the ubiquitination of the conserved cysteine of Pex5p, the peroxisomal import receptor." *J Biol Chem* 283(21): 14190-14197.

Grunau, S, Schliebs, W, Linnepe, R, Neufeld, C, Cizmowski, C, Reinartz, B, Meyer, HE, Warscheid, B, Girzalsky, W & Erdmann, R (2009). "Peroxisomal targeting of PTS2 pre-import complexes in the yeast Saccharomyces cerevisiae." *Traffic* 10(4): 451-460.

Guo, T, Kit, YY, Nicaud, JM, Le Dall, MT, Sears, SK, Vali, H, Chan, H, Rachubinski, RA & Titorenko, VI (2003). "Peroxisome division in the yeast Yarrowia lipolytica is regulated by a signal from inside the peroxisome." *J Cell Biol* 162(7): 1255-1266.

Guo, Y, Cordes, KR, Farese, RV, Jr. & Walther, TC (2009). "Lipid droplets at a glance." *J Cell Sci* 122(Pt 6): 749-752.

Gurvitz, A, Hiltunen, JK, Erdmann, R, Hamilton, B, Hartig, A, Ruis, H & Rottensteiner, H (2001). "Saccharomyces cerevisiae Adr1p governs fatty acid beta-oxidation and peroxisome proliferation by regulating POX1 and PEX11." *J Biol Chem.* 276(34): 31825-31830.

Gurvitz, A & Rottensteiner, H (2006). "The biochemistry of oleate induction: transcriptional upregulation and peroxisome proliferation." *Biochim Biophys Acta* 1763(12): 1392-1402.

Haan, GJ, Baerends, RJ, Krikken, AM, Otzen, M, Veenhuis, M & Klei, IJ (2006). "Reassembly of peroxisomes in Hansenula polymorpha pex3 cells on reintroduction of Pex3p involves the nuclear envelope." *FEMS Yeast Res.* 6(2): 186-194.

Hadden, DA, Phillipson, BA, Johnston, KA, Brown, LA, Manfield, IW, El-Shami, M, Sparkes, IA & Baker, A (2006). "Arabidopsis PEX19 is a dimeric protein that binds the peroxin PEX10." *Mol Membr Biol* 23(4): 325-336.

Halbach, A, Landgraf, C, Lorenzen, S, Rosenkranz, K, Volkmer-Engert, R, Erdmann, R & Rottensteiner, H (2006). "Targeting of the tail-anchored peroxisomal membrane proteins PEX26 and PEX15 occurs through C-terminal PEX19-binding sites." *J Cell Sci* 119(Pt 12): 2508-2517.

Halbach, A, Lorenzen, S, Landgraf, C, Volkmer-Engert, R, Erdmann, R & Rottensteiner, H (2005). "Function of the PEX19-binding site of human adrenoleukodystrophy protein as targeting motif in man and yeast. PMP targeting is evolutionarily conserved." *J.Biol.Chem.* 280(22): 21176-21182.

Hales, KG & Fuller, MT (1997). "Developmentally regulated mitochondrial fusion mediated by a conserved, novel, predicted GTPase." *Cell* 90(1): 121-129.

Heinemann, P & Just, WW (1992). "Peroxisomal protein import. In vivo evidence for a novel translocation competent compartment." *FEBS Lett* 300(2): 179-182.

Helm, M, Luck, C, Prestele, J, Hierl, G, Huesgen, PF, Frohlich, T, Arnold, GJ, Adamska, I, Gorg, A, Lottspeich, F & Gietl, C (2007). "Dual specificities of the glyoxysomal/peroxisomal processing protease Deg15 in higher plants." *Proc Natl Acad Sci U S A* 104(27): 11501-11506.

Hess, R, Staubli, W & Riess, W (1965). "Nature of the hepatomegalic effect produced by ethyl-chlorophenoxy-isobutyrate in the rat." *Nature.* 208(13): 856-858.

Hettema, EH & Motley, AM (2009). "How peroxisomes multiply." *J Cell Sci* 122(Pt 14): 2331-2336.

Heupel, R & Heldt, HW (1994). "Protein organization in the matrix of leaf peroxisomes. A multi-enzyme complex involved in photorespiratory metabolism." *Eur J Biochem* 220(1): 165-172.

Heymann, JA & Hinshaw, JE (2009). "Dynamins at a glance." *J Cell Sci* 122(Pt 19): 3427-3431.

Heymans, HS, Schutgens, RB, Tan, R, van den Bosch, H & Borst, P (1983). "Severe plasmalogen deficiency in tissues of infants without peroxisomes (Zellweger syndrome)." *Nature* 306(5938): 69-70.

Hicks, L & Fahimi, HD (1977). "Peroxisomes (microbodies) in the myocardium of rodents and primates. A comparative Ultrastructural cytochemical study." *Cell Tissue Res* 175(4): 467-481.

Hoepfner, D, Schildknegt, D, Braakman, I, Philippsen, P & Tabak, HF (2005). "Contribution of the endoplasmic reticulum to peroxisome formation." *Cell* 122(1): 85-95.

Hoepfner, D, van den Berg, M, Philippsen, P, Tabak, HF & Hettema, EH (2001). "A role for Vps1p, actin, and the Myo2p motor in peroxisome abundance and inheritance in Saccharomyces cerevisiae." *J Cell Biol* 155(6): 979-990.

Hogenboom, S, Tuyp, JJ, Espeel, M, Koster, J, Wanders, RJ & Waterham, HR (2004). "Mevalonate kinase is a cytosolic enzyme in humans." *J Cell Sci* 117(Pt 4): 631-639.

Hohfeld, J, Veenhuis, M & Kunau, WH (1991). "PAS3, a Saccharomyces cerevisiae gene encoding a peroxisomal integral membrane protein essential for peroxisome biogenesis." *J Cell Biol* 114(6): 1167-1178.

Honsho, M & Fujiki, Y (2001). "Topogenesis of peroxisomal membrane protein requires a short, positively charged intervening-loop sequence and flanking hydrophobic segments. study using human membrane protein PMP34." *J.Biol.Chem.* 276(12): 9375-9382.

Honsho, M, Hiroshige, T & Fujiki, Y (2002). "The membrane biogenesis peroxin Pex16p. Topogenesis and functional roles in peroxisomal membrane assembly." *J.Biol.Chem.* 277(46): 44513-44524.

Honsho, M, Tamura, S, Shimozawa, N, Suzuki, Y, Kondo, N & Fujiki, Y (1998). "Mutation in PEX16 is causal in the peroxisome-deficient Zellweger syndrome of complementation group D." *Am J Hum Genet.* 63(6): 1622-1630.

Hoppins, S, Lackner, L & Nunnari, J (2007). "The machines that divide and fuse mitochondria." *Annu Rev Biochem* 76: 751-780.

Hruban, Z & Swift, H (1964). "Uricase: Localization in Hepatic Microbodies." *Science* 146(3649): 1316-1318.

Hruban, Z, Vigil, EL, Slesers, A & Hopkins, E (1972). "Microbodies: constituent organelles of animal cells." *Lab Invest* 27(2): 184-191.

Hu, J (2010). "Molecular basis of peroxisome division and proliferation in plants." *Int Rev Cell Mol Biol* 279: 79-99.

Hu, J & Desai, M (2008). "Light control of peroxisome proliferation during Arabidopsis photomorphogenesis." *Plant Signal Behav* 3(10): 801-803.

Huber, A, Koch, J, Kragler, F, Brocard, C & Hartig, A (2011). "A Subtle Interplay Between Three Pex11 Proteins Shapes De Novo Formation and Fission of Peroxisomes." *Traffic* 13(1): 157-167.

Huber, CM, Saffrich, R, Ansorge, W & Just, WW (1999). "Receptor-mediated regulation of peroxisomal motility in CHO and endothelial cells." *Embo J* 18(20): 5476-5485.

Hulshagen, L, Krysko, O, Bottelbergs, A, Huyghe, S, Klein, R, Van Veldhoven, PP, De Deyn, PP, D'Hooge, R, Hartmann, D & Baes, M (2008). "Absence of functional peroxisomes from mouse CNS causes dysmyelination and axon degeneration." *J Neurosci* 28(15): 4015-4027.

Hunt, JE & Trelease, RN (2004). "Sorting pathway and molecular targeting signals for the Arabidopsis peroxin 3." *Biochem.Biophys.Res.Commun.* 314(2): 586-596.

Huybrechts, SJ, Van Veldhoven, PP, Brees, C, Mannaerts, GP, Los, GV & Fransen, M (2009). "Peroxisome dynamics in cultured mammalian cells." *Traffic* 10(11): 1722-1733.

Immenschuh, S & Baumgart-Vogt, E (2005). "Peroxiredoxins, oxidative stress, and cell proliferation." *Antioxid Redox Signal* 7(5-6): 768-777.

Imoto, M, Tachibana, I & Urrutia, R (1998). "Identification and functional characterization of a novel human protein highly related to the yeast dynamin-like GTPase Vps1p." *J Cell Sci* 111(Pt 10): 1341-1349.

Ishihara, N, Nomura, M, Jofuku, A, Kato, H, Suzuki, SO, Masuda, K, Otera, H, Nakanishi, Y, Nonaka, I, Goto, Y, Taguchi, N, Morinaga, H, Maeda, M, Takayanagi, R, Yokota, S & Mihara, K (2009). "Mitochondrial fission factor Drp1 is essential for embryonic development and synapse formation in mice." *Nat Cell Biol* 11(8): 958-966.

Islinger, M, Cardoso, MJ & Schrader, M (2010). "Be different--the diversity of peroxisomes in the animal kingdom." *Biochim Biophys Acta* 1803(8): 881-897.

Islinger, M, Li, KW, Seitz, J, Volkl, A & Luers, GH (2009). "Hitchhiking of Cu/Zn superoxide dismutase to peroxisomes--evidence for a natural piggyback import mechanism in mammals." *Traffic* 10(11): 1711-1721.

Islinger, M, Luers, GH, Li, KW, Loos, M & Volkl, A (2007). "Rat liver peroxisomes after fibrate treatment. A survey using quantitative mass spectrometry." *J Biol Chem* 282(32): 23055-23069.

Issemann, I & Green, S (1990). "Activation of a member of the steroid hormone receptor superfamily by peroxisome proliferators." *Nature.* 347(6294): 645-650.

Ivashchenko, O, Van Veldhoven, PP, Brees, C, Ho, YS, Terlecky, SR & Fransen, M (2011). "Intraperoxisomal redox balance in mammalian cells: oxidative stress and interorganellar cross-talk." *Mol Biol Cell* 22(9): 1440-1451.

Iwata, J, Ezaki, J, Komatsu, M, Yokota, S, Ueno, T, Tanida, I, Chiba, T, Tanaka, K & Kominami, E (2006). "Excess peroxisomes are degraded by autophagic machinery in mammals." *J Biol Chem* 281(7): 4035-4041.

James, A, Plank, MJ & Edwards, AM (2011). "Assessing Levy walks as models of animal foraging." *J R Soc Interface* 8(62): 1233-1247.

Jansen, GA & Wanders, RJ (2006). "Alpha-oxidation." *Biochim Biophys Acta* 1763(12): 1403-1412.

Jedd, G & Chua, NH (2000). "A new self-assembled peroxisomal vesicle required for efficient resealing of the plasma membrane." *Nat.Cell Biol.* 2(4): 226-231.

Jedd, G & Chua, NH (2002). "Visualization of peroxisomes in living plant cells reveals acto-myosin-dependent cytoplasmic streaming and peroxisome budding." *Plant Cell Physiol.* 43(4): 384-392.

Jones, JM, Morrell, JC & Gould, SJ (2001). "Multiple distinct targeting signals in integral peroxisomal membrane proteins." *J.Cell Biol.* 153(6): 1141-1150.

Jones, JM, Morrell, JC & Gould, SJ (2004). "PEX19 is a predominantly cytosolic chaperone and import receptor for class 1 peroxisomal membrane proteins." *J Cell Biol* 164(1): 57-67.

Jung, S, Marelli, M, Rachubinski, RA, Goodlett, DR & Aitchison, JD (2010). "Dynamic changes in the subcellular distribution of Gpd1p in response to cell stress." *J Biol Chem* 285(9): 6739-6749.

Kabeya, Y, Kamada, Y, Baba, M, Takikawa, H, Sasaki, M & Ohsumi, Y (2005). "Atg17 functions in cooperation with Atg1 and Atg13 in yeast autophagy." *Mol Biol Cell* 16(5): 2544-2553.

Kalbfleisch, T, Cambon, A & Wattenberg, BW (2007). "A bioinformatics approach to identifying tail-anchored proteins in the human genome." *Traffic* 8(12): 1687-1694.

Kammerer, S, Arnold, N, Gutensohn, W, Mewes, HW, Kunau, WH, Hofler, G, Roscher, AA & Braun, A (1997). "Genomic organization and molecular characterization of a gene encoding HsPXF, a human peroxisomal farnesylated protein." *Genomics* 45(1): 200-210.

Karnik, SK & Trelease, RN (2005). "Arabidopsis peroxin 16 coexists at steady state in peroxisomes and endoplasmic reticulum." *Plant Physiol* 138(4): 1967-1981.

Karpichev, IV & Small, GM (1998). "Global regulatory functions of Oaf1p and Pip2p (Oaf2p), transcription factors that regulate genes encoding peroxisomal proteins in Saccharomyces cerevisiae." *Mol Cell Biol.* 18(11): 6560-6570.

Kaur, N & Hu, J (2009). "Dynamics of peroxisome abundance: a tale of division and proliferation." *Curr Opin Plant Biol* 12(6): 781-788.

Kiel, JA, Emmrich, K, Meyer, HE & Kunau, WH (2005a). "Ubiquitination of the peroxisomal targeting signal type 1 receptor, Pex5p, suggests the presence of a quality control mechanism during peroxisomal matrix protein import." *J Biol Chem* 280(3): 1921-1930.

Kiel, JA, Komduur, JA, van der Klei, IJ & Veenhuis, M (2003). "Macropexophagy in Hansenula polymorpha: facts and views." *FEBS Lett* 549(1-3): 1-6.

Kiel, JA, van der Klei, IJ, van den Berg, MA, Bovenberg, RA & Veenhuis, M (2005b). "Overproduction of a single protein, Pc-Pex11p, results in 2-fold enhanced penicillin production by Penicillium chrysogenum." *Fungal Genet Biol* 42(2): 154-164.

Kiel, JA, Veenhuis, M & van der Klei, IJ (2006). "PEX genes in fungal genomes: common, rare or redundant." *Traffic.* 7(10): 1291-1303.

Kikuchi, M, Hatano, N, Yokota, S, Shimozawa, N, Imanaka, T & Taniguchi, H (2004). "Proteomic analysis of rat liver peroxisome: presence of peroxisome-specific isozyme of Lon protease." *J Biol Chem* 279(1): 421-428.

Kim, J & Klionsky, DJ (2000). "Autophagy, cytoplasm-to-vacuole targeting pathway, and pexophagy in yeast and mammalian cells." *Annu Rev Biochem* 69: 303-342.

Kim, PK, Mullen, RT, Schumann, U & Lippincott-Schwartz, J (2006). "The origin and maintenance of mammalian peroxisomes involves a de novo PEX16-dependent pathway from the ER." *J Cell Biol.* 173(4): 521-532.

Klaunig, JE, Babich, MA, Baetcke, KP, Cook, JC, Corton, JC, David, RM, DeLuca, JG, Lai, DY, McKee, RH, Peters, JM, Roberts, RA & Fenner-Crisp, PA (2003). "PPARalpha agonist-induced rodent tumors: modes of action and human relevance." *Crit Rev Toxicol* 33(6): 655-780.

Kleinmann, HK, Goodwin, EB, Rennard, SL & Martin, GR (1981). "Preparation of collagen substrates for cell attachment: Effect of collagen concentration and phosphate buffer." *Anal Biochem* 94.

Klionsky, DJ & Ohsumi, Y (1999). "Vacuolar import of proteins and organelles from the cytoplasm." *Annu Rev Cell Dev Biol* 15: 1-32.

Kluwe, WM, Haseman, JK, Douglas, JF & Huff, JE (1982). "The carcinogenicity of dietary di(2-ethylhexyl) phthalate (DEHP) in Fischer 344 rats and B6C3F1 mice." *J Toxicol Environ Health.* 10(4-5): 797-815.

Knoblach, B & Rachubinski, RA (2010). "Phosphorylation-dependent activation of peroxisome proliferator protein PEX11 controls peroxisome abundance." *J Biol Chem* 285(9): 6670-6680.

Kobayashi, S, Tanaka, A & Fujiki, Y (2007). "Fis1, DLP1, and Pex11p coordinately regulate peroxisome morphogenesis." *Exp Cell Res* 313(8): 1675-1686.

Koch, A, Schneider, G, Luers, GH & Schrader, M (2004). "Peroxisome elongation and constriction but not fission can occur independently of dynamin-like protein 1." *J Cell Sci* 117(Pt 17): 3995-4006.

Koch, A, Thiemann, M, Grabenbauer, M, Yoon, Y, McNiven, MA & Schrader, M (2003). "Dynamin-like protein 1 is involved in peroxisomal fission." *J Biol Chem* 278(10): 8597-8605.

Koch, A, Yoon, Y, Bonekamp, NA, McNiven, MA & Schrader, M (2005). "A role for fis1 in both mitochondrial and peroxisomal fission in Mammalian cells." *Mol Biol Cell* 16(11): 5077-5086.

Koch, J, Pranjic, K, Huber, A, Ellinger, A, Hartig, A, Kragler, F & Brocard, C (2010). "PEX11 family members are membrane elongation factors that coordinate peroxisome proliferation and maintenance." *J Cell Sci* 123(Pt 19): 3389-3400.

Koepke, JI, Wood, CS, Terlecky, LJ, Walton, PA & Terlecky, SR (2008). "Progeric effects of catalase inactivation in human cells." *Toxicol Appl Pharmacol* 232(1): 99-108.

Kollatakudy, PE, Bohnet, S, Roberts, E & Rogers, L (1987). "Peroxisomes in sebaceous glands: Biosynthetic role and hormonal regulation.". *Peroxisomes in Biology and Medicine*. Fahimi, HD and Sies, H. Berlin, Heidelberg, Springer-Verlag**:** 18-31.

Koshiba, T, Detmer, SA, Kaiser, JT, Chen, H, McCaffery, JM & Chan, DC (2004). "Structural basis of mitochondrial tethering by mitofusin complexes." *Science* 305(5685): 858-862.

Kou, J, Kovacs, GG, Hoftberger, R, Kulik, W, Brodde, A, Forss-Petter, S, Honigschnabl, S, Gleiss, A, Brugger, B, Wanders, R, Just, W, Budka, H, Jungwirth, S, Fischer, P & Berger, J (2011). "Peroxisomal alterations in Alzheimer's disease." *Acta Neuropathol* 122(3): 271-283.

Kragler, F, Lametschwandtner, G, Christmann, J, Hartig, A & Harada, JJ (1998). "Identification and analysis of the plant peroxisomal targeting signal 1 receptor NtPEX5." *Proc Natl Acad Sci U S A* 95(22): 13336-13341.

Kragt, A, Voorn-Brouwer, T, van den Berg, M & Distel, B (2005). "Endoplasmic reticulum-directed Pex3p Routes to peroxisomes and restores peroxisome formation in a Saccharomyces cerevisiae pex3Delta strain." *J Biol Chem* 280(40): 34350-34357.

Krikken, AM, Veenhuis, M & van der Klei, IJ (2009). "Hansenula polymorpha pex11 cells are affected in peroxisome retention." *FEBS J* 276(5): 1429-1439.

Kulic, IM, Brown, AE, Kim, H, Kural, C, Blehm, B, Selvin, PR, Nelson, PC & Gelfand, VI (2008). "The role of microtubule movement in bidirectional organelle transport." *Proc Natl Acad Sci U S A* 105(29): 10011-10016.

Kunau, WH (2001). "Peroxisomes: the extended shuttle to the peroxisome matrix." *Curr Biol* 11(16): R659-662.

Kunau, WH, Buhne, S, de la Garza, M, Kionka, C, Mateblowski, M, Schultz-Borchard, U & Thieringer, R (1988). "Comparative enzymology of beta-oxidation." *Biochem Soc Trans* 16(3): 418-420.

Kunze, M, Pracharoenwattana, I, Smith, SM & Hartig, A (2006). "A central role for the peroxisomal membrane in glyoxylate cycle function." *Biochim Biophys Acta* 1763(12): 1441-1452.

Kural, C, Kim, H, Syed, S, Goshima, G, Gelfand, VI & Selvin, PR (2005). "Kinesin and dynein move a peroxisome in vivo: a tug-of-war or coordinated movement?" *Science.* 308(5727): 1469-1472.

Kuravi, K, Nagotu, S, Krikken, AM, Sjollema, K, Deckers, M, Erdmann, R, Veenhuis, M & van der Klei, IJ (2006). "Dynamin-related proteins Vps1p and Dnm1p control peroxisome abundance in Saccharomyces cerevisiae." *J Cell Sci.* 119(Pt 19): 3994-4001.

Kurochkin, IV, Mizuno, Y, Konagaya, A, Sakaki, Y, Schonbach, C & Okazaki, Y (2007). "Novel peroxisomal protease Tysnd1 processes PTS1- and PTS2-containing enzymes involved in beta-oxidation of fatty acids." *Embo J* 26(3): 835-845.

Kyhse-Andersen, J (1984). "Electroblotting of multiple gels: a simple apparatus without buffer tank for rapid transfer of proteins from polyacrylamide to nitrocellulose." *J Biochem Biophys Methods* 10(3-4): 203-209.

Labrousse, AM, Zappaterra, MD, Rube, DA & van der Bliek, AM (1999). "C. elegans dynamin-related protein DRP-1 controls severing of the mitochondrial outer membrane." *Mol Cell* 4(5): 815-826.

Laemmli, UK (1970). "Cleavage of structural proteins during the assembly of the head of bacteriophage T4." *Nature* 227(259): 680-685.

Lagerwerf, S, Vrouwe, MG, Overmeer, RM, Fousteri, MI & Mullenders, LH (2011). "DNA damage response and transcription." *DNA Repair (Amst)* 10(7): 743-750.

Lam, SK, Yoda, N & Schekman, R (2011). "A vesicle carrier that mediates peroxisome protein traffic from the endoplasmic reticulum." *Proc Natl Acad Sci U S A* 108(14): E51-52.

Lametschwandtner, G, Brocard, C, Fransen, M, Van Veldhoven, P, Berger, J & Hartig, A (1998). "The difference in recognition of terminal tripeptides as peroxisomal targeting signal 1 between yeast and human is due to different affinities of their receptor Pex5p to the cognate signal and to residues adjacent to it." *J Biol Chem* 273(50): 33635-33643.

Lanyon-Hogg, T, Warriner, SL & Baker, A (2010). "Getting a camel through the eye of a needle: the import of folded proteins by peroxisomes." *Biol Cell* 102(4): 245-263.

Lauer, C, Volkl, A, Riedl, S, Fahimi, HD & Beier, K (1999). "Impairment of peroxisomal biogenesis in human colon carcinoma." *Carcinogenesis* 20(6): 985-989.

Lawrence, JW, Wollenberg, GK, Frank, JD & DeLuca, JG (2001). "Dexamethasone selectively inhibits WY14,643-induced cell proliferation and not peroxisome proliferation in mice." *Toxicol Appl Pharmacol* 170(2): 113-123.

Lazarow, PB & De Duve, C (1976). "A fatty acyl-CoA oxidizing system in rat liver peroxisomes; enhancement by clofibrate, a hypolipidemic drug." *Proc Natl Acad Sci U S A* 73(6): 2043-2046.

Lazarow, PB & Fujiki, Y (1985). "Biogenesis of peroxisomes." *Annu Rev Cell Biol* 1: 489-530.

Lazarow, PB, Shio, H & Leroy-Houyet, MA (1982). "Specificity in the action of hypolipidemic drugs: increase of peroxisomal beta-oxidation largely dissociated from hepatomegaly and peroxisome proliferation in the rat." *J Lipid Res.* 23(2): 317-326.

Leao-Helder, AN, Krikken, AM, van der Klei, IJ, Kiel, JA & Veenhuis, M (2003). "Transcriptional down-regulation of peroxisome numbers affects selective peroxisome degradation in Hansenula polymorpha." *J Biol Chem.* 278(42): 40749-40756.

Lee, MS, Kao, SC, Lemere, CA, Xia, W, Tseng, HC, Zhou, Y, Neve, R, Ahlijanian, MK & Tsai, LH (2003). "APP processing is regulated by cytoplasmic phosphorylation." *J Cell Biol* 163(1): 83-95.

Lee, SS, Pineau, T, Drago, J, Lee, EJ, Owens, JW, Kroetz, DL, Fernandez-Salguero, PM, Westphal, H & Gonzalez, FJ (1995). "Targeted disruption of the alpha isoform of the peroxisome proliferator-activated receptor gene in mice results in abolishment of the pleiotropic effects of peroxisome proliferators." *Mol Cell Biol.* 15(6): 3012-3022.

Legakis, JE, Koepke, JI, Jedeszko, C, Barlaskar, F, Terlecky, LJ, Edwards, HJ, Walton, PA & Terlecky, SR (2002). "Peroxisome senescence in human fibroblasts." *Mol Biol Cell* 13(12): 4243-4255.

Leighton, F, Poole, B, Beaufay, H, Baudhuin, P, Coffey, JW, Fowler, S & De Duve, C (1968). "The large-scale separation of peroxisomes, mitochondria, and lysosomes from the livers of rats injected with triton WR-1339. Improved isolation procedures, automated analysis, biochemical and morphological properties of fractions." *J Cell Biol* 37(2): 482-513.

Leon, S, Goodman, JM & Subramani, S (2006a). "Uniqueness of the mechanism of protein import into the peroxisome matrix: transport of folded, co-factor-bound and oligomeric proteins by shuttling receptors." *Biochim Biophys Acta* 1763(12): 1552-1564.

Leon, S, Zhang, L, McDonald, WH, Yates, J, 3rd, Cregg, JM & Subramani, S (2006b). "Dynamics of the peroxisomal import cycle of PpPex20p: ubiquitin-dependent localization and regulation." *J Cell Biol* 172(1): 67-78.

Li, X, Baumgart, E, Dong, GX, Morrell, JC, Jimenez-Sanchez, G, Valle, D, Smith, KD & Gould, SJ (2002a). "PEX11alpha Is Required for Peroxisome Proliferation in Response to 4-Phenylbutyrate but Is Dispensable for Peroxisome Proliferator-Activated Receptor Alpha-Mediated Peroxisome Proliferation." *Mol Cell Biol* 22(23): 8226-8240.

Li, X, Baumgart, E, Morrell, JC, Jimenez-Sanchez, G, Valle, D & Gould, SJ (2002b). "PEX11 beta deficiency is lethal and impairs neuronal migration but does not abrogate peroxisome function." *Mol Cell Biol* 22(12): 4358-4365.

Li, X & Gould, SJ (2002). "PEX11 promotes peroxisome division independently of peroxisome metabolism." *J Cell Biol* 156(4): 643-651.

Li, X & Gould, SJ (2003). "The dynamin-like GTPase DLP1 is essential for peroxisome division and is recruited to peroxisomes in part by PEX11." *J Biol Chem* 278(19): 17012-17020.

Li, Z, Okamoto, K, Hayashi, Y & Sheng, M (2004). "The importance of dendritic mitochondria in the morphogenesis and plasticity of spines and synapses." *Cell* 119(6): 873-887.

Lill, R & Muhlenhoff, U (2005). "Iron-sulfur-protein biogenesis in eukaryotes." *Trends Biochem Sci* 30(3): 133-141.

Lin-Cereghino, GP, Godfrey, L, de la Cruz, BJ, Johnson, S, Khuongsathiene, S, Tolstorukov, I, Yan, M, Lin-Cereghino, J, Veenhuis, M, Subramani, S & Cregg, JM (2006). "Mxr1p, a key regulator of the methanol utilization pathway and peroxisomal genes in Pichia pastoris." *Mol Cell Biol.* 26(3): 883-897.

Lingard, MJ, Gidda, SK, Bingham, S, Rothstein, SJ, Mullen, RT & Trelease, RN (2008). "Arabidopsis PEROXIN11c-e, FISSION1b, and DYNAMIN-RELATED PROTEIN3A Cooperate in Cell Cycle-Associated Replication of Peroxisomes." *Plant Cell* 20(6): 1567-1585.

Lingard, MJ & Trelease, RN (2006). "Five Arabidopsis peroxin 11 homologs individually promote peroxisome elongation, division without elongation, or aggregation." *J. Cell Sci.* 119: 1961-1972.

Listenberger, LL, Ostermeyer-Fay, AG, Goldberg, EB, Brown, WJ & Brown, DA (2007). "Adipocyte differentiation-related protein reduces the lipid droplet association of adipose triglyceride lipase and slows triacylglycerol turnover." *J Lipid Res* 48(12): 2751-2761.

Litwin, JA & Bilinska, B (1995). "Morphological heterogeneity of peroxisomes in cultured mouse Leydig cells." *Folia Histochem Cytobiol* 33(4): 255-258.

Liu, X, Weaver, D, Shirihai, O & Hajnoczky, G (2009). "Mitochondrial 'kiss-and-run': interplay between mitochondrial motility and fusion-fission dynamics." *EMBO J* 28(20): 3074-3089.

Logsdon, CD, Moessner, J, Williams, JA & Goldfine, ID (1985). "Glucocorticoids increase amylase mRNA levels, secretory organelles, and secretion in pancreatic acinar AR42J cells." *J Cell Biol* 100(4): 1200-1208.

Logsdon, CD, Perot, KJ & McDonald, AR (1987). "Mechanism of glucocorticoid-induced increase in pancreatic amylase gene transcription." *J Biol Chem* 262(32): 15765-15769.

Longnecker, DS, Lilja, HS, French, J, Kuhlmann, E & Noll, W (1979). "Transplantation of azaserine-induced carcinomas of pancreas in rats." *Cancer Lett* 7(4): 197-202.

Lopez-Huertas, E, Charlton, WL, Johnson, B, Graham, IA & Baker, A (2000). "Stress induces peroxisome biogenesis genes." *Embo J* 19(24): 6770-6777.

Luers, G, Hashimoto, T, Fahimi, HD & Volkl, A (1993). "Biogenesis of peroxisomes: isolation and characterization of two distinct peroxisomal populations from normal and regenerating rat liver." *J Cell Biol* 121(6): 1271-1280.

Luers, GH, Thiele, S, Schad, A, Volkl, A, Yokota, S & Seitz, J (2006). "Peroxisomes are present in murine spermatogonia and disappear during the course of spermatogenesis." *Histochem Cell Biol* 125(6): 693-703.

Ma, C, Haslbeck, M, Babujee, L, Jahn, O & Reumann, S (2006). "Identification and characterization of a stress-inducible and a constitutive small heat-shock protein targeted to the matrix of plant peroxisomes." *Plant Physiol* 141(1): 47-60.

Ma, C & Subramani, S (2009). "Peroxisome matrix and membrane protein biogenesis." *IUBMB Life* 61(7): 713-722.

Madrid, KP, De Crescenzo, G, Wang, S & Jardim, A (2004). "Modulation of the Leishmania donovani peroxin 5 quaternary structure by peroxisomal targeting signal 1 ligands." *Mol Cell Biol* 24(17): 7331-7344.

Maier, A, Lorenz, P, Voncken, F & Clayton, C (2001). "An essential dimeric membrane protein of trypanosome glycosomes." *Mol Microbiol* 39(6): 1443-1451.

Mannaerts, GP & Van Veldhoven, PP (1993). "Metabolic pathways in mammalian peroxisomes." *Biochimie* 75(3-4): 147-158.

Mannaerts, GP, Van Veldhoven, PP & Casteels, M (2000). "Peroxisomal lipid degradation via beta- and alpha-oxidation in mammals." *Cell Biochem Biophys* 32 Spring: 73-87.

Mano, S, Nakamori, C, Hayashi, M, Kato, A, Kondo, M & Nishimura, M (2002). "Distribution and characterization of peroxisomes in Arabidopsis by visualization with GFP: dynamic morphology and actin-dependent movement." *Plant Cell Physiol.* 43(3): 331-341.

Mano, S, Nakamori, C, Kondo, M, Hayashi, M & Nishimura, M (2004). "An Arabidopsis dynamin-related protein, DRP3A, controls both peroxisomal and mitochondrial division." *Plant J* 38(3): 487-498.

Marone, M, Mozzetti, S, De Ritis, D, Pierelli, L & Scambia, G (2001). "Semiquantitative RT-PCR analysis to assess the expression levels of multiple transcripts from the same sample." *Biol Proced Online* 3: 19-25.

Marshall, PA, Dyer, JM, Quick, ME & Goodman, JM (1996). "Redox-sensitive homodimerization of Pex11p: a proposed mechanism to regulate peroxisomal division." *J Cell Biol.* 135(1): 123-137.

Marshall, PA, Krimkevich, YI, Lark, RH, Dyer, JM, Veenhuis, M & Goodman, JM (1995). "Pmp27 promotes peroxisomal proliferation." *J Cell Biol* 129(2): 345-355.

Mathur, J, Mathur, N & Hulskamp, M (2002). "Simultaneous visualization of peroxisomes and cytoskeletal elements reveals actin and not microtubule-based peroxisome motility in plants." *Plant Physiol* 128(3): 1031-1045.

Matsumoto, N, Tamura, S & Fujiki, Y (2003). "The pathogenic peroxin Pex26p recruits the Pex1p-Pex6p AAA ATPase complexes to peroxisomes." *Nat Cell Biol* 5(5): 454-460.

Matsuzaki, T & Fujiki, Y (2008). "The peroxisomal membrane protein import receptor Pex3p is directly transported to peroxisomes by a novel Pex19p- and Pex16p-dependent pathway." *J Cell Biol* 183(7): 1275-1286.

Matsuzono, Y & Fujiki, Y (2006). "In vitro transport of membrane proteins to peroxisomes by shuttling receptor Pex19p." *J Biol Chem* 281(1): 36-42.

Matsuzono, Y, Kinoshita, N, Tamura, S, Shimozawa, N, Hamasaki, M, Ghaedi, K, Wanders, RJ, Suzuki, Y, Kondo, N & Fujiki, Y (1999). "Human PEX19: cDNA cloning by functional complementation, mutation analysis in a patient with Zellweger syndrome, and potential role in peroxisomal membrane assembly." *Proc Natl Acad Sci U S A.* 96(5): 2116-2121.

Matsuzono, Y, Matsuzaki, T & Fujiki, Y (2006). "Functional domain mapping of peroxin Pex19p: interaction with Pex3p is essential for function and translocation." *J Cell Sci* 119(Pt17): 3539-3550.

Mattenberger, Y, James, DI & Martinou, JC (2003). "Fusion of mitochondria in mammalian cells is dependent on the mitochondrial inner membrane potential and independent of microtubules or actin." *FEBS Lett* 538(1-3): 53-59.

Mayerhofer, PU, Kattenfeld, T, Roscher, AA & Muntau, AC (2002). "Two splice variants of human PEX19 exhibit distinct functions in peroxisomal assembly." *Biochem Biophys Res Commun* 291(5): 1180-1186.

Maynard, EL & Berg, JM (2007). "Quantitative analysis of peroxisomal targeting signal type-1 binding to wild-type and pathogenic mutants of Pex5p supports an affinity threshold for peroxisomal protein targeting." *J Mol Biol* 368(5): 1259-1266.

McBride, HM, Neuspiel, M & Wasiak, S (2006). "Mitochondria: more than just a powerhouse." *Curr Biol* 16(14): R551-560.

McCammon, MT, Veenhuis, M, Trapp, SB & Goodman, JM (1990). "Association of glyoxylate and beta-oxidation enzymes with peroxisomes of Saccharomyces cerevisiae." *J Bacteriol* 172(10): 5816-5827.

McNew, JA & Goodman, JM (1994). "An oligomeric protein is imported into peroxisomes in vivo." *J Cell Biol* 127(5): 1245-1257.

Meinecke, M, Cizmowski, C, Schliebs, W, Kruger, V, Beck, S, Wagner, R & Erdmann, R (2010). "The peroxisomal importomer constitutes a large and highly dynamic pore." *Nat Cell Biol* 12(3): 273-277.

Mi, J, Garcia-Arcos, I, Alvarez, R & Cristobal, S (2007). "Age-related subproteomic analysis of mouse liver and kidney peroxisomes." *Proteome Sci* 5(1): 19.

Michels, PA, Bringaud, F, Herman, M & Hannaert, V (2006). "Metabolic functions of glycosomes in trypanosomatids." *Biochim Biophys Acta* 24: 24.

Michels, PA, Moyersoen, J, Krazy, H, Galland, N, Herman, M & Hannaert, V (2005). "Peroxisomes, glyoxysomes and glycosomes (review)." *Mol Membr Biol* 22(1-2): 133-145.

Mitchell, AM, Bridges, JW & Elcombe, CR (1984). "Factors influencing peroxisome proliferation in cultured rat hepatocytes." *Arch Toxicol* 55(4): 239-246.

Miyata, N & Fujiki, Y (2005). "Shuttling mechanism of peroxisome targeting signal type 1 receptor Pex5: ATP-independent import and ATP-dependent export." *Mol Cell Biol* 25(24): 10822-10832.

Monastyrska, I & Klionsky, DJ (2006). "Autophagy in organelle homeostasis: peroxisome turnover." *Mol Aspects Med* 27(5-6): 483-494.

Moody, DE, Reddy, JK, Lake, BG, Popp, JA & Reese, DH (1991). "Peroxisome proliferation and nongenotoxic carcinogenesis: commentary on a symposium." *Fundam Appl Toxicol* 16(2): 233-248.

Moreno, M, Lark, R, Campbell, KL & Goodman, JM (1994). "The peroxisomal membrane proteins of Candida boidinii: gene isolation and expression." *Yeast* 10(11): 1447-1457.

Motley, A, Hettema, E, Distel, B & Tabak, H (1994). "Differential protein import deficiencies in human peroxisome assembly disorders." *J Cell Biol* 125(4): 755-767.

Motley, AM & Hettema, EH (2007). "Yeast peroxisomes multiply by growth and division." *J Cell Biol* 178(3): 399-410.

Motley, AM, Hettema, EH, Ketting, R, Plasterk, R & Tabak, HF (2000). "Caenorhabditis elegans has a single pathway to target matrix proteins to peroxisomes." *EMBO Rep* 1(1): 40-46.

Motley, AM, Ward, GP & Hettema, EH (2008). "Dnm1p-dependent peroxisome fission requires Caf4p, Mdv1p and Fis1p." *J Cell Sci* 121(Pt 10): 1633-1640.

Mozdy, AD, McCaffery, JM & Shaw, JM (2000). "Dnm1p GTPase-mediated mitochondrial fission is a multi-step process requiring the novel integral membrane component Fis1p." *J Cell Biol* 151(2): 367-380.

Muench, DG & Mullen, RT (2003). "Peroxisome dynamics in plant cells: a role for the cytoskeleton." *Plant Science* 164: 307-315.

Mukai, S & Fujiki, Y (2006). "Molecular mechanisms of import of peroxisome-targeting signal type 2 (PTS2) proteins by PTS2 receptor Pex7p and PTS1 receptor Pex5pL." *J Biol Chem* 281(49): 37311-37320.

Mullen, RT, Flynn, CR & Trelease, RN (2001). "How are peroxisomes formed? The role of the endoplasmic reticulum and peroxins." *Trends Plant Sci* 6(6): 256-261.

Mullen, RT, Lisenbee, CS, Miernyk, JA & Trelease, RN (1999). "Peroxisomal membrane ascorbate peroxidase is sorted to a membranous network that resembles a subdomain of the endoplasmic reticulum." *Plant Cell* 11(11): 2167-2185.

Mullen, RT & Trelease, RN (2006). "The ER-peroxisome connection in plants: development of the "ER semi-autonomous peroxisome maturation and replication" model for plant peroxisome biogenesis." *Biochim Biophys Acta* 1763(12): 1655-1668.

Munck, JM, Motley, AM, Nuttall, JM & Hettema, EH (2009). "A dual function for Pex3p in peroxisome formation and inheritance." *J Cell Biol* 187(4): 463-471.

Muntau, AC, Mayerhofer, PU, Paton, BC, Kammerer, S & Roscher, AA (2000). "Defective peroxisome membrane synthesis due to mutations in human PEX3 causes Zellweger syndrome, complementation group G." *Am J Hum Genet* 67(4): 967-975.

Nagotu, S, Veenhuis, M & van der Klei, IJ (2010). "Divide et impera: the dictum of peroxisomes." *Traffic* 11(2): 175-184.

Nakada, K, Inoue, K, Ono, T, Isobe, K, Ogura, A, Goto, YI, Nonaka, I & Hayashi, JI (2001). "Inter-mitochondrial complementation: Mitochondria-specific system preventing mice from expression of disease phenotypes by mutant mtDNA." *Nat Med* 7(8): 934-940.

Nashiro, C, Kashiwagi, A, Matsuzaki, T, Tamura, S & Fujiki, Y (2011). "Recruiting Mechanism of the AAA peroxins, Pex1p and Pex6p, to Pex26p on Peroxisome Membrane." *Traffic* 12(6): 774-788.

Natarajan, SK, Eapen, CE, Pullimood, AB & Balasubramanian, KA (2006). "Oxidative stress in experimental liver microvesicular steatosis: role of mitochondria and peroxisomes." *J Gastroenterol Hepatol* 21(8): 1240-1249.

Nedergaard, J, Alexson, S & Cannon, B (1980). "Cold adaptation in the rat: increased brown fat peroxisomal beta-oxidation relative to maximal mitochondrial oxidative capacity." *Am J Physiol* 239(5): C208-216.

Neuspiel, M, Schauss, AC, Braschi, E, Zunino, R, Rippstein, P, Rachubinski, RA, Andrade-Navarro, MA & McBride, HM (2008). "Cargo-selected transport from the mitochondria to peroxisomes is mediated by vesicular carriers." *Current Biology* 18(2): 102-108.

Newman, MEJ (2005). "Power laws, Pareto distributions and Zipf's law." *Contemp Phys* 46(5): 323-351.

Nicholls, DG & Locke, RM (1984). "Thermogenic mechanisms in brown fat." *Physiol Rev.* 64(1): 1-64.

Niemann, A, Ruegg, M, La Padula, V, Schenone, A & Suter, U (2005). "Ganglioside-induced differentiation associated protein 1 is a regulator of the mitochondrial network: new implications for Charcot-Marie-Tooth disease." *J Cell Biol* 170(7): 1067-1078

Novikoff, AB & Essner, E (1960). "The liver cell. Some new approaches to its study." *Am J Med.* 29: 102-131.

Novikoff, AB & Goldfischer, S (1969). "Visualization of peroxisomes (microbodies) and mitochondria with diaminobenzidine." *J Histochem Cytochem* 17(10): 675-680.

Novikoff, AB & Shin, WY (1964). "The endoplasmic reticulum in the Golgi zone and its relations to microbodies, Golgi apparatus, and autophagic vacuoles in rat liver cells." *J Microscopy* 3: 187-206.

Novikoff, PM & Novikoff, AB (1972). "Peroxisomes in absorptive cells of mammalian small intestine." *J Cell Biol.* 53(2): 532-560.

Nuttall, JM, Motley, A & Hettema, EH (2011). "Peroxisome biogenesis: recent advances." *Curr Opin Cell Biol* 23(4): 421-426.

Nyathi, Y & Baker, A (2006). "Plant peroxisomes as a source of signalling molecules." *Biochim Biophys Acta* 1763(12): 1478-1495.

Okamoto, K & Shaw, JM (2005). "Mitochondrial Morphology and Dynamics in Yeast and Multicellular Eukaryotes." *Annu Rev Genet* 39: 503-536.

Olichon, A, Elachouri, G, Baricault, L, Delettre, C, Belenguer, P & Lenaers, G (2007). "OPA1 alternate splicing uncouples an evolutionary conserved function in mitochondrial fusion from a vertebrate restricted function in apoptosis." *Cell Death Differ* 14(4): 682-692.

Ono, T, Isobe, K, Nakada, K & Hayashi, JI (2001). "Human cells are protected from mitochondrial dysfunction by complementation of DNA products in fused mitochondria." *Nat Genet* 28(3): 272-275.

Opalinski, L, Kiel, JA, Williams, C, Veenhuis, M & van der Klei, IJ (2011). "Membrane curvature during peroxisome fission requires Pex11." *EMBO J* 30(1): 5-16.

Opperdoes, FR (1988). "Glycosomes may provide clues to the import of peroxisomal proteins." *Trends Biochem.Sci.* 13(7): 255-260.

Orth, T, Reumann, S, Zhang, X, Fan, J, Wenzel, D, Quan, S & Hu, J (2007). "The PEROXIN11 protein family controls peroxisome proliferation in Arabidopsis." *Plant Cell* 19(1): 333-350.

Osteryoung, KW & Nunnari, J (2003). "The division of endosymbiotic organelles." *Science* 302(5651): 1698-1704.

Otera, H, Harano, T, Honsho, M, Ghaedi, K, Mukai, S, Tanaka, A, Kawai, A, Shimizu, N & Fujiki, Y (2000). "The mammalian peroxin Pex5pL, the longer isoform of the mobile peroxisome targeting signal (PTS) type 1 transporter, translocates the Pex7p.PTS2 protein complex into peroxisomes via its initial docking site, Pex14p." *J Biol Chem* 275(28): 21703-21714.

Otera, H & Mihara, K (2011). "Molecular mechanisms and physiologic functions of mitochondrial dynamics." *J Biochem* 149(3): 241-251.

Otera, H, Wang, C, Cleland, MM, Setoguchi, K, Yokota, S, Youle, RJ & Mihara, K (2010). "Mff is an essential factor for mitochondrial recruitment of Drp1 during mitochondrial fission in mammalian cells." *J Cell Biol* 191(6): 1141-1158.

Otzen, M, Wang, D, Lunenborg, MG & van der Klei, IJ (2005). "Hansenula polymorpha Pex20p is an oligomer that binds the peroxisomal targeting signal 2 (PTS2)." *J Cell Sci* 118(Pt 15): 3409-3418.

Ozimek, P, Veenhuis, M & van der Klei, IJ (2005). "Alcohol oxidase: a complex peroxisomal, oligomeric flavoprotein." *FEMS Yeast Res* 5(11): 975-983.

Palmer, CS, Osellame, LD, Laine, D, Koutsopoulos, OS, Frazier, AE & Ryan, MT (2011). "MiD49 and MiD51, new components of the mitochondrial fission machinery." *EMBO Rep* 12(6): 565-573.

Passreiter, M, Anton, M, Lay, D, Frank, R, Harter, C, Wieland, FT, Gorgas, K & Just, WW (1998). "Peroxisome biogenesis: involvement of ARF and coatomer." *J Cell Biol* 141(2): 373-383.

Perry, RJ, Mast, FD & Rachubinski, RA (2009). "Endoplasmic reticulum-associated secretory proteins Sec20p, Sec39p, and Dsl1p are involved in peroxisome biogenesis." *Eukaryot Cell* 8(6): 830-843.

Perry, RJ & Rachubinski, RA (2007). "The yeast Dsl1p secretory complex is involved in peroxisome biogenesis." *47th ASCB Annual Meeting, Washington* 183 (abstr.).

Pidoux, G, Witczak, O, Jarnaess, E, Myrvold, L, Urlaub, H, Stokka, AJ, Kuntziger, T & Tasken, K (2011). "Optic atrophy 1 is an A-kinase anchoring protein on lipid droplets that mediates adrenergic control of lipolysis." *EMBO J* 30(21): 4371-4386.

Pinto, MP, Grou, CP, Alencastre, IS, Oliveira, ME, Sa-Miranda, C, Fransen, M & Azevedo, JE (2006). "The import competence of a peroxisomal membrane protein is determined by Pex19p before the docking step." *J Biol Chem* 281(45): 34492-34502.

Pinto, MP, Grou, CP, Fransen, M, Sa-Miranda, C & Azevedo, JE (2009). "The cytosolic domain of PEX3, a protein involved in the biogenesis of peroxisomes, binds membrane lipids." *Biochim Biophys Acta* 1793(11): 1669-1675.

Plant, NJ, Horley, NJ, Savory, RL, Elcombe, CR, Gray, TJ & Bell, DR (1998). "The peroxisome proliferators are hepatocyte mitogens in chemically-defined media: glucocorticoid-induced PPAR alpha is linked to peroxisome proliferator mitogenesis." *Carcinogenesis* 19(5): 925-931.

Platta, HW, El Magraoui, F, Baumer, BE, Schlee, D, Girzalsky, W & Erdmann, R (2009). "Pex2 and pex12 function as protein-ubiquitin ligases in peroxisomal protein import." *Mol Cell Biol* 29(20): 5505-5516.

Platta, HW, El Magraoui, F, Schlee, D, Grunau, S, Girzalsky, W & Erdmann, R (2007). "Ubiquitination of the peroxisomal import receptor Pex5p is required for its recycling." *J Cell Biol* 177(2): 197-204.

Platta, HW & Erdmann, R (2007). "The peroxisomal protein import machinery." *FEBS Lett* 581(15): 2811-2819.

Platta, HW, Grunau, S, Rosenkranz, K, Girzalsky, W & Erdmann, R (2005). "Functional role of the AAA peroxins in dislocation of the cycling PTS1 receptor back to the cytosol." *Nat Cell Biol* 7(8): 817-822.

Poirier, Y, Antonenkov, VD, Glumoff, T & Hiltunen, JK (2006). "Peroxisomal beta-oxidation--a metabolic pathway with multiple functions." *Biochim Biophys Acta* 1763(12): 1413-1426.

Praefcke, GJ & McMahon, HT (2004). "The dynamin superfamily: universal membrane tubulation and fission molecules?" *Nat Rev Mol Cell Biol* 5(2): 133-147.

Pratt, WB (1998). "The hsp90-based chaperone system: involvement in signal transduction from a variety of hormone and growth factor receptors." *Proc Soc Exp Biol Med* 217(4): 420-434.

Ptacek, J, Devgan, G, Michaud, G, Zhu, H, Zhu, X, Fasolo, J, Guo, H, Jona, G, Breitkreutz, A, Sopko, R, McCartney, RR, Schmidt, MC, Rachidi, N, Lee, SJ, Mah, AS, Meng, L, Stark, MJ, Stern, DF, De Virgilio, C, Tyers, M, Andrews, B, Gerstein, M, Schweitzer, B, Predki, PF & Snyder, M (2005). "Global analysis of protein phosphorylation in yeast." *Nature* 438(7068): 679-684.

Puigserver, P, Adelmant, G, Wu, Z, Fan, M, Xu, J, O'Malley, B & Spiegelman, BM (1999). "Activation of PPARgamma coactivator-1 through transcription factor docking." *Science* 286(5443): 1368-1371.

Puigserver, P, Wu, Z, Park, CW, Graves, R, Wright, M & Spiegelman, BM (1998). "A cold-inducible coactivator of nuclear receptors linked to adaptive thermogenesis." *Cell.* 92(6): 829-839.

Purdue, PE & Lazarow, PB (1996). "Targeting of human catalase to peroxisomes is dependent upon a novel COOH-terminal peroxisomal targeting sequence." *J Cell Biol.* 134(4): 849-862.

Purdue, PE & Lazarow, PB (2001). "Peroxisome biogenesis." *Annu Rev Cell Dev Biol* 17: 701-752.

Pyper, SR, Viswakarma, N, Yu, S & Reddy, JK (2010). "PPARalpha: energy combustion, hypolipidemia, inflammation and cancer." *Nucl Recept Signal* 8: e002.

Qi, C, Zhu, Y & Reddy, JK (2000). "Peroxisome proliferator-activated receptors, coactivators, and downstream targets." *Cell Biochem Biophys.* 32(Spring): 187-204.

Rabu, C & High, S (2007). "Membrane protein chaperones: a new twist in the tail?" *Curr.Biol.* 17(12): R472-R474.

Rachubinski, RA & Subramani, S (1995). "How proteins penetrate peroxisomes." *Cell* 83(4): 525-528.

Rambold, AS, Kostelecky, B, Elia, N & Lippincott-Schwartz, J (2011a). "Tubular network formation protects mitochondria from autophagosomal degradation during nutrient starvation." *Proc Natl Acad Sci U S A* 108(25): 10190-10195.

Rambold, AS, Kostelecky, B & Lippincott-Schwartz, J (2011b). "Together we are stronger: Fusion protects mitochondria from autophagosomal degradation." *Autophagy* 7(12).

Rao, MS & Subbarao, V (1997). "Effect of dexamethasone on ciprofibrate-induced cell proliferation and peroxisome proliferation." *Fundam Appl Toxicol* 35(1): 78-83.

Rapp, S, Saffrich, R, Anton, M, Jakle, U, Ansorge, W, Gorgas, K & Just, WW (1996). "Microtubule-based peroxisome movement." *J Cell Sci* 109(Pt 4): 837-849.

Raychaudhuri, S & Prinz, WA (2008). "Nonvesicular phospholipid transfer between peroxisomes and the endoplasmic reticulum." *Proc Natl Acad Sci U S A* 105(41): 15785-15790.

Reddy, JK, Azarnoff, DL & Hignite, CE (1980). "Hypolipidaemic hepatic peroxisome proliferators form a novel class of chemical carcinogens." *Nature* 283(5745): 397-398.

Reddy, JK & Hashimoto, T (2001). "Peroxisomal beta-oxidation and peroxisome proliferator-activated receptor alpha: an adaptive metabolic system." *Annu Rev Nutr.* 21: 193-230.

Reddy, JK & Lalwani, ND (1983). "Carcinogenesis by hepatic peroxisome proliferators: Evaluation of the risk of hypolipidemic drugs and industrial plasticizers to humans." *CRC Critical Rev. Tox.* 12: 1-58.

Reddy, JK, Warren, JR, Reddy, MK & Lalwani, ND (1982). "Hepatic and renal effects of peroxisome proliferators: biological implications." *Ann N Y Acad Sci* 386: 81-110.

Rehling, P, Marzioch, M, Niesen, F, Wittke, E, Veenhuis, M & Kunau, WH (1996). "The import receptor for the peroxisomal targeting signal 2 (PTS2) in Saccharomyces cerevisiae is encoded by the PAS7 gene." *EMBO J* 15(12): 2901-2913.

Rehling, P, Skaletz-Rorowski, A, Girzalsky, W, Voorn-Brouwer, T, Franse, MM, Distel, B, Veenhuis, M, Kunau, WH & Erdmann, R (2000). "Pex8p, an intraperoxisomal peroxin of Saccharomyces cerevisiae required for protein transport into peroxisomes binds the PTS1 receptor pex5p." *J Biol Chem* 275(5): 3593-3602.

Reily, MM, Pantoja, C, Hu, X, Chinenov, Y & Rogatsky, I (2006). "The GRIP1:IRF3 interaction as a target for glucocorticoid receptor-mediated immunosuppression." *EMBO J* 25(1): 108-117.

Reumann, S, Quan, S, Aung, K, Yang, P, Manandhar-Shrestha, K, Holbrook, D, Linka, N, Switzenberg, R, Wilkerson, CG, Weber, AP, Olsen, LJ & Hu, J (2009). "In-depth proteome analysis of Arabidopsis leaf peroxisomes combined with in vivo subcellular targeting verification indicates novel metabolic and regulatory functions of peroxisomes." *Plant Physiol* 150(1): 125-143.

Reumann, S & Weber, AP (2006). "Plant peroxisomes respire in the light: Some gaps of the photorespiratory C(2) cycle have become filled-Others remain." *Biochim Biophys Acta* 1763(12): 1496-1510.

Rhodes, CJ & Anderson, RM (1996). "Power laws governing epidemics in isolated populations." *Nature* 381(6583): 600-602.

Rhodin, J (1954). "Correlation of ultrastructural organization and function in normal experimentally changed convoluted tubule cells of the mouse kidney.". Ph. D. thesis. *Stockholm*, Aktiebolaget Godvil.

Ribeiro, D, Castro, I, Fahimi, D & Schrader, M (2011). "Peroxisome morphology in pathology." *HISTOLOGY AND HISTOPATHOLOGY - Cellular and Molecular Biology* in press.

Rikova, K, Guo, A, Zeng, Q, Possemato, A, Yu, J, Haack, H, Nardone, J, Lee, K, Reeves, C, Li, Y, Hu, Y, Tan, Z, Stokes, M, Sullivan, L, Mitchell, J, Wetzel, R, Macneill, J, Ren, JM, Yuan, J, Bakalarski, CE, Villen, J, Kornhauser, JM, Smith, B, Li, D, Zhou, X, Gygi, SP, Gu, TL, Polakiewicz, RD, Rush, J & Comb, MJ (2007). "Global survey of phosphotyrosine signaling identifies oncogenic kinases in lung cancer." *Cell* 131(6): 1190-1203.

Rizzuto, R, Bernardi, P & Pozzan, T (2000). "Mitochondria as all-round players of the calcium game." *J Physiol* 529 Pt 1: 37-47.

Rodriguez-Rocha, H, Garcia-Garcia, A, Panayiotidis, MI & Franco, R (2011). "DNA damage and autophagy." *Mutat Res* 711(1-2): 158-166.

Rodriguez-Serrano, M, Romero-Puertas, MC, Sparkes, I, Hawes, C, del Rio, LA & Sandalio, LM (2009). "Peroxisome dynamics in Arabidopsis plants under oxidative stress induced by cadmium." *Free Radic Biol Med* 47(11): 1632-1639.

Roels, F, Espeel, M, Pauwels, M, De Craemer, D, Egberts, HJ & van der Spek, P (1991). "Different types of peroxisomes in human duodenal epithelium." *Gut* 32(8): 858-865.

Rojo, M, Legros, F, Chateau, D & Lombes, A (2002). "Membrane topology and mitochondrial targeting of mitofusins, ubiquitous mammalian homologs of the transmembrane GTPase Fzo." *J Cell Sci* 115(Pt 8): 1663-1674.

Rottensteiner, H, Kal, AJ, Filipits, M, Binder, M, Hamilton, B, Tabak, HF & Ruis, H (1996). "Pip2p: a transcriptional regulator of peroxisome proliferation in the yeast Saccharomyces cerevisiae." *Embo J.* 15(12): 2924-2934.

Rottensteiner, H, Kramer, A, Lorenzen, S, Stein, K, Landgraf, C, Volkmer-Engert, R & Erdmann, R (2004). "Peroxisomal membrane proteins contain common Pex19p-binding sites that are an integral part of their targeting signals (mPTS)." *Mol Biol Cell* 15: 3406-3417.

Rottensteiner, H, Stein, K, Sonnenhol, E & Erdmann, R (2003a). "Conserved function of pex11p and the novel pex25p and pex27p in peroxisome biogenesis." *Mol Biol Cell* 14(10): 4316-4328.

Rottensteiner, H, Wabnegger, L, Erdmann, R, Hamilton, B, Ruis, H, Hartig, A & Gurvitz, A (2003b). "Saccharomyces cerevisiae PIP2 mediating oleic acid induction and peroxisome proliferation is regulated by Adr1p and Pip2p-Oaf1p." *J Biol Chem.* 278(30): 27605-27611. Epub 22003 May 27614.

Rouiller, C & Jezequel, AM (1963). "Electron microscopy of the liver". *The Liver: Morphology, Biochemistry, Physiology*. Rouiller, C and Jezequel, AM. New York, Academic Press**:** 195-264.

Rucktaschel, R, Girzalsky, W & Erdmann, R (2011). "Protein import machineries of peroxisomes." *Biochim Biophys Acta* 1808(3): 892-900.

Rucktaschel, R, Halbach, A, Girzalsky, W, Rottensteiner, H & Erdmann, R (2010). "De novo synthesis of peroxisomes upon mitochondrial targeting of Pex3p." *Eur J Cell Biol* 89(12): 947-954.

Rucktaschel, R, Thoms, S, Sidorovitch, V, Halbach, A, Pechlivanis, M, Volkmer, R, Alexandrov, K, Kuhlmann, J, Rottensteiner, H & Erdmann, R (2009). "Farnesylation of pex19p is required for its structural integrity and function in peroxisome biogenesis." *J Biol Chem* 284(31): 20885-20896.

Sacksteder, KA & Gould, SJ (2000). "The genetics of peroxisome biogenesis." *Annu Rev Genet* 34: 623-652.

Sacksteder, KA, Jones, JM, South, ST, Li, X, Liu, Y & Gould, SJ (2000). "PEX19 binds multiple peroxisomal membrane proteins, is predominantly cytoplasmic, and is required for peroxisome membrane synthesis." *J Cell Biol* 148(5): 931-944.

Sakai, Y, Marshall, PA, Saiganji, A, Takabe, K, Saiki, H, Kato, N & Goodman, JM (1995). "The Candida boidinii peroxisomal membrane protein Pmp30 has a role in peroxisomal proliferation and is functionally homologous to Pmp27 from Saccharomyces cerevisiae." *J Bacteriol* 177(23): 6773-6781.

Santel, A, Frank, S, Gaume, B, Herrler, M, Youle, RJ & Fuller, MT (2003). "Mitofusin-1 protein is a generally expressed mediator of mitochondrial fusion in mammalian cells." *J Cell Sci* 116(Pt 13): 2763-2774.

Santel, A & Fuller, MT (2001). "Control of mitochondrial morphology by a human mitofusin." *J Cell Sci* 114(Pt 5): 867-874.

Santos, MJ, Imanaka, T, Shio, H, Small, GM & Lazarow, PB (1988). "Peroxisomal membrane ghosts in Zellweger syndrome--aberrant organelle assembly." *Science* 239(4847): 1536-1538.

Santos, MJ, Quintanilla, RA, Toro, A, Grandy, R, Dinamarca, MC, Godoy, JA & Inestrosa, NC (2005). "Peroxisomal proliferation protects from beta-amyloid neurodegeneration." *J Biol Chem.* 280(49): 41057-41068.

Saraya, R, Krikken, AM, Veenhuis, M & van der Klei, IJ (2011). "Peroxisome reintroduction in Hansenula polymorpha requires Pex25 and Rho1." *J Cell Biol* 193(5): 885-900.

Saraya, R, Veenhuis, M & van der Klei, IJ (2010). "Peroxisomes as dynamic organelles: peroxisome abundance in yeast." *FEBS J* 277(16): 3279-3288.

Schad, A, Fahimi, HD, Volkl, A & Baumgart, E (1996). "Nonradioactive in situ hybridization for detection of mRNAs encoding for peroxisomal proteins: heterogeneous hepatic lobular distribution after treatment with a single dose of bezafibrate." *J Histochem Cytochem.* 44(8): 825-834.

Scheele, GA (1993). "Regulation of pancreatic gene expression in response to hormones and nutritional substrates". *The Pancreas: Biology, Pathobiology and Disease, Second Edition.* Vay Liang, W. New York, Raven Press, Ltd.

Schettini, G, Govoni, S, Racchi, M & Rodriguez, G (2010). "Phosphorylation of APP-CTF-AICD domains and interaction with adaptor proteins: signal transduction and/or transcriptional role--relevance for Alzheimer pathology." *J Neurochem* 115(6): 1299-1308.

Schliebs, W & Kunau, WH (2006). "PTS2 co-receptors: diverse proteins with common features." *Biochim Biophys Acta* 1763(12): 1605-1612.

Schluter, A, Fourcade, S, Ripp, R, Mandel, JL, Poch, O & Pujol, A (2006). "The evolutionary origin of peroxisomes: an ER-peroxisome connection." *Mol Biol Evol* 23(4): 838-845.

Schneiter, R, Brugger, B, Sandhoff, R, Zellnig, G, Leber, A, Lampl, M, Athenstaedt, K, Hrastnik, C, Eder, S, Daum, G, Paltauf, F, Wieland, FT & Kohlwein, SD (1999). "Electrospray ionization tandem mass spectrometry (ESI-MS/MS) analysis of the lipid molecular species composition of yeast subcellular membranes reveals acyl chain-based sorting/remodeling of distinct molecular species en route to the plasma membrane." *J Cell Biol* 146(4): 741-754.

Schollenberger, L, Gronemeyer, T, Huber, CM, Lay, D, Wiese, S, Meyer, HE, Warscheid, B, Saffrich, R, Peranen, J, Gorgas, K & Just, WW (2010). "RhoA regulates peroxisome association to microtubules and the actin cytoskeleton." *PLoS One* 5(11): e13886.

Schonfeld, P & Wojtczak, L (2008). "Fatty acids as modulators of the cellular production of reactive oxygen species." *Free Radic Biol Med* 45(3): 231-241.

Schoonjans, K, Staels, B & Auwerx, J (1996). "Role of the peroxisome proliferator-activated receptor (PPAR) in mediating the effects of fibrates and fatty acids on gene expression." *J Lipid Res.* 37(5): 907-925.

Schrader, M (2001). "Tubulo-reticular clusters of peroxisomes in living COS-7 cells: dynamic behavior and association with lipid droplets." *J Histochem Cytochem* 49(11): 1421-1429.

Schrader, M (2006). "Shared components of mitochondrial and peroxisomal division." *Biochim Biophys Acta* 1763(5-6): 531-541.

Schrader, M, Baumgart, E, Volkl, A & Fahimi, HD (1994). "Heterogeneity of peroxisomes in human hepatoblastoma cell line HepG2. Evidence of distinct subpopulations." *Eur J Cell Biol* 64(2): 281-294.

Schrader, M, Bonekamp, NA & Islinger, M (2011). "Fission and proliferation of peroxisomes." *Biochim Biophys Acta*.

Schrader, M, Burkhardt, JK, Baumgart, E, Luers, G, Spring, H, Volkl, A & Fahimi, HD (1996a). "Interaction of microtubules with peroxisomes. Tubular and spherical peroxisomes in HepG2 cells and their alterations induced by microtubule-active drugs." *Eur J Cell Biol* 69(1): 24-35.

Schrader, M, Burkhardt, JK, Baumgart, E, Luers, G, Volkl, A & Fahimi, HD (1996b). "The importance of microtubules in determination of shape and intracellular distribution of peroxisomes." *Ann N Y Acad Sci* 804: 669-671.

Schrader, M & Fahimi, HD (2006). "Growth and division of peroxisomes." *Int Rev Cytol* 255: 237-290.

Schrader, M & Fahimi, HD (2008). "The peroxisome: still a mysterious organelle." *Histochem Cell Biol* 129(4): 421-440.

Schrader, M, King, SJ, Stroh, TA & Schroer, TA (2000). "Real time imaging reveals a peroxisomal reticulum in living cells." *J Cell Sci* 113(Pt 20): 3663-3671.

Schrader, M, Krieglstein, K & Fahimi, HD (1998a). "Tubular peroxisomes in HepG2 cells: selective induction by growth factors and arachidonic acid." *Eur J Cell Biol* 75(2): 87-96.

Schrader, M, Reuber, BE, Morrell, JC, Jimenez-Sanchez, G, Obie, C, Stroh, TA, Valle, D, Schroer, TA & Gould, SJ (1998b). "Expression of PEX11beta mediates peroxisome proliferation in the absence of extracellular stimuli." *J Biol Chem* 273(45): 29607-29614.

Schrader, M, Thiemann, M & Fahimi, HD (2003). "Peroxisomal motility and interaction with microtubules." *Microsc Res Tech* 61(2): 171-178.

Schrader, M, Wodopia, R & Fahimi, HD (1999). "Induction of tubular peroxisomes by UV irradiation and reactive oxygen species in HepG2 cells." *J Histochem Cytochem* 47(9): 1141-1148.

Schrader, M & Yoon, Y (2007). "Mitochondria and peroxisomes: Are the 'Big Brother' and the 'Little Sister' closer than assumed?" *Bioessays* 29(11): 1105-1114.

Schulz, JB, Matthews, RT, Klockgether, T, Dichgans, J & Beal, MF (1997). "The role of mitochondrial dysfunction and neuronal nitric oxide in animal models of neurodegenerative diseases." *Mol Cell Biochem* 174(1-2): 193-197.

Sell, H, Deshaies, Y & Richard, D (2004). "The brown adipocyte: update on its metabolic role." *Int J Biochem Cell Biol* 36(11): 2098-2104.

Sesaki, H & Jensen, RE (1999). "Division versus fusion: Dnm1p and Fzo1p antagonistically regulate mitochondrial shape." *J Cell Biol* 147(4): 699-706.

Shen, YQ & Burger, G (2009). "Plasticity of a key metabolic pathway in fungi." *Funct Integr Genomics* 9(2): 145-151.

Sheridan, C & Martin, SJ (2010). "Mitochondrial fission/fusion dynamics and apoptosis." *Mitochondrion* 10(6): 640-648.

Shibata, H, Kashiwayama, Y, Imanaka, T & Kato, H (2004). "Domain architecture and activity of human Pex19p, a chaperone-like protein for intracellular trafficking of peroxisomal membrane proteins." *J.Biol.Chem.* 279(37): 38486-38494.

Shimizu, M, Takeshita, A, Tsukamoto, T, Gonzalez, FJ & Osumi, T (2004). "Tissue-selective, bidirectional regulation of PEX11 alpha and perilipin genes through a common peroxisome proliferator response element." *Mol Cell Biol.* 24(3): 1313-1323.

Shiozawa, K, Konarev, PV, Neufeld, C, Wilmanns, M & Svergun, DI (2009). "Solution structure of human Pex5.Pex14.PTS1 protein complexes obtained by small angle X-ray scattering." *J Biol Chem* 284(37): 25334-25342.

Simon, M, Binder, M, Adam, G, Hartig, A & Ruis, H (1992). "Control of peroxisome proliferation in Saccharomyces cerevisiae by ADR1, SNF1 (CAT1, CCR1) and SNF4 (CAT3)." *Yeast.* 8(4): 303-309.

Sinclair, AM, Trobacher, CP, Mathur, N, Greenwood, JS & Mathur, J (2009). "Peroxule extension over ER-defined paths constitutes a rapid subcellular response to hydroxyl stress." *Plant J* 59(2): 231-242.

Singh, AK, Dhaunsi, GS, Gupta, MP, Orak, JK, Asayama, K & Singh, I (1994). "Demonstration of glutathione peroxidase in rat liver peroxisomes and its intraorganellar distribution." *Arch Biochem Biophys* 315(2): 331-338.

Singh, I (1996). "Mammalian peroxisomes: metabolism of oxygen and reactive oxygen species." *Ann N Y Acad Sci* 804: 612-627.

Smith, JJ, Marelli, M, Christmas, RH, Vizeacoumar, FJ, Dilworth, DJ, Ideker, T, Galitski, T, Dimitrov, K, Rachubinski, RA & Aitchison, JD (2002). "Transcriptome profiling to identify genes involved in peroxisome assembly and function." *J Cell Biol* 158(2): 259-271.

Snyder, WB, Koller, A, Choy, AJ & Subramani, S (2000). "The peroxin Pex19p interacts with multiple, integral membrane proteins at the peroxisomal membrane." *J.Cell Biol.* 149(6): 1171-1178.

Song, Z, Chen, H, Fiket, M, Alexander, C & Chan, DC (2007). "OPA1 processing controls mitochondrial fusion and is regulated by mRNA splicing, membrane potential, and Yme1L." *J Cell Biol* 178(5): 749-755.

Sornette, D (2006). "Critical Phenomena in Natural Sciences, Chaos, Fractals, Self-organization and Disorder: Concepts and Tools", *Springer, Berlin*.

Soukupova, M, Sprenger, C, Gorgas, K, Kunau, WH & Dodt, G (1999). "Identification and characterization of the human peroxin PEX3." *Eur J Cell Biol* 78(6): 357-374.

South, ST & Gould, SJ (1999). "Peroxisome synthesis in the absence of preexisting peroxisomes." *J Cell Biol* 144(2): 255-266.

South, ST, Sacksteder, KA, Li, X, Liu, Y & Gould, SJ (2000). "Inhibitors of COPI and COPII do not block PEX3-mediated peroxisome synthesis." *J Cell Biol* 149(7): 1345-1360.

Stahn, C, Lowenberg, M, Hommes, DW & Buttgereit, F (2007). "Molecular mechanisms of glucocorticoid action and selective glucocorticoid receptor agonists." *Mol Cell Endocrinol* 275(1-2): 71-78.

Steinberg, SJ, Dodt, G, Raymond, GV, Braverman, NE, Moser, AB & Moser, HW (2006). "Peroxisome biogenesis disorders." *Biochim Biophys Acta* 1763(12): 1733-1748.

Stier, H, Fahimi, HD, Van Veldhoven, PP, Mannaerts, GP, Volkl, A & Baumgart, E (1998). "Maturation of peroxisomes in differentiating human hepatoblastoma cells (HepG2): possible involvement of the peroxisome proliferator-activated receptor alpha (PPAR alpha)." *Differentiation* 64(1): 55-66.

Stohs, SJ & Bagchi, D (1995). "Oxidative mechanisms in the toxicity of metal ions." *Free Radic Biol Med* 18(2): 321-336.

Stolz, DB, Zamora, R, Vodovotz, Y, Loughran, PA, Billiar, TR, Kim, YM, Simmons, RL & Watkins, SC (2002). "Peroxisomal localization of inducible nitric oxide synthase in hepatocytes." *Hepatology* 36(1): 81-93.

Suzuki, M, Jeong, SY, Karbowski, M, Youle, RJ & Tjandra, N (2003). "The solution structure of human mitochondria fission protein Fis1 reveals a novel TPR-like helix bundle." *J Mol Biol* 334(3): 445-458.

Suzuki, M, Neutzner, A, Tjandra, N & Youle, RJ (2005). "Novel structure of the N terminus in yeast Fis1 correlates with a specialized function in mitochondrial fission." *J Biol Chem* 280(22): 21444-21452.

Svoboda, DJ & Azarnoff, DL (1966). "Response of hepatic microbodies to a hypolipidemic agent, ethyl chlorophenoxyisobutyrate (CPIB)." *J Cell Biol* 30(2): 442-450.

Swarovsky, B, Steinhilber, W, Scheele, GA & Kern, HF (1988). "Coupled induction of exocrine proteins and intracellular compartments involved in the secretory pathway in AR4-2J cells by glucocorticoids." *Eur J Cell Biol* 47(1): 101-111.

Sweitzer, SM & Hinshaw, JE (1998). "Dynamin undergoes a GTP-dependent conformational change causing vesiculation." *Cell* 93(6): 1021-1029.

Swinkels, BW, Gould, SJ, Bodnar, AG, Rachubinski, RA & Subramani, S (1991). "A novel, cleavable peroxisomal targeting signal at the amino-terminus of the rat 3-ketoacyl-CoA thiolase." *Embo J.* 10(11): 3255-3262.

Tabak, HF, Hoepfner, D, Zand, A, Geuze, HJ, Braakman, I & Huynen, MA (2006). "Formation of peroxisomes: present and past." *Biochim Biophys Acta* 1763(12): 1647-1654.

Takei, K, Haucke, V, Slepnev, V, Farsad, K, Salazar, M, Chen, H & De Camilli, P (1998). "Generation of coated intermediates of clathrin-mediated endocytosis on protein-free liposomes." *Cell* 94(1): 131-141.

Takei, K, Slepnev, VI, Haucke, V & De Camilli, P (1999). "Functional partnership between amphiphysin and dynamin in clathrin-mediated endocytosis." *Nat Cell Biol* 1(1): 33-39.

Tam, YY, Fagarasanu, A, Fagarasanu, M & Rachubinski, RA (2005). "Pex3p Initiates the Formation of a Preperoxisomal Compartment from a Subdomain of the Endoplasmic Reticulum in Saccharomyces cerevisiae." *J Biol Chem* 280(41): 34933-34939.

Tam, YY & Rachubinski, RA (2002). "Yarrowia lipolytica cells mutant for the PEX24 gene encoding a peroxisomal membrane peroxin mislocalize peroxisomal proteins and accumulate membrane structures containing both peroxisomal matrix and membrane proteins." *Mol Biol Cell.* 13(8): 2681-2691.

Tam, YY, Torres-Guzman, JC, Vizeacoumar, FJ, Smith, JJ, Marelli, M, Aitchison, JD & Rachubinski, RA (2003). "Pex11-related proteins in peroxisome dynamics: a role for the novel peroxin Pex27p in controlling peroxisome size and number in Saccharomyces cerevisiae." *Mol Biol Cell* 14(10): 4089-4102.

Tanabe, Y, Maruyama, J, Yamaoka, S, Yahagi, D, Matsuo, I, Tsutsumi, N & Kitamoto, K (2011). "Peroxisomes are involved in biotin biosynthesis in Aspergillus and Arabidopsis." *J Biol Chem* 286(35): 30455-30461.

Tanaka, A, Kobayashi, S & Fujiki, Y (2006). "Peroxisome division is impaired in a CHO cell mutant with an inactivating point-mutation in dynamin-like protein 1 gene." *Exp Cell Res* 312: 1671-1684.

Tanaka, A, Okumoto, K & Fujiki, Y (2003). "cDNA cloning and characterization of the third isoform of human peroxin Pex11p." *Biochem Biophys Res Commun.* 300(4): 819-823.

Terlecky, SR, Koepke, JI & Walton, PA (2006). "Peroxisomes and aging." *Biochim Biophys Acta* 1763(12): 1749-1754.

Terlecky, SR, Nuttley, WM, McCollum, D, Sock, E & Subramani, S (1995). "The Pichia pastoris peroxisomal protein PAS8p is the receptor for the C-terminal tripeptide peroxisomal targeting signal." *EMBO J* 14(15): 3627-3634.

Thiemann, M, Schrader, M, Volkl, A, Baumgart, E & Fahimi, HD (2000). "Interaction of peroxisomes with microtubules. In vitro studies using a novel peroxisome-microtubule binding assay." *Eur J Biochem* 267(20): 6264-6275.

Thoms, S & Erdmann, R (2005). "Dynamin-related proteins and Pex11 proteins in peroxisome division and proliferation." *Febs J* 272(20): 5169-5181.

Titorenko, VI & Mullen, RT (2006). "Peroxisome biogenesis: the peroxisomal endomembrane system and the role of the ER." *J Cell Biol.* 174(1): 11-17.

Titorenko, VI & Rachubinski, RA (1998). "Mutants of the yeast Yarrowia lipolytica defective in protein exit from the endoplasmic reticulum are also defective in peroxisome biogenesis." *Mol Cell Biol* 18(5): 2789-2803.

Titorenko, VI & Rachubinski, RA (2000). "Peroxisomal membrane fusion requires two AAA family ATPases, Pex1p and Pex6p." *J Cell Biol* 150(4): 881-886.

Titorenko, VI & Rachubinski, RA (2001a). "Dynamics of peroxisome assembly and function." *Trends Cell Biol* 11(1): 22-29.

Titorenko, VI & Rachubinski, RA (2001b). "The life cycle of the peroxisome." *Nat Rev Mol Cell Biol* 2(5): 357-368.

Titorenko, VI & Terlecky, SR (2011). "Peroxisome metabolism and cellular aging." *Traffic* 12(3): 252-259.

Tolbert, NE (1981). "Metabolic pathways in peroxisomes and glyoxysomes." *Annu Rev Biochem* 50: 133-157.

Tondera, D, Grandemange, S, Jourdain, A, Karbowski, M, Mattenberger, Y, Herzig, S, Da Cruz, S, Clerc, P, Raschke, I, Merkwirth, C, Ehses, S, Krause, F, Chan, DC, Alexander, C, Bauer, C, Youle, R, Langer, T & Martinou, JC (2009). "SLP-2 is required for stress-induced mitochondrial hyperfusion." *EMBO J* 28(11): 1589-1600.

Toro, AA, Araya, CA, Cordova, GJ, Arredondo, CA, Cardenas, HG, Moreno, RE, Venegas, A, Koenig, CS, Cancino, J, Gonzalez, A & Santos, MJ (2009). "Pex3p-dependent peroxisomal biogenesis initiates in the endoplasmic reticulum of human fibroblasts." *J Cell Biochem* 107(6): 1083-1096.

Towbin, H, Staehelin, T & Gordon, J (1992). "Electrophoretic transfer of proteins from polyacrylamide gels to nitrocellulose sheets: procedure and some applications. 1979." *Biotechnology* 24: 145-149.

Tsukamoto, T, Yokota, S & Fujiki, Y (1990). "Isolation and characterization of Chinese hamster ovary cell mutants defective in assembly of peroxisomes." *J Cell Biol* 110(3): 651-660.

Tuttle, DL & Dunn, WA, Jr. (1995). "Divergent modes of autophagy in the methylotrophic yeast Pichia pastoris." *J Cell Sci* 108 (Pt 1): 25-35.

Van Ael, E & Fransen, M (2006). "Targeting signals in peroxisomal membrane proteins." *Biochim Biophys Acta* 1763(12): 1629-1638.

van den Bosch, H, Schutgens, RB, Wanders, RJ & Tager, JM (1992). "Biochemistry of peroxisomes." *Annu Rev Biochem* 61: 157-197.

van der Klei, I & Veenhuis, M (2002). "Peroxisomes: flexible and dynamic organelles." *Curr Opin Cell Biol* 14(4): 500-505.

van der Klei, IJ & Veenhuis, M (2006). "PTS1-independent sorting of peroxisomal matrix proteins by Pex5p." *Biochim Biophys Acta* 1763(12): 1794-1800.

van der Klei, IJ, Yurimoto, H, Sakai, Y & Veenhuis, M (2006). "The significance of peroxisomes in methanol metabolism in methylotrophic yeast." *Biochim Biophys Acta* 1763(12): 1453-1462.

van der Zand, A, Braakman, I & Tabak, HF (2010). "Peroxisomal membrane proteins insert into the endoplasmic reticulum." *Mol Biol Cell* 21(12): 2057-2065.

van Leyen, K, Duvoisin, RM, Engelhardt, H & Wiedmann, M (1998). "A function for lipoxygenase in programmed organelle degradation." *Nature* 395(6700): 392-395.

van Roermund, CW, Visser, WF, Ijlst, L, van Cruchten, A, Boek, M, Kulik, W, Waterham, HR & Wanders, RJ (2008). "The human peroxisomal ABC half transporter ALDP functions as a homodimer and accepts acyl-CoA esters." *FASEB J* 22(12): 4201-4208.

Veenhuis, M, Kiel, JA & Van Der Klei, IJ (2003). "Peroxisome assembly in yeast." *Microsc Res Tech.* 61(2): 139-150.

Veenhuis, M, Mateblowski, M, Kunau, WH & Harder, W (1987). "Proliferation of microbodies in Saccharomyces cerevisiae." *Yeast* 3(2): 77-84.

Veenhuis, M, Sulter, G, van der Klei, I & Harder, W (1989). "Evidence for functional heterogeneity among microbodies in yeasts." *Arch Microbiol.* 151(2): 105-110.

Viswanathan, GM, Bartumeus, F, Buldyrev, SV, Catalan, J, Fulco, UL, Havlin, S, da Luz, MGE, Lyra, ML, Raposo, EP & Stanley, HE (2002). "Levy flight random searches in biological phenomena." *Physica A* 314(1-4): 208-213.

Vizeacoumar, FJ, Torres-Guzman, JC, Tam, YY, Aitchison, JD & Rachubinski, RA (2003). "YHR150w and YDR479c encode peroxisomal integral membrane proteins involved in the regulation of peroxisome number, size, and distribution in Saccharomyces cerevisiae." *J Cell Biol.* 161(2): 321-332.

Völkl, A, Baumgart, E & Fahimi, HD (1996). "Isolation and characterization of peroxisomes.". *Subcellular Fractionation: A Practical Approach*. Graham, J and Rickwood, D. Oxford, U. K., Oxford University Press**:** 143-167.

Voncken, F, van Hellemond, JJ, Pfisterer, I, Maier, A, Hillmer, S & Clayton, C (2003). "Depletion of GIM5 causes cellular fragility, a decreased glycosome number, and reduced levels of ether-linked phospholipids in trypanosomes." *J Biol Chem* 278(37): 35299-35310.

Voorn-Brouwer, T, Kragt, A, Tabak, HF & Distel, B (2001). "Peroxisomal membrane proteins are properly targeted to peroxisomes in the absence of COPI- and COPII-mediated vesicular transport." *J Cell Sci* 114(Pt 11): 2199-2204.

Wakabayashi, J, Zhang, Z, Wakabayashi, N, Tamura, Y, Fukaya, M, Kensler, TW, Iijima, M & Sesaki, H (2009). "The dynamin-related GTPase Drp1 is required for embryonic and brain development in mice." *J Cell Biol* 186(6): 805-816.

Walton, PA, Hill, PE & Subramani, S (1995). "Import of stably folded proteins into peroxisomes." *Mol.Biol.Cell* 6(6): 675-683.

Wanders, RJ (2004). "Peroxisomes, lipid metabolism, and peroxisomal disorders." *Mol Genet Metab* 83(1-2): 16-27.

Wanders, RJ, Ferdinandusse, S, Brites, P & Kemp, S (2010). "Peroxisomes, lipid metabolism and lipotoxicity." *Biochim Biophys Acta* 1801(3): 272-280.

Wanders, RJ & Waterham, HR (2005). "Peroxisomal disorders I: biochemistry and genetics of peroxisome biogenesis disorders." *Clin Genet.* 67(2): 107-133.

Wanders, RJ & Waterham, HR (2006a). "Peroxisomal disorders: the single peroxisomal enzyme deficiencies." *Biochim Biophys Acta* 1763(12): 1707-1720.

Wanders, RJA & Waterham, HR (2006b). "Biochemistry of mammalian peroxisomes revisited." *Annu. Rev. Biochem.* 75: 295-332.

Wang, H & Joseph, JA (1999). "Quantifying cellular oxidative stress by dichlorofluorescein assay using microplate reader." *Free Radic Biol Med* 27(5-6): 612-616.

Waterham, HR, Koster, J, van Roermund, CW, Mooyer, PA, Wanders, RJ & Leonard, JV (2007). "A lethal defect of mitochondrial and peroxisomal fission." *N Engl J Med* 356(17): 1736-1741.

Wessel, D & Flugge, UI (1984). "A method for the quantitative recovery of protein in dilute solution in the presence of detergents and lipids." *Anal.Biochem.* 138(1): 141-143.

Westermann, B (2010). "Mitochondrial fusion and fission in cell life and death." *Nat Rev Mol Cell Biol* 11(12): 872-884.

Wiebel, FF & Kunau, WH (1992). "The Pas2 protein essential for peroxisome biogenesis is related to ubiquitin-conjugating enzymes." *Nature* 359(6390): 73-76.

Wiemer, EA, Wenzel, T, Deerinck, TJ, Ellisman, MH & Subramani, S (1997). "Visualization of the peroxisomal compartment in living mammalian cells: dynamic behavior and association with microtubules." *J Cell Biol* 136(1): 71-80.

Wiese, S, Gronemeyer, T, Ofman, R, Kunze, M, Grou, CP, Almeida, JA, Eisenacher, M, Stephan, C, Hayen, H, Schollenberger, L, Korosec, T, Waterham, HR, Schliebs, W, Erdmann, R, Berger, J, Meyer, HE, Just, W, Azevedo, JE, Wanders, RJ & Warscheid, B (2007). "Proteomic characterization of mouse kidney peroxisomes by tandem mass spectrometry and protein correlation profiling." *Mol Cell Proteomics* 6(12): 2045-2057.

Wikstrom, AC (2003). "Glucocorticoid action and novel mechanisms of steroid resistance: role of glucocorticoid receptor-interacting proteins for glucocorticoid responsiveness." *J Endocrinol* 178(3): 331-337.

Williams, C, van den Berg, M, Geers, E & Distel, B (2008). "Pex10p functions as an E3 ligase for the Ubc4p-dependent ubiquitination of Pex5p." *Biochem Biophys Res Commun* 374(4): 620-624.

Williams, C, van den Berg, M, Sprenger, RR & Distel, B (2007). "A conserved cysteine is essential for Pex4p-dependent ubiquitination of the peroxisomal import receptor Pex5p." *J Biol Chem* 282(31): 22534-22543.

Wriessnegger, T, Gubitz, G, Leitner, E, Ingolic, E, Cregg, J, de la Cruz, BJ & Daum, G (2007). "Lipid composition of peroxisomes from the yeast Pichia pastoris grown on different carbon sources." *Biochim Biophys Acta* 1771(4): 455-461.

Yamamoto, K & Fahimi, HD (1987). "Three-dimensional reconstruction of a peroxisomal reticulum in regenerating rat liver: evidence of interconnections between heterogeneous segments." *J Cell Biol* 105(2): 713-722.

Yang, X, Purdue, PE & Lazarow, PB (2001). "Eci1p uses a PTS1 to enter peroxisomes: either its own or that of a partner, Dci1p." *Eur J Cell Biol* 80(2): 126-138.

Yano, T, Oku, M, Akeyama, N, Itoyama, A, Yurimoto, H, Kuge, S, Fujiki, Y & Sakai, Y (2010). "A novel fluorescent sensor protein for visualization of redox states in the cytoplasm and in peroxisomes." *Mol Cell Biol* 30(15): 3758-3766.

Yokota, S (1993). "Formation of autophagosomes during degradation of excess peroxisomes induced by administration of dioctyl phthalate." *Eur J Cell Biol* 61(1): 67-80.

Yonekawa, S, Furuno, A, Baba, T, Fujiki, Y, Ogasawara, Y, Yamamoto, A, Tagaya, M & Tani, K (2011). "Sec16B is involved in the endoplasmic reticulum export of the peroxisomal membrane biogenesis factor peroxin 16 (Pex16) in mammalian cells." *Proc Natl Acad Sci U S A* 108(31): 12746-12751.

Yoon, Y (2004). "Sharpening the scissors: mitochondrial fission with aid." *Cell Biochem Biophys* 41(2): 193-206.

Yoon, Y, Krueger, EW, Oswald, BJ & McNiven, MA (2003). "The mitochondrial protein hFis1 regulates mitochondrial fission in mammalian cells through an interaction with the dynamin-like protein DLP1." *Mol Cell Biol* 23(15): 5409-5420.

Yoon, Y, Pitts, KR, Dahan, S & McNiven, MA (1998). "A novel dynamin-like protein associates with cytoplasmic vesicles and tubules of the endoplasmic reticulum in mammalian cells." *J Cell Biol* 140(4): 779-793.

Yoon, Y, Pitts, KR & McNiven, MA (2001). "Mammalian dynamin-like protein DLP1 tubulates membranes." *Mol Biol Cell* 12(9): 2894-2905.

Yoshikawa, S, Shinzawa-Itoh, K, Nakashima, R, Yaono, R, Yamashita, E, Inoue, N, Yao, M, Fei, MJ, Libeu, CP, Mizushima, T, Yamaguchi, H, Tomizaki, T & Tsukihara, T (1998). "Redox-coupled crystal structural changes in bovine heart cytochrome c oxidase." *Science* 280(5370): 1723-1729.

Zaar, K, Volkl, A & Fahimi, HD (1991). "Purification of marginal plates from bovine renal peroxisomes: identification with L-alpha-hydroxyacid oxidase B." *J Cell Biol* 113(1): 113-121.

Zhang, X-C & Hu, J-P (2008). "FISSION1A and FISSION1B Proteins Mediate the Fission of Peroxisomes and Mitochondria in Arabidopsis." *Mol Plant* 1(6): 1036-1047.

Zhang, X & Hu, J (2010). "The Arabidopsis chloroplast division protein DYNAMIN-RELATED PROTEIN5B also mediates peroxisome division." *Plant Cell* 22(2): 431-442.

Zhao, J, Liu, T, Jin, S, Wang, X, Qu, M, Uhlen, P, Tomilin, N, Shupliakov, O, Lendahl, U & Nister, M (2011). "Human MIEF1 recruits Drp1 to mitochondrial outer membranes and promotes mitochondrial fusion rather than fission." *EMBO J* 30(14): 2762-2778.

Zorzano, A, Liesa, M, Sebastian, D, Segales, J & Palacin, M (2010). "Mitochondrial fusion proteins: dual regulators of morphology and metabolism." *Semin Cell Dev Biol* 21(6): 566-574.

8 APPENDIX

8.1 SUPPLEMENTARY MATERIAL

8.1.1 Supplementary Information

8.1.1.1 Theoretical Model explaining power law behaviour

A simple model could explain why the number of contacts lasting for a time τ decays as a power law: $N(\tau) \sim \tau^{-3}$. Consider that two interacting organelles have a probability $p \times dt$ of terminating their interaction between τ and $t + dt$. Then, the probability that the interaction is terminated only after $\tau = ndt$ units of time is $(1 - pdt)^{n-1} pdt$. To calculate $N(\tau)$ a sum over all types of organelle interactions has to be considered. Writing $P = pdt$ we have: $N(\tau) \sim \int f_p (1-P)^{n-1} PdP$. Here f_p is the number of organelles interacting with a probability p of terminating their contact. Assuming that $f_p \sim p$ as there are more organelles performing fast bindings available for making new bindings, then the integral can be straightforwardly integrated by parts. If the lower bound starts near zero, than the integral diverges as τ^{-3} and the cumulative frequency distribution decays as τ^{-2}, as observed. If the lower bound is a finite number (for instance, 0.1), then $N(\tau)$ falls exponentially to zero. Hence, to explain the observed data, one needs to assume that organelle interactions differ considerably in contact lifetimes. In particular, some contacts have to be extremely stable, i.e. $p \cong 0.$ These results require further studies, because many different models have been shown to display power law behavior, as discussed in (Sornette, 2006). If further experiments reveal that power law exponent is slightly different from the one we found, then more elaborate theoretical models could be developed, for instance, taking into account the impact of the cytoskeleton on organelle traffic (Kulic et al., 2008). This may have an impact on the weighting factor f_p considered above. Alternatively, it could also be necessary to describe the details of inter-organelle interactions, which may entail a diversity of mechanisms. The later mechanisms, however, should only provide corrections to the exponent we found, which relates to the complexity of peroxisomal interactions.

8.1.1.2 Results Phospho-Screen HsPex11pβ

NetPhos 2.0		DISPHOS		NetPhosK		ScanProSite		Scansite Motif Scan	
Position	Score	Position	Score	Position	Score (*Motif*)	Position	*Motif*	Position	Score (*Motif*)
S11	0.949	**S154**	0.75	**S70**	0.84 (*PKC*)	**S70**	*PKC phospho site*	**T178**	0.171% (*Erk1*)
S38	0.981	**S160**	0.801	**S154**	0.85 (*PKC*)	**S123**		**I220**	0.144% (*Erk bdg*)
S70	0.982	**S 168**	0.866			**S154**			
Y140	0.917	**T178**	0.793						

KinasePhos 2.0		ELM	
Position	Score (*Motif*)	Position	*Motif*
S11	0.955 (*ATM*)	**S8**	*PKA*
S38	0.953 (*ATM*)	**S11**	*CK1* *PIKK*
S50	0.972 (*ATM*)	**S54**	*CK1*
S53	0.973 (*ATM*)	**T149**	*CK1*
S70	0.909 (*ATM*)	**S150/S151**	*PLK*
S78	0.960 (*ATM*)	**S154**	*GSK3*
S150	0.982 (*ATM*)	**T178**	*ProDKinase*
S151	0.983 (*ATM*)	**S246**	*CK1*
S154	0.908 (*ATM*) 0.897 (*GSK3*)		
S160	0.894 (*CK1*)		
S168	0.956 (*ATM*)		
S243	0.940 (*ATM*)		
S246	0.918 (*ATM*)		

8.1.2 Supplementary Figures

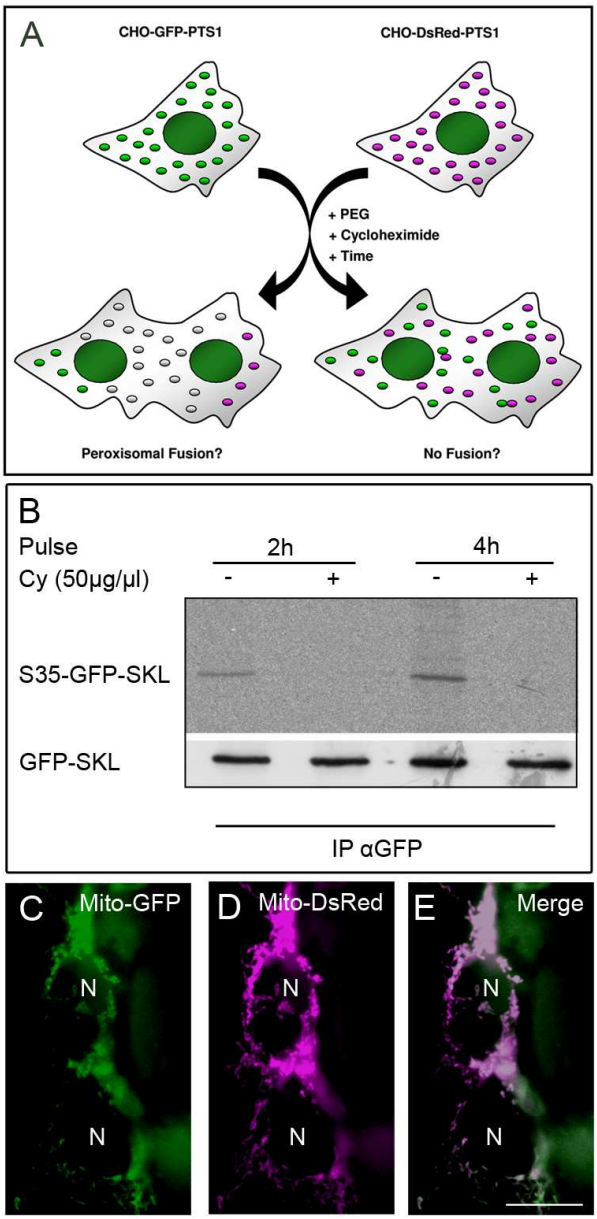

Fig. 3.1 (alternative): Establishing a peroxisomal *in vivo* fusion assay. (A) Principle of the peroxisomal *in vivo* fusion assay established in this study. CHO cell lines either stably expressing a matrix-targeted peroxisomal GFP (CHO-GFP-PTS1) or DsRed construct (CHO-DsRed-PTS1) were generated. To assess peroxisomal fusion, the cell lines were mixed and fused using PEG-6000. Hybridoma cells were incubated at 37° C in the presence of cycloheximide to avoid false positive events by peroxisomal protein import. The appearance of yellow peroxisomes (marker for co-localization) and peroxisomal dynamics were investigated by fluorescence microscopy and live cell imaging.
(B) Protein translation is efficiently blocked over the course of the observation period. Control (-) and cycloheximide (Cy, +)-blocked CHO-GFP-PTS1 cells were pulse labeled with S^{35}-methionine for 2 and 4 hours, respectively. Cell lysates were split and subjected to immunoprecipitation with anti-GFP. One set of samples was subjected to SDS-PAGE and autoradiographs were developed by PhosphoImaging (upper panel). As a loading control, the other set of samples was separated by SDS-PAGE, immunoblotted and incubated with anti-GFP (lower panel).
(C - E) Mitochondrial fusion in CHO cells. As a positive control, CHO-K1 cells were transiently transfected with Mito-GFP (C) and Mito-DsRed (D), respectively. Differentially labeled cells were subjected to the *in vivo* fusion assay. After 4 hours, cells were fixed and processed for fluorescence microscopy. Overlay of fluorescent signals from (C) and (D) is shown in (E). N, nucleus. Bar, 20µm.

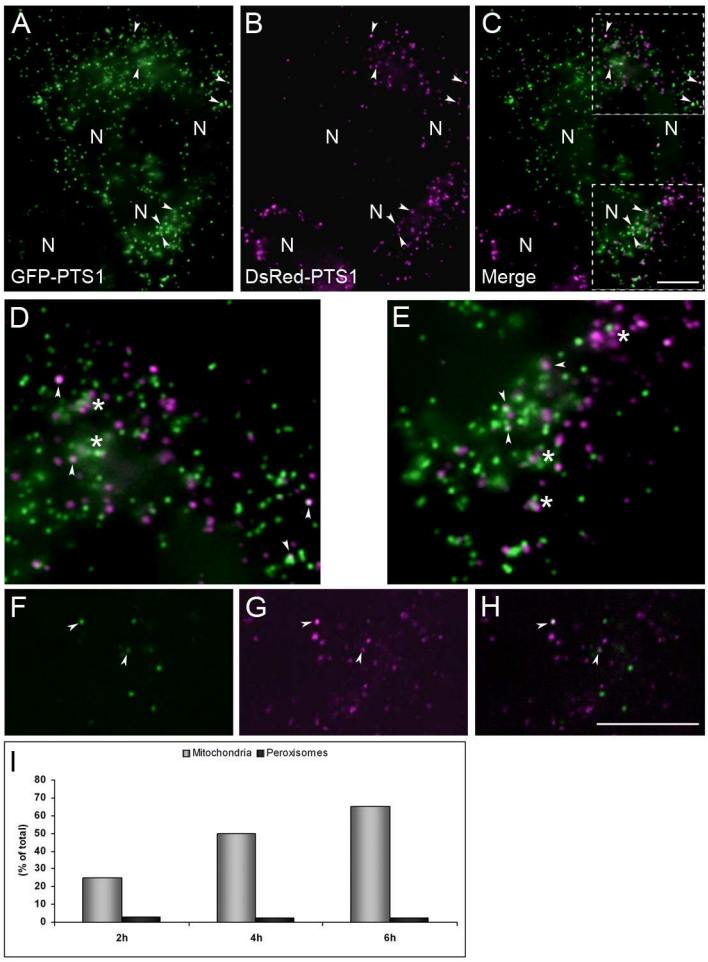

Fig. 3.2 (alternative): Peroxisomal matrix signals co-localize in fixed cells.
CHO-GFP-PTS1 (A, F) and CHO-DsRed-PTS1 cells (B, G) were mixed and subjected to the peroxisomal *in vivo* fusion assay. Hybridoma cells were incubated for 4 hours, fixed and processed for epifluorescence (A – E) or confocal microscopy (F – H). Higher magnification images of the boxed regions in (C) are shown in (D) and (E). Arrowheads point to yellow peroxisomes. Asterisks highlight red and green peroxisomes engaged in intimate contacts.
(I) Quantitative analysis of mitochondrial and putative peroxisomal matrix intermixing (yellow organelles). CHO cell lines either transfected with differential mitochondrial or peroxisomal markers were subjected to the *in vivo* fusion assay. After the indicated time points, cells were fixed and processed for fluorescence microscopy. The percentage of yellow peroxisomes (% of total organelle number per hybridoma cell) at different time points of a representative experiment is shown. To assess mitochondrial fusion, the overall number of hybridoma cells with yellow mitochondria (full fusion) was determined. N, nucleus. Bars, 20µm.

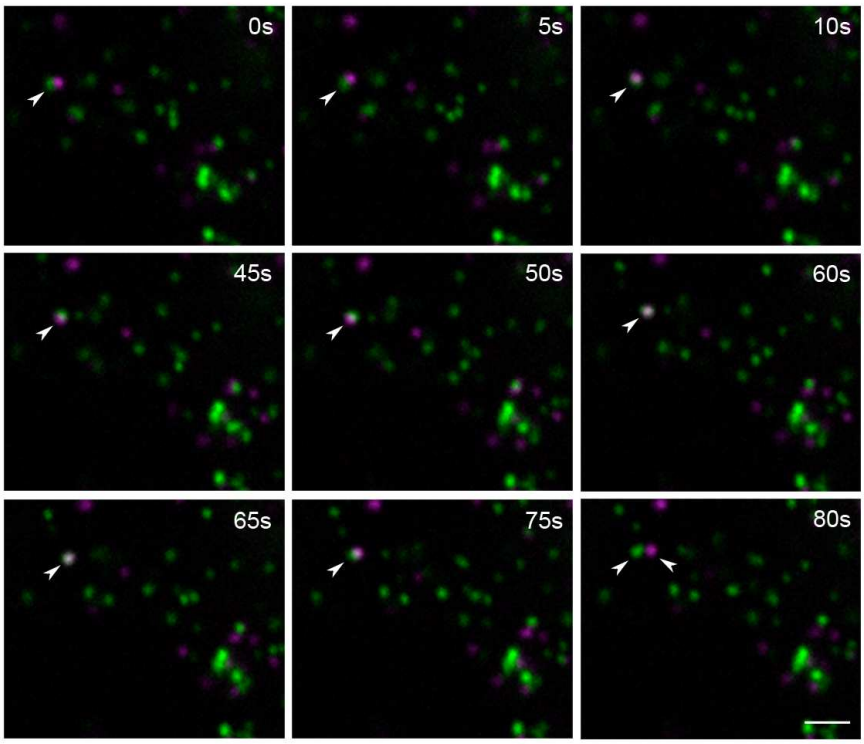

Fig. 3.3 (alternative): Time-lapse confocal microscopy reveals that peroxisomes interact extensively, but do not exchange matrix proteins.
CHO-GFP-PTS1 and CHO-DsRed-PTS1 cells were subjected to the peroxisomal *in vivo* fusion assay. Hybridoma cells were allowed to recover for 30 minutes and were then analyzed by time-lapse confocal microscopy. Images were taken every 5 seconds using 488 and 561 laser lines, respectively (see also Movies S1 and S2). Arrows indicate interaction events. Note the close (60 – 65s), but transient (80s) overlap of differentially labelled peroxisomes. Bar, 5µm.

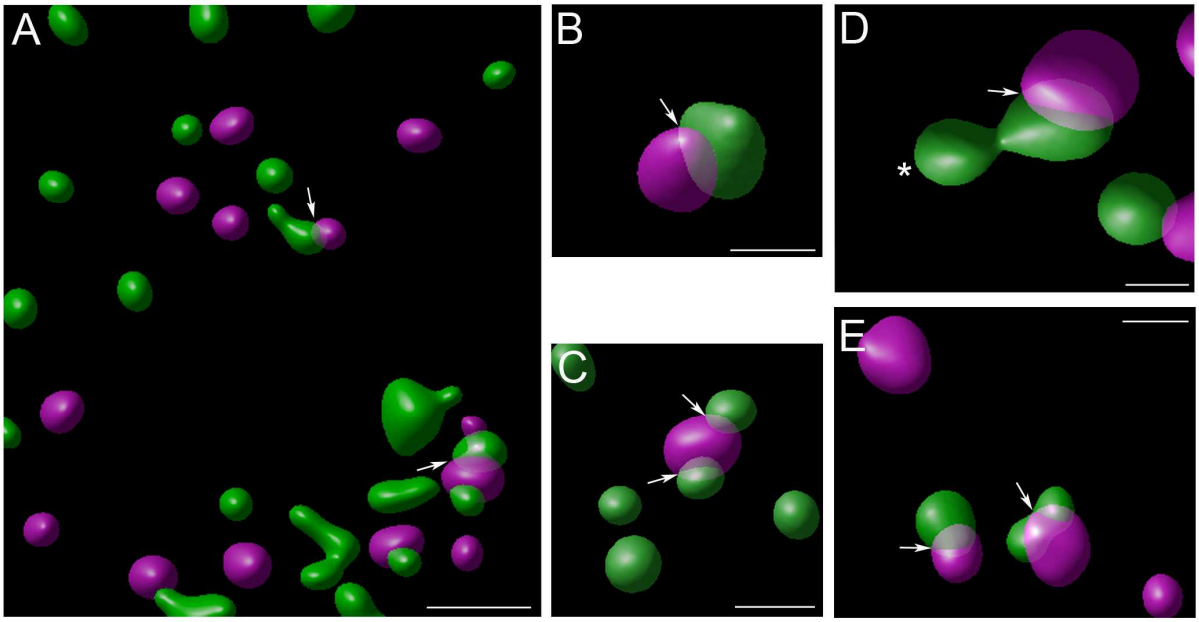

Fig. 3.4 (alternative): High resolution images of peroxisomal interactions.
Differentially labelled CHO cell lines were subjected to the in vivo peroxisomal fusion assay and processed for confocal microscopy. Image deconvolution was performed using Huygens Professional software. A selection of peroxisomal interaction events is shown (A-E). Arrows highlight overlap of markers; a potential fission event is labelled by an asterisk. Note the close, intimate contacts between interacting peroxisomes. In (E, peroxisomes on the right) one peroxisome appears to embrace another (estimated colocalisation of signals: approx. 50% (green) and 24% (red)). Data analysis revealed a mean distance between interacting peroxisomes of about 0.07 µm +/- 0.029 µm. As data evaluation only allowed for the calculation of distances between the centre of one mass to the nearest surface point (but not for the surface-to-surface distance), the actual distance is most probably even smaller. Bars, 1µm (A); 0.25µm (B); 0.5µm (C-E).

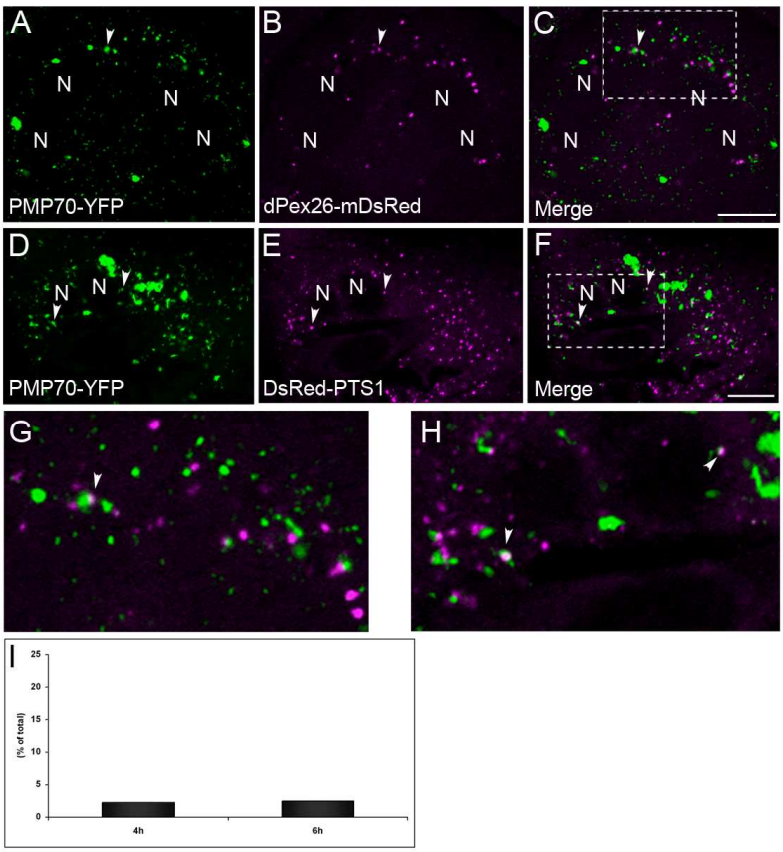

Fig. 3.8 (alternative): Peroxisomes do not exchange membrane components.
CHO-K1 cells stably expressing the peroxisomal membrane markers PMP70-YFP (A) or DsRed-dPex26 (B) were subjected to the peroxisomal *in vivo* fusion assay and assayed for the exchange of membrane components (C). In a second set of experiments, CHO-PMP70-YFP (D) and CHO-DsRed-PTS1 cells (E) were fused. Overlay of signals is shown in (F). Higher magnification images of (C) and (F) are shown in (G) and (H), respectively. Arrowheads point to intimate interactions. (I) Quantitative analysis of putative peroxisomal membrane intermixing. The percentage of yellow organelles (% of total organelle number per hybridoma cell) at different time points of a representative experiment is shown. N, nucleus. Bars, 20µm.

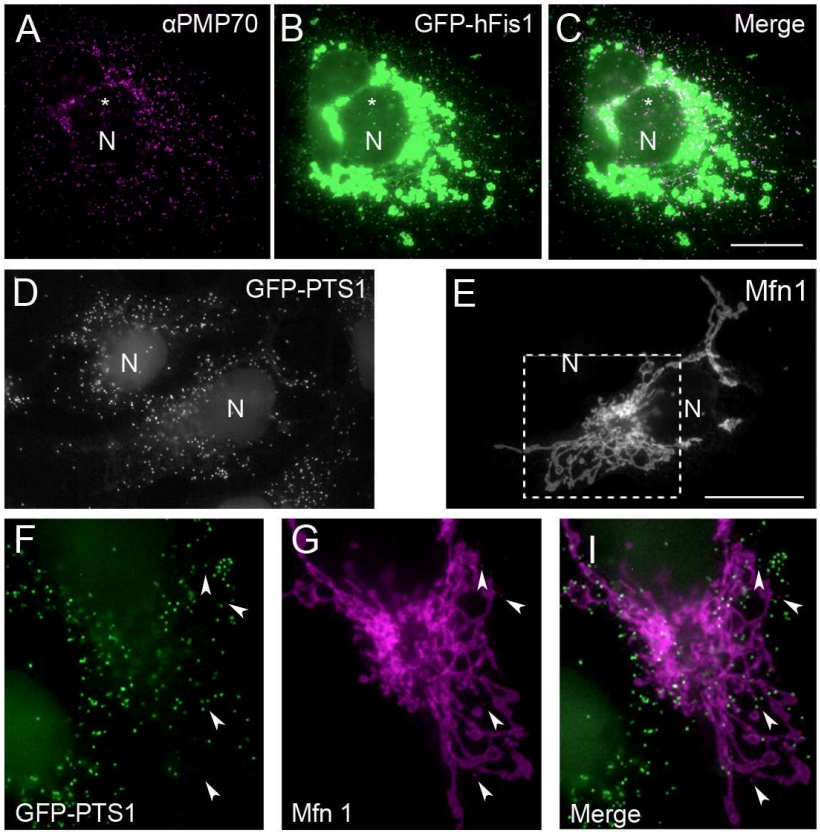

Fig. 3.10 (alternative): The mitochondrial fusion protein Mfn1 does not localize to peroxisomes.
(A–C) Fis1 is dually targeted to peroxisomes and mitochondria. As a positive control, COS-7 cells were transfected with GFP-hFis1 (B) and processed for immunofluorescence with anti-PMP70 (A). (C) Overlay of (A, B). Note the localization of GFP-Fis1 at peroxisomes (asterisks) and clustering of mitochondria.
(D–G) Mfn1 does not localize to peroxisomes. COS-7 cells stably expressing GFP-PTS1 (D) were transfected with Mfn1-myc (E) and processed for immunofluorescence using anti-myc. Higher magnification image of the boxed area in (E) is shown in (F–H). Overlay (Merge) of (F, G) is shown in (H). Note that although small punctuate Mfn1 positive structures can be seen, there is no co-localization with peroxisomal markers (arrowheads).
N, nucleus. Bars, 20µm.

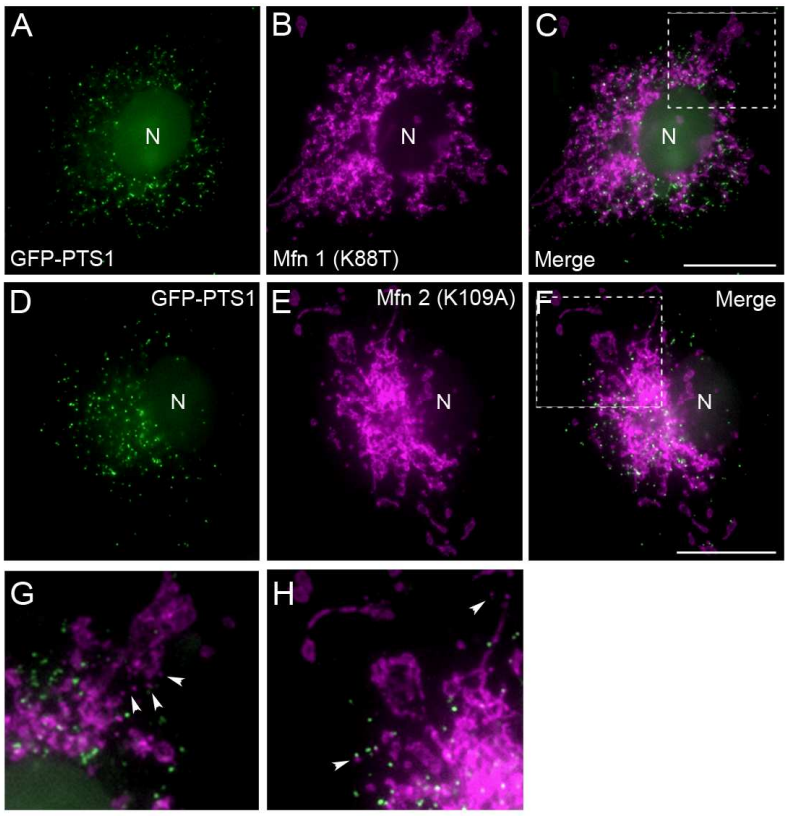

Fig. 3.11 (alternative): Expression of activity-deficient mitofusin variants does not affect peroxisome morphology.
COS-7 cells stably expressing GFP-PTS1 (A, D) were transfected with activity-deficient variants of Mfn1 (K38T) (B) and Mfn2 (K109A) (E). After 24 hours, cells were processed for immunofluorescence using anti-myc antibodies. Overlays (Merge) of (A, B) and (D, E) are shown in (C) and (F). Higher magnification images of boxed areas in (C) and (F) are shown in (G) and (H). Asterisks highlight mitofusin-positive punctuate structures that do not co-localize with peroxisomal markers. Note that although mitochondria are prone to fragmentation upon overexpression of Mfn mutants, peroxisomal morphology remains unaffected. N, nucleus. Bars, 20µm.

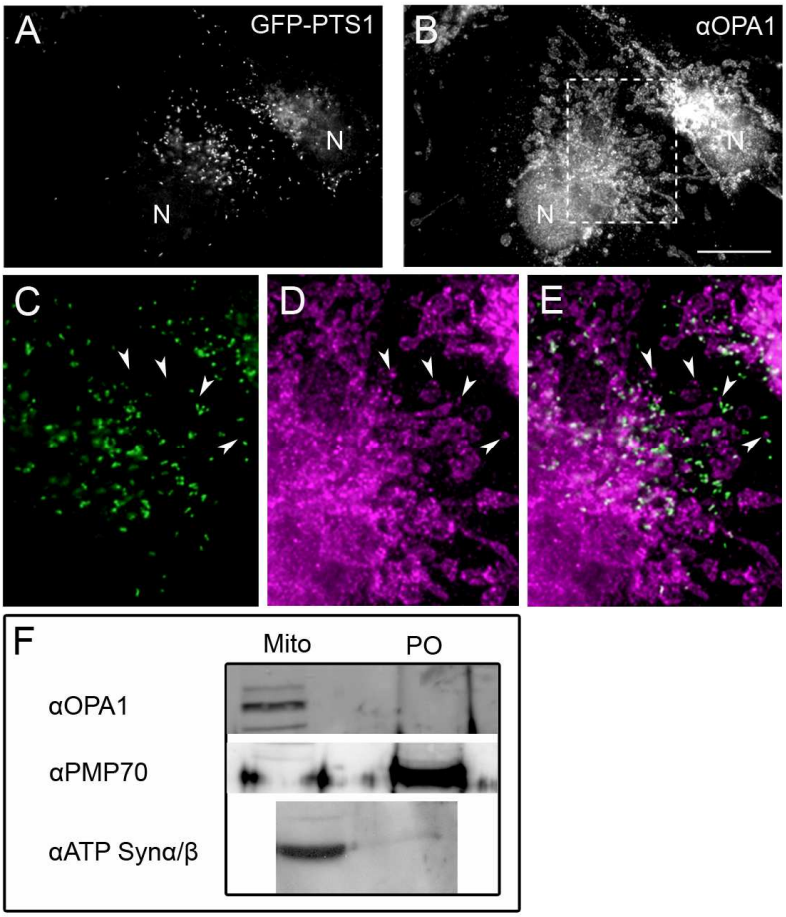

Fig. 3.12: The mitochondrial inner membrane fusion protein OPA1 does not localize to peroxisomes.
OPA1 is not a peroxisomal protein. (A–E) COS-7 cells stably expressing GFP-PTS1 (A) processed for immunofluorescence using anti-OPA1 (B). Higher magnification images of the boxed area in (B) are shown in (C–E). (E) Overlay (Merge) of (C, D). Note that some punctuate structures are positive for OPA1, but do not co-localize with the peroxisomal marker. N, nucleus. Bar, 20µm.
(F) Highly purified peroxisomes (PO) and mitochondria (Mito) were separated by 12.5% SDS-PAGE and immunoblotted using anti-OPA1, anti-PMP70 and anti-ATP synthase antibodies. Equal amounts of protein (50µg) were applied. Multiple OPA1 bands correspond to different splice variants.

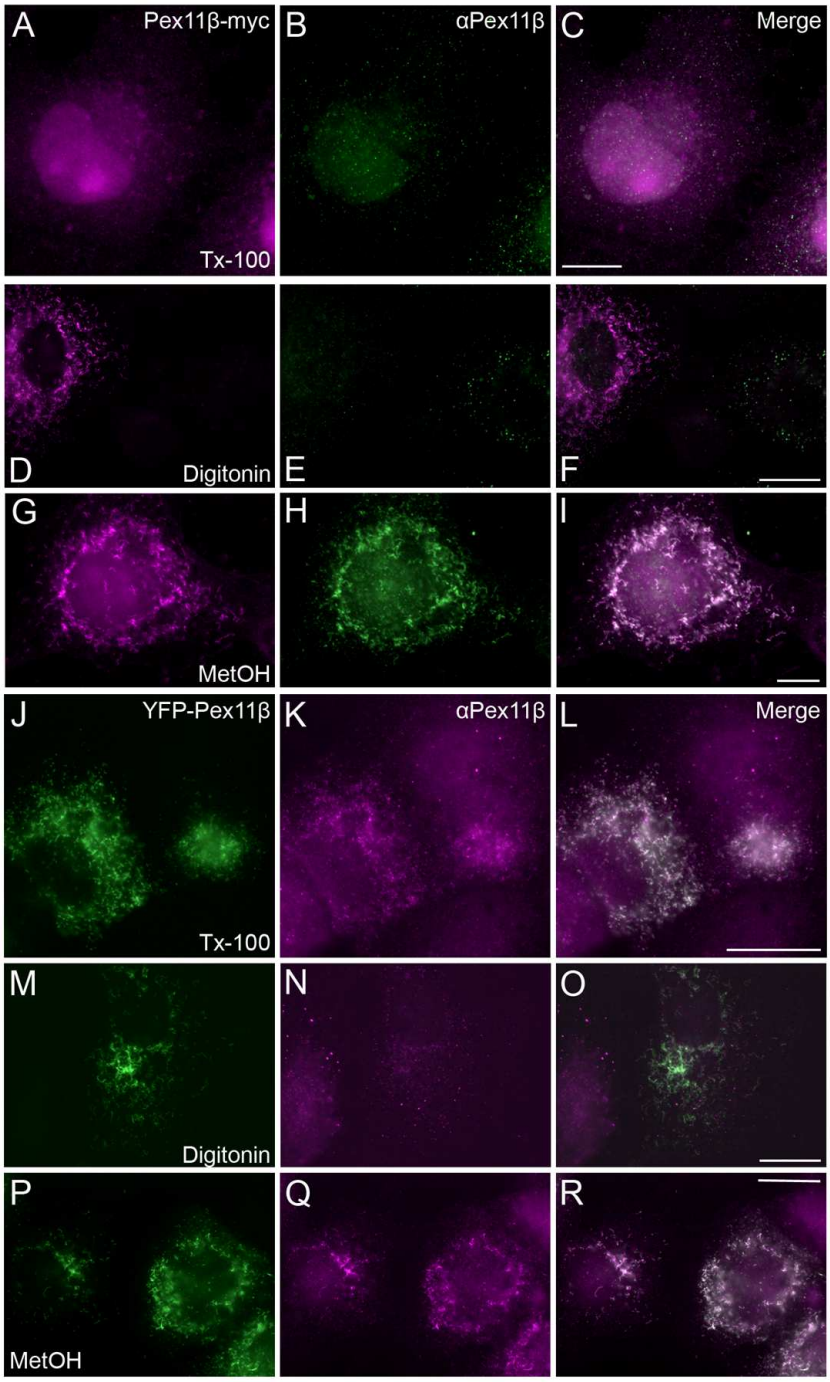

Fig. 3.16 (alternative): The Pex11pβ antibody only recognizes its epitope after peroxisomal membrane permeabilization.
Cos-7 cells were transfected with either Pex11b-myc (A-I) or YFP-Pex11b (J – R) and fixed after 24h. Membrane (and organelle membrane) permeabilisation was achieved by incubating fixed cells with either 0.2 % Tx100 (A – C; J – L), 25µg/ml digitonin (D – F; M – O) or Methanol (MetOH; G – I; P – R), before immunostaining against the myc epitope and an internal part of Pex11β (A – I) or Pex11β alone (J – R) was performed.
Note that Pex11β-myc is absent/extracted from the peroxisomal membrane after Tx100 permeabilisation (A – C), while YFP-Pex11pβ is retained after fixation (J – L).
Bars, 20µm.

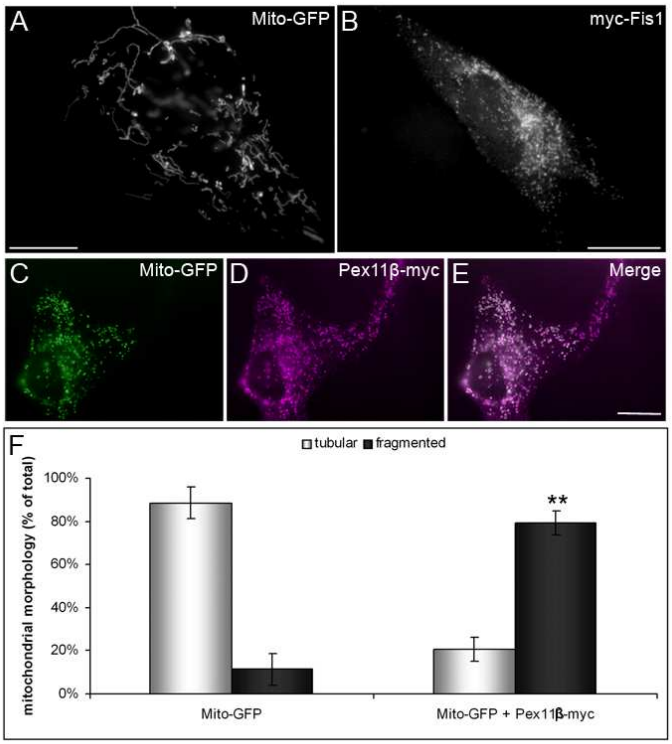

Fig. 3.19.: In ΔPEX19 cells, Pex11pβ mistargets to mitochondria and leads to their fragmentation.
(A, B) ΔPEX19 fibroblasts were transfected with either the mitochondrial matrix marker Mito-GFP (A) or myc-Fis1, a tail-anchored protein known to fragment mitochondria (B). Cells were fixed and in the case of (B) processed for immunofluorescence against the myc epitope.
(C-E) ΔPex19 fibroblasts were co-transfected with Mito-GFP and Pex11β-myc and processed for immunofluorescence against the myc epitope. Merge of signals is seen in E. Bars, 20µm.
(F) For statistical analysis, ΔPex19 fibroblasts were either transfected with Mito-GFP alone or co-transfected with Mito-GFP and Pex11β-myc and processed for immunofluorescence. Mitochondrial morphology was assessed to be either tubular (A) or fragmented (B) and 100 cells/coverslip (2 coverslips/condition) were grouped accordingly. Data is shown as means +/- S.D.

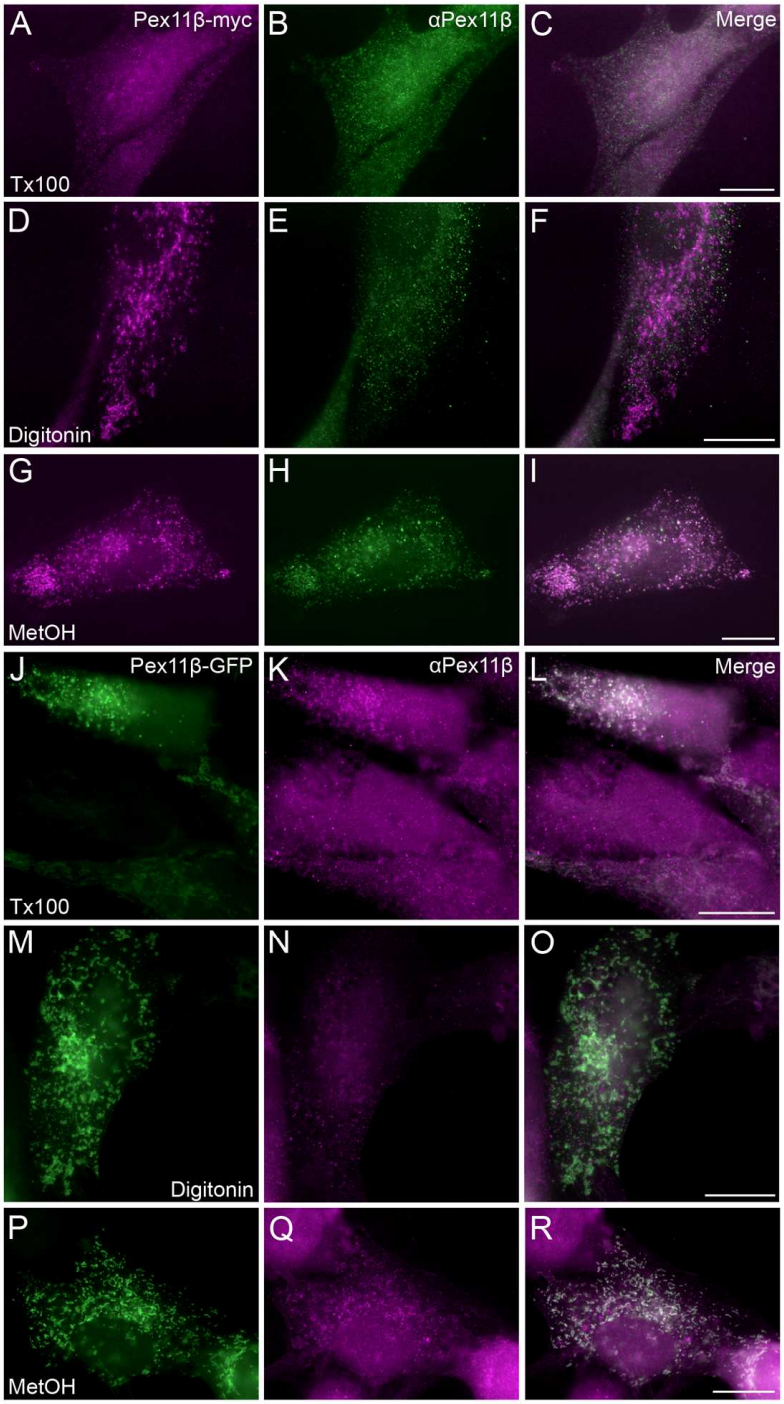

Fig. 3.21: Pex11pβ retains its topology upon mistargeting to mitochondria.
(A-I) ΔPex19 fibroblasts were transfected with Pex11βb-myc, fixed after 24 hours and permeabilized using either Tx100 (A-C), digitonin (D-F) or methanol (G-I). Subsequently, they were co-stained with antibodies against the myc epitope (A, D, G) and Pex11β (B, E, H).
(J-R) In a similar approach, ΔPex19 fibroblasts were transfected with Pex11β-GFP before permeabilizion using either Tx100 (J-L), digitonin (M-O) or methanol (P-R).
Subsequently, staining against Pex11β was performed (K, N, Q).
Bars, 20µm

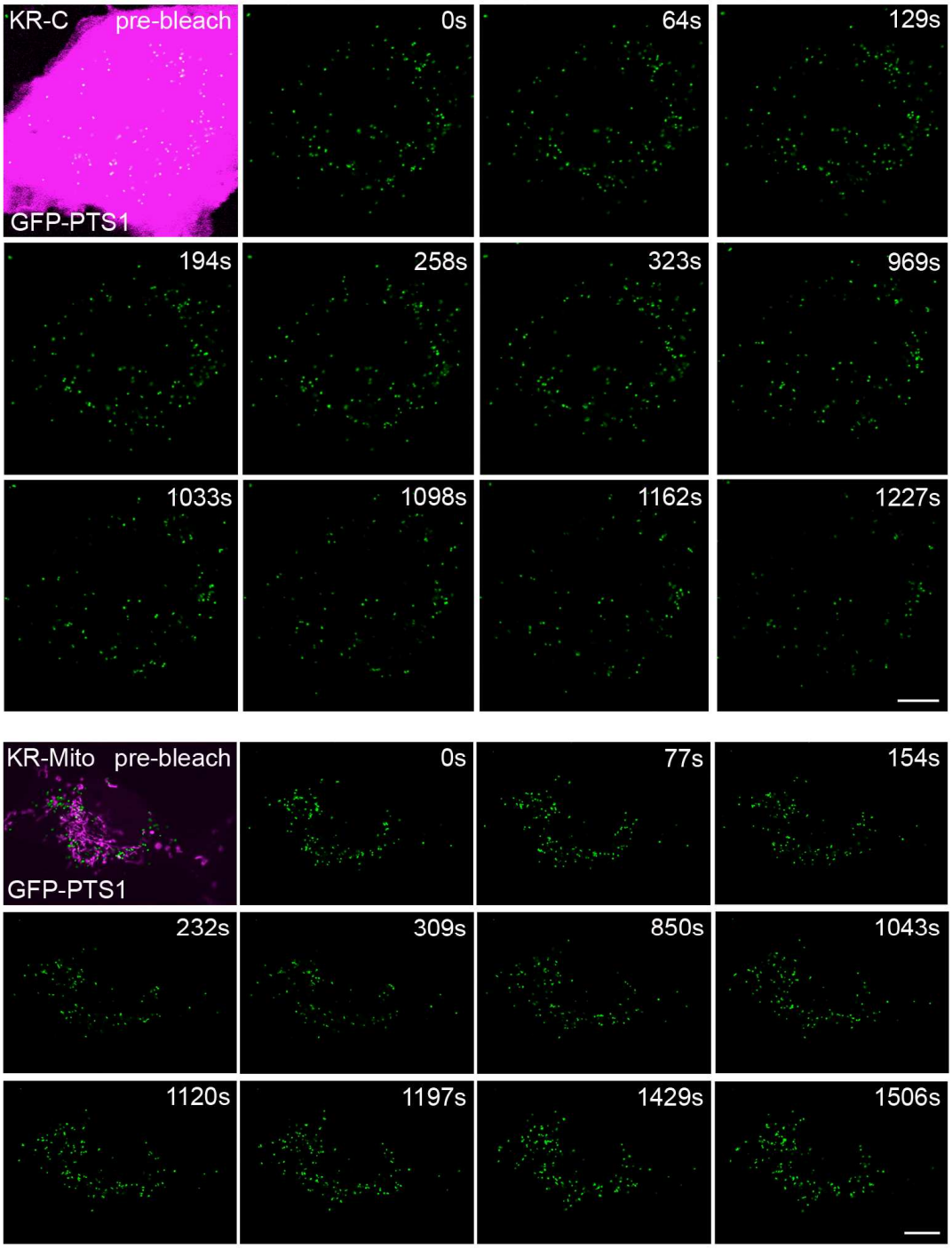

Fig. 3.29 (alternative): Activation of KillerRed targeted to the cytosol or mitochondria does not alter peroxisome dynamics.
COS-7-GFP-PTS1 cells were transfected with either KillerRed-C (upper panel) or KillerRed-Mito (lower panel). 24 hours later, cells were subjected to live cell imaging using a LSM 510 Meta confocal microscope. Before activation of KillerRed images of single cells were taken (Pre-bleach). After photobleaching of KillerRed, images were collected every 60 seconds for 30-90 minutes.
Bars, 20µm.

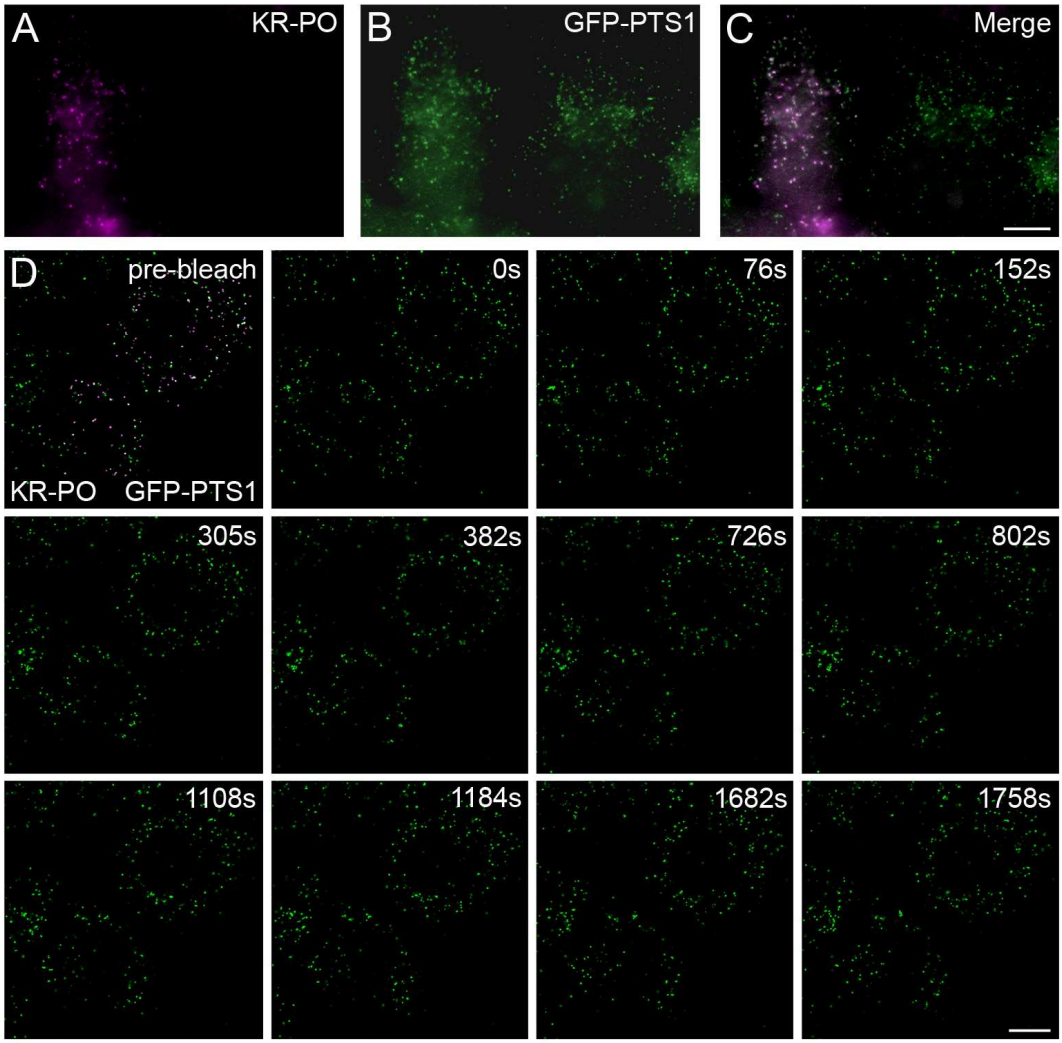

Fig. 3.30 (alternative): Activation of peroxisomal KillerRed does not affect peroxisome dynamics.
(A-C) COS-7-GFP-PTS1 (B) cells were transfected with KillerRed-PO (KR-PO, A). 24 hours later, cells were fixed and mounted for epifluorescence microscopy. Merge of signal is shown in C.
(D) KR-PO was transfected into COS-7-GFP-PTS1 cells. 24 hours later, cells were subjected to live cell imaging using a LSM 510 Meta confocal microscope. Before activation of KillerRed images of single cells were taken (Pre-bleach). After photobleaching of KillerRed, images were collected every 60 seconds for 30-90 minutes.
Bars, 20µm.

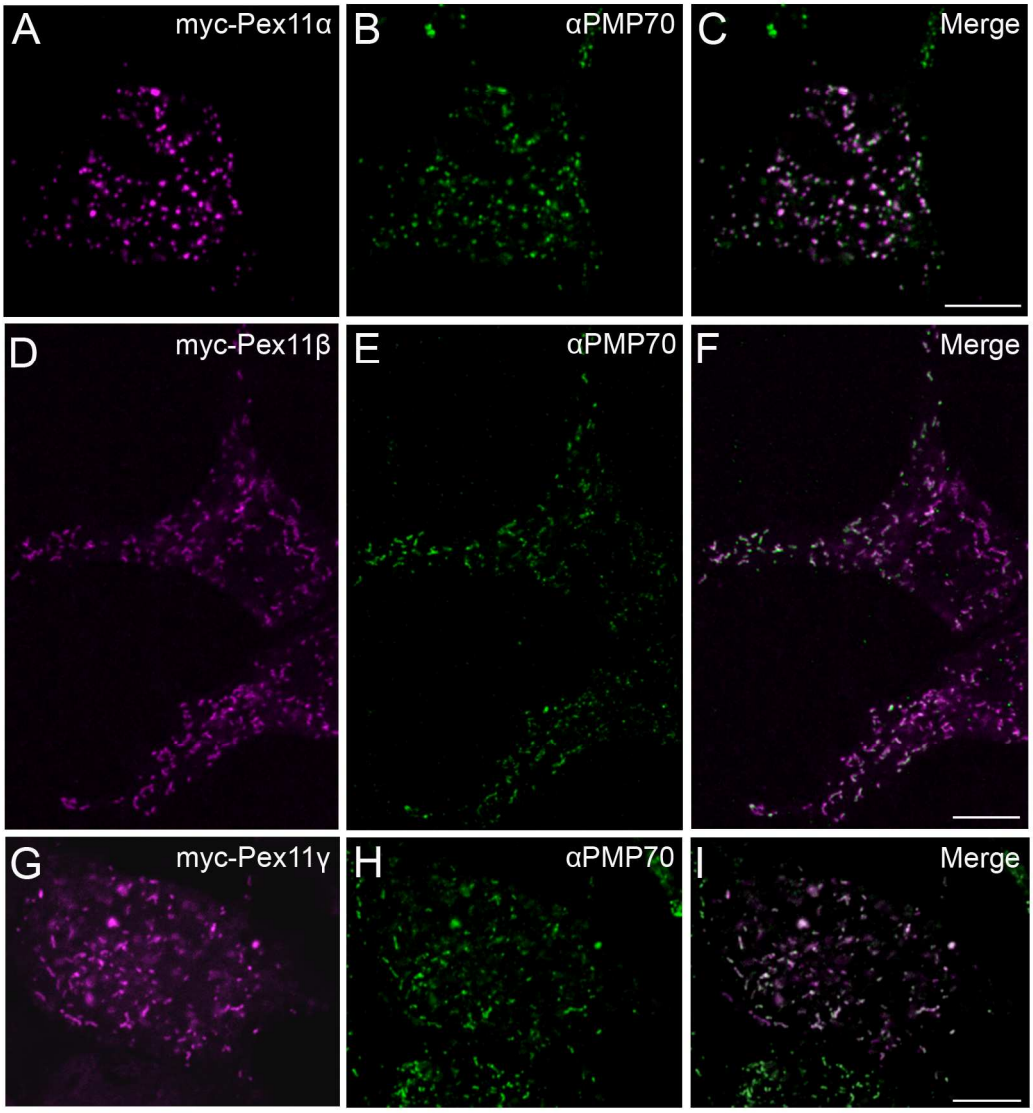

Fig. 3.34 (alternative): Overexpression of the 3 human isoforms of Pex11 in AR42J cells.
AR42J cells were transfected with myc-tagged variants of the 3 human isoforms of Pex11, Pex11α (A-C), Pex11β (D-F) and Pex11γ (G-I). After 24 hours, cells were fixed and processed for immunofluorescence against the myc epitope (A, D, G) and the peroxisomal membrane protein PMP70 (B, E, H). Images were taken using a LSM 510 Meta confocal microscope. Merge of signals is shown in C, F and I, respectively.
Bars, 20µm.

8.1.3 Supplementary Movies

Supplementary Movie S1. Peroxisomal interaction in vivo.
CHO-GFP-PTS1 and CHO-DsRed-PTS1 cells were subjected to the peroxisomal *in vivo* fusion assay (see Materials and Methods). After cell fusion, cells were incubated for 1 hour at 37°C and then analyzed by time-lapse confocal microscopy. Images were acquired every 5 seconds, shown here as two frames per second. Arrows indicate interaction events.

Supplementary Movie S2. Peroxisomal interaction in vivo.
See legend Supplementary Movie S1.

Supplementary Movie S3. Peroxisomal fission in time-lapse confocal microscopy.
COS-7 cells were transfected with YFP-Pex11β to stimulate peroxisome elongation and subsequent DLP1-dependent fission and analyzed by time-lapse confocal microscopy. Note the membrane extension/elongation of a spherical peroxisome and the subsequent division into two spherical organelles (arrowheads). Higher magnification view of the selected peroxisome is shown in the upper left corners. Bar, 10µm.

8.2 LIST OF ABBREVIATIONS

µ	micro
aa	amino acids
AAA-ATPase	ATPase associated with various cellular activities
ABC	ATP binding cassette
AGT	alanine: glyoxylate aminotransferase
ALD	adrenoleukodystrophy
Amp	ampicillin
AOX	Acyl-CoA oxidase
APS	ammonium persulfate
APX	ascorbate peroxidase
At, A. thaliana	*Arabidopsis thaliana*
ATP	adenosine triphosphate
bp	base pair
BSA	bovine serum albumin
C. elegans	*Caenorhabditis elegans*
CAT	catalase
cDNA	complementary deoxyribonucleic acid
Ci	Curie
CL	cardiolipin
CLSM	Confocal laser scanning microscopy
CMV	cytomegalovirus
DAB	3, 3'-Diaminebenzidine tetrahydrochloride
DaM	Donkey anti-mouse
DaR	Donkey anti-rabbit
DBP	D-bifunctional protein
DCF	dichlorofluorescein
DEAE	diethylaminoethyl
DEPC	diethylpyrocarbonate
dH20	destilled water
DHAP	dihydroxy acetone phosphate
DHCA	dihydroxycholestanoic acid
DLP	Dynamin-like protein
DMEM	Dulbecco`s modified Eagle´s medium
DMSO	dimethylsulfoxid
DNA	deoxyribonucleic acid
dNTP	desoxynucleoside triphosphate
Drp	Dynamin-related protein
DsRed	*Discosoma species* Red
dT	desoxythymidine
DTT	dithiothreitol
E. coli	*Escherischia coli*
e.g.	exemplia gratia (for example)
ECL	enhanced Chemiluminescence
EDTA	ethylenediaminetetraacetic acid
EM	electron microscopy
ER	endoplasmic reticulum
Et al	et alii (and others)
EtBr	ethidium bromide
ETC	electron transfer chain

EtOH	Ethanol
ETYA	5 ,8, 11, 14-Eicosatetraynoic Acid
F	Farad
FAD	flavin-adenine-dinucleotide
FCS	fetal calf serum
FITC	Fluorescein isothiocyanate
FOY	Ethyl-4-(6 - Guadininohexanoyloxy)-benzoate
Fzo	fuzzy onions
g	x 9,81 m/s²
G	Gauche
g	gram
GaM	Goat anti-mouse
GAPDH	glycerinaldehyde-3-phosphate dehydrogenase
GaR	Goat anti-rabbit
GED	GTPase effector domain
GFP	Green Fluorescent Protein
GSH	glutathione
GTP	guanosine triphosphate
HBS	Hepes buffered saline
Hepes	4-(2-Hydroxyethyl)-1-piperazinethansulfonic acid
Hp, H. polymorpha	*Hansenula polymorpha*
HRP	horseradish peroxidase
Hs, H. sapiens	*Homo sapiens*
i.e.	id est (which means)
IF	immunofluorescence
IMM	inner mitochondrial membrane
IMS	intermembrane space
IP	immunoprecipitation
Kana	Kanamycin
kb	kilo base pairs
kD	kilodalton
l	liter
LB	Luria - Bertani
m	metre
M	Molar
mA	milliampere
mc	monoclonal
Mff	mitochondrial fission factor
Mfn	mitofusin
Mgm	mitochondrial genome maintenance
Min	minutes
Mito	mitochondria
mL	milliliter
mM	millimolar
MOPS	3-(N-Morpholino)-propanesulfonic acid
mPTS	peroxisomal membrane targeting signal
mRNA	messenger RNA
ms	millisecond
mtDNA	mitochondrial DNA
n	nano
Nc, N. Crassa	*Neurospora crassa*

nm	nanometre
OD	optical density
OMM	outer mitochondrial membrane
OPA1	Optic atrophy 1
ORE	oleate response element
P. chrysogenum	*Penicillum chrysogenum*
P. pastoris	*Pichia pastoris*
PAA	polyacrylamide
PAGE	polyacrylamide gel electrophoresis
PAS	protein A sepharose
PBD	peroxisome biogenesis disorder
PBS	phosphat buffered saline
PC	phosphatidylcholine
pc	polyklonal
PCR	polymerase chain reaction
PE	phosphatidylethanolamine;
PED	peroxisomal enzyme deficiency
PEG	polyethyleneglykol
PEI	polyethylenimine
Pex	peroxin
pFA	para-formaldehyde
PH	Pleckstrin homology
PI	phosphatidylinositol
PMP	peroxisomal membrane protein
PMSF	phenylmethylsulfonylfluoride
PO	peroxisome
PP	peroxisome proliferator
PPAR	peroxisome proliferator activated receptor
PPRE	peroxisome proliferator respose element
PRD	proline-rich domain
PS	phosphatidylserine
PTS	peroxisomal targeting sequence
RE	restriction endonuclease
RING	Really interesting new gene
RNA	ribonucleic acid
ROS	reactive oxygen species
rpm	rotations per minute
RT	reverse transcription
RT	room temperature
s	second
Sc, S. cerevisiae	*Saccharomyces cerevisiae*
SD	standard deviation
SDS	sodiumdodecyl sulfate
SH3	src homology 3
siRNA	small interfering ribonucleic acid
SOD	superoxide dismutase
SRP	signal recognition particle
TAE	Tris/Acetate/EDTA
Tb, T. brucei	*Trypanosoma brucei*
TBS	Tris buffered saline
TBS-T	TBS-Tween

TE	Tris / EDTA
TEMED	tetramethylendiamine
THCA	trihydroxycholestanoic acid
TM	transmembrane domain
TOM	translocator of outer membrane
TPR	tetratricopeptide repeats
Tris	Tris- (Hydroxyl) - aminomethane
TRITC	tetramethylrhodamine isothiocyanate
Tx100	Triton - X -100
U	Units
UT	untransfected
UV	ultraviolet
v / v	volume per volume
V	Volt
VLCFA	very long chain fatty acid
Vol	Volumen
w / v	weight per volume
WD	tryptophan-aspartic acid
WT	wild type
X-ALD	X-chromosomal linked adrenoleukodystrophy
YFP	yellow fluorescent protein
Yl, Y. lipolytica	*Yarrowia lipolytica*
ZS	Zellweger spectrum
Ω	Ohm

8.3 LIST OF FIGURES

8.4 CURRICULUM VITAE

Name:	Nina Anna Maria Bonekamp
Date of birth:	14.06.1982
Place of birth:	Würselen, Germany
Nationality:	German
Marital status:	single; no children
Address:	Ahrstraße 1, 51371 Leverkusen, Germany

School Education

1988 - 1990	Primary School "*Nathrater Straße*", Wuppertal, Germany
1990 - 1992	Primary School "*Im Steinfeld*", Leverkusen-Bürrig, Germany
1992 - 2001	Secondary School "*Landrat-Lucas-Gymnasium*", Leverkusen-Opladen, Germany
2001	University entrance qualification (Grade: 1.0, very good)

University Education

2001 - 2007	Studies of Human biology at *Philipps-University of Marburg*, Germany
Apr 2006-Mar 2007	Diploma thesis at the Institute for Cytobiology and Cytopathology; Philipps-University Marburg (PD Dr. M. Schrader) • Title: "*Untersuchungen zur Fusion von Peroxisomen in Säugerzellen*"
Mar 2007	Granting of the academical degree "*Diplom-Humanbiologe"* (Grade: 1.1, very good)
May 2007-Dec 2007	PhD fellowship at the Centro de Biologia Celular, University of Aveiro, Portugal (PD Dr. M. Schrader)
Jan 2008-Dec 2011	PhD fellowship at the Centro de Biologia Celular, University of Aveiro, Portugal (PD Dr. M. Schrader), funded by the "*Fundacao para a Ciencia e a Tecnologia*" (FCT) • Title: "*Towards an understanding of peroxisome dynamics in mammalian cells*"

8.5 VERZEICHNIS DER AKADEMISCHEN LEHRER

Meine akademischen Lehrer in Marburg waren die Damen und Herren Professoren, Doktoren und Dozenten:

Bastians
Bauer
Bernd
Bette
Dalpke
Daut
Del Rey
Dietrich
Eickmann
Eilers
Elsässer
Feuser
Garn
Garten
Gebhard
Gudermann
Hasilik
Hassel
Huber
Jacob
Jungclas
Kirchner
Klenk
Knöller
Koolmann
Krebber
Kunz
Lang
Lill
Liss
Löffler
Lohoff
Lorberth
Lüers
Maisner
Moll
Müller
Müller-Brüsselbach
Renkawitz-Pohl
Renz
Röhm
Röper
Schäfer
Schrader
Schulz
Steiniger
Stöckmann
Suske
Voigt
Weihe
Westermann

8.6 ACKNOWLEDGEMENTS

First of all, I would like to thank PD Dr. Michael Schrader for the supervision of my thesis. His unwavering optimism, passionate attitude towards all things peroxisome and his continued trust in my abilities were immeasurable when investigating my various projects. I am very greatful for his advice and mentoring which enabled me to learn different aspects of scientific everyday life, well beyond benchwork.

Furthermore, I would like to thank Prof. Dr. Roland Lill for supervising and representing my thesis.

Many thanks to Prof. Dr. Georg Lüers for his thoughtful advice in the lab and beyond. I would like to deeply thank Dr. Paula Sampaio for her thorough expertise and support in regard to the different aspects of microscopy. Moreover, I would like to thank Dr. Fernão Vistelo de Abreu for introducing us to the exciting possibilities of biomathematical analysis. Furthermore, many thanks to Dr. Joaquin Jordan Bueso for his support and expertise on the field of mitochondrial dynamics.

I would like to kindly thank the *Fundação para a Ciência e a Tecnologia* (FCT) and the *Conselho dos Reitores Portugueses* (CRUP) for their financial support in the course of this thesis (SFRH/BD/37647/2007 and N° A-20/08, resp.). Also, many thanks to the members of the *Centro de Biologia Celular* at the University of Aveiro and the *Institut für Zytobiologie und Zytopathologie* of the University of Marburg for their continued support and advice over the years.

A heartfelt thank you to all past and present members of the Schrader-Lab. Thank you all for the warm welcome into a foreign country and your continuous within the lab and beyond, especially Monica Almeida, Miguel Aroso, Fatima Camões, Maria João Cardoso and Markus Islinger. I would like to deeply thank Hannah Delille, Maria Gomez Lazaro, Sandra Grille, Sofia Guimarães and Cornelia Rinn for their never-wavering efforts to support me and make me feel at home, despite myself.

Many, many thanks to Stephanie Brand, Annett Koch, Cornelia Ringer and Nadime Ünver. You managed to listen and ease my doubts in spite of the long distance and the years passing. Thank you very much, I couldn't have done it without you.

Last not but definitely not least, special thanks to my family: my mother Inge Bonekamp and my brother Bernd Bonekamp (whom I hereby thank explicitly!). I am more than greatful for the help, love and support over the years, more than I can say. Vielen, vielen Dank!

8.7 EHRENWÖRTLICHE ERKLÄRUNG EHRENWÖRTLICHE ERKLÄRUNG (MIT PUBLIKATIONSLISTE)

Ich erkläre ehrenwörtlich, dass ich die dem Fachbereich Medizin der Philipps-Universität Marburg zur Promotionsprüfung eingereichte Arbeit mit dem Titel „*Towards an understanding of peroxisome dynamics in mammalian cells*“ im Institut für Zytobiologie und Zytopathologie unter Leitung von Prof. Dr. Roland Lill mit Unterstützung durch PD Dr. Michael Schrader (externe Betreuung) ohne sonstige Hilfe selbst durchgeführt und bei der Abfassung der Arbeit keine anderen als die in der Dissertation aufgeführten Hilfsmittel benutzt habe. Ich habe bisher an keinem in- oder ausländischen Medizinischen Fachbereich ein Gesuch um Zulassung zur Promotion eingereicht, noch die vorliegende oder eine andere Arbeit als Dissertation vorgelegt.

Marburg Nina Bonekamp

Teile der Arbeit wurden/werden wie folgt publiziert:

Gomez-Lazaro, M**., N. A. Bonekamp**, M. F. Galindo, J. Jordan and M. Schrader: 6-OHDA induces Drp1-dependent mitochondrial fragmentation in SH-SY5Y cells. Free Radic Biol Med., 44 (11), 1960-69, 2008.

Camoes, F, **N. A. Bonekamp**, H. K. Delille, and M. Schrader: Organelle dynamics and dysfunction: A closer link between mitochondria and peroxisomes. J Inherit Metab Dis. **32**(2), 163-80, 2009. *Review*.

Bonekamp, N. A., A. Volkl, H. D. Fahimi, and M. Schrader: Reactive oxygen species and peroxisomes: struggling for balance. BioFactors **35**(4), 346-355, 2009. *Review*.

Bonekamp, N. A., H. D. Fahimi, and M. Schrader: Oxidative stress in peroxisomes. In: Principles of Free Radical Biomedicine, eds. K. Pantopoulos, H. Schipper, Nova Science Publishers Inc. (2011). *Book chapter* (in press).

Bonekamp, N.A., M. Islinger, M. Gomez-Lazaro, and M. Schrader: Cytochemical detection of peroxisomes and mitochondria. In: "Cell Imaging Techniques: Methods and Protocols", Methods in Molecular Biology Series, eds. J. Roth & D. Taatjes, Springer Science + Business Media; 2nd edition (2011). *Book chapter* (in press)

Schrader, M., **N.A. Bonekamp**, and M. Islinger: Fission and proliferation of peroxisomes. Biochim Biophys Acta – Molecular Basis of Disease (2012) *Review* (in press).

Bonekamp, N. A., F. Vistulo de Abreu, P. Sampaio, G. Luers and M. Schrader: Transient interactions of mammalian peroxisomes without exchange of matrix or membrane marker proteins. (2011) (Traffic, in revision).

Bonekamp, N. A., M. Almeida, S. Guimaraes, S. Tavares and M. Schrader: Mammalian Pex11pβ is a peroxisomal transmembrane protein. (2012, in preparation)

Cardoso, MJ., S. Grille, **N.A. Bonekamp** and M. Schrader: Regulation of mammalian Pex11pβ during peroxisomal growth and division. (2012, in preparation)

Vorträge:

"Peroxisomal dynamics: Do mammalian peroxisomes fuse with each other?" **N.A. Bonekamp**, P. Sampaio, G. H. Lüers, and M. Schrader. Open European Peroxisome Meeting, October 20-21, 2010. Lunteren, The Netherlands. *Oral presentation*

"Quo vadis, Pex11pb? - Re-examining Pex11pb membrane topology" **N. A. Bonekamp**, M. Almeida, S. Guimaraes, M. J. Cardoso, and M. Schrader. Open European Peroxisome Meeting, October 20-21, 2010, Lunteren, The Netherlands. *Oral presentation*

Posterpräsentationen:

"6-Hydroxydopamine and 3-nitropropionic acid: two ways towards the final end?" Gomez-Lazaro M, **Bonekamp N.A.**, Jordan J and Schrader M. International symposium. New advances in Parkinson's disease. May 27-28, 2008. Salamanca, Spain.

"Peroxisome dynamics in health and disease" **N. A. Bonekamp**, and M. Schrader. Research Day, June 8, 2011, University of Aveiro, Aveiro, Portugal.

Betreute Masterarbeiten:

S. Pinho: Induction and determination of ROS and their effect on peroxisome proliferation, (Master in Biomolecular Methods, University of Aveiro 2009-2010); Supervisor: M. Schrader, Co-Supervisor: **N.A. Bonekamp**

Weitere Publikationen:

Koch, A., Y. Yoon, **N. A. Bonekamp**, M. A. McNiven and M. Schrader: A role for Fis1 in both mitochondrial and peroxisomal fission in mammalian cells. Mol. Biol. Cell 16 (11), 5077-86, 2005.

Delille, H. K., **N. A. Bonekamp** and M. Schrader: Peroxisomes and Disease - An overview. IJBC Vol. **2**(4), 308-314, 2006. *Review*

Bonekamp, N. A., K. Vormund, R. Jacob and M. Schrader: Dynamin-like protein 1 at the Golgi complex: A novel component of the sorting/targeting machinery en route to the plasma membrane. Exp Cell Res. 316(20), 3454-67, 2010

Islinger, M., **N. A. Bonekamp**, F. Camoes, I. Castro, M. Almeida, S. Gomes, M. Schrader: New insights into the targeting process of tail-anchored proteins to peroxisomes. 2012 (in preparation)

Delille, H., **N. A. Bonekamp**, S. Pinho, M. Schrader: Hypertubulation of peroxisomes by multiple stimuli. 2012 (in preparation).

Pinho, S., **N. A. Bonekamp**, M. G. Lazaro, J. Jordan, M. Schrader: Effect of Rotenone on peroxisomal dynamics and motility. (2012, in preparation).

Weitere Präsentationen:

"Mitochondrial fission proteins DLP1 and Fis1 participate in peroxisomal fission". A. Koch, Y. Yoon, **N. A. Bonekamp**, M. McNiven, and M. Schrader. International Meeting of the SFB 593 "Mechanisms of cellular compartmentalization". 2005. Marburg, Germany.

Vormund, K., **N. A. Bonekamp**, R. Jacob, M. Schrader: A novel function of Dynamin-like protein 1 at the Golgi complex. Eur. J. Cell Biol. **87S1** (Suppl. 58), S1-8 (abstr.), 2008.

"Dynamin-like protein 1 – a single protein with multiple locations and functions". **N. A. Bonekamp**, K. Vormund, R. Jacob, and M. Schrader. EMBO Meeting, August 29–September 1, 2009. Amsterdam, The Netherlands.

28th Workshop of the German Anatomical Society, Wuerzburg, Germany (September 28-30, 2011) Islinger, M., **N.A. Bonekamp**, M. Almeida, S. Guimaraes, I. Castro, F. Camoes, M. Schrader: "Tail-anchored proteins on peroxisomes: common targeting to a 3rd subcellular compartment"